c. 2

# GENESIS OF SKARN-POLYMETALLIC DEPOSITS IN THE HANOVER-FIERRO AREA AND A GEOTECHNICAL EVALUATION OF PIT SLOPE STABILITY AT THE CONTINENTAL MINE, FIERRO, NEW MEXICO

Volume I

by

Mohammed Vali Yousefpour

1979

T-2119

A thesis submitted to the Faculty and the Board of Trustees of the Colorado School of Mines in partial fulfillment of the requirements for the degree of Doctor of Philosophy (Geological Engineering).

Signed: M. V. Yousefpour
Mohammed Vali Yousefpour

Golden, Colorado
Date 12/13/, 1979

Approved: Robert H. Carpenter
Robert H. Carpenter
Thesis Advisor

Joseph J. Finney
Head of Department

Golden, Colorado
Date 12/13, 1979

## ABSTRACT

Skarn deposits in the Hanover-Fierro area of the Central Mining District, New Mexico, U.S.A. are localized around the margin of a granodiorite stock. Paleozoic and Mesozoic sedimentary rocks were extensively thermally altered by intrusion of the stock in Lower Tertiary time. High-temperature skarn assemblages were subsequently altered and replaced by low-temperature ore minerals. Intense fracturing of the wallrock, which began prior to the development of the skarns, continued during the formation of the skarns and during emplacement of the ore minerals. The southern lobe of the granodiorite stock is an equigranular facies and is different from the main mass to the north which is porphyritic. The skarn associated with the equigranular facies is richer in manganese and iron than those at the northern margin.

Two environments of skarns are recognized: (1) "endoskarn" which formed within the margins of the stock is very limited in size and is composed mainly of epidote and (2) "exoskarns" which formed in adjacent sedimentary rocks. Exoskarns in the investigated area are much more extensive and are rich in the elements Ca, Mg, Mn, Fe, and Al, and they are the only hosts to ore deposits. Exoskarns here are of two types: (1) limy-siliceous skarn which is the result of replacement and partial recrystallization of calcareous shale. This is the skarn of hornfels type, and (2) replacement skarns which are the major skarn types and contain the commercial grade of ore deposits.

The ore-bearing skarns are separated into "magnesian" and "limy" types. The magnesian skarn is formed at the contact of dolomite with the stock whereas the limy skarn occurs in the limestone unit.

Magnesian skarn is composed of high-temperature magnesium minerals such as forsterite, diopside, magnetite, periclase and spinel. These minerals later were replaced by humite, chondrodite, clinohumite, phlogopite, serpentine, tremolite, talc, magnesite and brucite during low-temperature alteration. The magnesian skarn is the best host for magnetite mineralization. Limy skarn is characterized by development of high-temperature lime-magnesium-iron-manganese-aluminum silicates which include garnet of andradite to grossularite, pyroxene of diopside to hedenbergite, manganhedenbergite, johannsenite, pyroxmangite, and rhodonite. Wollastonite is one of the least abundant of the high-temperature silicates occurring in the marble zone. Idocrase usually occurs in trace amounts associated with garnet. The limy skarn is the best host for the copper-zinc-and iron ores.

Intensive development of vein-like bodies of garnet and pyroxene represents a second stage of skarnization. This was followed by the formation of actinolite and epidote. Actinolite characteristically has replaced diopside and salite, but it did not form in manganiferous varieties of pyroxene. The Mn-bearing varieties of pyroxene are replaced by ilvaite, calcite and quartz.

The factors controlling zonation may be separated into two groups: (1) changes in the mobility of the constituents in the fluids, and (2) changes in the concentration of the key elements, Mg, Si, Mn, Fe, Al,

Cl, and F in these fluids. The wallrock alteration after the main stage of skarnization includes nests and veins of greisen materials replacing the previously formed silicates.

The replacement of carbonate rocks was accompanied by introduction of all constituents except for calcium and carbon dioxide. Silica, iron, manganese, potassium, sodium, and magnesium were, for the most part, brought in by magmatic fluids from the granodiorite stock. Alumina was mainly redistributed in the shale units and went into formation of epidote.

The earliest stage of ore mineralization developed at the end of the alkaline stage of the skarnization. Continued precipitation of ore minerals was accompanied by an increasing acidity of the fluids that provided cation replacement reactions in which the weaker cations take the place of stronger ones. Formation of ore minerals was controlled by the solubility of skarn silicates in acid solutions,and followed by decreasing insolubility of ore minerals. Among skarn-polymetallic deposits, magnetite, copper sulfides and sphalerite are the only economic minerals.

A geotechnical evaluation of slope-stability at the Continental pit was anticipated. This investigation included rock weathering and engineering classification of rock masses, role of fractures in slope-stability, stereoplots of structural conditions and evaluation of potential slope problems, groundwater conditions and drainage systems and effects of blasting. On-going investigations have been recommended to assess and to monitor the stability of particular slopes on the basis of the geologic structures.

# TABLE OF CONTENTS

# LIST OF FIGURES

# LIST OF TABLES

# LIST OF PLATES

# Dedication

To my parents, who provided the moral and financial supports throughout my educational training.

# GENESIS OF SKARN-POLYMETALLIC DEPOSITS IN THE HANOVER-FIERRO AREA, NEW MEXICO

## INTRODUCTION

### Location and Accessibility

The general area of study is part of the Central mining district in Grant County, New Mexico, located about 13 miles northeast of Silver City and 4 miles north of the Chino Pit. The topography consists of a series of mountains and hills with a relief of about 1180 feet. The area studied is surrounded by Fierro Mountain to the east, Hermosa Mountain to the west and northwest, Hanover Mountain to the north, and Hanover City to the south. The location of this area in the state of New Mexico is shown in Figure 1.

The district has very good accessibility. Highway 90 connects Silver City with Hillsboro, and passes through Central, Hanover, and Santa Rita. Highway 180 connects Silver City with Deming, New Mexico, passes through Bayard, and intersects Highway 90 at Central, New Mexico. One branch of Highway 180 extends northeastward from Bayard and intersects Highway 90 at Hanover, New Mexico. A branch of the Atchison, Topeka and Santa Fe Railroad

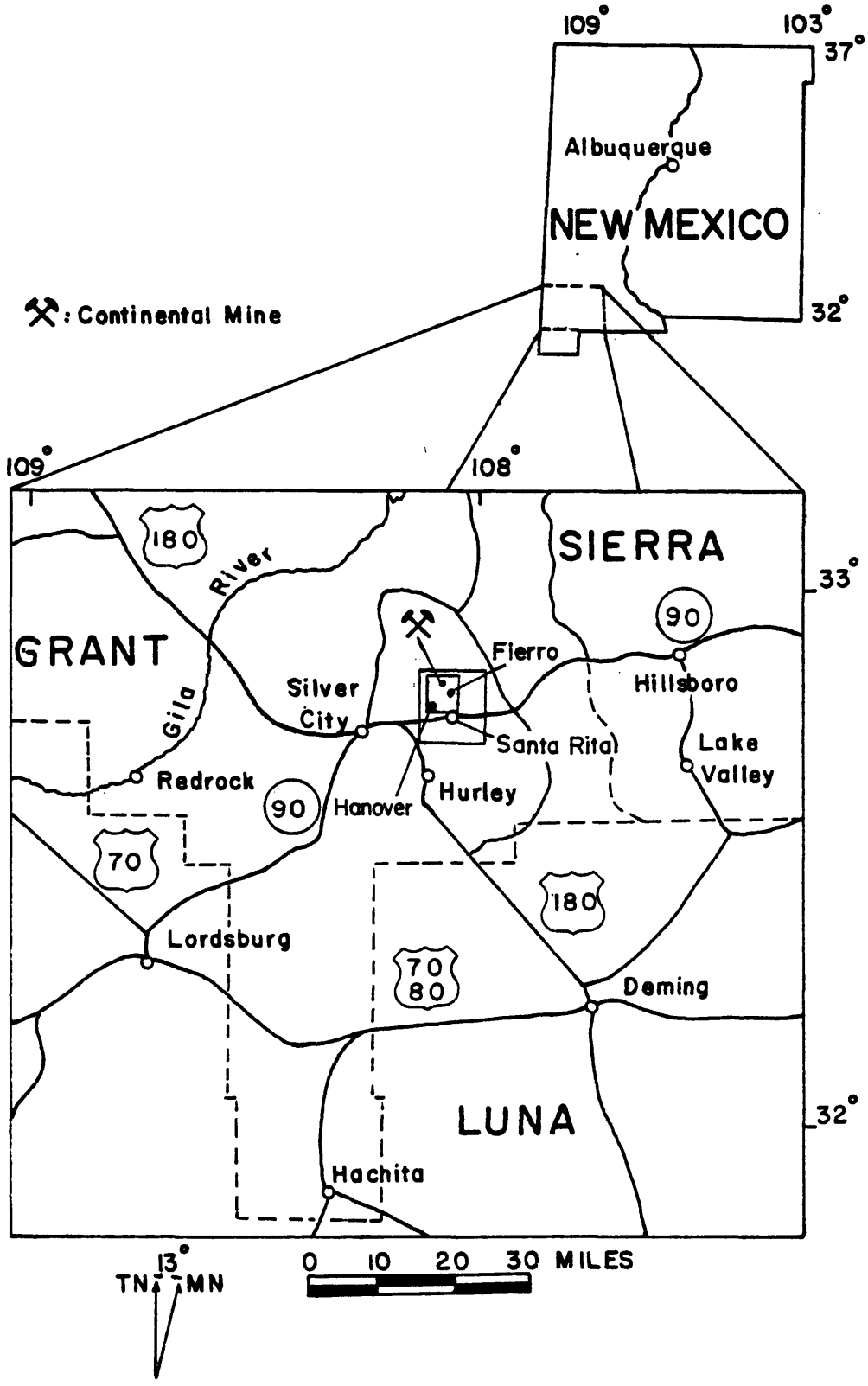


Figure 1. Index map of the Hanover-Fierro area, New Mexico. The larger rectangle represents Santa Rita quadrangle, and the smaller one indicates area studied (modified from Jones and others, 1967).

extends from Bayard to Fierro and the Continental mine, and serves the open pit and underground mine of the United States Smelting, Refining and Mining Company.

The Continental, Union Hill, New Jersey Zinc, Annie Fox, Pewabic, El Paso, Jim Fair, and Hugo mines are located around the margin of the granodiorite porphyry of the Hanover-Fierro stock, in the metasomatized and metamorphosed Paleozoic sediments (Figure 2).

## History

The Santa Rita area is one of the oldest mining districts in the west. Native copper was discovered for the first time by an Apache Indian in the late eighteenth century (Lindgren, 1910, p. 306). The discovery was reported to Colonel Carrasco, an officer of the Spanish army. The Central Mining District appears to have been organized about 1860. The copper production in the latter part of the nineteenth century was reported to be 20,000 mule loads, or about 4,000,000 pounds per year. The production was reduced during the late nineteenth century, but mining activity was sustained intermittently until the end of the century.

The Hanover mine near the present town of Fierro was probably known to the Indians in the early eighteenth century. It was producing copper as early as 1858. Between

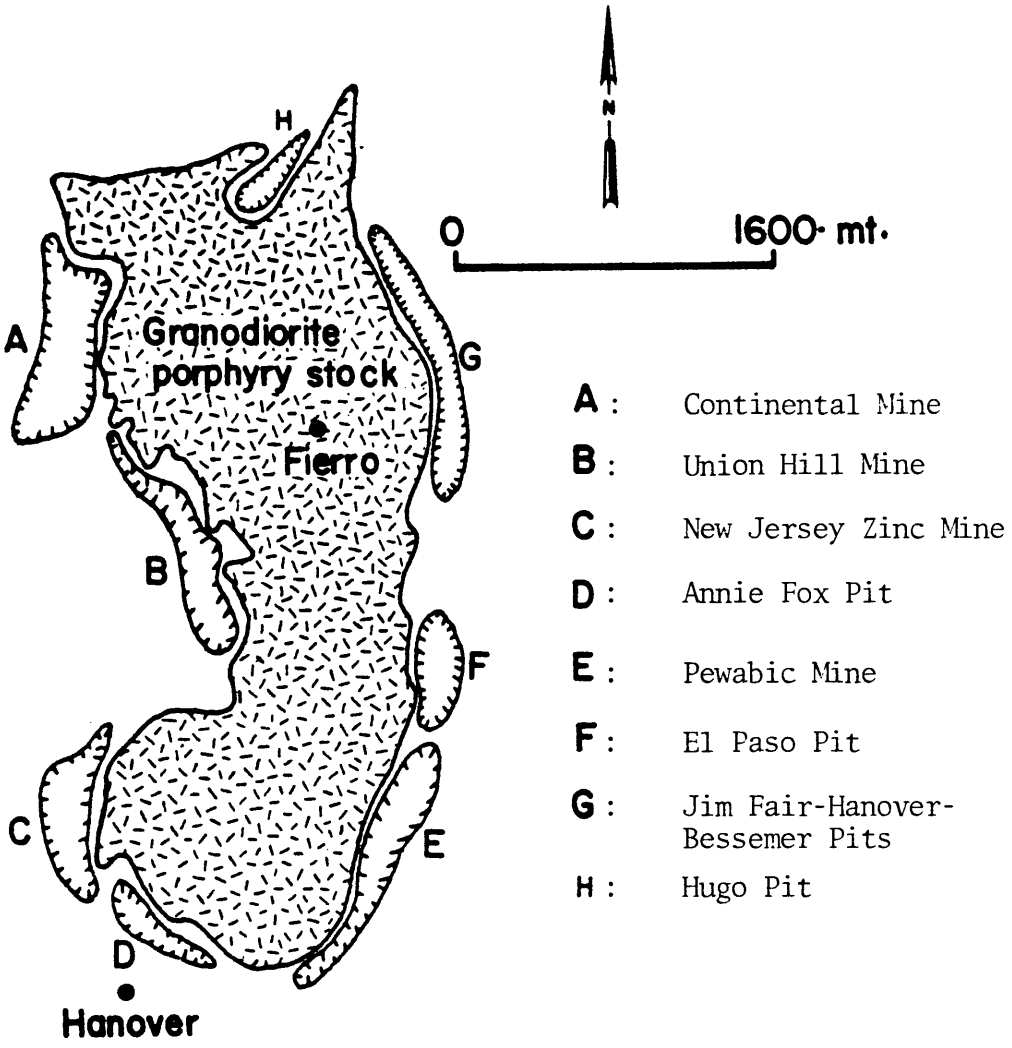


Figure 2. Generalized map showing location of the major open-pit mines around the margin of the granodiorite of the Hanover-Fierro stock.

1858 and 1861 the Hanover mine is said to have produced nearly 1,000,000 pounds of copper. The average price of copper at that time was 23 cents per pound. It was closed shortly after the beginning of the Civil War. This mine and other properties in the vicinity were purchased by Phelps Dodge in 1902. The deposits of iron ore in the vicinity of Fierro had long been regarded as an important asset, and mining of these deposits by Colorado Fuel and Iron Company began in 1891. Another operator in the region, the Hermosa Copper Company, began mining in 1904. Copper production in the district reached its maximum in 1929 (Spencer and Paige, 1935, p. 10). Production of lead and zinc did not begin until 1902 (Hernon, 1949, p. 9), with significant production increases occurring in 1930.

The United States Smelting, Refining and Mining Company, which had operated iron mines at Fierro, but had not participated in the zinc mining until 1941, has been the chief producer in recent years. In 1962 an extensive drilling program was carried out in the district, resulting in the present Continental open pit and underground mine with production of over 8,000 tons of copper, iron, and some zinc ores per day (written communication, 1976). Assuming favorable economic conditions over the long term, future production may be expected to increase.

## Previous Geologic Work

The geology of the Central Mining District has been investigated by many authors since 1875. Early reports by Graton (1910) and Paige (1909, 1912, 1916, 1935) emphasize general geology and ore deposits in this region. Metamorphism in the area has been investigated by Landon (1929). Schmitt's (1939a, 1948) work emphasizes the pyrometasomatic deposits in the Pewabic mine along the southern margin of the Hanover-Fierro stock. More interesting geologic features of the region were described by Hernon and others (1953). In 1956 Jones and others completed geologic maps of the Central Mining District. Kelley (1949) described the geology and economic aspects of the ore deposits. Kniffin (1930) investigated the iron ore deposits around the Hanover-Fierro stock. Lead and zinc deposits around the southern margin of the Hanover-Fierro stock were described by Schmitt (1939a, b) and by Hoagland and Lasky (1948).

The first investigation of wall-rock alteration was performed by Landon (1932) and a second by Lasky (1936). Alteration associated with the Santa Rita Stock was studied by Kerr and others (1950), and mineral zoning of this stock was the subject of Nielsen's study (1968).

The publications prior to 1959 are summarized by

Jones and others (1967). Most of these papers deal with the general geology and economic aspects of the Central Mining District. The most recent study was by Aldrich (1972) who summarized the structural features and performed a joint system analysis of the Santa Rita-Hanover area. Forrester (1972) has discussed metamorphic zoning and mineralization at the Continental mine. His investigation is based on drilling data which lacks geologic maps and avoids many critical details.

## Present Investigation

The purpose of the present investigation was to study and map the various facies of metamorphism, examining their interrelationships and in turn their relations to the metamorphic wall-rocks in order to understand the concept of metamorphic facies and to consider associations of mineral assemblages from diverse bulk composition. These studies include detail mapping of selected localities in the open pits and accessible underground working (see Figure 2). The following subjects have been investigated during this work:

1. Thermal metamorphism of calcareous and non-calcareous sediments.
2. Description of metamorphic minerals.
3. Role of temperature and $CO_2$ pressure in the

formation of ore-bearing skarn.

4. Distribution of certain elements in metasediments adjacent to ore bodies.
5. The major structural control of ore deposits.
6. Geotechnical evaluation of pit slope stability.

Methods of Investigation

Field work for gathering the necessary data was conducted during the spring of 1978. Geologic mapping of the pits and underground working has been completed on a scale of 1 inch to 30 feet, 1 inch to 50 feet, and 1 inch to 200 feet. Rock chip samples of both fresh and altered materials were collected for geochemical trace element analysis, petrographic thin sections, and ore-microscopy study.

Laboratory investigations included petrographic study of 250 thin sections for mineral identification, rock type determination and detection of alteration minerals suites, and microscope study of various polished sections and polished thinsections or ore samples. Some thin sections were stained to facilitate differentiation of calcite from dolomite and cordierite from plagioclase. The universal-stage was used to determine the 2V and optical orientation of various rock-forming minerals.

Atomic absorption spectrometry was used to determine the distribution of several elements in metasedimentary

rocks. X-ray diffraction powder was utilized to identify Mn-bearing pyroxenes. X-ray fluorescence analysis was used to determine the concentration of the major oxides present in the samples. Garnet composition was determined by microprobe analysis.

Acknowledgements

The writer wishes to express his thanks to the following people who helped in the completion of this investigation. Sincere appreciation goes to the members of his thesis committee: Drs. Robert H. Carpenter, Advisor, L. Trowbridge Grose, L. Graham Closs, Maurice Brock; John F. Abel, Professors Charles O. Frush and Donald I Dickinson. Each of these men maintained patience and interest, and supplied continuing encouragement throughout this study. Dr. Carpenter's help is most sincerely appreciated for securing permission to do geologic mapping and sampling at Fierro, New Mexico, from the United States Smelting, Refining, and Mining Company.

Acknowledgement also goes to the Western Division of the United States Smelting, Refining, and Mining Company for its financial support. The very valuable assistance of the vice president, Mr. R. C. Weagel, and the geology staff of the company, particularly that of Mr. B. Worthington, is greatly appreciated.

The author also wishes to gratefully acknowledge the financial support from the Ministry of Higher Education and Sciences of the Iranian Government, without whose aid this study would not have been possible.

Microprobe analysis for determining the garnet composition was done by Dr. Greg S. Holden. His help and useful discussions are gratefully appreciated. The writer is grateful to Dr. J. Krause from the CSM Research Institute for his generous help in x-ray fluorescence analysis. Extremely helpful reviews of some parts of the dissertation were held with Mr. Stan Obernyer, and his ideas and suggestions are gratefully appreciated.

## GENERAL GEOLOGY

According to McKee (1951) and King and others (1944), the Santa Rita Quadrangle lies near the southeastern tip of the Colorado Plateau and on the north margin of the Sonora geosyncline. The Central Mining District is located in the transition zone between the Mexican Highland section of the Basin and Range Physiographic Province and the southern volcanic lobe of the Colorado Plateau, at a place where the sub-horizontal Miocene(?) volcanic rocks of the Colorado Plateau have been stripped away, exposing the complicated geology of the older rocks and the ore

deposits in them. The regional setting of the study area is shown in Figure 3. The conspicuous structures of the northern and southern part of this quadrangle are faults with general northwest and northeast trends. The interested reader is referred to the above references and also to the geologic map of southwestern New Mexico (Dane and Bachman, 1961).

The area studied is characterized by the Paleozoic and Mesozoic sediments intruded by various igneous rock types. Exposure of Precambrian rock is restricted to a small area on the east rim of the Hanover-Fierro stock.

## Precambrian Rocks

The following description including Precambrian, sedimentary, and igneous rocks is a summary of previous work and the reader is referred to the Master's thesis (Yousefpour, 1977) for more detailed information.

In the area studied, the Precambrian rock underlies a lenticular area exposed along the eastern contact of the Hanover-Fierro stock. Precambrian rock is also penetrated in one of the deep drill holes near the Number 3 shaft of the Continental mine. A few small lenses and fragments of Precambrian rock were mapped in the Union Hill mine. The rock is a finely crystalline gneiss with abundant lenses of black biotite in a groundmass of potassic

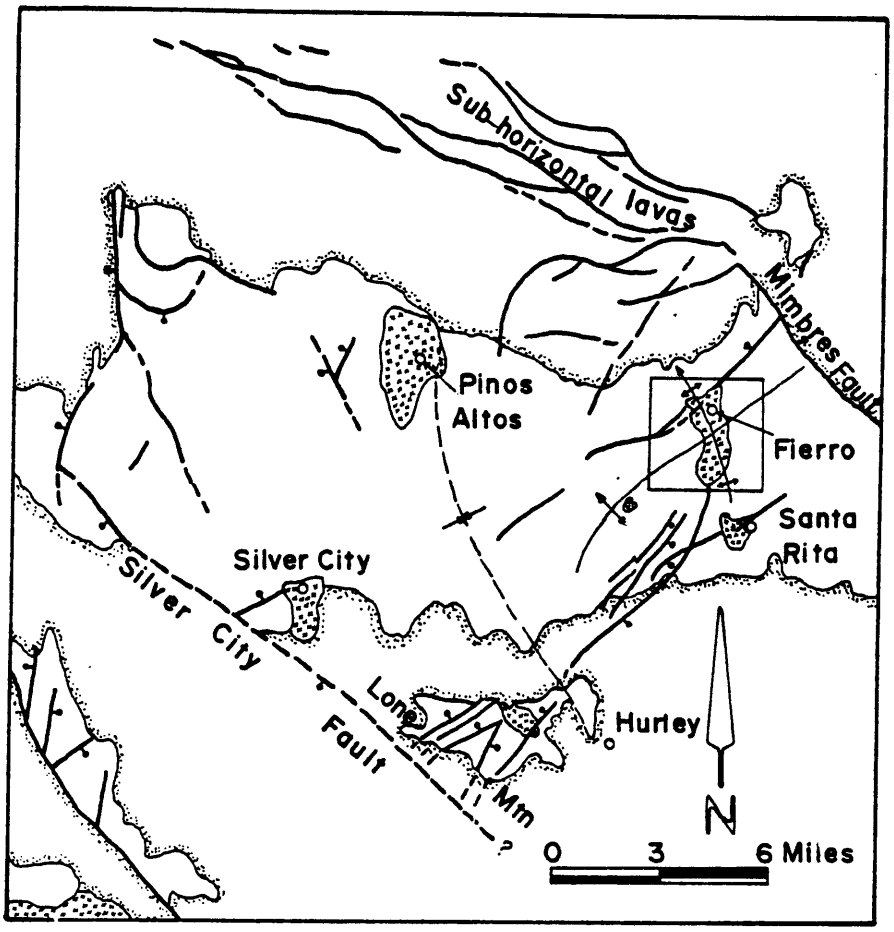


Figure 3. Regional setting of the study area is shown in the rectangle (modified from Paige, 1916, and Lasky, 1949).

EXPLANATION

Edge of Tertiary volcanic rocks

Stocks

Normal fault, ball on downthrown side

Trace of axial plane and plunge of axis

Anticline

Syncline

feldspar and quartz giving a foliated fabric to the rock. Zoisite, magnetite and zircon are observed in thin section as accessory minerals; also some biotite is altered to muscovite and chlorite.

Bliss Formation of Cambrian and Lower Ordovician Age

The Bliss Formation, of upper Cambrian to lower Ordovician age, is the basal Paleozoic unit. It is not extensively exposed in the area. The upper contact is obscured because it is covered by old mine dumps. Where the contacts are well exposed, they are gradational and very irregular. The Bliss Formation is metamorphosed and strongly sheared by the intrusion of the Hanover-Fierro stock. This formation is locally intruded by younger dikes.

The Bliss Formation is interbedded green to brown, medium- to coarse-grained glauconitic, ferruginous quartzite, serpentinized, glauconitic dolomite containing Precambrian fragments toward the base, and green, brown and black calcareous shale highly metamorphosed to fine-grained hornfels. The black color is the result of magnetite. Other common minerals are biotite, clinopyroxene and hematite. The best exposure of the Bliss Formation is on the east side of the Hanover-Fierro stock, the east side of Union Hill, and to the southwest of the Continental pit. The total

thickness of formation is 140-188 feet (Spencer and Paige, 1935, p. 13; Jones and others, 1967, p. 10).

El Paso Limestone of Ordovician Age

The El Paso Limestone is conformable with the underlying Bliss Formation and the overlying Montoya Dolomite (Jones, 1967, p. 12). It has been divided into two members by Kelley and Silver (1952, p. 40). In the area studied, the El Paso Limestone is exposed only in small areas on the east and west side of the Hanover-Fierro stock. This formation and other early Paleozoic sediments are faulted and domed by the forceful injection of the pluton. Around the pluton, the El Paso Limestone, where exposed, is a white dolomitic and siliceous limestone containing chert nodules and thin layers of shale. It is metamorphosed to marble and clinopyroxene hornfels with blebs of green to yellowish-green serpentine, magnetite veins and disseminated chalcopyrite. The south edge of the Continental pit shows a higher concentration of chalcopyrite. The total thickness measured in the Fierro district is 323 feet (Jones and others, 1967, p. 13). In other areas of the Santa Rita quadrangle the thickness of unaltered El Paso Limestone has been reported to be 519-534 feet (Jones, 1959). Drilling data has shown that

the El Paso Limestone is much thicker to the southwest of the present Continental pit.

Montoya and Fusselman Dolomites of Ordovician and Silurian Age

The Upper Ordovician Montoya Dolomite and the overlying Silurian Fusselman Dolomite have been thermally metamorphosed in the Continental mine area. It is difficult to map them as separate units. Elsewhere, in the eastern part of the Santa Rita quadrangle where they are not metamorphosed, they have been mapped separately. In the area studied these formations consist of white to light gray, coarse- to fine-grained dolomitic marble with chert nodules and interbedded with coarse-grained gray limestone near the top. The lower part of these formations are highly metamorphosed and contain blebs of marble, banded green to light green and locally black serpentine alternating with massive magnetite and disseminated chalcopyrite mineralization. The lower unit locally contains tremolite. At the Continental mine area, the Montoya and Fusselman Dolomites are intruded by dikes of varied lithologies. South of the Santa Rita quadrangle, Jones and others (1967, p. 17) found the Montoya Dolomite to measure approximately 352 feet of limy dolomite, cherty dolomite, mudstone, and sandy dolomite. The Montoya and

Fusselman Dolomites measured 460 feet on the east side of the Hanover-Fierro stock (Jones and others, 1967, p. 20).

Percha Shale of Devonian Age

The Percha Shale disconformably overlies the Fusselman Dolomite and is overlain by the Lake Valley Limestone. Stevenson (1945, p. 24), divided the Percha Shale into a lower member, the Ready Pay Member, and an upper member, the Box Member.

The Ready Pay Member is a black, fissile, carbonaceous shale which is somewhat more calcareous at the base. The Upper Box Member is white to light-gray,calcareous shale with local concentrations of gray limestone nodules. This formation is well exposed on the east and west sides of the Hanover-Fierro stock. The Box Member is thicker on the west side. On the west side of the area studied it is intruded by a hornblende syenodiorite porphyry. Along the contact with this intrusion, the Percha Shale is metamorphosed to a fine-grained, brownish to black, diopsidic hornfels. The limy unit is usually diopsidic hornfels with arsenopyrite and pyrite mineralization adjacent to the contact of the intrusive. East of the pluton, the Percha Shale is intruded by a narrow hornblende-quartz diorite sill, which is mappable in a small area to the northwest of Fierro Hill. To the west of the pluton

the Percha Shale and younger Paleozoic sediments are in fault contact with Fusselman Dolomite. There is not enough data to identify this formation from others in the present Continental pit area. The thickness of Percha Shale was measured by different authors. Spencer and Paige (1935, p. 19) reported 280-350 feet east of the Hanover-Fierro stock. Jones and others (1967, p. 22) reported 315 feet total thickness, with the Upper Box Member being 95 feet thick. Other reports from different areas show more variable thicknesses.

Lake Valley Limestone of Lower Mississippian Age

The rocks of Carboniferous and Permian age in the Central Mining District were called the Fierro Limestone by Paige (1916). He correlated the lowermost part with the Lake Valley Limestone. The crinoidal limestone of the upper part of Lake Valley Limestone was called the Hanover Limestone by Schmitt (1933b, p. 188) but is known as the Tierra Blanca Member of the Lake Valley Limestone (Laudon and Bowsher, 1949, p. 10).

The Lake Valley Limestone has been divided into four members. They are, from oldest to youngest: the Andrecito, the Alamogordo, the Nunn, and the Tierra Blanca. The Lake Valley Limestone is underlain conformably by Percha Shale, and overlain disconformably by the Parting Shale of the

Oswaldo Formation.

The Andrecito Member consists of fossiliferous limestone, interbedded with gray shale and marl with local black chert nodules. The thickness varies from 15 to 60 feet in the Santa Rita quadrangle (Jones and others, 1967, p. 22).

The Alamogordo Member is characterized by intensive internal shearing of dark gray, slightly fossiliferous limestone beds with abundant lenses of black chert. Total thickness of this member in the area studied is reportedly 40 feet (Jones and others, 1967, p. 25).

The Nunn Member contains dark to light gray, very fine-grained, fossiliferous, marly limestone with abundant gray chert nodules and lenses of shale. The purity of the limestone increases upward. Total thickness is reported to be 166-182 feet (Jones and others, 1967, p. 25). The Alamogordo and Nunn Members are termed the Lower Blue Limestone by local mine geologists. The Lower Blue Limestone close to the igneous contact is metamorphosed to marble and garnet-clinopyroxene skarn. Locally it has been replaced by ore minerals.

The Tierra Blanca Member, where unmetamorphosed, is a coarsely crystalline, white to grayish-white, massive, non-magnesian limestone with abundant crinoid stems and

local white chert nodules. Petrographic studies show that, except for the chert, this member is almost pure calicte. Schmitt (1939a, p. 801) reported 0.19-0.44 percent MgO from analyzed samples. It is metamorphosed to marble and garnet close to the contact with the Hanover-Fierro stock, and contains a large portion of the zinc, and copper ore in the Continental mine area. The lower contact of this member can be identified by a downward color change from white to dark gray limestone and from white chert nodules to black chert lenses of the Nunn Member. The upper contact is marked by a disconformity with the overlying Parting Shale. Total thickness of the Tierra Blanca is reportedly 35-220 feet (Jones and others, 1967, p. 25). Some of the variation in thickness may be due to erosion before the deposition of the overlying Oswaldo Formation.

Magdalena Group of Pennsylvanian Age

Rocks of Pennsylvanian age were called the Magdalena Group by Gordon (1907). Spencer and Paige (1935, p. 23) divided the Magdalena Group into two formations: the lower part, the Oswaldo Formation, and the upper part, the Syrena Formation. At the base of the Oswaldo Formation there is a siliceous shale member, 20-40 feet thick, called the Parting Shale, which rests disconformably on the Lake Valley Limestone. To the northeast of the area studied,

the Parting Shale is intruded by a quartz diorite sill. Above the Parting Shale, the Oswaldo Formation consists of gray crinoidal, argillaceous and silty limestone, containing chert nodules and interlayered with many thin siliceous shale layers. The lower portion of the Oswaldo Formation is called Middle Blue Limestone. The upper portion is called Upper Blue Limestone. The basal Parting Shale is intruded by several granodiorite sills with the same composition and texture as that of the Hanover-Fierro stock at the pit area. In the Continental mine area, the shale beds are metamorphosed to clinopyroxene-quartz-feldspar hornfels with accessory retrograde chlorite and epidote. The same unit has been altered to epidote skarn at the New Jersey Zinc mine and the Powabic mine. The limy units are metamorphosed to garnet, garnet-clinopyroxene, and marble at the Continental mine, but to garnet, hedenbergite, pyroxmangite and marble along the southern margin of the stock.

Total thickness of the Oswaldo Formation is 405-437 feet (Jones and others, 1967, p. 27).

The Syrena Formation lies conformably above the Oswaldo Formation. The base of the Syrena Formation is a black,limy shale unit about 30-40 feet thick. The upper limit is gray, argillaceous limestone and shaly limestone interbedded

with a 2-6-foot thick siliceous shale. The effect of metamorphism is the same as that of the Oswaldo Formation. The shaly units have accessory chlorite and epidote. Within the area studied the Syrena Formation is identified only at the Continental pit and west of the New Jersey Zinc mine. The thickness of the Syrena Formation is reported to be 170-390 feet (Laskey, 1936, p. 19) and 320-350 feet (Jones and others, 1967, p. 29).

Abo Formation of Permian Age

Overlying the Syrena Formation are the red mudstone and shale beds correlated with the Abo Formation by Spencer and Paige (1935, p. 27). In the area studied, the Abo Formation consists of reddish to greenish shale, calcareous mudstone, and siltstone with abundant lenses of silty and argillaceous limestone. The lower part of the Abo Formation, near the Number 2 shaft along the shaft fault zone, is intruded by granodiorite dikes and sills. The Abo Formation crops out in two places within the area studied: to the north near the Number 3 shaft, and to the northwest in the pit area.

The Abo Formation is metamorphosed to garnet, clinopyroxene, chlorite, and epidote hornfels. The entire formation is a dark green hornfels with lenses of garnet and locally ferriferrous hornfels with accessory muscovite.

Total thickness of the Abo Formation is reported to be 0-200 feet (Laskey and Hoagland, 1949, p. 12). Jones and others (1967, p. 32) have recorded 265 feet from the northern part of the Santa Rita quadrangle.

Mesozoic Rocks

Rocks of Triassic, Jurassic, and Lower Cretaceous ages are not present in the area studied. Rocks of the Upper Cretaceous include the Beartooth Quartzite and Colorado Formation (Laskey, 1936; Paige, 1916; Darton, 1917).

The Upper Cretaceous Beartooth Quartzite lies unconformably on the Abo Formation. Within the area studied the Beartooth Quartzite is exposed on the west side of the Continental pit and to the north and northeast of the mill where it is in direct contact with the Hanover-Fierro stock and to the southeast of the area. The original rock is a light gray to buff, fine- to very fine-grained sandstone interbedded with thin, dark green to black shale near the top. It is metamorphosed everywhere at the Continental mine to light gray and white quartzite by silicification and is locally weathered to reddish-brown quartzite.

The Beartooth Quartzite contains abundant pyrite veins and veinlets. Locally azurite, a result of supergene enrichment, is present. This formation is intruded by quartz monzonite breccia and pyroxene andesite dikes. The

total thickness is reported to be 50 to 140 feet (Laskey and Hoagland, 1949, p. 12), and 142 feet (Jones and others, 1967, p. 34).

The Upper Cretaceous-Colorado Formation lies conformably on the Beartooth Quartzite. The lower part of the Colorado Formation is exposed at the pit area and extends to the west and northwest. Farther from the pit area, it is intruded by Upper Cretaceous syenodiorite porphyry and covered by volcanic rocks of the Late Tertiary. The lower part of the Colorado Formation is bounded by the Barringer fault southwest of the Continental pit. In this area it is extensively intruded by several types of mafic dikes and sills. The lower part of the Colorado Formation is severely fractured and altered. This part of the Colorado Formation is a well-bedded, black fissile shale characterized by abundant thin beds of silty to very fine-grained sandstone and sparse lenses of calcareous shale. Total thickness of the lower member is reportedly 225 feet (Jones and others, 1967, p. 36). The upper part of this shale member consists of a series of interbedded shales and siltstones and very fine-grained sandstones. In various publications this interbedded shale and siltstone is interpreted as being the lower part of the upper sandstone member.

The sandstone member of the Colorado Formation consists of fine- to coarse-grained, locally arkosic sandstone with some dark gray to green shale at the base. The sandstone beds are yellowish-tan, white, light green, and brown ferrigenous. Near the base of the member there is some mudstone and thin beds of limestone grading upward to calcareous sandstone. Fossiliferous limestone is reported by Jones and others (1967, p. 37).

The upper part of the sandstone member is commonly conglomeratic sandstone, containing pebbles of quartz, chert, granite, and fragments of feldspar. Total thickness of the Colorado Formation is reported to be 2000 feet in the Silver City quadrangle (Jones and others, 1967, p. 36), and over 1000 feet in the Central Mining District (Laskey and Hoagland, 1949, p. 12). The Colorado Formation at the Continental mine area is metamorphosed to biotite and diopsidic hornfels. The succession and thickness of sedimentary rocks in the Santa Rita quadrangle is shown in Figure 4.

The Paleozoic and overlain Cretaceous rocks are severely fractured, faulted, and intruded by different types of igneous dikes and sills.

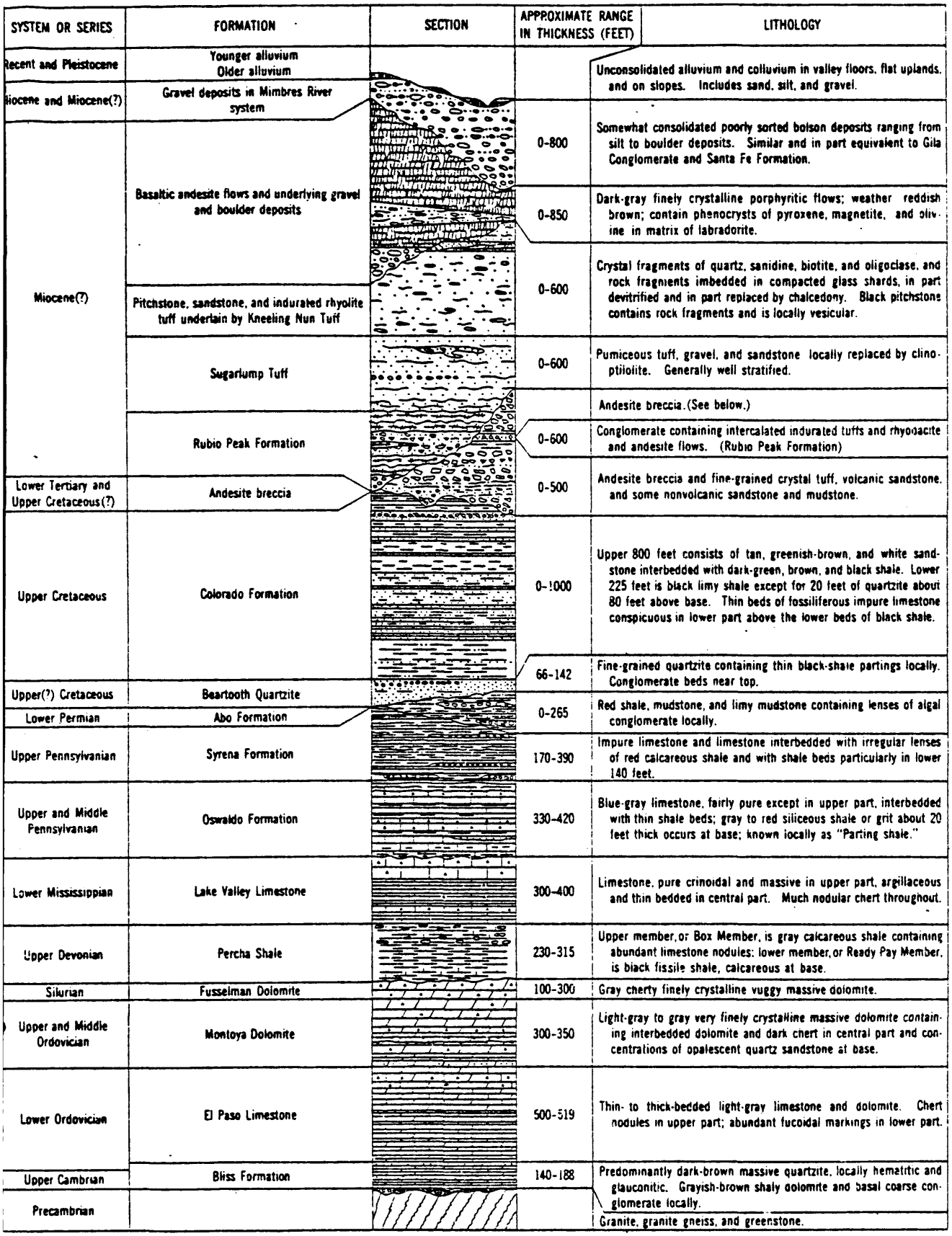


Figure 4. Columnar section of sedimentary rocks at the Santa Rita quadrangle, Grant County, New Mexico (from Jones and others, 1967).

## IGNEOUS ROCKS

Twelve general categories of intrusive rocks crop out within the area studied, probably in the interval between Late Cretaceous and Miocene time. The intrusives form sills, stock and dikes. All of the igneous rocks appear to have been emplaced during a single episode. Evidently, some deep-seated fractures existed in the Paleozoic and Mesozoic sedimentary rocks within the area prior to the initial intrusives. Magmas of slightly different composition invaded Devonian shale and carboniferous carbonate rocks in preference to more competent sediments. The intrusion of sills into the sequence of sedimentary rocks increased its thickness and competency. Outward dipping of strata adjacent to the Hanover-Fierro stock indicates that the stock was emplaced by arching and faulting of strata above the preferred horizon. The stock and the adjacent country rocks were intruded by composite dikes. The intrusive rocks are nearly similar in color and texture. The matrix of most rocks constitutes 40 to 70 percent of their volume.

The type and relative abundance of alteration differs from older to younger rocks. The most abundant phenocrysts in all varieties of intrusives, except for pyroxene andesite porphyry dikes, are those of plagioclase. Potassium feldspar

phenocrysts occur abundantly in most rocks. Hornblende and biotite are the main mafic constituents in most of the rocks, but pyroxene is predominant in andesite dikes. When hornblende is predominant in quartz monzonite dikes, biotite is absent or at least very rare. The reverse situation is also present.

The distribution, geologic relation, and mineralogy of each igneous rock unit are described only briefly. For more detailed information, the reader is referred to the M. Sc. thesis (Yousefpour, 1977).

Hornblende-Quartz Diorite Sills

Hornblende-quartz diorite forms extensive sills throughout the Santa Rita quadrangle. In the area studied, the hornblende-quartz diorite sills intrude the Parting Shale near the base of the Oswaldo Formation. The sills also intrude the Percha Shale, but are more localized than in the Parting Shale.

The hornblende-quartz diorite is a mottled greenish-gray, fine- to medium-grained, nearly holocrystalline, somewhat porphyritic and generally weathers to a dull pink. The following are the essential primary minerals found in the hornblende-quartz diorite: plagioclase, hornblende, orthoclase and quartz. The accessories are apatite,

magnetite, and trace amounts of pyroxene.

Hornblende-Augite Syenodiorite Porphyry

Three masses of hornblende-augite syenodiorite porphyry crop out in the western and northwestern parts of the study area. Each of the masses of hornblende-augite syenodiorite porphyry is slightly different from the others in composition and texture. In general they are dark-gray to greenish-gray in outcrop. The rock is a holocrystalline prophyry with a hypidiomorphic, medium-grained matrix.

The essential minerals are: hornblende, plagioclase, orthoclase and pyroxene. The accessory minerals include: magnetite, apatite, and zircon. Biotite occurs in trace amounts.

None of the masses of hornblende-augite syenodiorite has caused any intensive alteration at the contact with the invaded sediments except for several feet at the most.

Pyroxene Andesite Porphyry Dikes

Pyroxene andesite porphyry dikes crop out extensively to the northwest of the studied area, and in the Continental pit, where they cut the Syrena, Abo and Colorado Formations (Plates 1 and 2). Most dikes were emplaced along pre-existing fractures and conform to the regional and local fault pattern. On the west side of the Continental pit, both

faults and dikes have northwest trends and dip steeply to the southwest. Away from the pit, the trend is mostly to the west. Some dikes are solid units, but frequent wide, anastomosing bodies include masses of country rock further to the northwest of Hermosa Mountain. This feature may be explained as the result of intrusion along a complex series of linked fractures.

The pyroxene andesite porphyry dikes show variation in texture and composition. The rock is dark-green to black on fresh surface and dark-brown on the weathered part. A large variety of pyroxene andesite dikes have prophyritic aphanitic texture. Over 60 percent of the rock is cryptocrystalline and microcrystalline groundmass, and phenocrysts constitute 35 to 40 percent. The essential minerals include macrophenocrysts of pyroxene (augite, hypersthene, and trace amounts of diopside). The microphenocrysts are plagioclase. Accessory minerals are hornblende, apatite, tridymite and crystoballite.

Hornblende Andesite Porphyry Sills and Dikes

Generally the hornblende andesite sills exposures are discontinuous. The lenses of the sills tend to lie near the base of the Colorado Formation on the west side of the Continental pit. This rock has not been recognized anywhere else in the area. Therefore, the source and

relative age are not identified. Based on petrology and composition, it might be an apophysis of the gabbro plug cropping out in the North Star Basin.

The rock of the sills is medium-gray to greenish-gray on fresh surface, and has a porphyritic texture with 50 percent aphanitic groundmass. The phenocrysts are hornblende, plagioclase, pyroxene, orthoclase, biotite, and apatite. This rock is usually more siliceous and alkaline than pyroxene andesite and hence grades somewhat into dacite.

Diorite Porphyry Dike

One small body of unusual rock has been classified as diorite, cropping out to the south edge of the Continental pit, where it intrudes Montoya and Fusselman dolomites. The age of the diorite and its igneous affiliation are uncertain. The rock is hydrothermally altered by the intrusion of the Hanover-Fierro stock. As far as its relation to other rocks is concerned, it may belong to the late Cretaceous or early Tertiary period of intrusion.

The diorite is dark-green to black, a variably textured rock and is characterized by angular fragments due to injection of the granodiorite stock. The main mass is hollocrystalline, porphyritic, with a hypidiomorphic, medium-grained groundmass.

The essential minerals are plagioclase, pyroxene, and hornblende. Accessory minerals include apatite, orthoclase, magnetite, biotite and olivine.

The diorite is severely altered. Alteration ranges from intensive saussuritization of plagioclase, moderate garnetization of calcitized feldspar, chloritization of hornblende and biotite, and uralitization of pyroxene. Along the contact with the Fusselman dolomite, alteration is characterized by the development of magnetite, pyrite, and molybdenite mineralization along fracture and joint surfaces.

Granodiorite Porphyry of the Hanover-Fierro Stock

The Hanover-Fierro Stock is a stock named by Spencer and Paige (1935). It is the largest granodiorite body of the district. The stock has a length of about 2½ miles (4 kilometers) from north to south, and is 0.5-1 mile (800-1600 meters) wide. It is exposed principally in the valley extending from Hanover to the north of Fierro (Figure 1).

The walls of the stock are almost everywhere vertical and generally crosscutting with respect to the surrounding metasedimentary rock. Based on the structural features and intensity of alteration of the invaded rocks, it is suggested that the stock has more lateral extension at depth.

In different places the stock is in contact with different Paleozoic formations. To the north, along the zone of the Barringer fault, the main mass is in contact at the surface with Syrena and Abo Formations, the Beartooth Quartzite, and the Colorado Formation. Wherever the contact is exposed, the Paleozoic Formations are steeply dipping away from the stock. The average dip ranges from $10^{o}$ to $50^{o}$. The steeper dips lie adjacent to the contact, but along the south margin of the stock, the invaded rocks dip gently toward the stock. In many places the contact rocks are moderately brecciated. Contact metamorphosed sediments contain fragments of granodiorite and the reverse situation is also possible. The southern part of the stock includes xenoliths of sedimentary rocks which have been highly altered (plate 6).

Two distinct facies are recognized in the stock; one is the light-colored, medium- to coarse-grained, hornblende-biotite granodiorite porphyry which includes the main mass. The other a greenish-gray, finer-grained and nearly equigranular with a hypidiomorphic texture. It is intermediate in composition between granodiorite and quartz diorite. This facies is confined to the Hanover lobe and continues marginally to the east of Union Hill (Figure 6). The masses of granodiorite porphyry are cut

by many dikes.

As mentioned previously, the Hanover-Fierro stock is surrounded by a wide zone of contact metamorphic rocks. The intensity of metamorphism decreases rapidly away from the contact, except along the fractures and fault zones where alteration occurs for thousands of feet from the contact. It is evident that the domal structure, at least locally exhibited by the Paleozoic formations, was produced as a result of the forceful injection of the granodiorite stock. Outward dips and intrusive faults in the Paleozoic rocks indicate that the stock was emplaced by arching of the strata above the roof of the intrusion. The magma probably inserted itself as a relatively fluid wedge at this horizon. Based on the field observation, the equigranular facies is possibly slightly older. This interpretation must be verified by geochronology.

The porphritic facies of the Hanover-Fierro stock is light-gray and coarsely crystalline rock. Under the microscope the porphyritic texture is even more pronounced. The phenocrysts lie in a holocrystalline, fine-grained groundmass. In general, the rock is characterized by a xenomorphic, granular fabric with partly granophyric texture. The essential minerals are: plagioclase, hornblende, biotite, orthoclase, and quartz. Accessory minerals include sphene,

apatite, magnetite, and zircon.

The white to light-gray, euhedral to subhedral plagioclase crystals constitute the main phenocrysts. The plagioclase is predominantly andesine ($Ab_{69}$-$Ab_{60}$) with minor calcic oligoclase ($Ab_{72}$). The crystals show albite-pericline twinning and lesser amounts of carlsbad twinning. Some crystals exhibit zoning with $An_{40}$ in inner zones, surrounded by an outer zone where the An content is 31. Selective sericitization and calcitization of andesine is rare. Plagioclase phenocrysts contain euhedral hornblende, indicating earlier crystallization of hornblende.

The hornblende phenocrysts are green and strongly pleochroic, euhedral to subhedral, measuring as much as 8.0 millimeters long. They are marginally replaced by biotite and chlorite and some contain aggregates of quartz, pyrite, hematite, and magnetite. In most thin sections which have been studied, hornblende predominates over biotite. Inclusions of apatite in hornblende are common.

The biotite is brown to green in color, and is strongly pleochroic, euhedral to subhedral and up to 4.0 millimeters across. Some crystals are embayed by the matrix and have irregular outlines. Few crystals contain plagioclase indicating later crystallization of biotite. Green biotite has inclusion of euhedral sphene, which suggests

contemporaneous crystallization of the two minerals. Biotite marginally has been replaced by chlorite; chloritization also occurs along cleavage planes and commonly is rimmed by quartz, sericite, calcite, and iron oxide.

The quartz phenocrysts are anhedral to subhedral. A few are euhedral. Most quartz crystals have been embayed by the groundmass and have irregular outlines. Some grains are moderately rounded and have apatite and zircon inclusions.

The orthoclase crystals are the least abundant phenocrysts. They are light yellow to colorless, with irregular outlines due to strong embayment by the groundmass. Orthoclase commonly contains crystals of plagioclase. Partial corrosion of enclosed plagioclase indicates that the crystallization of plagioclase preceded that of orthoclase. Orthoclase phenocrysts also contain euhedral crystals of sphene and apatite which indicates contemporaneous crystallization of these minerals.

The accessory minerals occur both in the groundmass and as inclusions in the phenocryst crystals. In most samples, sphene predominates over apatite and zircon.

The matrix consists of microgranular plagioclase, quartz, orthoclase, and subordinate amounts of hornblende, biotite, and opaque minerals. The estimated abundance of

the rock forming minerals is: feldspar 60-70 percent, hornblende 10-20 percent, quartz 10-15 percent, and biotite 5-10 percent.

The granodiorite porphyry stock is fairly fresh. Selective sericitization and calcitization of feldspar, partial replacement of hornblende by biotite, chlorite, calcite, and quartz, and marginal replacement of biotite by pennine and calcite are the common alteration products. Along the contact with surrounding rocks, where the stock is broken by closely spaced joints and fractures, albitization and suassuritization of feldspar is relatively extensive. Along the same fractures, argillic-sericitic alteration is well developed. On the east side of the stock, in the transitional zone between equigranular and porphyritic facies, near the contact with lower Paleozoic metasedimentary rocks, irregular and discontinuous lenses of epidote skarn have formed. A similar zone has developed in a small area on the western margin of the stock. In this area and elsewhere, several narrow zones of hornblende and dark green actinolite occur along fracture planes in the stock. These units have been mapped as endoskarn (plates 4 and 6).

The chemical composition of both porphyritic and equigranular facies have been reported by previous

investigators. A compilation of these analyses are given in table 1.

Quartz Monzonite Breccia Column

A dike-like fragmented rock known locally as the breccia columns or breccia are exposed in three areas on the west and north sides of the Continental pit, where they cut steeply across gently westward dipping Paleozoic and Mesozoic metasedimentary rocks. The larger body is dike-like and about 7 feet wide, and has a sharp contact with host rock. Evidently its dimensions increase downward below the present level of the open pit. The second body is much smaller and is found further north in the pit and intrudes the Beartooth orthoquartzite. The third body, which is slightly different in texture and composition, is characterized by intensive galena mineralization. It is found in the northwest corner of the pit where it intrudes the Oswaldo Formation (Plate 1). It is likely that the breccias have formed along fissures and fault intersections and they may be less pipe-like in form. For this reason, the term "breccia column" will be used for this interpretation.

The breccia forms a mass of angular, subangular to well-rounded or rotated fragments tightly cemented with

Table 1 - Compilation of chemical analyses of the granodiorite porphyry of the Hanover-Fierro Stock.

(nd, not determined; ng, not given)

| | 1 | 2 | 3 | 4 | 5 |
|---|---|---|---|---|---|
| $SiO_2$ | 61.26 | 60.4 | 65.36 | 62.7 | 65.50 |
| $Al_2O_3$ | 16.22 | 18.7 | 16.29 | 17.6 | 15.65 |
| $Fe_2O_3$ | 3.0 | 3.9 | 1.94 | 2.9 | 1.63 |
| FeO | 2.38 | 3.6 | 1.88 | 2.7 | 2.79 |
| MgO | 2.57 | 1.0 | 1.76 | 1.1 | 1.86 |
| CaO | 6.12 | 5.8 | 4.05 | 3.9 | 4.1 |
| $Na_2O$ | 4.34 | 3.5 | 3.90 | 3.2 | 3.84 |
| $K_2O$ | 2.61 | 2.3 | 3.29 | 4.8 | 3.01 |
| $H_2O+$ | .20 | nd | .52 | nd | .69 |
| $H_2O-$ | .15 | nd | .20 | nd | ng |
| $TiO_2$ | .52 | nd | .45 | nd | .61 |
| $P_2O_5$ | .48 | nd | .24 | nd | .23 |
| MnO | .08 | nd | .04 | nd | .09 |
| $CO_2$ | .09 | nd | .06 | nd | ng |
| S | .05 | nd | ng | nd | ng |
| Total | 100.07 | 99.2 | 99.98 | 98.9 | 100 |

1. Granodiorite from Empire zinc mine at Hanover, N. Mex. (Kerr and others, 1950, p. 299).
2. Analysis calculated from average mode of equigranular facies.
3. Granodiorite porphyritic facies (Schmitt, 1939a, p. 78).
4. Analysis calculated from average of 10 modes of porphyritic facies (Jones and others, 1967, p. 69).
5. Average hornblende-biotite granodiorites (Nockolds, 1954).

chlorite, carbonate, silica, and clay associated with pyrite, galena and copper mineralization. Broken pieces of quartz monzonite porphyry predominate each fragment. Angular and rounded fragments of indurated shale, limestone, and quartzite which were derived from host rocks are abundant.

Since the base of the Beartooth Quartzite occurs above the breccia column, the quartzite fragments within the breccia body must have slumped downward and reached their present location near the bottom of the pit. This field relation clearly indicates major downward slumping within a steeply dipping breccia wall. The fragments of quartz monzonite porphyry are locally highly altered to sericite and calcite. On the whole, the breccia is compact and firmly cemented, but small microlitic cavities appear occasionally in the matrix and crystalline fragments.

Fragments of the breccia range from microscopic dimensions to blocks of 5 to 8 inches in diameter. The fragments are angular to well-rounded. They include rocks from the adjoining walls and of the rock that forms the wall of the breccia column.

The quartz monzonite fragments vary from nearly equigranular to coarsely porphyritic. Phenocrysts of quartz, orthoclase, andesine, and rare oligoclase are the essential

constituents. Accessory minerals include hornblende, biotite, apatite, zircon, and rutile. Quartz usually contains inclusions of apatite and zircon. Recrystallized interlocking quartz grains compose the bulk of these rock fragments. Fresh hornblende and biotite are very rare. They are entirely replaced by chlorite and calcite. Variable amounts of chlorite, calcite and clay minerals occur interstitially with quartz and other phenocrysts.

The green-colored aphanitic matrix of breccia consists of chlorite (pennine and chloritoid), calcite and clay minerals with disseminated pyrite and minor chalcopyrite. Some fragments are characterized by the presence of native copper in the matrix. Minor magnetite occurs as irregular grains associated with pyrite. The matrix may comprise from 10-80 percent of the rock volume, but an average specimen consists of 70 percent fragments and 30 percent matrix. However, the matrix itself is a microbreccia, at least half of which consists of fragments.

Aplite

Aplite dikes are confined to the granodiorite stock, but a few extend into the surrounding rocks on the east and south margins of the stock (Plate 5). Some of the aplite dikes occur as stringer zones in the stock.

The aplite is pink to pale-pink in color and is charac-

terized by sugary texture. Under the microscope it reveals a typically fine-grained, equigranular texture, consisting chiefly of 50 percent quartz, 40 percent orthoclase, 5-10 percent plagioclase, and subordinate amounts of biotite. The percentage of quartz and orthoclase changes from dike to dike.

Granodiorite Porphyry Dikes

Granodiorite porphyry dikes are very prominent and abundant in the Central Mining District. In the area mapped, they are confined to the west of the Union Hill mine. where they intrude the Montoya and Fusselman Dolomites (Plate 3).

The composition of the granodiorite dike rock is similar to that of the granodiorite stock, but it is not clear whether the former is an apophysis of the latter. Obviously the dikes fill fractures and tend to form a similar pattern following the same direction as the fractures. However, there is no close association between the dikes and the stock. Therefore, they have been classified into two different phases of granodiorite intrusion.

The granodiorite porphyry dikes show variations both in color and in the proportion of the different minerals. The most common variety is a light-gray to greenish-gray, coarse-grained porphyry. The phenocrysts make up 50 to

60 percent of the rock volume, and are embedded in a finely crystalline to aphanitic groundmass. The following essential minerals were revealed under microscope: plagioclase, hornblende, biotite, orthoclase, and quartz. The accessory minerals are apatite, magnetite, sphene, zircon, allanite, and rutile.

Quartz Monzonite Porphyry Dikes

Based on the biotite-hornblende ratio, the quartz monzonite porphyry dikes can be classified into two groups. The biotite-quartz monzonite and the hornblende-quartz monzonite.

The biotite-quartz monzonite dikes are localized to the west and southwest of Union Hill where they intrude the Fusselman Dolomite. Here they generally trend northeast and cut granodiorite dikes. Further to the southwest of Union Hill, northerly-trending quartz monzonite dikes intrude the hornblende-augite syenodiorite porphyry.

The hornblende-quartz monzonite porphyry dikes crop out to the west and northwest of Fierro village, where they intrude the granodiorite porphyry of the Hanover-Fierro stock. The general trend of this group is north-northeast. Some have been cut by younger dike swarms.

The intrusion of quartz monzonite porphyry dikes has not had much effect on the host rock. Wall rock alteration

is slightly more extensive where they intrude sedimentary rocks, but it does not exceed more than a few feet. Relatively intense pyrite mineralization is present a few inches into the Fusselman Dolomite along the porphyry dike-dolomite contact.

The hornblende-quartz monzonite dikes are gray to light-gray on a fresh surface and possess fine- to medium-grained porphyritic texture. The mineral composition is more or less the same as in the case of the biotite-quartz monzonite. However, the main differences in the two monzonites are the sparse distribution of hornblende in the biotite-quartz monzonite dikes and some variation in the accessory minerals.

The biotite-quartz monzonite dikes are light greenish-gray, medium- to coarse-grained, and porphyritic in texture. The groundmass is very fine-grained to aphanitic and constitutes 50-60 percent of the rock volume. The essential minerals are plagioclase, biotite, orthoclase, quartz, and trace amounts of hornblende. Accessory minerals include sphene, apatite, magnetite, allanite, and zircon.

Quartz Latite Porphry Dikes

The quartz latite porphyry dikes crop out extensively in the Hanover-Fierro stock (Plates 4 and 6). Field relations indicate that the quartz latite porphyry dikes were injected after the intrusion of the quartz monzonite dikes.

Several of the dikes are exposed to the west of the Union Hill mine where they cut the granodiorite dike, the bedded Percha Shale and the Montoya and Fusselman Dolomites (Plate 3).

Two different mappable facies can be distinguished in the large masses of quartz latite (Plate 6). The interior facies is typically light-colored, whereas the marginal facies is a dark-gray rock. Quartz latite dikes cut previously contact-metamorphosed rock on the east margin of the Hanover-Fierro stock and contact-metasomatic iron ores in the Republic mine at Fierro.

The rock of the interior facies is coarse- to medium-grained. The matrix is very fine to aphanitic, constituting 60-65 percent of the rock volume. The marginal facies is dark-gray, fine- to medium-grained, and contains more than 70 percent dark-gray aphanitic groundmass. The essential minerals are: plagioclase, quartz, orthoclase, biotite and hornblende. Accessory minerals include apatite, sphene, magnetite, allanite, zircon, and rutile.

Dacite Porphyry Dikes

The dikes designated dacite porphyry include three types of rocks that were emplaced at closely spaced intervals, possibly after intrusion of the quartz latite porphyry dikes. Their absence from the area covered by tuffs and flows of Miocene(?) age suggests the dikes are older

and were emplaced prior to the volcanic episode.

The mineralogic composition of the three rocks, particularly feldspar and heavy minerals and their alteration characteristics, is especially suggestive of a close genetic relationship between them. The most obvious likeness is the similar composition of the plagioclase feldspar. The main difference between them is the proportions of hornblende and biotite. The reader is referred to the M. Sc. thesis (Yousefpour, 1977) for more detailed description of the three rock types.

## Relative Ages of Intrusive Rocks

The relative ages of the intrusive rocks are summarized in the following paragraphs.

The hornblende-quartz diorite sills and hornblende-augite syenodiorite porphyry are possibly the oldest intrusives in the area mapped. The relative age of the two rocks is not known because of lack of outcrops to study their contact relationships. Fragments of hornblende-augite syenodiorite porphyry are found in the andesite breccia to the northwest of the area where it crops out on Hermosa Mountain (Jones and others, 1967). Later pyroxene andesite, hornblende andesite, and diorite dikes cut through the syenodiorite porphyry. The relative ages of these rocks are not known. The hornblende-augite syenodiorite porphyry

west of Union Hill has been cut by an apophysis of the Hanover-Fierro Pluton.

The hornblende-quartz diorite sill is cut by granodiorite porphyry dikes which intruded after the granodiorite of the Hanover-Fierro stock. Crosscutting relations in many places in the Santa Rita quadrangle (Jones and others, 1967) indicate the intermediate age of the Hanover-Fierro stock between that of the hornblende-quartz diorite sill and the younger aplite and granodiorite dikes.

The quartz monzonite porphyry breccia column is highly altered and characterized by extensive mineralization. The relative age of the breccia and the granodiorite porphyry stock is not known because of lack of contact of the two rocks. Extensive alteration and presence of mineralization in the breccia column are due to later stage hydrothermal solutions resulting from a deep-seated magma. Possibly the breccia is a pre-mineralization structure that originated after the granodiorite of the Hanover-Fierro Stock.

The quartz monzonite porphyry dikes cut the hornblende-augite syenodiorite porphyry, the Hanover-Fierro Stock, the aplite dikes, and the granodiorite porphyry dikes. In turn, the quartz monzonite dikes are cut by quartz latite porphyry dikes and dacite porphyry dikes. The dikes grouped as dacite porphyry are considered to be younger

than the quartz latite dikes because some of them cut the quartz latite porphyry dikes.

# SKARN DEPOSITS

## DEFINITION

Skarns are limy-magnesium-manganese-ferrugineous metasomatic silicates and aluminosilicates formed in high-temperature halos which surround plutons. They originate by interaction of magmatic solutions with invaded carbonate rocks. This includes only rocks formed by contact reactional metasomatism. The ore deposits associated with skarns are called "contact," "contact metamorphic," "contact metasomatic," and "pyrometasomatic" ore deposits.

The following definition and terminology have been reported in various papers by different skarn geologists. The reader is referred to the best one by Zharikov (1970) for more detailed information. In the present paper those types of skarns which have occurred in the Hanover-Fierro area are considered.

### Endoskarn and Exoskarn Deposits

Relative to the contact of the granodiorite of the Hanover-Fierro stock, two environments of skarns are recognized: (1) endoskarn which forms inside the periphery of the granodiorite stock and replaces the granodiorite. It has a very limited distribution and forms in irregular,

discontinuous lenses at the contact of the stock with the surrounding sedimentary rocks. This skarn is exposed in several places along the eastern contact of the intrusive (Plate 6 and Figure 48). (2) Exoskarn includes those rocks which occur on the outside of the intrusive and replaces sedimentary rocks.

As shown in Figure 5, most of the skarn deposits in the study area fall into the exoskarn category which generally occurs in the enclosing sedimentary host rocks along the contact of the granodiorite stock. The exoskarn deposit generally occurs between 0 and 1,500 feet from the exposed contact, but in a few places it extends to over 4000 feet.

Skarn formation in the Hanover-Fierro area, like other ore-bearing skarns, are Ca, Mg, Mn, Fe, and Al silicate minerals and include ore deposits of different origins.

## Classification of Skarn Deposits

The mineral assemblages of skarn formations are genetically classified as follows:

### Magnesian skarn

This includes metasomatic rocks characterized by high-temperature magnesium minerals such as forsterite, spinel, diopside, phlogopite and periclase formed at the contact of Montoya and Fusselman Dolomites with the granodiorite

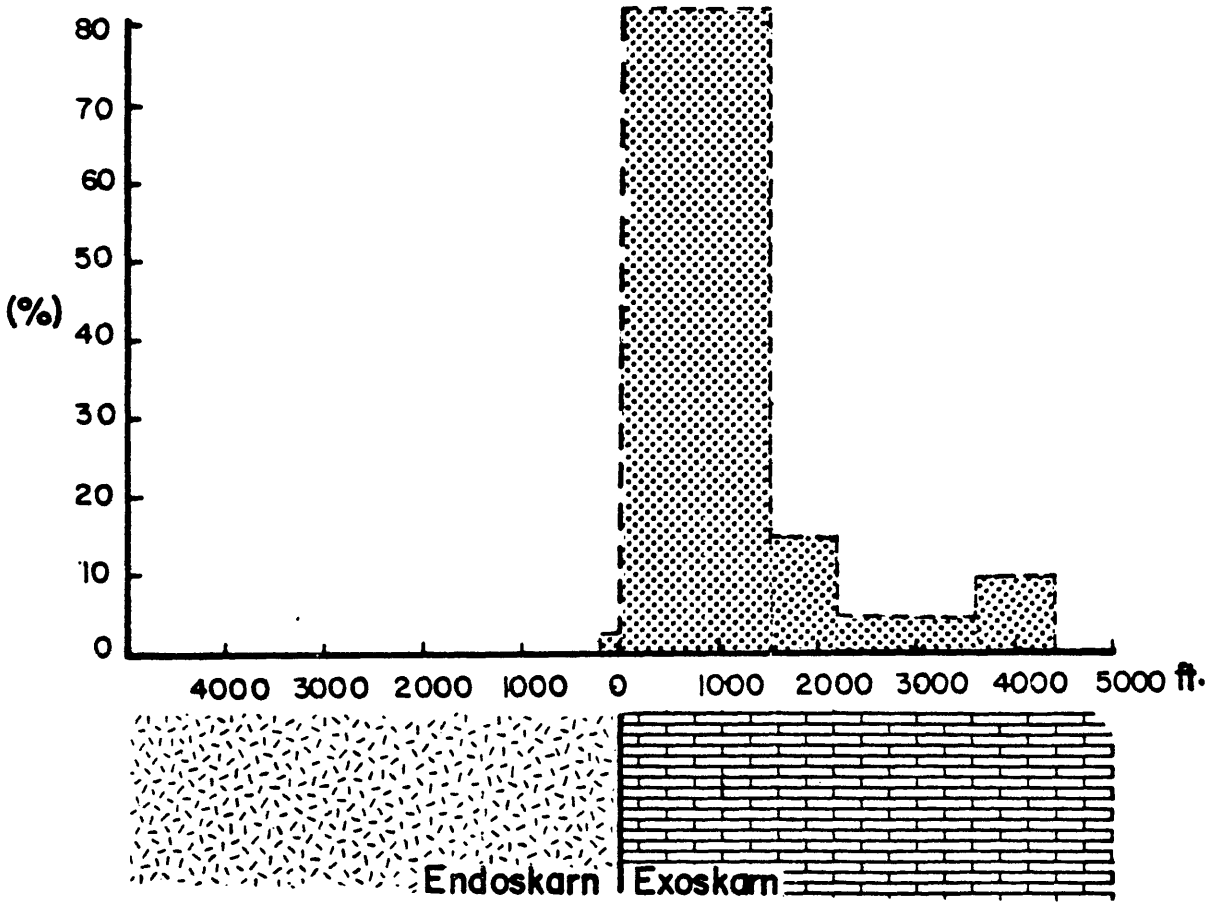


Figure 5. Distribution of endoskarn and exoskarn deposits relative to the exposed contact of the granodiorite and altered sedimentary rocks (modified from Smirnov, 1976). The horizontal axis shows distance from the intrusive contact and the vertical axis represents the percent of endoskarn and exoskarn deposits.

intrusion. This skarn is exposed in the Continental pit and the Union Hill mine, and along the eastern contact of the stock. Table 2 presents major mineral associations in magnesian skarn in the study area.

Limy skarn

This includes metasomatic rocks characterized by high-temperature lime-magnesium-iron-manganese-aluminum silicates such as garnet which ranges in composition from andradite to grossularite, pyroxene that ranges in composition from diopside to hedenbergite, pyroxmangite and rhodonite. These minerals develop at the contact of the granodiorite intrusion with limestone units of Paleozoic sedimentary rocks. This skarn develops everywhere in the study area. Table 3 presents major mineral associations in limy skarn in the Hanover-Fierro area.

## STAGE OF ORE MINERALIZATION

Two principal genetic families of ore minerals have been developed in the Hanover-Fierro area. There is an earlier attendant type of ore which is related to the skarn family and which formed immediately after silication in a relatively similar alkaline environment. This includes the magnetite ore of the magnesian skarn, and the early

Table 2 - Mineral assemblages of magnesian skarns.

| Mineral Group | Major Minerals | Minor Minerals |
|---|---|---|
| Silicates | Forsterite, clinopyroxene (mainly diopside), garnet (mainly andradite to grossularite) and quartz | Monticellite, K feldspar (mainly orthoclase), plagioclase, scapolite and cordierite. |
| Hydrosilicates | Serpentine (antigorite and chrysotile), humite, clinohumite, chondrodite, pennine, clinochlore, phlogopite and chrysocolla | Zeolite, epidote, and amphiboles |
| Oxides and Sulfates | Magnetite, specularite, earthy hematite, limonite, brucite and periclase | Spinel, selenite, chalchanthite and epsomite |
| Sulfides | Pyrite, chalcopyrite, and marmatite | Chalcocite, digenite and pyrrhotite |
| Carbonates and others | Dolomite, calcite, magnesite, and malachite | Apatite, and sphene |

Table 3 - Mineral assemblages of limy skarns.

| Mineral Group | Major Minerals | Minor Minerals |
|---|---|---|
| Silicates | Garnet (mainly andradite to grassularite and some pyrope), clinopyrokene (mainly diopside, hedenbergite to salite and ferfosalite), pyroxmangite, wollastonite, and quartz | K feldspars (mainly orthoclase), plagioclase, cordierite, scalpolite, andalusite, rhodonite, zircon, bustamite, johannsenite |
| Hydrosilicates | Epidote, chlorite, muscovite, actinolite, tremolite, ilvaite, nontronite, and chrysocolla | Zeolite, phlogopite, anthophyllite, axinite, biotite, sericite, montmorillonite, and kaolinite |
| Oxides and Sulfates | Magnetite, specularite, earthy hematite, limonite, chalcanthite, selenite, and epsomite | Chalcedony, jasper, and rutile |
| Sulfides | Sphalerite, chalcopyrite, pyrite, marmatite, bornite, and chalcocite | Covellite, tetrahedrite, digenite, molybdenite, galena, and pyrrhotite |
| Carbonates and others | Calcite, fluorite, malachite, azurite and smithsonite | Apatite and sphene |

sulfide skarn. A later, superimposed ore mineral formed by late stage hydrothermal processes in a more acid environment. This stage includes the main sulfide mineralization which tends to replace previously formed skarns.

One more stage of ore mineralization needs to be recognized for completion of the genetic classification. This includes ore minerals formed simultaneously with vein-type skarn and is related to greisenization.

## GENESIS OF SKARN DEPOSITS

Skarnization is a process involving decarbonatization. The following occur during skarnization:

a. Formation of skarn minerals from calcite, dolomite, and silicate minerals in original rocks.
b. Escape of carbon dioxide.
c. Migration of materials.

The Hanover-Fierro area is characterized by zones containing different assemblages of metasomatic minerals each of which represent a specific range of temperatures and pressures and which are controlled, in part, by the composition and permeability of the parent rocks. The resulting assemblages are also a function of the chemical potential of the mobilized constituents in the system.

The following conditions for the formation of skarn are important:

a. Elevated temperature

b. Presence of high temperature fluids.

Korzhinskii (1954, and 1970) and Philips and Hess (1936) thought that the existence of a stream of aqueous fluids in the contact zone is necessary for the contact reaction, because migration of material is easier in fluids.

During skarnization or high-temperature metasomatism, migration of materials is believed to involve diffusion of material through the crystal lattice of minerals or along the surface layers of crystal grains, combined with migration of materials through infiltration. If both processes were not involved, mineral grains of the original rock could not be completely replaced. Partial replacement was observed at the Continental mine in low-temperature alteration during retrogressive metasomatism.

Migration of material through infiltration played an important role in forming the ore deposits during low-temperature metasomatism. The local concentration of massive sulfides near fractures supports the idea of fracture control and infiltrational skarn during low-temperature metasomatic ore formation.

Volatile materials such as water vapor, and carbon

dioxide are considered to be very mobile. In the case of the Continental mine, transportation of carbon dioxide possibly was strongly controlled by the structural behavior of rock. The intensive fracturing in the ore-bearing skarns acted not only as channelways for the ore forming solutions, but also as a mechanism to release excess $CO_2$ pressure. Shoji (1975) reported that garnet is not stable in fluids containing high $CO_2$ pressure at approximately 400°C. Since garnet is the most common skarn-formed mineral in the Hanover-Fierro area, the skarn and ore deposits seem to have formed at moderate $CO_2$ pressure.

In the deep environment fluid pressure may be lower than the rock pressure, but in the geologic environment of the Continental mine area, where shallow depths were probable during the magmatic activity, the lithostatic pressure may not have been higher than fluid pressure. Therefore, the fluid pressure may play an important role in the contact reactions which developed through "infiltrational metasomatism", in which components are transferred by a stream of aqueous fluids percolating through pores in the rock. The presence of microbreccia and fractures in the original rocks was especially favorable for fluids to permeate the wall rock.

Factors Controlling Zonation in Skarn Deposits

Based on Zharikov's contribution, these factors may be summarized as follows:

1. Changes in the mobility of the constituents in solution. This is marked by the concentration of particular minerals in special zones.
2. Changes in the content of the key elements and their concentration in solution, particularly the elements Mg, Si, Al, Mn, Fe, Cl and F.

According to Korzhinskii (1970), unlike other skarns, the formation of magnesian skarn at magmatic stage occurs under uniform temperature and fully mobile constituents. Zharikov (1970) has mentioned that the differences between various facies of metasomatism are controlled by depth of formation and changes in the carbon dioxide regime. However, development of various zones of skarns in the Hanover-Fierro area mainly depends on the fracture pattern, composition of the original sedimentary rocks and orderly distribution of minerals formed during high-temperature and low-temperature alteration.

The most variable zonation of the magnesian skarn occurs where magnesium minerals of high-temperature stage were subjected to early low-temperature alteration.

Sequence of events that accompanied the intrusion of the granodiorite stock

The sequence of processes following the intrusion of the granodiorite of the Hanover-Fierro stock may fall into four stages: (1) fracturing and brecciating of sedimentary host rock, (2) thermal metamorphism, (3) pneumatolysis, and (4) invasion of iron-bearing solutions and introduction of sulfides.

The essential aspects of the chemical process by which magnesian skarn is formed are summarized by Zharikov (1970) and in some aspects are modified by the writer as follows:

1. The addition of silica to hydrothermal solutions during development of the various skarn rocks.
2. The addition of additional magnesium to the original carbonate rocks during magmatic activity.
3. The addition of iron to solutions, particularly during low-temperature alteration.
4. The addition of aluminum, fluorine, boron and chlorine to hydrothermal solutions during late magmatic activity.
5. A general outflow of magnesium from the inner zones of replacement is conspicuous by accumulation

of this element in the outer zones of the magnesian skarn where its higher content is obvious by formation of magnesium-rich minerals.

6. A general outflow of calcium and escape of carbon dioxide from inner zones is another characteristic.
7. The role played by oxygen in the magmatic processes is not clearly understood, but its general constant content in skarn of different zones is recognized by various investigators.

Characteristics of magmatic-stage of skarnization

Based on the field relationship, the following interpretation may be applied for magmatic-stage skarnization in the Hanover-Fierro area:

1. The contact of the granodiorite stock with invaded sedimentary rocks is relatively sharp and no interaction with the intrusion is obvious over most of its length. In other words, no skarnization of the granodiorite was observed except for very local areas along the southern contact (see Plates 3, 4, 5 and 6).
2. No skarnization is observed within the apophyses of the stock that extend from the stock for tens of meters into the host rock (see Plates 1, 3, 4 and Figure 8).

3. Skarn rocks are pre-dike formations because everywhere in the area they are intruded by aplite and younger dikes.
4. Silicate skarns possibly formed after the crystallization of upper portions of the granodiorite stock.

## ORIGINAL LITHOLOGY AND CONTACT METAMORPHIC AUREOLES ABOUT THE HANOVER-FIERRO STOCK

In the Hanover-Fierro region, various mafic, acidic and neutral plutonic and hypabyssal intrusives are present which were intruded in the Paleozoic and Mesozoic sedimentary rocks. Based on field observation, no intrusive other than the granodiorite of the Hanover-Fierro stock has caused any intensive alteration in the invaded host rock. In general, where sedimentary rocks were intruded by other types of rocks including intrusions of late Cretaceous age and Tertiary time, they are unmetamorphosed or at the most, have suffered only a slight alteration outward from the contact for distances of not more than several feet.

The intensive skarn halo around the margin of the granodiorite stock and the major fractures are shown in Figure 6. The average thermal effect extends approximately

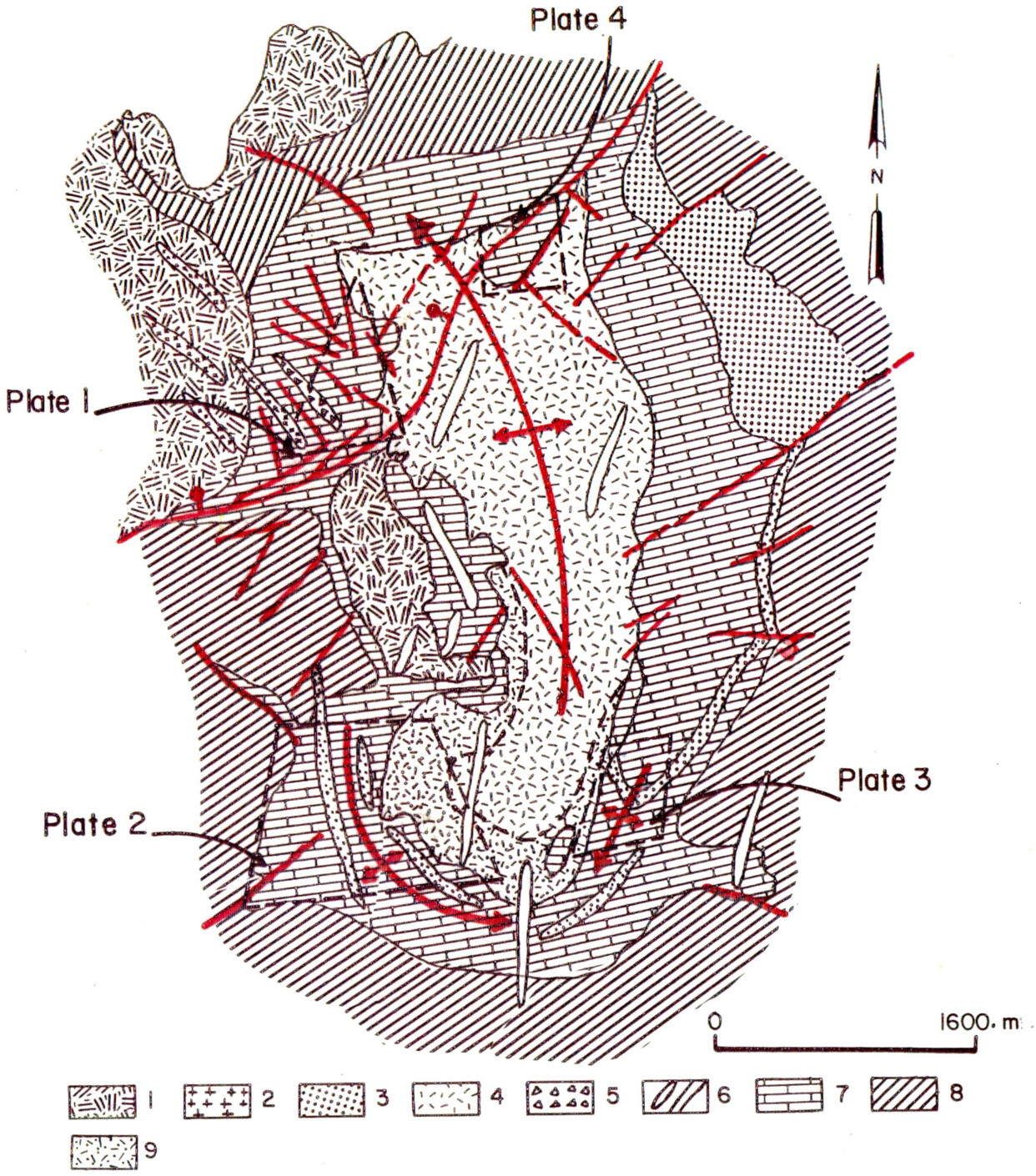


Figure 6 - Simplified geologic map of the Continental mine area showing the major structure and skarn distribution (modified from Jones and others, 1967).
(1) Hornblende-augite syenodiorite porphyry, (2) pyroxene andesite porphyry dikes, (3) hornblende-quartz diorite sills, (4) granodiorite stock (porphyritic facies), (5) quartz monzonite breccia, (6) granodiorite, quartz monzonite, quartz latite and dacite porphyry dikes, (7) skarn and hornfels, (8) unaltered sedimentary rocks, and (9) granodiorite stock (equigranular facies). (10) The red lines are faults and anticline axes.

600-800 meters outward from the contact, but as shown in the figure, skarnization extends along faults over 1400 meters.

Detailed investigations made during this study show local variations in the paragenesis of silicate minerals, in types of metals in the deposits, in types of deposits, and in periods of formation of deposits. These characteristics are summarized in the discussion of the four plates. These include: Plate 1 (the Continental mine), Plate 2 (the New Jersey Zinc mine and the Annie Fox pit), Plate 3 (the Pewabic mine) and Plate 4 (the Hugo pit). In addition to the above mines, the discussion will also include the Union Hill mine (see Figure 2).

The block diagram in Figure 7 represents a schematic model showing the products of metasomatism and metamorphism associated with the granodiorite of the Hanover-Fierro stock. In different places, the stock is in contact with different Paleozoic and Mesozoic formations.

As shown in the diagram, the altered sedimentary rocks show well developed zonation about the contact, and the types of mineral assemblages are also determined in part by the composition and permeability of the original host sedimentary rock. The shale units of the Colorado, Abo

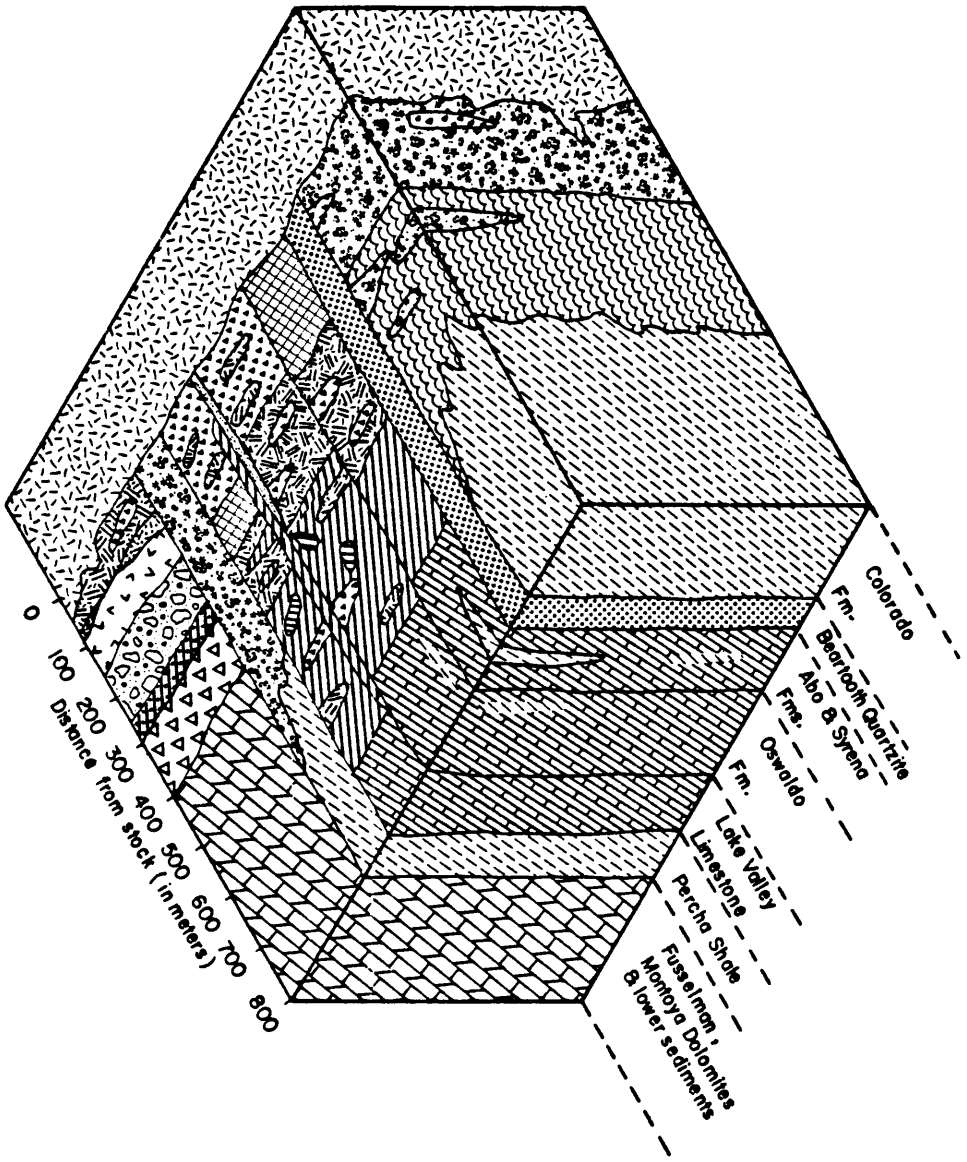


Figure 7 - Schematic model of the alteration zone developed about the granodiorite of the Hanover-Fierro stock.

## EXPLANATION

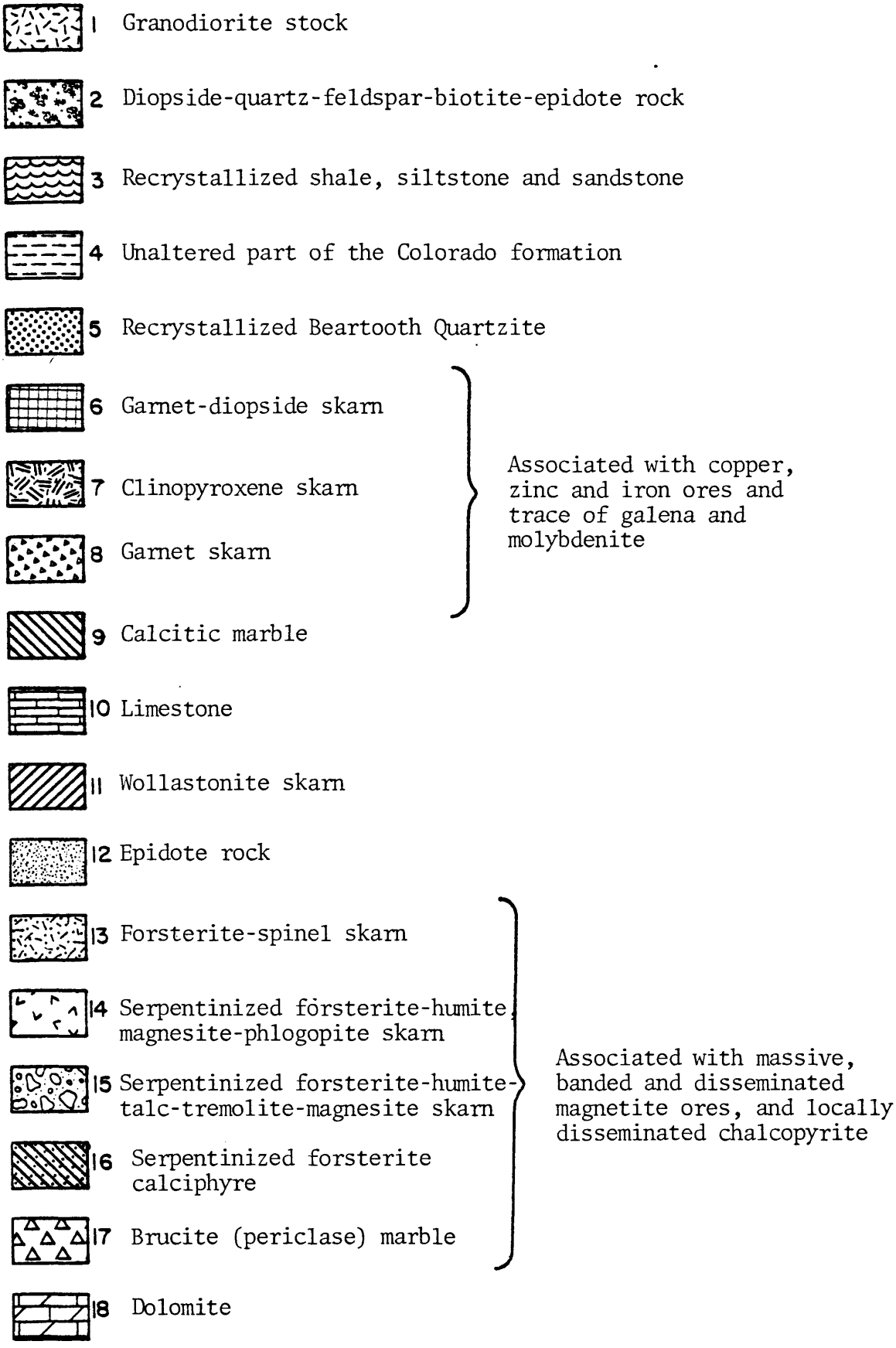

Syrena, and Oswaldo Formations and the Percha Shale at the Continental mine nearly everywhere are metamorphosed to a fine-grained to aphanitic, medium- to dark-green diopside-quartz-feldspar-biotite-epidote hornfels close to the contact. The texture is variable from equigranular, granoblastic to porphyroblastic. The grade of metamorphism decreases away from the intrusive contact. The main metamorphic constituents in the shale units around the southern margin of the stock are epidote, zoisite and clinozoisite and accessory quartz, scapolite, feldspar and diopside. This is shown at the base of the Oswaldo Formation in the diagram. The limestone, shaly limestone, marl and calcareous shale of the Abo, Syrena, and Oswaldo Formations and the lower Lake Valley Limestone at the Continental mine are altered to brown garnet (andradite to grossularite) with lenses of diopside-quartz-feldspar hornfels close to the contact and grade into clinopyroxene (diopside to salite and ferrosalite) and marble away from the contact. At the Continental mine, the marble zone occasionally contains nodules and discontinuous lenses of wollastonite skarn. The same limestone units around the southern margin of the stock are altered to green garnet (mainly andradite to some grossularite) with lenses of epidote and hedenbergite skarn close to the contact, and grade into

hedenbergite-johannsenite-pyroxmangite skarn and marble away from the contact. As shown in Figure 7, a pure limestone in the upper part of the Lake Valley Limestone (the Hanover Limestone) is only slightly affected and recrystallized to calcite marble near the contact with the granodiorite stock.

The Montoya and Fusselman Dolomites (at the base of the block diagram, Figure 7) are altered to magnesian skarns which include the following zones: diopside skarn with lenses of forsterite-spinel skarn close to the contact which grade into forsterite-humite-tremolite-talc-magnesite skarn, forsterite calciphyre, and brucite (periclase) marble away from the contact.

The forsterite later was altered to green and black, magnetite-rich serpentine with spots of yellowish-green serpentine.

The Beartooth orthoquartzite has been moderately to slightly affected by thermal metamorphism and converted to metaquartzite.

Almost everywhere in the region, in the limestone host rock, massive garnet skarn includes alternating lenses of clinopyroxene skarn and marble. The same situation is true for clinopyroxene zone which includes lenses of garnet skarn and marble.

One of the most important features of skarn formation in the Hanover-Fierro area is the differences of alteration and mineralization between the northern and the southern margins of the stock. As can be seen in Figure 6, the southern lobe of the stock differs from the main mass to the north in that the porphyritic facies of the stock is enclosed in a thick mantle of equigranular granodiorite facies. This mantling of the equigranular facies may represent the earlier of the two facies. The following major differences are noticed between the skarn zones near the northern and southern contacts of the granodiorite stock.

| Northern Contact (silicate minerals) | Southern Contact (silicate minerals) |
|---|---|
| 1. Brown garnet skarn (andradite to grossularite) | 1. Green garnet skarn (mainly andradite, some grossularite) |
| 2. Clinopyroxene skarn (diopside to salite and ferrosalite) | 2. Clinopyroxene skarn (hedenbergite-johannsenite, pyroxmangite-rhodonite, and ilvaite |
| 3. Diopside-quartz-feldspar-mica rock in Parting Shale at the base of the Oswaldo Formation | 3. Epidote-zoisite-clinozoisite-quartz-feldspar rock in Parting Shale at the base of the Oswaldo Formation |
| 4. Presence of magnesian skarns and actinolite zone | 4. Absence of magnesian skarns and actinolite zone |
| 5. Abundant veins of quartz, calcite, feldspar, diopside, garnet, epidote and amphiboles | 5. Abundant veins of quartz, calcite, and feldspar |

| Hypogene Ore Minerals | Hypogene Ore Minerals |
|---|---|
| Magnetite, specularite, pyrrhotite, chalcopyrite, pyrite, bornite, chalcocite, sphalerite, marmatite and trace of molybdenite | Sphalerite, galena, pyrite, pyrrhotite, trace of magnetite, and chalcopyrite |

Note: Galena-rich veins observed only in breccia at Continental pit

The most influential factor that determines the composition of the resulting mineral assemblage is the composition of the original lithology. Figure 8 shows a banded sediment composed of layers that reflect original texture and composition. The lower part was a fine-grained grit, recrystallized to quartz-feldspar hornfels. The middle part was a very fine-grained calcareous shale metamorphosed to a fine-grained diopside-garnet-quartz-feldspar hornfels, and the upper part was a fine- to medium-grained calcareous shale metamorphosed to diopside-quartz-garnet hornfels. As can be seen from the photograph, metamorphism has not converted the three parts to one average type. The thin beds remain distinct, each represented by its own assemblage of new minerals that reflect original grain size, and the relationship remains obvious even among beds of microscopic scale.

One special case is worthy of notice: diffusivity is a function of temperature, increasing with rise of temperature. For this and other reasons, the dimension of migration

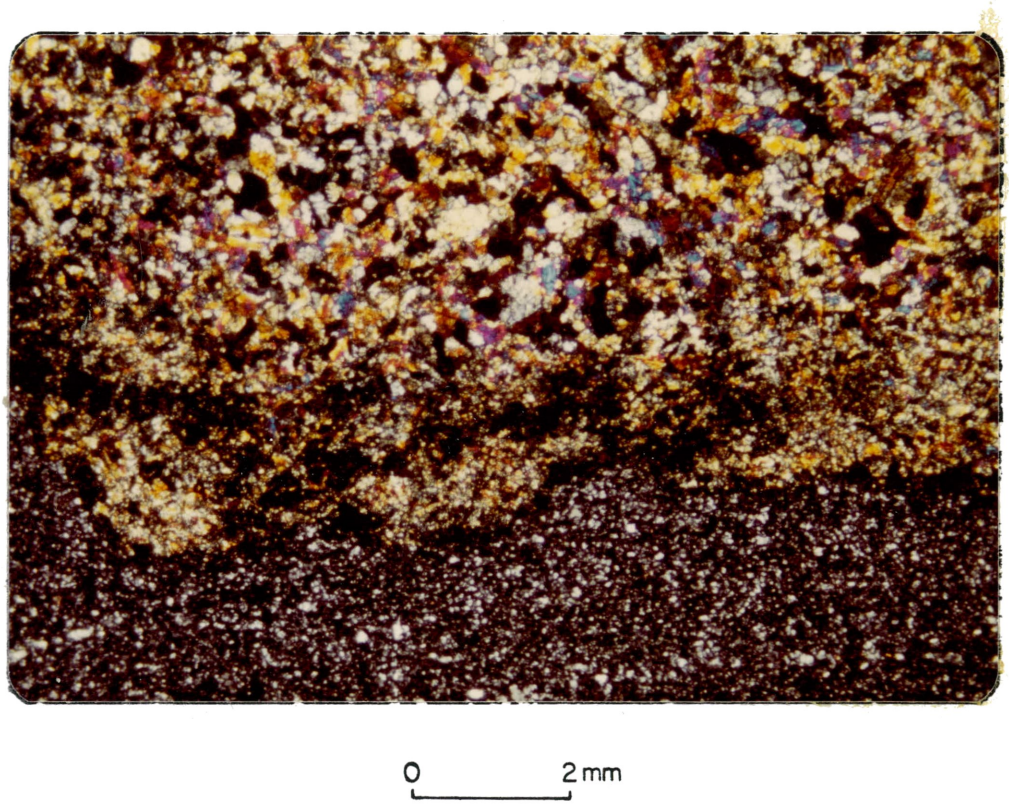


Figure 8. Photomicrograph of banded metasediments showing granoblastic texture of recrystallized grit (lower part), very fine-grained to aphanitic diopside-garnet-quartz-feldspar hornfels (middle part); and medium-grained diopside-quartz-garnet hornfels (upper part).
Location: Syrena Formation in the Continental pit.

of material is always relatively small in the lower temperature zone of alteration and somewhat enlarged in the higher temperature environment.

Where internal differential movement is involved, pre-existing sedimentary structures in the original host are likely to be obliterated, but in many cases they are recognizable. The rocks in the higher temperature zone show less preservation of the original structure, possibly due to more enlarged amplitude of diffusion.

In the high-temperature skarn zone, the contact separating formations of similar compositions is in most cases obscured by the addition of skarn minerals. On the other hand, where lithologic units which differ in chemical composition are subjected to such a grade, the contact between the units can be identified by contrast in mineralogy. For more detailed description, the reader is referred to the following pages.

## SKARN DEPOSITS AT THE CONTINENTAL MINE

Montoya and Fusselman Dolomites, Lake Valley Limestone, Oswaldo, Syrena and Abo Formations, Beartooth Quartzite and Colorado Shale are the dominant wall rock lithologies at the Continental mine. These rocks are intruded by the pyroxene andesite dikes of late Cretaceous age.

The lack of intensive alteration at the contact of pyroxene andesite dikes can be attributed to the fact that the high initial temperature is released prior to emplacement of the dike and the magmas of this composition contain less water than granodiorite.

The shale units of Oswaldo, Syrena, and Abo Formations, and Colorado Shale have been metamorphosed to a medium- to dark-green, very fine-grained to aphanitic clinopyroxene-quartz-feldspar hornfels. The calcareous beds of the above formations are altered to a fine- to medium-grained aggregate of brown garnet and diopside.

The rocks in the Continental mine are extremely fractured and sheared. The author's Plates 1 and 2 are the first maps compiled to depict the interrelationship of the skarn, ores, and structures of the pit area. Here the pre-stock structures such as Barringer, Zuniga and Modoc faults played an important role in the localization of metasomatic and metamorphic rocks and ore minerals. The rocks of this area yield evidence of numerous periods of deformation although the dominant structural pattern was acquired during the Sevier orogeny of the Laramide and therefore predates the metamorphism and mineralization.

As far as the genetic relation is concerned, the new rocks developed in the wall rocks at the Continental mine as a consequence of plutonism include magnesian skarn,

limy skarn, hornfels and metaquartzite. Copper, magnetite and some zinc are the only ore deposits.

Figure 9 represents alteration and major structure in the Continental pit (for the exact location, compare this figure with Plate 1 of Figure 6). Table 4 shows ages of sedimentary rocks, lithology and mineralization of the rocks present at the Continental pit.

## Formation of Magnesian Skarns

Genetically, magnesian skarns at the Continental mine area can be classified into two groups:

### High-temperature magnesian skarn

The minerals of this skarn are olivine (forsterite), periclase, magnetite, specularite, diopside, calcite and trace amounts of spinel. Table 5 is adapted from Zharikov (1970) which represents the list of principal minerals of the high-temperature stage of magnesian skarns in the U.S.S.R. This table shows a general characteristic of the average content and ordinary compositions of each mineral by zones.

Considering the characteristics present in this table, the following differences are observed at the Continental mine: (1) absence of endoskarn, (2) the clinopyroxenes are mainly diopside to salite and very rarely occur in the outer zone or in the calciphyre, (3) absence of

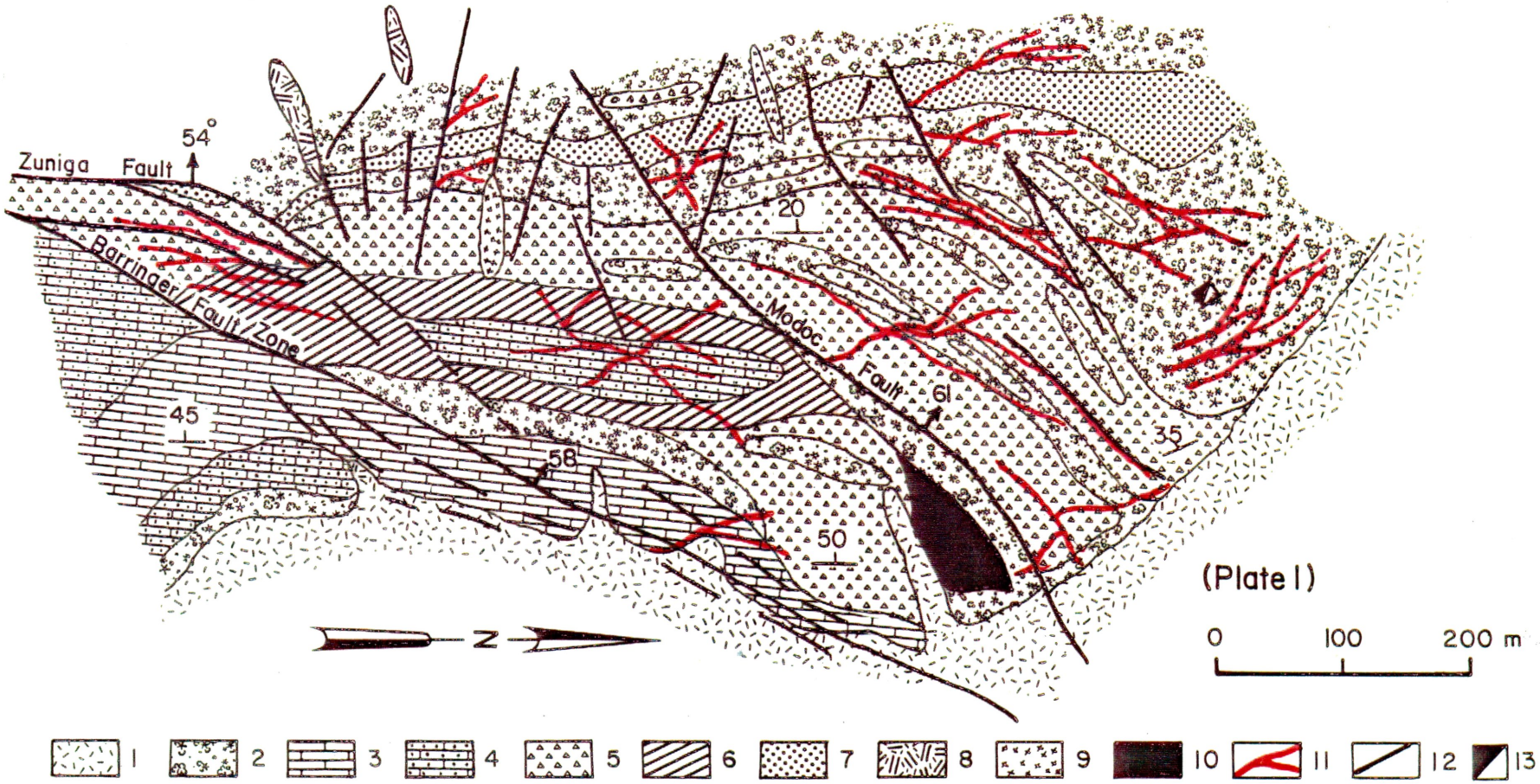


Figure 9. Map showing principal faults, plutons, and skarn units in the Continental pit.

(1) Granodiorite stock
(2) Hornfels zones
(3) Magnesian skarn
(4) Calcitic marble
(5) Brown garnet } Mineralized skarn
(6) Green garnet
(7) Beartooth Quartzite
(8) Pyroxene andesite dikes
(9) Quartz monzonite breccia
(10) Massive magnetite
(11) Veins of pyroxene, amphibole, garnet, epidote, opaque minerals, quartz
(12) Fault
(13) No. 2 shaft

Table 4. Ages and dominant lithologies of sedimentary and metasedimentary rocks and major ore minerals at the Continental pit.

| Formation | Age | Lithology | | Hypogene Ore Minerals |
|---|---|---|---|---|
| | | Sedimentary rocks | Metamorphic rocks | |
| Colorado Formation | Upper Cretaceous | Shale, siltstone and sandstone | Diopside-quartz feldspar hornfels | |
| Beartooth Quartzite | Upper Cretaceous | Orthoquartzite<br>UNCONFORMITY | Metaquartzite | Pyrite-rich veins |
| Abo Formation | Lower Permian | Shale, calcareous mudstone, silty and argillaceous limestone | Diopside-salite-quartz-feldspar hornfels, garnet-diopside skarn | Pyrite and minor chalcopyrite and bornite in garnet zone |
| Syrena Formation | Upper Pennsylvanian | Argillaceous and shaly limestone interbedded with siliceous shale and limy shale | Alternating garnet, garnet-diopside skarn, diopside-quartz-feldspar hornfels with veins of garnet, diopside, amphiboles and epidote | Veins of pyrite, disseminated and veins of chalcopyrite, pyrite, bornite and chalcocite in garnet zone |

Table 4. (Continued)

| Formation | Age | Lithology | | Hypogene Ore Minerals |
|---|---|---|---|---|
| | | Sedimentary rocks | Metamorphic rocks | |
| Oswaldo Formation | Upper and Middle Pennsylvanian | Limestone, argillaceous and silty limestone with chert nodules interlayered with siliceous shale. Marked bed of Parting Shale at base<br><br>DISCONFORMITY | Garnet skarn, garnet-diopside-salite skarn, diopside-salite-quartz-feldspar hornfels with veins of garnet, diopside, amphiboles and epidote and wollastonite skarn | Disseminated and veins of chalcopyrite bornite, pyrite, magnetite, sphalerite, molybdenite, and trace of galena |
| Lake Valley Limestone | Lower Mississippian | Upper part crinoidal limestone with nodules and lenses of chert. Lower part siliceous and marly limestone with lenses of shaly limestone | Marble, garnet skarn, garnet-diopside-quartz-calcite skarn, diopside-quartz-feldspar hornfels and nodules of wollastonite skarn | Chalcopyrite, sphalerite, marmatite, magnetite, bornite, pyrite, and trace of molybdenite |

Table 4. (Continued)

| Formation | Age | Lithology | | Hypogene Ore Minerals |
|---|---|---|---|---|
| | | Sedimentary rocks | Metamorphic rocks | |
| Percha Shale | Upper Devonian | Black shale<br><br>DISCONFORMITY | Diopside-quartz-feldspar-mica hornfels | |
| Fusselman and Montoya Dolomites | Silurian<br><br>Upper and Middle Ordovician | Cherty dolomite with lenses of limy and sandy dolomite | Forsterite-serpentine skarn, humite-forsterite-spinel skarn, tremolite-talc skarn, brucite-periclase marble | Massive magnetite, disseminated magnetite, chalcopyrite and pyrrhotite |

orthopyroxene, (4) trace amounts of spinel formed in the transitional zone between inner and outer zones, but not present in the calciphyre, (5) more abundant magnetite in both inner and outer zones, (6) absence of plagioclase throughout the zones, (7) presence of periclase in the calciphyre, and (8) presence of specularite in all three zones.

Zharikov reportedly indicated that clinopyroxene composition ranges between diopside and the hedenbergite series, containing high quantities of alumina. The alumina content of pyroxene ranges from 1 to 16 percent by weight and the most typical pyroxenes there contain 4 to 9 percent $Al_2O_3$.

Low-temperature magnesian skarn

These skarns are metasomatic rocks made up of lower-temperature magnesium minerals in comparison with those of the high-temperature stage.

Petrographic observation reveals that magnesian skarn of the high-temperature stage is replaced by skarn minerals of the lower temperature stage.

Two groups of minerals are identifiable in these connections: (1) the humite group (humite, clinohumite, and chondrodite), phlogopite, magnesite, tremolite, serpentine, chlorite, and talc which has replaced forsterite, and brucite which has replaced periclase, (2) minerals connected with

Table 5. Characteristics of principal minerals in magnesian skarns of high-temperature stage in U.S.S.R. (from Zharikov, 1970).

| Skarns / Minerals | Peri-skarnal rocks[a] and endoskarns | | Inner zones of exo-skarns | | Outer zones of exo-skarns | | Calciphyres | | Remarks |
|---|---|---|---|---|---|---|---|---|---|
| | Content, % | Composition, f | Content, % | Composition, f | Content, % | Composition, f | Content, % | Composition, f | |
| Olivine (forsterite) | – | – | – | – | 30-90 | 5-15 | 20-40 | 0-5 | In all cases, $f = \frac{\Sigma Fe}{\Sigma Fe + Mg}$ mol-% |
| Clinopyroxenes | 10-50 | 30-40 | 60-90 | 12-15 | 0 or 20-40 | 3-15 | None, as a rule or negligible diopside | | |
| Orthopyroxenes | 20-50 | 35-45 | 60-90 | 15-20 | – | – | – | – | So far, are known only in the abyssal depth facies of skarns |
| Spinel | 0 or 0-20 | 40-50 | 8-35 | 20-30 | 3-12 | 12-20 | 2-8 | 0-12 | |
| Magnetite | – | – | 0-35 | – | 3-5 | – | 1-3 | – | |
| Plagioclases | 40-60 | 40-90 mol-% anorthite | – | – | – | – | – | – | Same |
| Calcite | – | – | 0-20 | – | 0-35 | – | 50-70 | – | |

a superimposed ore mineralization include magnetite and specularite which, in turn, is followed by sulfide mineralization.

Investigation of the magnesian skarns with the aid of a microscope reveals that the concentration of particular minerals in some zones and the absence of those minerals in other zones are due to changes in degree of mobility and in concentration of the constituents in solution. An attempt is made to delineate the various zones of magnesian skarns and the general model of a small portion of these skarns and is presented in Figures 9 and 10.

An irregular, lenticular diopsidic zone of various thickness ranging from a fraction of a centimeter to a few meters developed at the contact with the granodiorite stock. The main mineral constituents of this zone are colorless to light-green, anhedral to subhedral, medium- to coarse-grained clinopyroxene (mainly diopside to ferrosalite), commonly ranging in composition from $Di_{90}$ to $Di_{50}$. Compositions were determined from index of refraction and optic angle.

Occasionally isolated grains of forsterite are present in the zone. Away from the contact of the intrusion the amounts of forsterite crystals increase. The transition from clinopyroxene skarn to forsterite-spinel skarn is

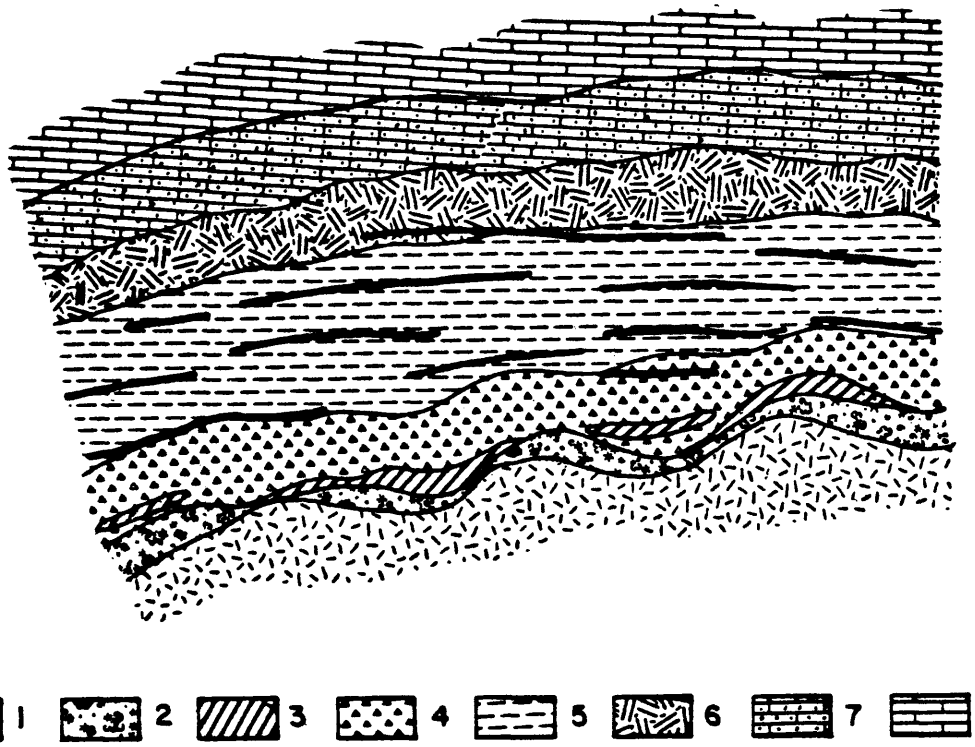


Figure 10 - Plan view metasomatic zoning of the magnesian skarns in the Continental pit associated with massive, banded and disseminated magnetite.

1. Granodiorite stock
2. Diopside skarn
3. Forsterite-spinel skarn
4. Serpentinized forsterite, humite, magnetite, magnesite and phlogopite skarn
5. Serpentinized forsterite, talc, magnetite, tremolite and magnesite skarn
6. Serpentinized forsterite calciphyre
7. Brucite (periclase) marble
8. Dolomite
9. Barringer fault zone

very complex. Forsterite forms abundant nodules within the diopside skarn.

The metasomatism of dolomites and partly dolomitic limestone in the Montoya and Fusselman Dolomites carry various impurities, and present some features of special interest. The first mineral to form in dolomite containing silica as its only impurity is the magnesian forsterite. Two other orthosilicates, monticellite and larnet are not present at the Continental mine area due to their unstable condition.

If the original dolomite rock contained more silica than would suffice to convert all the magnesia to forsterite, a lime-bearing silicate makes its appearance. This, however, is clinopyroxene of the diopside to hedenbergite series; the former is found accompaning forsterite. The clinopyroxene skarn formed in the lower portions of the Montoya and Fusselman Dolomites in the more siliceous limy dolomites.

Diopside skarn passes gradually into a zone of irregular and discontinuous lenses of forsterite skarn with trace amounts of spinel (Figure 10). Formation of spinel is restricted to remote areas within the forsterite zone close to the contact of diopside skarn. The diopside occurs as isolated, colorless, round to idioblastic grains

in the forsterite-spinel skarn. Partial serpentinization of forsterite is common.

The spinel present is fine- to medium-grained, colorless, and may be recognized by its isotropic condition and octahedral habit. It actually occurs very rarely.

Forsterite crystals occur as colorless, rounded to euhedral grains up to 10 mm in diameter. However, in the direction away from the intrusion, the forsterite-spinel skarn is followed by serpentinized forsterite-humite-magnetite-magnesite-phlogopite skarn and serpentinized forsterite-talc-tremolite-magnesite-magnetite skarn, serpentinized forsterite calciphyre, brucite (periclase) marble, and dolomitic marble (see Figure 10).

Figures 11 and 12 are photomicrographs from magnesian skarns and show magnetite minerals rimmed by forsterite.

In the early alkaline stage during low-temperature skarnization, the composition of magnesian minerals (forsterite, periclase and spinel) is changed by the formation of new minerals. Forsterite is replaced by humite, chondrodite, clinohumite, serpentine, chlorite, tremolite, talc, phlogopite, and magnesite, and periclase is replaced by brucite.

An interesting group of magnesian fluorosilicates is that which includes humite, chondrodite and clinohumite. Only the last two of these are common at the Continental

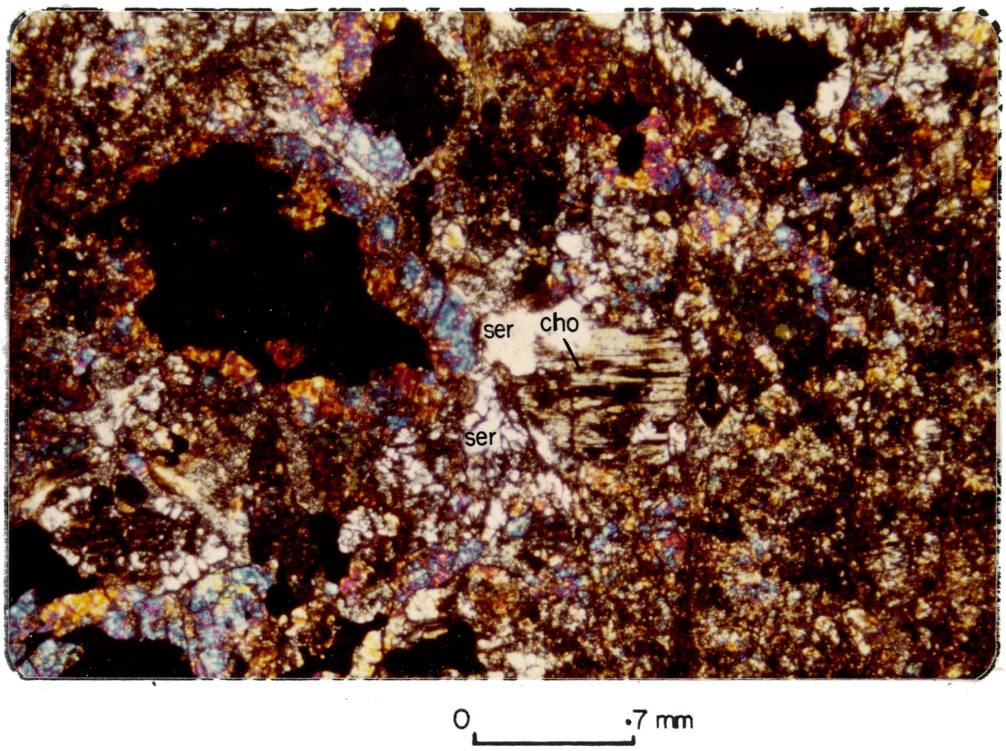


Figure 11. Magnetite-forsterite-chondrodite skarn showing magnetite (black) with inclusions of forsterite (yellow) rimmed by fine-grained forsterite (blue). Forsterite is replaced by chondrodite (cho) and serpentine (ser). Notice lamellar twinning in chondrodite. The dark-brown fibrous products are chlorite replacing humite group minerals. Location: Continental pit. X nicols.

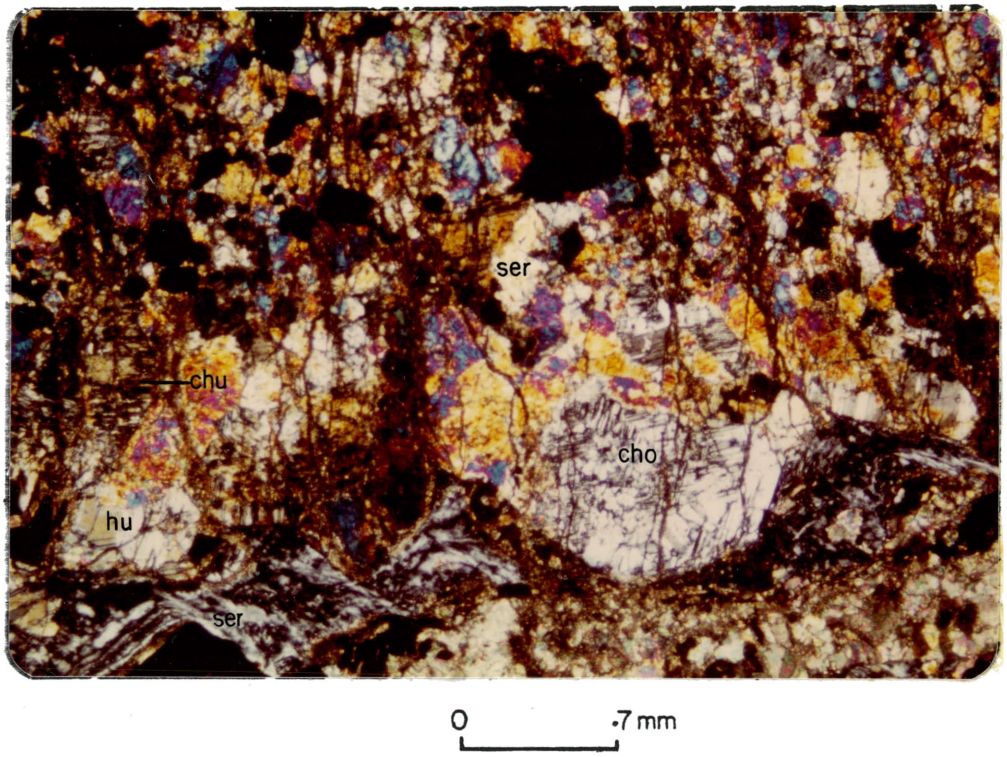


Figure 12. Magnetite-forsterite-humite-clinohumite-chondrodite-serpentine skarn showing magnetite (black) and forsterite (blue and yellow). Forsterite is replaced by humite (hu), chondrodite (cho), clinohumite (chu) and serpentine (ser). Notice lamellar twinning in clinohumite. The photograph also shows intensive serpentinization of forsterite along fracture (lower part). Location: Continental pit. X nicols.

mine area and the first one occurs very rarely.

Yellowish-brown, euhedral to subhedral crystals of chondrodite replace forsterite (Figure 11). They show abundant lamellar twinning on (001) plane. Humite occurs in colorless to pale yellow, euhedral to subhedral crystals with no twinning (Figure 12). Clinohumite appears in yellow to brown, euhedral to subhedral crystals with lamellar twinning on (001) plane (Figure 12).

It is sometimes difficult to distinguish the humite group minerals from forsterite, but they always have a lower birefringence and smaller optic angle than forsterite. The distinction between humite, untwinned chondrodite and clinohumite from optic properties may not be possible. The most reliable way to identify the individual members of the humite group is by x-ray powder techniques.

Formation of the humite group minerals indicates the introduction of iron, boron, fluorine and possibly titanium to the system. The two main substitutions in the minerals of the humite group are $Mg \rightleftarrows Fe^{+2}$ and $F \rightleftarrows (OH)$. The content of titanium in the olivine minerals is generally very small. Relatively high amounts of titanium in some humite group minerals particularly the clinohumite, which has been reported in various papers, is of considerable interest. Possibly Ti may replace Si in the humite series.

Petrographic observation reveals that the humite group minerals alter readily to serpentine, chlorite and calcite. Occasionally the relict cores of clinohumite in some thin-sections partially alter to a dark-brown fibrous product which is occasionally bordered by a narrow zone of pennine.

Distinct minerals such as phlogopite mica occur as the other postmagmatic product replacing forsterite. Phlogopite is found in flakes scattered through the forsterite-humite-phlogopite zone on the footwall of the Barringer fault (Figure 13). The formation of this mineral is possibly another indication of fluorine in the system.

The processes of formation of skarns and of their postmagmatic alteration in the crushed zone of the Barringer fault are slightly different and more complex. In this zone tectonic movements were repeatedly reactivated possibly throughout magmatic activity. Repeated opening, closing and formation of fractures resulted in pulsating introduction of solutions into the zones. As a result, the composition of previously formed minerals gradually changed from alkaline to acid and back to alkaline, as indicated by the formation of characteristic mineral assemblages.

A colorless to slightly pleochroic tremolite in fibrous and prismatic crystals is a mineral of less general distribution in the skarns of the Continental mine area. The

best example of the tremolite zone is exposed at the Union Hill mine (Plate 3). Where tremolite is found it is always associated with serpentine and talc. The photomicrograph in Figure 14 shows the association of serpentine (both antigorite and chrysotile) and fibrous talc from the Barringer fault zone.

Although the hydrothermal synthesis of chondrodite and humite together with serpentine and talc has been reported by some investigators, the close association of tremolite and talc at the Continental mine area possibly indicates the latter mineral is pseudomorphed after the former.

Away from the intrusion contact, the forsterite-serpentine-tremolite-talc zone passes gradually into a zone composed of calcite and serpentinized forsterite, producing a rock known as "forsterite calciphyre" or "ophicalcite" (Figures 10 and 15).

The forsterite calciphyre passes gradually into a zone known as "brucite (periclase) marble" (Figure 10). Development of various alteration zones in dolomite evidently indicates that the behavior of dolomite in thermal alteration is not the same at different distances from the granodiorite contact.

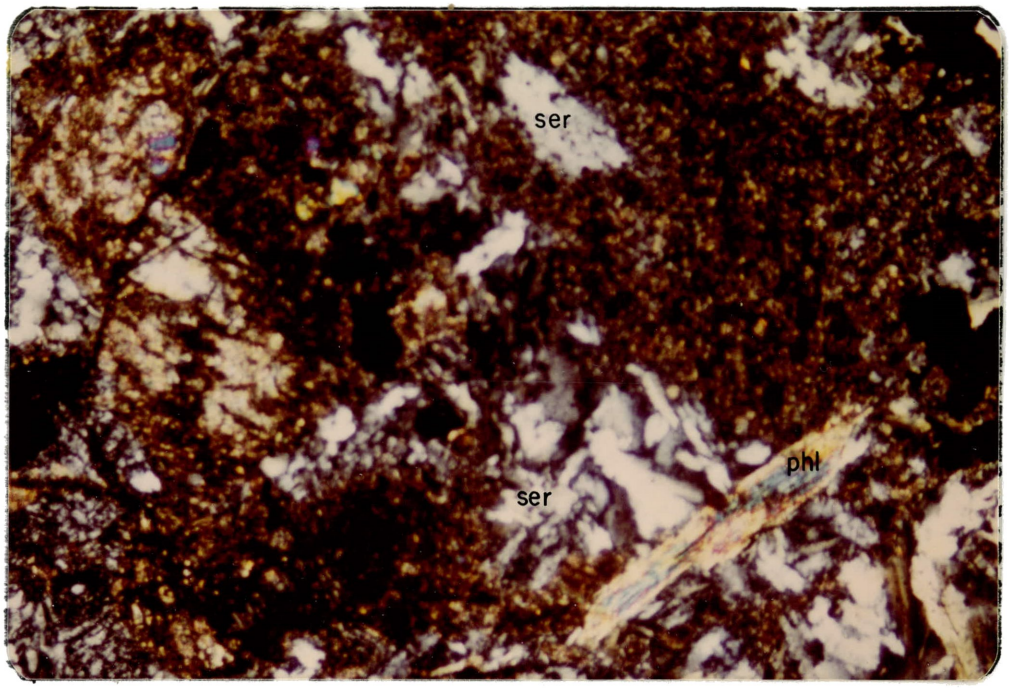


Figure 13. Forsterite-serpentine-phlogopite skarn, showing forsterite (blue) for the most part of the rock is completely replaced by serpentine (ser) and phlogopite (phl). Location: Continental pit. X nicols.

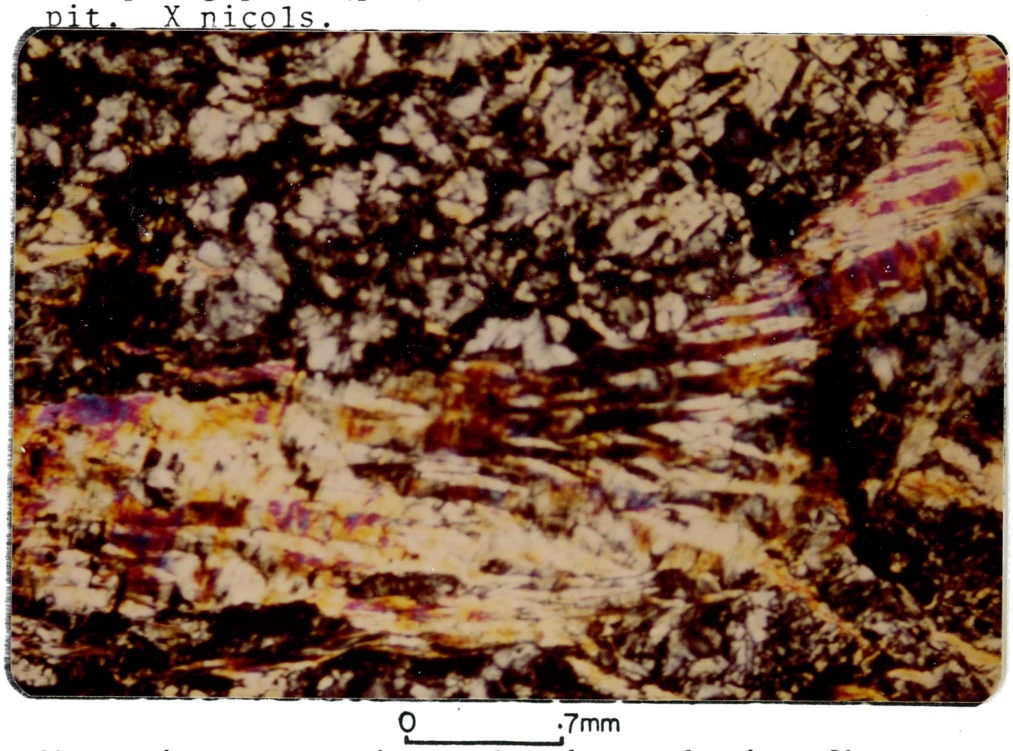


Figure 14. Magnetite-serpentine-talc skarn showing fine-grained magnetite (black), serpentine (white) and talc (birefringent minerals) after forsterite and tremolite. Location: Barringer fault zone, Continental pit. X nicols.

Under different conditions (low pressure and relatively high temperature) the magnesian part of dolomite dissociates and the reaction implies dedolomitization:

$$CaMg(CO_3)_2 = CaCO_3 + MgO + CO_2$$

The resulting rock is a "periclase marble" composed of periclase and calcite. In the later stage of metasomatism, the periclase is altered to brucite by circulating water.

Periclase marbles with no brucite are very seldom reported. This is to be expected for periclase to be stable in contact with water vapor occurs only at temperature above 600°C (Winkler, 1974, p. 124). Water at sufficient pressure to allow periclase to be converted to brucite must be present at some stage of alteration when the temperature is lower than this.

As shown in Figure 16, the periclase has suffered change by hydration, and in this particular example it is completely replaced by flaky minerals of brucite, and the resulting rock is "brucite marble." Relatively equal molecular distribution of calcite and brucite may indicate the original rock was a pure dolomite. This is called "pencatite." In contrast, if the crystallized rock has a larger proportion of calcite, it would be called "predazzite."

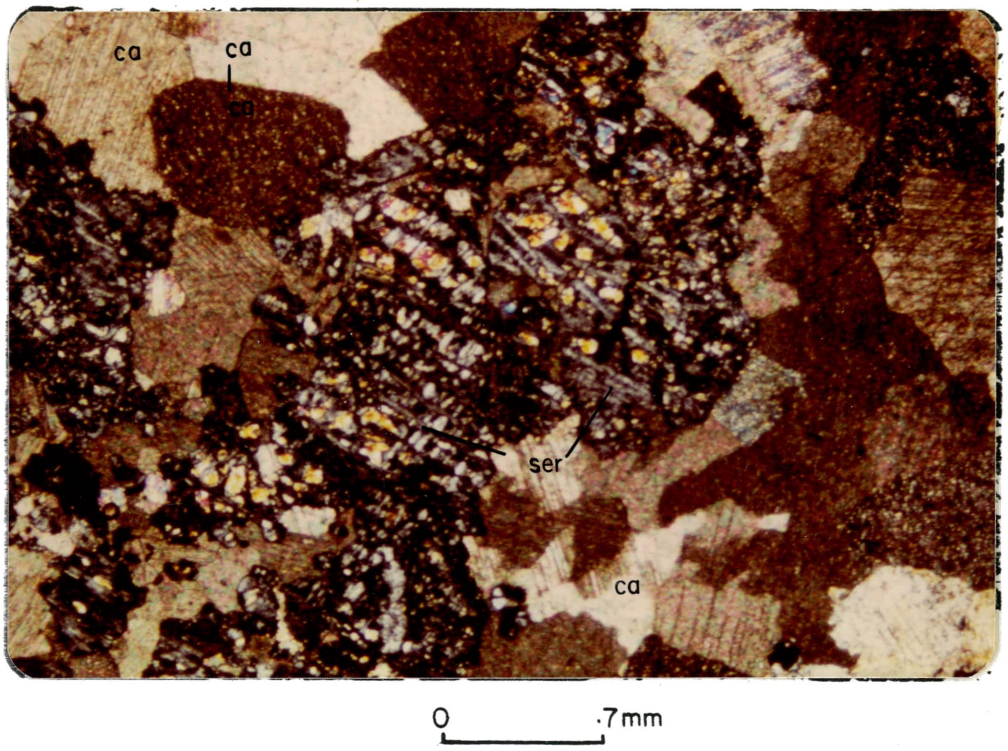


Figure 15. Forsterite calciphyre, showing remnant forsterite (blue and yellow) and calcite (Ca). Crystals of forsterite are set in a coarse-grained granoblastic matrix of calcite which shows irregular boundaries and triple-points. The forsterite has often been replaced by serpentine (ser), giving the rock known as ophicalcite. Location: Continental pit. X nicols.

Figure 16 also shows formations of ore minerals and hydrothermal dolomite which have followed hydration of periclase.

Banded magnetite-serpentine-magnesite skarn

As mentioned previously, the most common alternation product of forsterite is serpentine that contains both antigorite and chrysotile. Serpentine forms alternating layers with magnetite and magnesite, a pattern that persists throughout this skarn unit. Forsterite masses may be completely replaced by the rhythmically banded sequence of magnetite-serpentine-magnesite skarn (Figure 17). A diagrammatic example of this banded skarn is shown in Figure 18. The banding is a product of replacement and most likely formed by diffusion of ions outward from fractures.

Deposition of the early magnetite in the magnesian skarn actually started during high-temperature metasomatism, before the formation of serpentine and continued during and after the serpentinization of forsterite. Figure 19 shows at least two stages of magnetite mineralization (during and after serpentinization of forsterite).

Formation of Limy Skarns

The limy skarns always alternate with hornfels at the Continental mine due to a complex alternating distribution of limestone, shaly limestone, calcareous shale

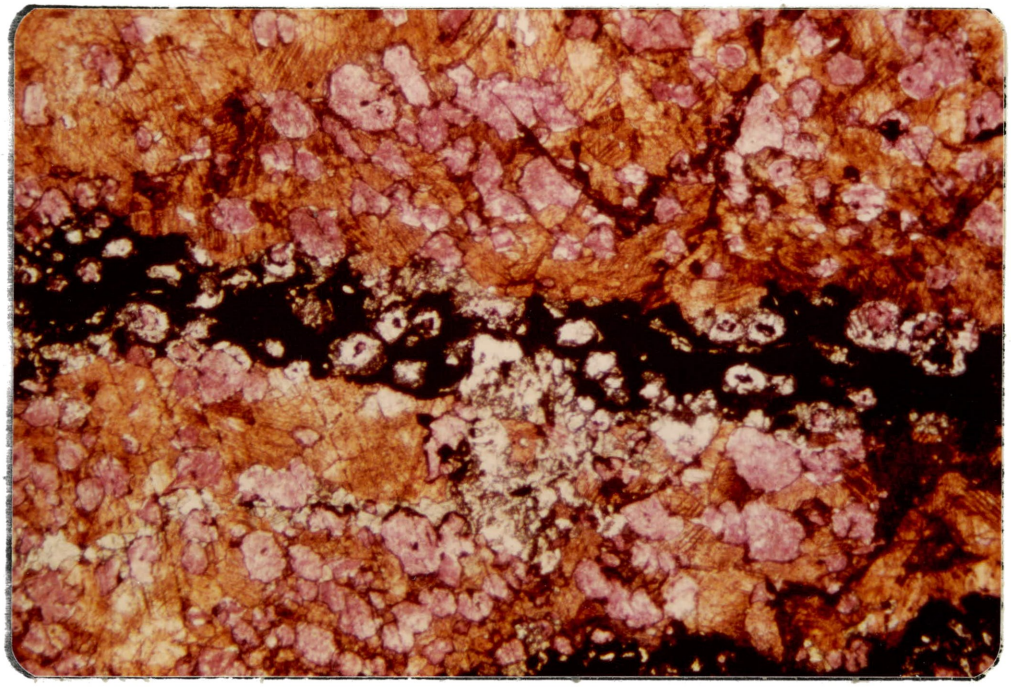


Figure 16. Granoblastic texture of brucite marble. The section is stained with Alizarin Red S (ARS) to emphasize the dedolomitization products (calcite and brucite). Brucite is embedded in calcite (yellowish-brown), but the periclase is almost entirely replaced by brucite (stained pink). The white minerals are hydrothermal dolomite produced in the vein form after dedolomitization of the original dolomite. The black materials in the vein are specularite, magnetite and sulfides. Notice the equal molecular distribution of calcite and brucite, giving the rock known as pencatite. Location: Continental pit. Plain light.

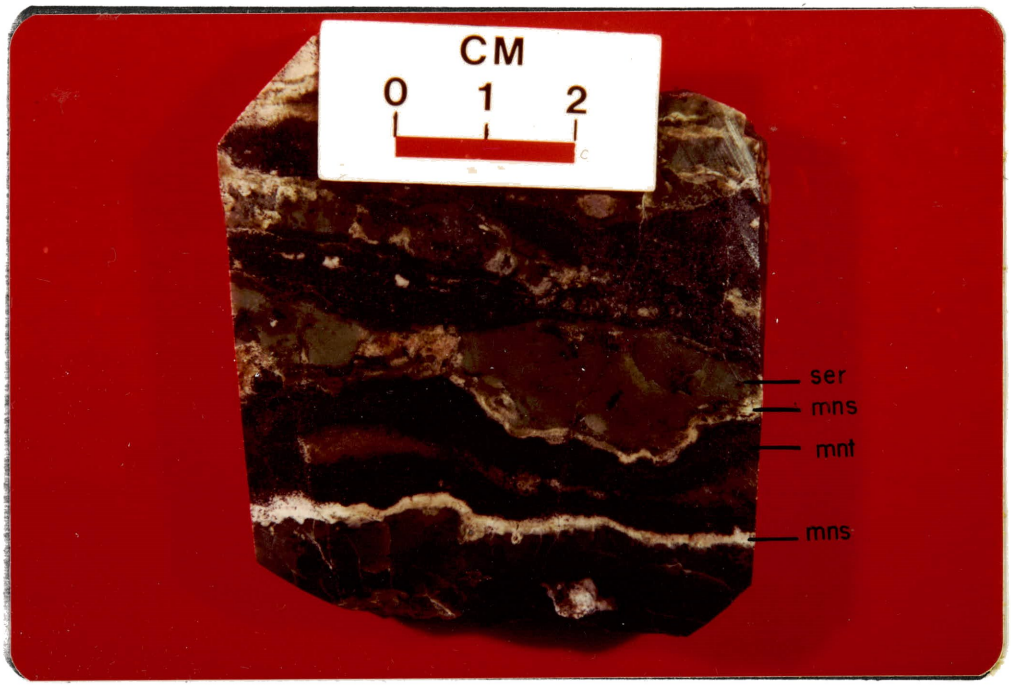


Figure 17. Polished surface hand sample, showing rhythmically zoned diffusional magnesian skarn including: serpentine (ser), magnesite (mns) and magnetite (mnt). Serpentine occasionally contains disseminated chalcopyrite. Location: Hanging wall of the Jim Fair pit.

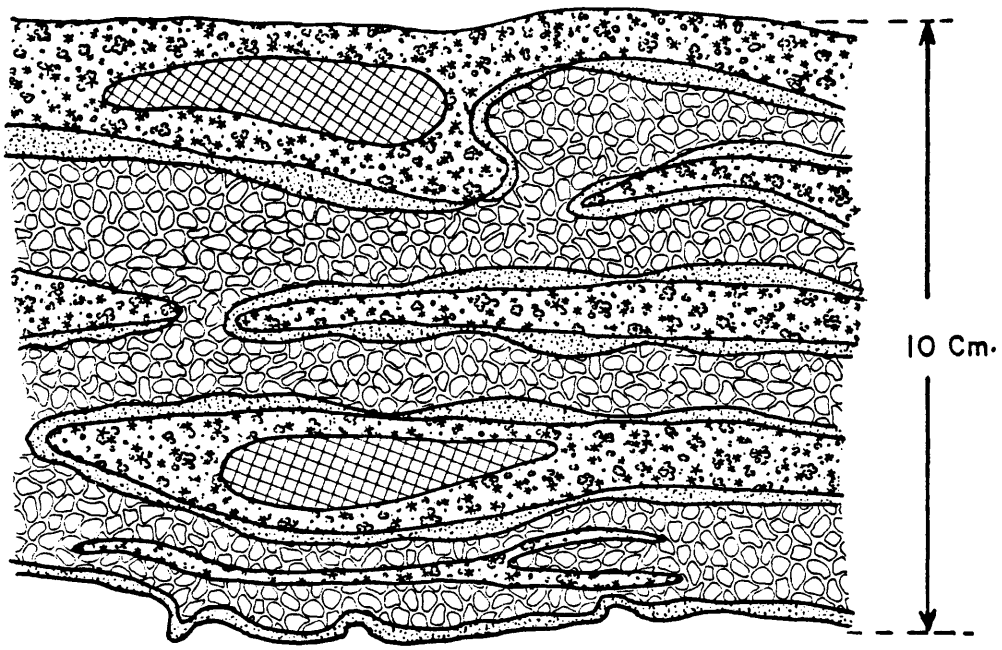


1) Serpentinized forsterite

2) Magnesite

3) Massive magnetite

4) Disseminated chalcopyrite and magnetite

Figure 18. Banded magnetite-serpentine-magnesite skarn from the hanging wall of the Jim Fair pit.

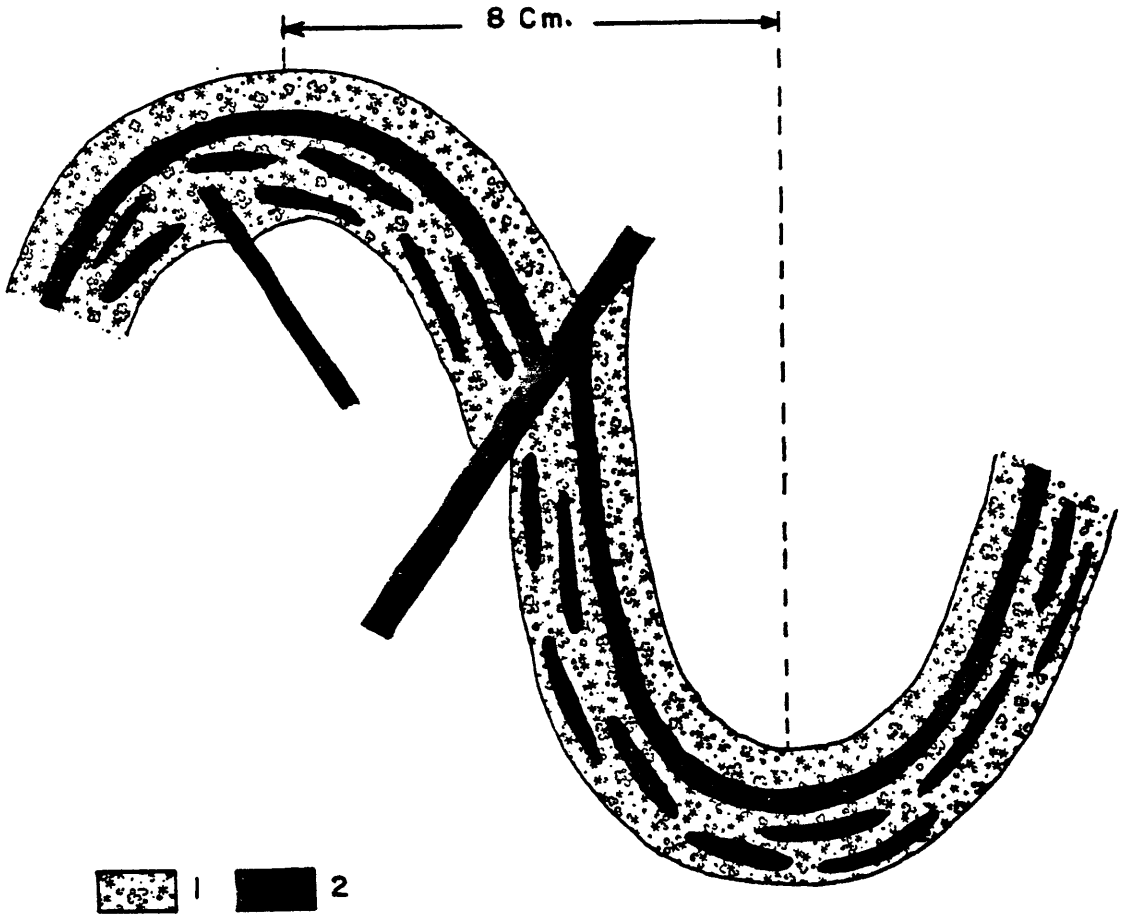


1) serpentinized forsterite and magnesite

2) massive magnetite

Figure 19. Rhythmically zoned and folded magnesian skarn. A sequence of alternating magnetite and serpentinized forsterite displaced by magnetite veins. Hanging wall of Union Hill mine, looking west.

and argillaceous sediments.

Alteration of Colorado Shale, Percha Shale and other shaly units of the Oswaldo, Syrena and Abo Formations shows different characteristics at various temperature zones.

The minute black particles in the Percha Shale and other black carbonaceous shales have a strong tendency to develop clots, patches and spotted structure at a distance from the granodiorite stock. The finely divided dark material which was composed mainly of limonite is largely converted to granules of magnetite.

The Beartooth Quartzite is essentially pure quartz and exhibits little change. It generally is recrystallized. When the Beartooth Quartzite is subjected to further rise in temperature, increasing coarseness of texture is a common change. Even in the highest temperature zones, the pure sandstone shows no chemical reaction and most of the crystals of detrital origin undergo no change other than recrystallization. However, the upper part of the Beartooth Quartzite which is composed of interbedded sandstone and shale, in general, undergoes the same sequence of mineralogical transformations as the more argillaceous sediments. The description of various rock types are given in the following pages.

Clinopyroxene

The clinopyroxene rock is one of the most abundant and variable types at the Continental mine. Almost everywhere in the area this rock is characterized by the following features:

(1) granoblastic and poikiloblastic texture with local porphyroblastic texture,

(2) very fine-grained to aphanitic with grain sizes ranging from 0.01 mm to 0.2 mm in diameter, dense and light- to dark-green in color,

(3) little variation in the relative percentages of minerals in each clinopyroxene hornfels,

(4) sharp contacts with the small lenses and lenticular bodies of garnet-clinopyroxene rocks which have been classified as "hornfels type skarn",

(5) the ore minerals in clinopyroxene include pyrite, trace amounts of chalcopyrite, bornite and chalcocite which are restricted to microfractures and small joints.

The pyroxenes at the Continental pit are diopside to ferrosalite, but the composition of most specimens is near $D_{90}$. Clinopyroxene rocks locally contain predominant amounts of quartz, calcite and feldspar which serve to bind the grains of diopside together.

Some pyroxene hornfels contain more muscovite than others. As shown in Plate 1 and Figure 9, some units are severely fractured and crushed as a result of movements on the Barringer, Zuniga and Modoc faults. The excess muscovite may suggest the presence of an excess of water in the system. However, it appears that with increased metamorphism some muscovite converted to orthoclase.

The pyroxene hornfels derived from marl and argillaceous units of the Oswaldo, Syrena, and Abo Formations is characterized by the presence of the high-alumina silicate minerals, andalusite and cordierite.

The pyroxene hornfels which formed from siliceous limestone is relatively monomineralic. Medium- to coarse-grained, anhedral to subhedral crystals of diopside are accompanied by garnet, minor quartz and calcite.

The clinopyroxene of the early stage of metamorphism is characterized by crosscutting veins of diopside of the later stage of metamorphism (Figure 20). Diopside veins are usually accompanied by epidote, quartz, calcite, feldspars and opaque minerals. The pyroxene hornfels always contain veins of garnet skarn.

Another type of metasomatism brought about by the agency of liquid solutions of magmatic origin is that which involves an accession of magnesium. A typical case is the formation of various amphiboles (hornblende, tremolite,

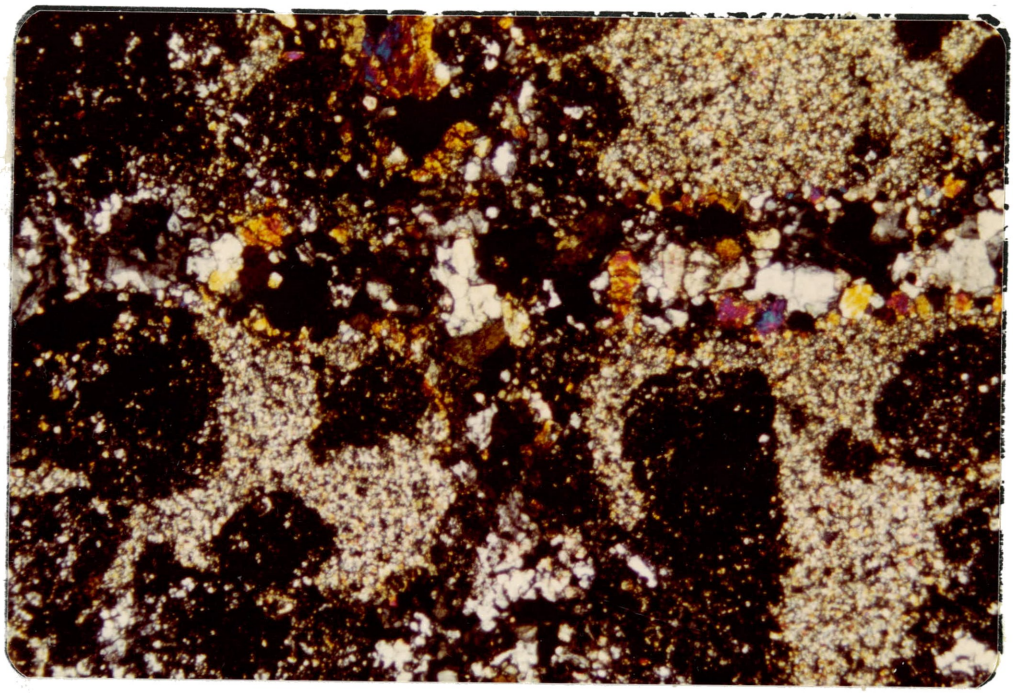


Figure 20. Photomicrograph showing diopside vein that replaced pyroxene hornfels. Diopside appears in blue to yellow and quartz and calcite present in gray to white. Location: Oswaldo Formation, Continental pit. X nicols.

actinolite and anthophyllite) along the zones of increased fracturing (Figures 21 and 22). Frequently amphibole veins include epidote, chlorite, quartz, calcite, feldspars and opaque minerals. The occurrence of these veins is shown in red lines in Figure 9. Here should perhaps be included certain metasomatic transformations in which heated water of magmatic origin seems to have been the sole agent.

The other accessory minerals present in the clinopyroxene zones are sphene, apatite, andalusite, cordierite, zircon and allanite. Axinite and fluorite were observed in a few thin sections. They mainly occur in vein form.

Garnet

The most common product of the alteration of limestone and shaly limestone is garnet which forms very readily. Garnet skarns are the most important rock type at the Continental mine since they host nearly all the economic ore minerals. Garnet skarn forms hard, dense, reddish-brown to light-green rocks. Under the microscope, they are yellow to light-brown isotropic to weakly birefringent (Figures 23 and 24). With respect to grain size, a wide range of difference may be observed. The coarser types are generally those made up mainly of one mineral or sometimes intergrown with diopside or calcite and quartz. Grain sizes range from

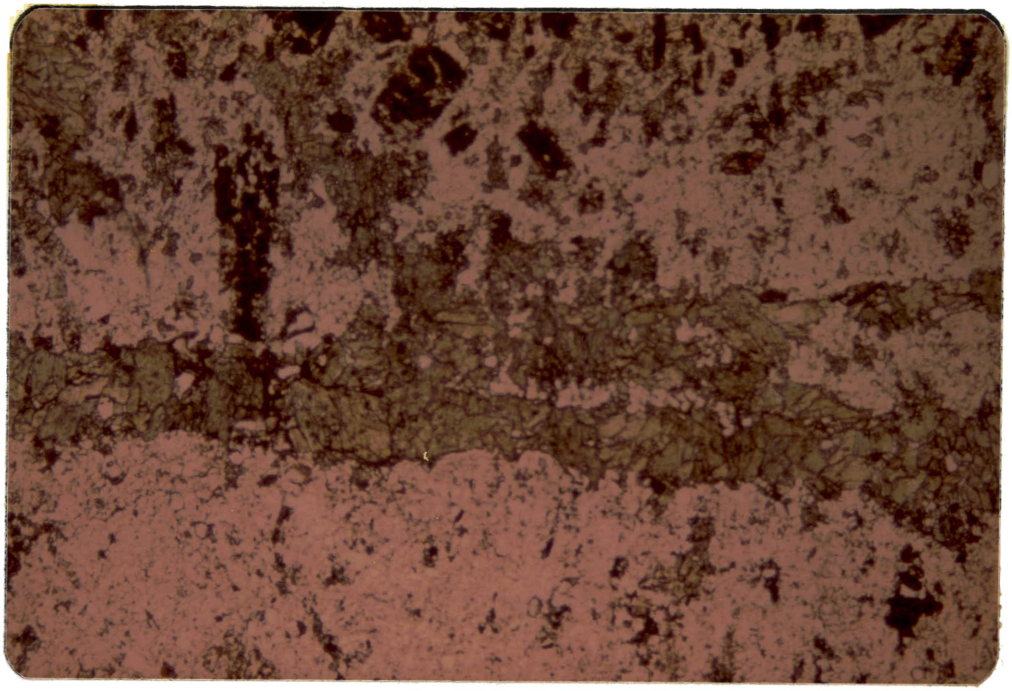

0 2 mm

Figure 21. Photomicrograph showing veins of amphibole (green) cutting clinopyroxene hornfels. Location: Abo Formation, Continental pit. Plain light.

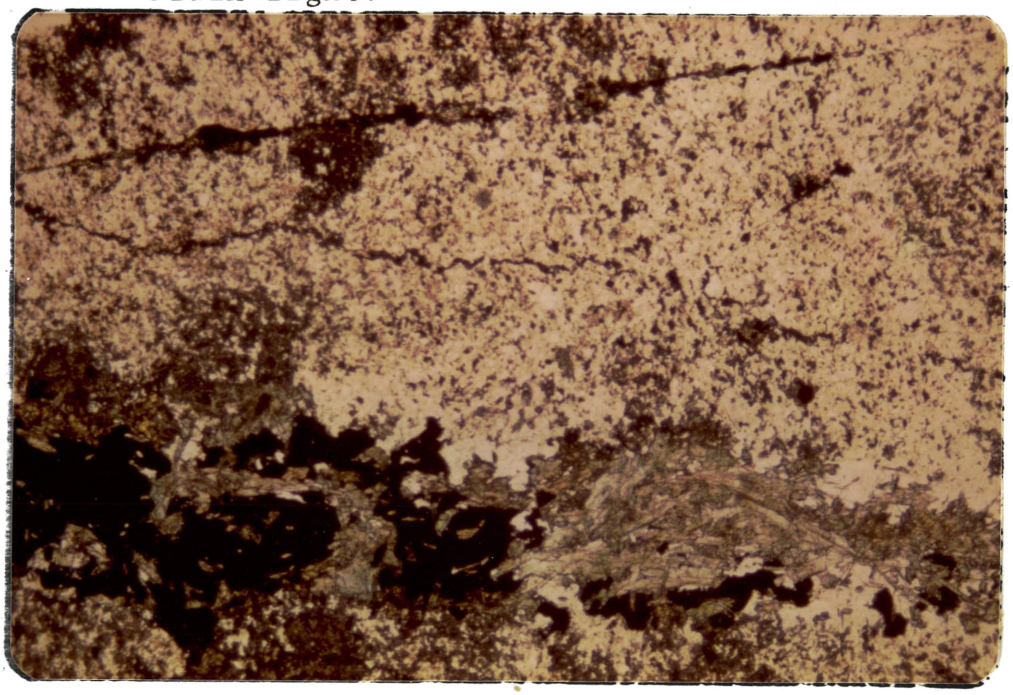

0 2 mm

Figure 22. Photomicrograph showing amphibole (green), epidote (greenish-yellow) and pyrite-chalcopyrite (black) veining and replacing pyroxene. Location: Syrena Formation, Continental pit. Plain light.

0.2 mm in the hornfels zone up to 1 cm in diameter in the garnet skarn zone derived from limestone.

The crystals are anhedral to subhedral in the hornfels zone, but the garnet derived from limestone units is idioblastic against most other minerals, due to their higher energy of crystallization. These are commonly dodecahedral and trapezohedral and show distinct zones of growth. In the plane of thinsection, some garnet crystals appear four-sided, which may indicate four faces of minerals, and others are six-sided. In some four-sided crystals, the square zoning on the rims usually has a cruciform twin with four small triangles in the center (Figure 24). These properties vary in the successive zones. Figure 9 and Plate 1 show the general distribution of brown and green garnet in the Continental pit.

Garnet compositions were determined by microprobe analysis. The results show that the brown garnets range in composition from 70-80 percent andradite, 18-29 percent grossularite and 1-2 percent pyrope, but the green garnets range in composition from 80-90 percent andradite and 10-20 percent grossularite.

A gabbroic diorite dike of late Cretaceous age is exposed in the Continental pit, and weathering products from the destruction of this rock were calcite and chlorite.

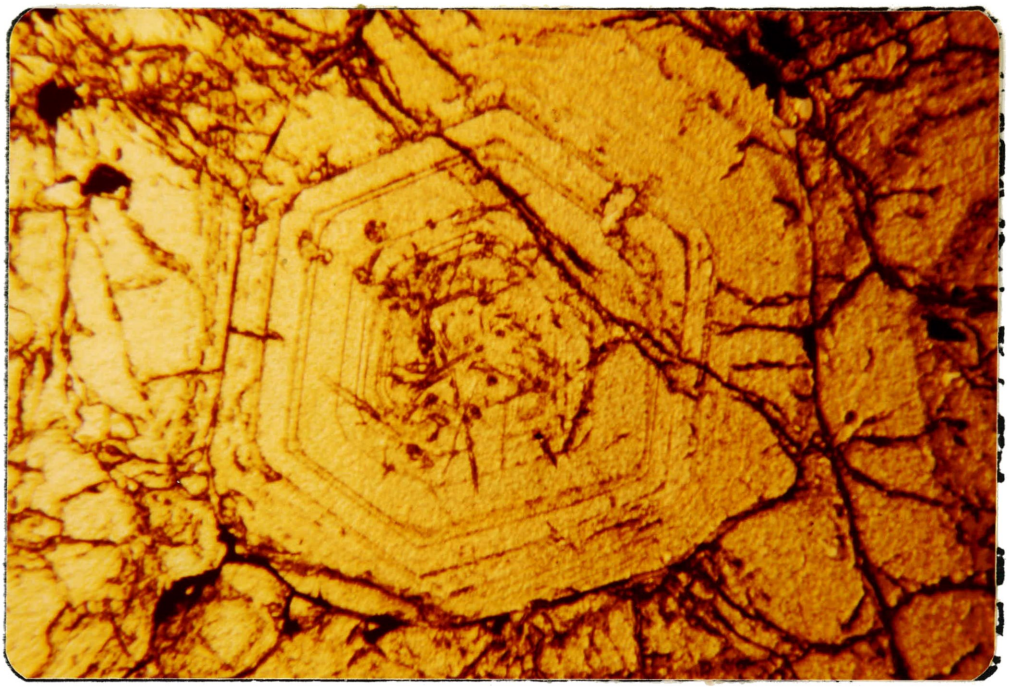


Figure 23. Andradite-grossularite garnet showing six-sided garnet crystal with zonary growth. Location: Oswaldo Formation, Continental pit. Plain light.

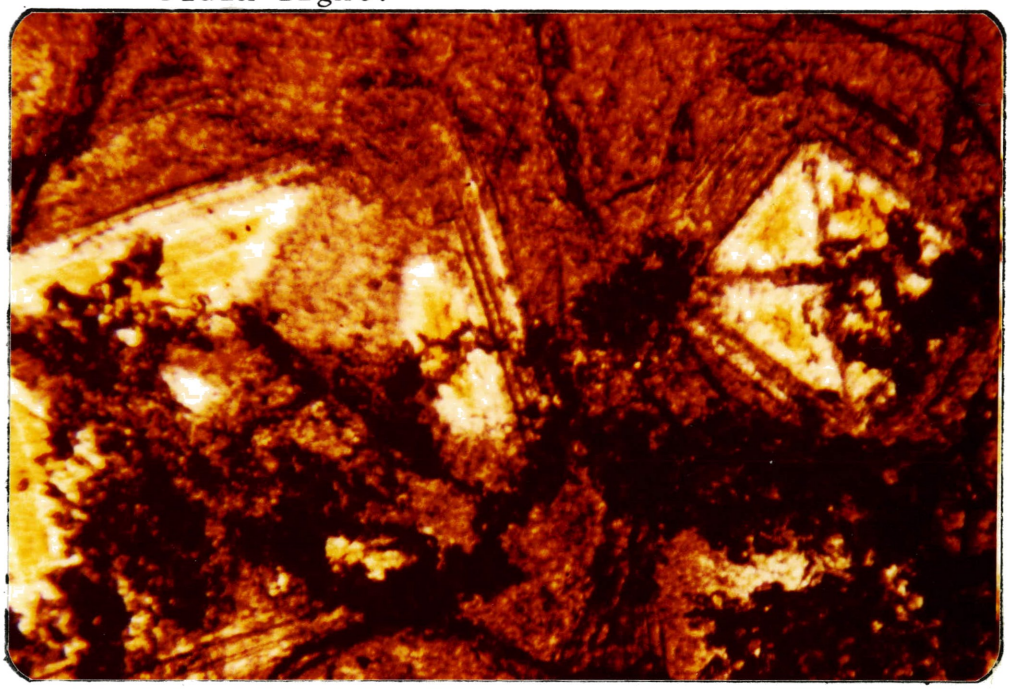


Figure 24. Andradite-grossularite garnet showing four faces of crystals with square zoning on the rims and cruciform twin with four small triangles in the center. Location: Oswaldo Formation, Continental pit. X nicols.

This rock has been metamorphosed by the granodiorite stock, and produced the same metamorphic mineral assemblage that occurs in an impure metamorphosed limestone. Abundant idocrase is the only exception in the gabbroic diorite dike.

The garnet derived from shaly limestones and calcareous shales is classified as a hornfels type skarn. The most typical product of such assemblages consists of colorless to brownish, fine- to medium-grained garnets of the andradite-grossularite series. Some are zoned and birefringent and are associated with non-pleochroic, fine-grained diopside, salite and pale-pinkish or brownish idocrase. In the more aluminous bands of calcareous shale, calcic plagioclase and epidote are the other accompanying minerals. Epidote-bearing hornfels frequently contain both zoisite and clinozoisite. Figure 25 shows a garnet skarn of the hornfels type produced as a result of replacement and partial recrystallization of either impure limestone, marl, argillaceous limestone and/or calcareous shale. This type of rock is partially formed in the upper part of the Syrena and Abo Formations and in the lower Oswaldo Formation and locally in the lower Colorado Shale (Figure 9 and Plate 1).

Along the zones of increased fracturing, the manifestations of garnet veins are frequently observed. The diffusional garnet-clinopyroxene rock of high temperature

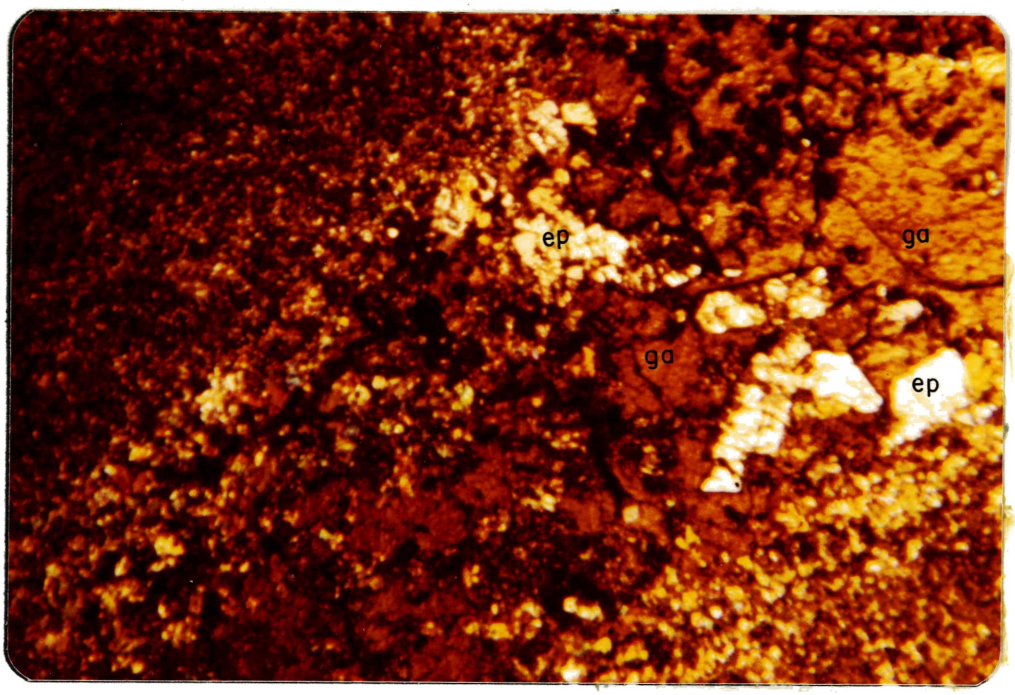


Figure 25. Garnet skarn of the hornfels type showing nodules and disseminated andradite-grossularite garnet (ga) associated with epidote (ep) and fine-grained to aphanitic crystals of diopside in the background. Location: Syrena Formation, Continental mine. X nicols.

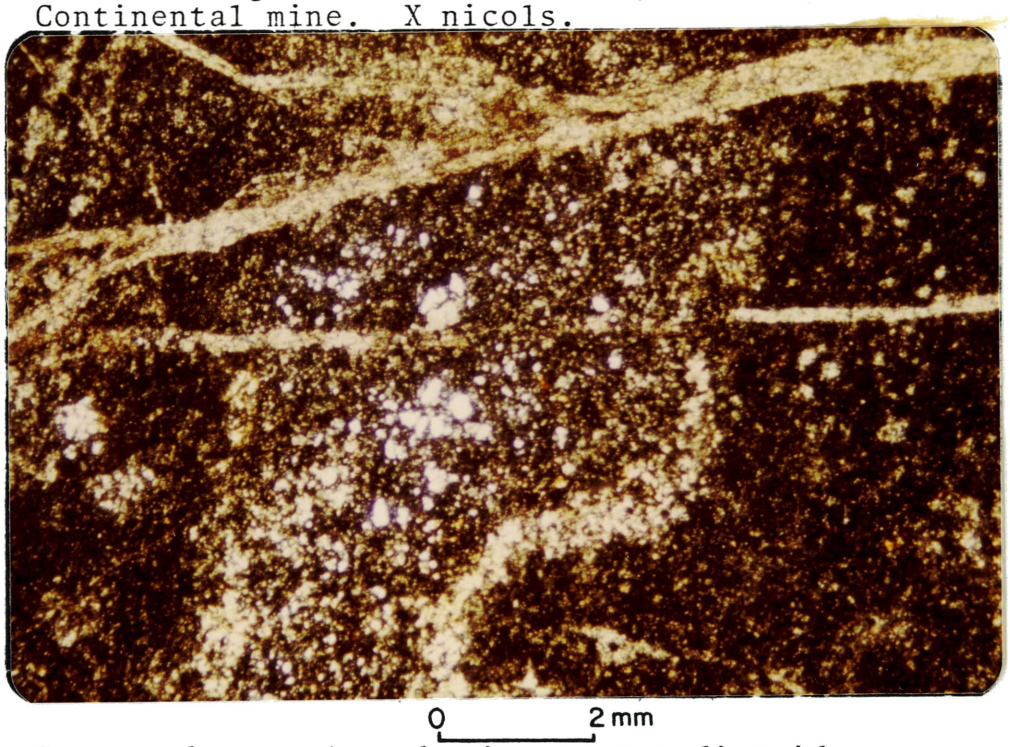


Figure 26. Garnet skarn veins showing garnet-diopside-quartz-feldspar rock of high-temperature stage cut by garnet veins of low-temperature stage.

stage is cut by infiltrational garnet skarn of the low-temperature stage (Figure 26). These garnets are fine- to medium-grained, light-brown, anhedral to subhedral and occasionally weakly birefringent.

Garnet skarn alternates with clinopyroxene hornfels. Alternating zones of garnet, clinopyroxene and marble were observed everywhere in the underground workings (Figure 27).

The massive garnet rocks which are the only host rock for economic copper-zinc-iron ore bodies, include accessory minerals of calcite, quartz, diopside and trace amounts of epidote, form in vugs and veins. These rocks are always brecciated. Towards the bottom of the pit the brown garnet rock of the Oswaldo Formation is transitional to green garnet rock possibly derived from the Lake Valley Limestone.

The diffusional skarns have been partially replaced by metallic minerals and hydrosilicates of epidote, chlorite and smectite in low-temperature alteration during post-magmatic metasomatism (Figures 28 and 29).

Extensive replacement of garnet by hydrosilicates in the zone of increased fracturing has altered the hard and tough garnet skarn to a white, soft and clayey material.

As mentioned previously, idocrase is one of the rare minerals formed at the Continental mine. It occurs within

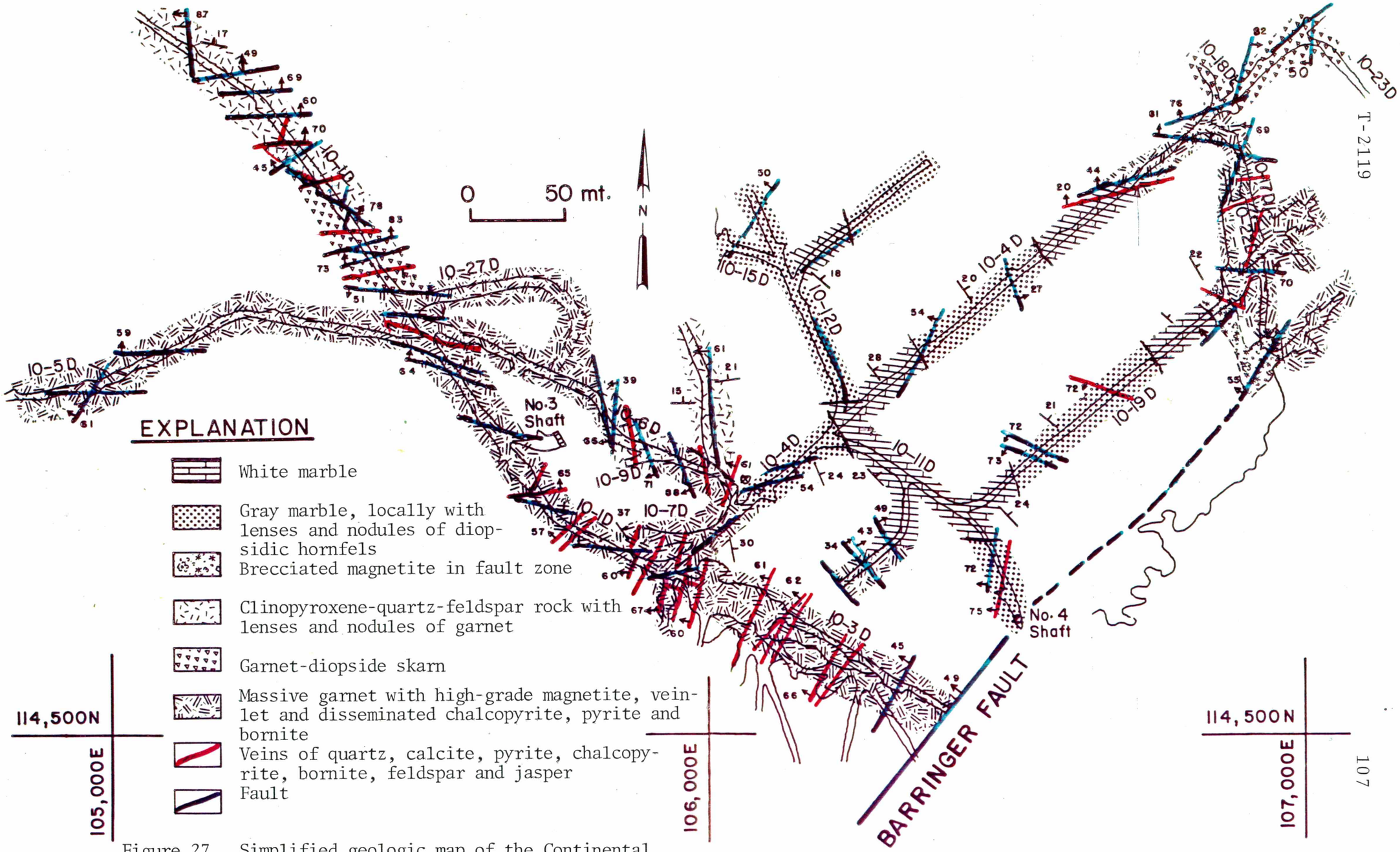


Figure 27. Simplified geologic map of the Continental Number 3 underground mine (1000 level).

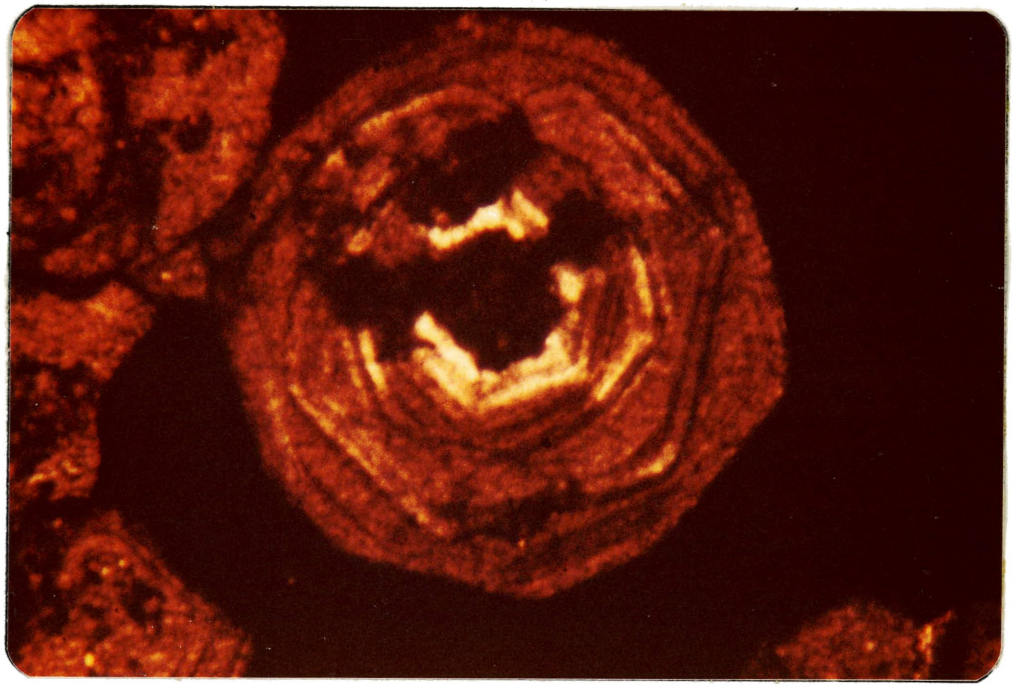


Figure 28. Infiltrational skarn showing zonal structure in garnet (brown) replaced by sulfides and magnetite (black) in grain boundaries during low-temperature metasomatism. Location: Oswaldo Formation, Continental pit. X nicols.

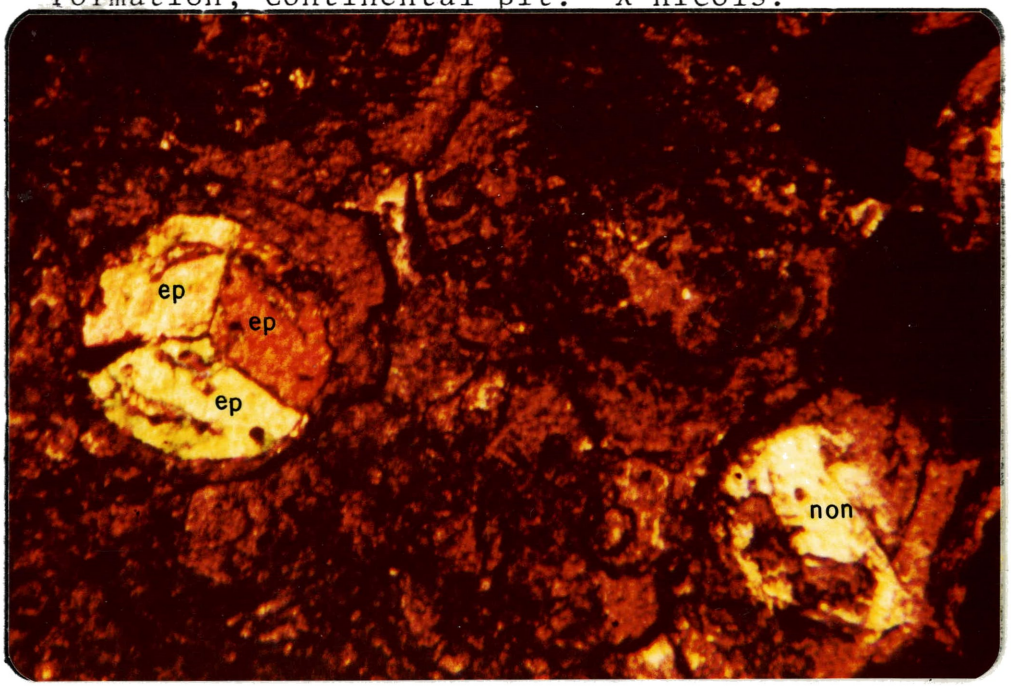


Figure 29. Retrogressive metasomatism showing garnet skarn of high-temperature stage (dark brown) replaced by epidote (ep) and nontronite (non) during retrogressive metasomatism. The garnet crystals are coated by hematite and pyrite (black). Location: Oswaldo Formation, Continental pit. X nicols.

the garnet zone as accessory isolated, brown to colorless prisms. The relationship between garnet and idocrase is not clear. Sometimes it appears intergrown with garnet, but usually it is pseudomorphic after garnet and indicates a later phase of skarnization than garnet skarn. When birefringent garnet is associated with idocrase, optical data give variable results, and differentiation of the two minerals is difficult. For some unknown reason in this type of occurrence, some anisotropic minerals range from uniaxial, both positive and negative, to biaxial, again both positive and negative.

Epidote

Within zones of extensive fracturing, epidote occurs in medium- to coarse-grained, anhedral to subhedral crystals that have replaced garnet and clinopyroxene rocks. They formed in fractures and along bedding planes. The epidote sometimes forms nodules and small clots in rock between the fractures. Zoisite, clinozoisite and epidote frequently occur together.

Epidote is also the main component of epidosites developed mainly in the hornfels zones of the Oswaldo, Syrena and Abo Formations. Careful petrographic study revealed that trace amounts of very fine-grained axinite and fluorite occur with epidote which indicates introduction

of boron and fluorine during the process in the formation of epidote.

Wollastonite

Wollastonite is commonly regarded as a high-temperature mineral. The mineral is absent in the upper level of the Continental mine, but it appears in the lower levels where it gradually increases with depth, a trend that may indicate that a wollastonite skarn facies may occur at even greater depth.

Abundant nodules and discontinuous small lenses of wollastonite were observed on the 1300 level of Number 3 underground mine. Here it occurs in gray and white marble. Wollastonite also occurs with garnet and diopside within the garnet-clinopyroxene zone. Garnet forms small spots and veinlets in the mass of wollastonite.

The limestone with nodules and lenses of chert favored the formation of wollastonite. The presence of such siliceous limestone in the high-temperature environment undoubtedly promoted many different reactions between the calcareous and non-calcareous constituents of the rock. The simplest type of reaction was

$$CaCO_3 + SiO_2 = CaSiO_3 + CO_2$$

As shown in the equation, formation of wollastonite required

local redistribution of calcium and silicate and the removal of carbon dioxide. The silica-free portions of the limestones recrystallized to pure marble. Figure 30 shows prismatic crystals of wollastonite in marble. The association of diopside and garnet with wollastonite may lead to the following interpretation: the presence of little magnesia is enough to produce some diopside, but with aluminous and ferruginous material present, it is likely to give rise to grandite garnet.

Marble

Marble occurs commonly as alternating layers with garnet and clinopyroxene rocks (Plate 1, Figures 9 and 27).

Pure limestone of the lower Lake Valley Limestone and Oswaldo Formation are recrystallized to a medium- to coarse-grained gray and white marble. The Tierra Blanca Member of the Lake Valley Limestone is a white to light-gray coarsely crystalline limestone and contains abundant crinoids. Except for some very localized nodules and lenses of chert, this member is nearly pure calcium carbonate. It contains only 0.19 to 0.44 percent MgO in samples analyzed by Schmitt (1939a, p. 801).

Petrographic study of this member where unmetamorphosed shows cementing material which serves to bind the calcite

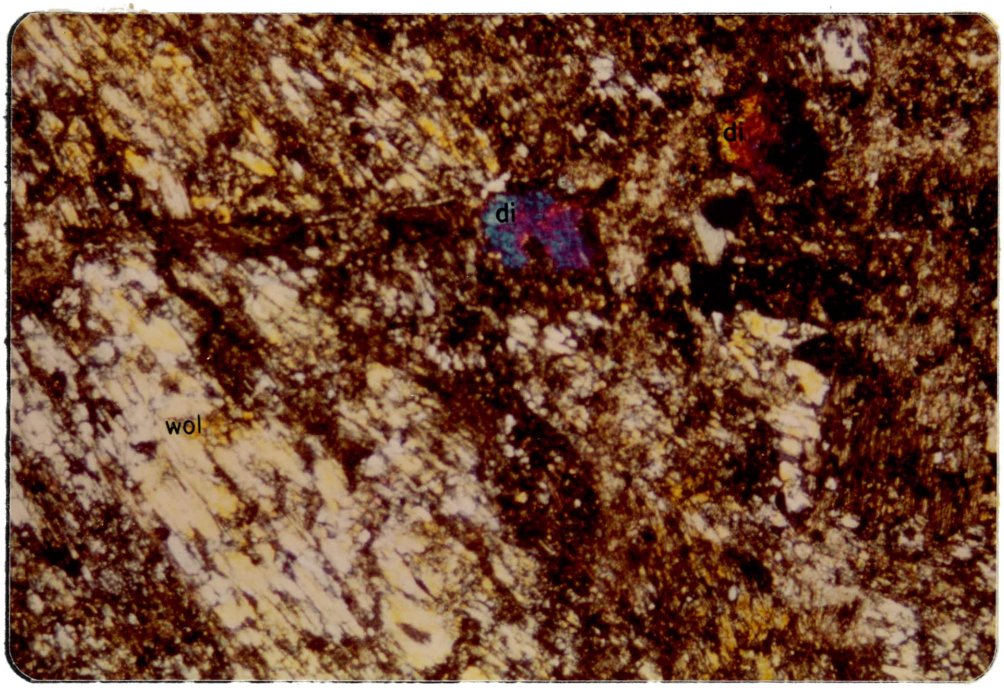


Figure 30. Prismatic crystals of wollastonite (wol) in association with diopside (di) grown in fine-grained, groundmass marble. Location: 1300 Level, Number 3 underground mine. X nicols.

grains together and again are furnished from the fine-grained calcite.

There is, however, one special case worthy of notice. That is the abundant beds and lenses of impure limestone within the member which are metasomatically altered to garnet and clinopyroxene skarn and later mineralized by sulfides and oxides and provide the highest grade ore deposits in the region.

## SKARN DEPOSITS AT THE HUGO PIT

The Hugo pit (Figure 31) is situated on the north edge of the granodiorite stock. Compare Figure 31 with Plate 4 of Figure 6.

Pyroxene rock, garnet-pyroxene skarn, garnet-magnetite-hematite skarn, actinolite-diopside-tremolite skarn, garnet-marble skarn and marble are the common skarn deposits in this area. Magnetite and hematite are the only economic ore minerals formed in the garnet skarn. Trace amounts of disseminated chalcopyrite and sphalerite are localized in the magnetite ore.

This area is structurally and mineralogically of particular interest. The characteristics of the original rock units and metamorphic products are presented in Table 6. The whole area has been affected by extensive multiple

stages of faulting.

Thermal alteration of sedimentary rocks in the Hugo pit is similar to that mentioned under the skarnization at the Continental pit. No mineralization occurs in the clinopyroxene rock except for minor pyrite veinlets. Green and brown garnet rocks are the only hosts of the ore minerals. Away from the intrusive contact, the garnet skarn passes gradually into the marble. The contact between garnet and marble is locally sharp, but usually it is gradational and lenses and nodules of green garnet frequently occur on the marble side. The occurrence of actinolite skarn is the exceptional case in this area.

Actinolite-Tremolite Skarn

The actinolite skarn here occurs at the contact with the stock in a rather thin zone in comparison with the thickness of marble or garnet skarn (Figure 31). This rock is dark-green and composed mainly of actinolite. In thin section it appears as a light- to dark-green, coarse-grained prismatic crystal (Figure 32) with trace amounts of intergrown colorless tremolite, calcite and quartz.

Inclusions of fine-grained, granular diopside were observed in the actinolite crystals. This may indicate pseudomorphic production of actinolite after diopside.

No actinolite replaces hedenbergite skarn in the southern

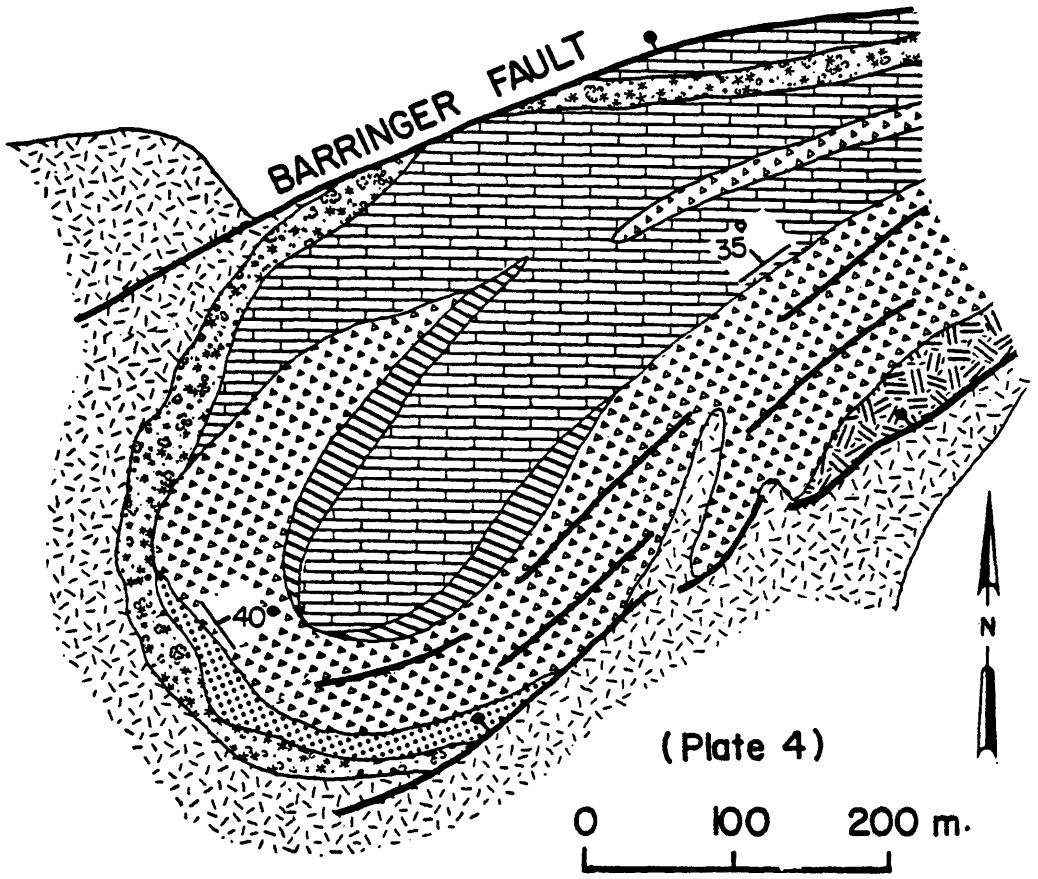



1. Granodiorite stock
2. Pyroxene rock
3. Garnet-pyroxene skarn
4. Garnet-magnetite-hematite skarn
5. Actinolite-diopside-tremolite skarn
6. Garnet marble skarn
7. Calcitic marble
8. Fault

Figure 31. Plan view of generalized diagram showing metasomatic zoning of skarn in the Barringer fault zone at the Hugo pit.

Table 6. Ages and dominant lithologies of sedimentary and metasedimentary rocks and major ore minerals at the Hugo pit.

| Formation | Age | Lithology | | Hypogene Ore Minerals |
|---|---|---|---|---|
| | | Sedimentary rocks | Metamorphic rocks | |
| Colorado Formation | Upper Cretaceous | Shale, siltstone and sandstone | Diopside-quartz-feldspar hornfels | --- |
| Beartooth Quartzite | Upper Cretaceous | Orthoquartzite<br><br>UNCONFORMITY | Metaquartzite | --- |
| Lake Valley Limestone | Lower Mississippian | Crinoidal limestone, with nodules and lenses of chert. Lower part siliceous and marly limestone | Marble, garnet skarn, garnet-marble skarn, garnet-diopside skarn. Actinolite-diopside-tremolite skarn | Magnetite, hematite and minor chalcopyrite |
| Percha Shale | Upper Devonian | Black shale | Diopside-quartz-feldspar-mica hornfels | --- |

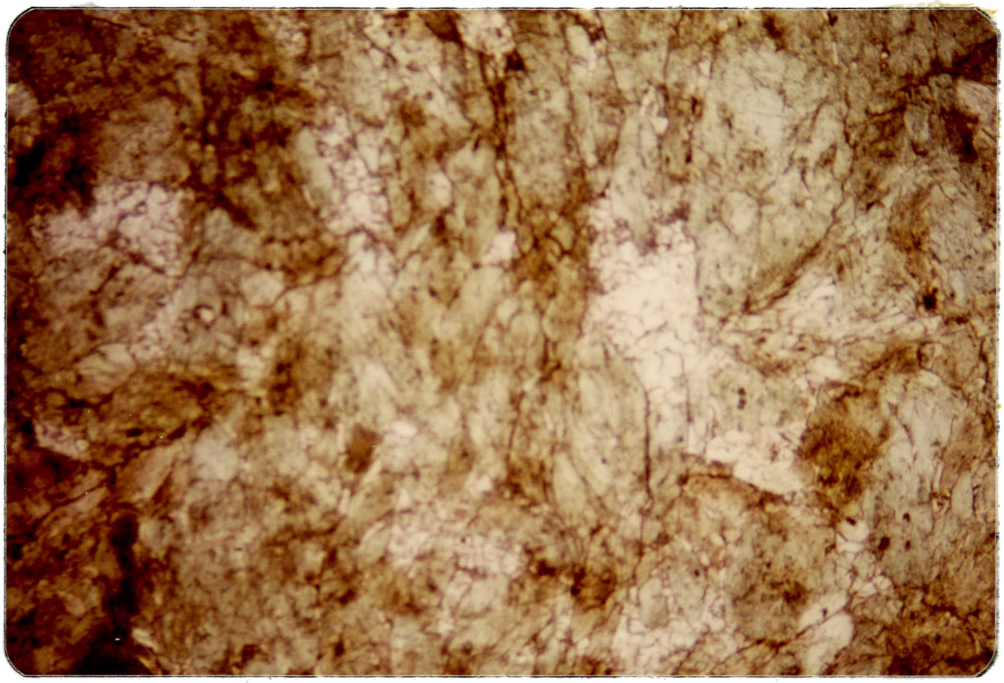


Figure 32. Actinolite skarn showing equigranular granoblastic texture of actinolite (green) with intergrown interstitial calcite and quartz (white). Location: Lake Valley Limestone at the contact with the granodiorite stock in the Hugo mine. Plain light.

area. Replacement of magnesium-rich clinopyroxene by actinolite in the Hugo and Continental mines may lead to the belief that actinolite usually forms in non-manganiferous varieties of pyroxene. However, in these two particular mines, iron sulfide mineralization is slight in the diopsidic-rich rock, except for minor pyrite. This may be explained by the fact that a considerable part of the iron was released during the extensive replacement of diopside by actinolite, and that this conversion left little iron available for the formation of pyrite.

## SKARN DEPOSITS AROUND THE SOUTHERN MARGIN OF THE STOCK

The Paleozoic formations exposed to the south include the Lake Valley Limestone and the Oswaldo Formation. No dolomitic carbonate rocks occur in this area. Therefore, the lack of magnesian skarn is due to the absence of the Fusselman-Montoya Dolomite.

The southern limb of the stock is characterized by the distribution of equigranular facies of the granodiorite rock and differs from the main porphyritic mass toward the northern part of the mapped area. However, the skarn at the contact with the equigranular facies is slightly genetically and mineralogically different from those formed

at the contact with the porphyritic facies.

The metasedimentary complex in this area is composed of a thick massive green garnet zone at the contact with the stock, followed by another massive zone of pale-green to olive-green manganhedenbergite skarn which hosts the sphalerite ore bodies throughout the region. Zinc is the only economic ore in any individual mine in the south area.

The garnet zone is commonly considerably thicker than the hedenbergite zone. The marker bed of the Parting Shale at the base of the Oswaldo Formation is altered everywhere in the area to epidote skarn with accessory garnet and clinopyroxene minerals (Plates 4, 5 and 6).

Development of the manganese-bearing pyroxene indicates that the equigranular facies of the granodiorite stock was higher in manganese than the porphyritic facies.

The garnet zone in the southern area commonly contains abundant lenses of fine-grained, light-green diopside-salite-quartz-feldspar hornfels, white marble and lenticular bodies of epidote and hedenbergite skarns. The hedenbergite zone likewise includes alternating lenses and lenticular bodies of marble, ilvaite, epidote and garnet skarns.

This sequence of skarn deposits is frequently intruded by dikes of various composition, including quartz monzonite, quartz latite, dacite and aplite.

## Selective Ore Mineralization

The principal ore minerals are black to reddish-brown sphalerite, pyrite, galena, and trace amounts of chalcopyrite, magnetite, pyrrhotite and hematite of metasomatic origin.

The hornfels and the epidote skarn are barren of ore-forming minerals except for minor pyrite. Neither marble nor garnet skarn contain an abundance of ore minerals, but very high-grade sphalerite ore occurs in the contact zone between these two rock types and the hedenbergite skarn. Localization of the ore in the manganhedenbergite skarn may lead to the following interpretation. Manganese and iron released from the replacement of pyroxene changed from the bivalent to higher oxidation states and played an important role as a reducing agent and provided a favorable condition for the precipitation of sulfide. This will be discussed in more detail.

## Skarn Deposits at the New Jersey Zinc Mine

The New Jersey Zinc mine is located along the southwest contact of the granodiorite stock. Plate 4 is the geologic map of the mine and adjacent area. Figure 33 is a generallized geologic map of the mine and immediate adjacent area. In order to visualize the exact location of the

mine, compare Figure 33 with Plate 2 of Figure 6. The deposits in this mine lie at the contact between the granodiorite stock and altered limestone which is folded into an anticline. Table 7 shows the distribution of sedimentary and skarn rocks and their mineralogic characteristics.

Characteristically, garnet forms in the impure limestone, hedenbergite forms in the more magnesium-rich limestone, epidote develops in shale units, and diopside-salite-quartz-feldspar rock forms in argillaceous limestone and calcareous shale. The pure and non-magnesian limestone recrystallizes and yields an even-grained, milky-white marble. The replacement of the sedimentary rocks was accompanied by introduction of many of the constituents except for calcium and carbon dioxide. A characteristic feature of the layered zones that conform to original bedding is the sharpness of the zonal boundaries marking the interface of two skarn layers, and the uniform mineralogy of the individual zones. This general scheme of the zonation is clearly seen on the flanks of the anticline at the mine.

Structural features

The New Jersey Zinc orebody is localized on the flanks and in the crest of an open, slightly asymmetrical anticline that plunges southward. Near the northern end of the New Jersey Zinc mine the fold is relatively open in comparison

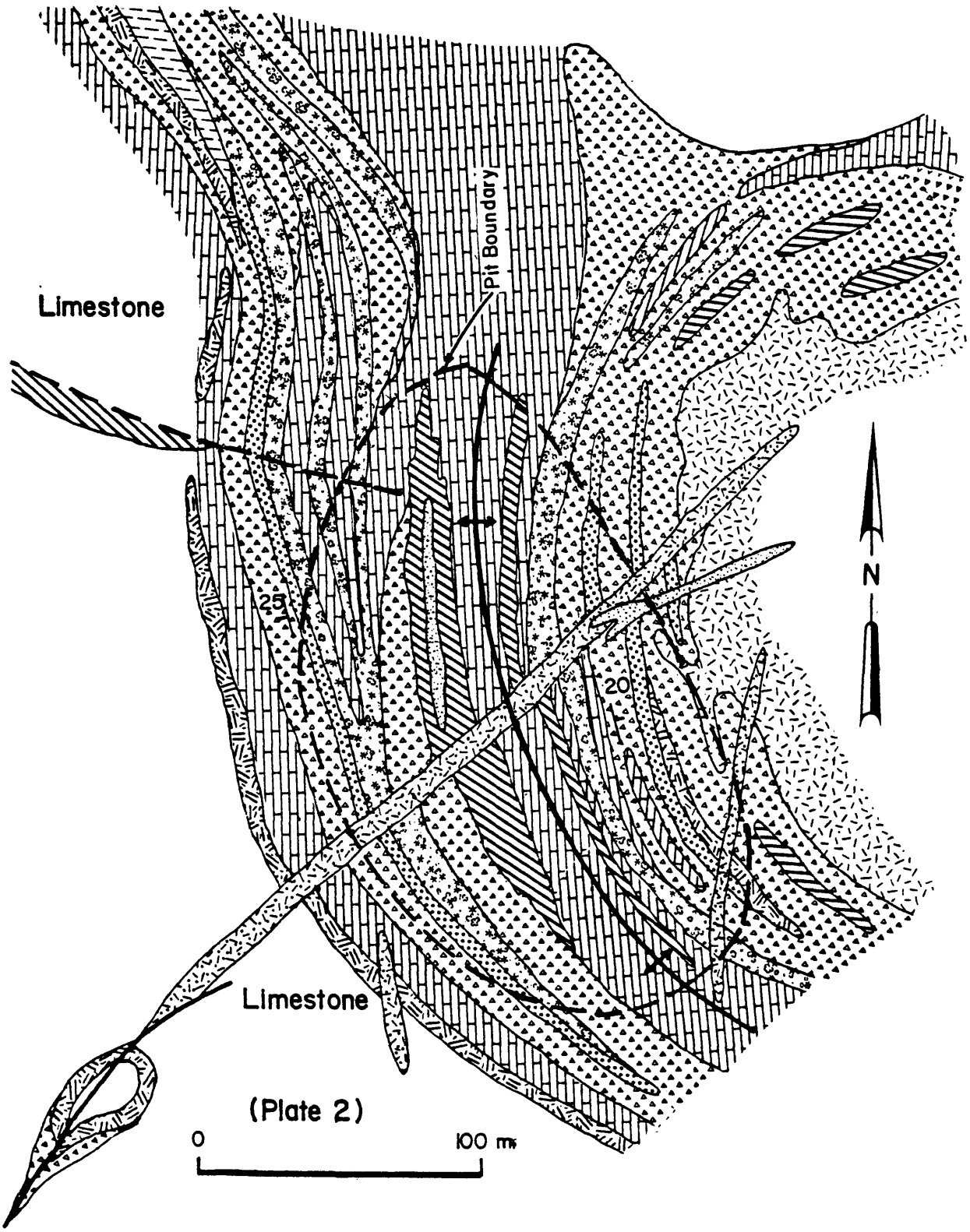


Figure 33. Generalized diagram of metasomatic zoning of skarn at the New Jersey Zinc mine.

EXPLANATION


Granodiorite stock


Quartz latite porphyry dikes


Dacite porphyry dikes


Hornblende-quartz diorite sills


Andradite-grossularite-sphalerite skarn


Calcite marble


Hedenbergite-ilvaite-pyrite skarn


Pyroxene rock


Hedenbergite-johannsenite-sphalerite skarn


Epidote skarn


Recrystallized shale


Axis of the anticline


Faults

Table 7. Ages and dominant lithologies of sedimentary and metasedimentary rocks and major ore minerals at the New Jersey Zinc mine.

| Formation | Age | Lithology | | Hypogene Ore Minerals |
|---|---|---|---|---|
| | | Sedimentary rocks | Metamorphic rocks | |
| Oswaldo Formation | Upper and Middle Pennsylvanian | Limestone, argillaceous limestone, and silty limestone interbedded with siliceous shale and limy shale<br><br>DISCONFORMITY | Garnet skarn, garnet-diopside skarn, hedenbergite-johannsenite skarn, hedenbergite-ilvaite skarn and epidote-scapolite skarn at base | Sphalerite, pyrite, trace of galena, magnetite and chalcopyrite |
| Lake Valley Limestone | Lower Mississippian | Upper part crinoidal limestone with nodules and lenses of chert. Lower part siliceous and marly limestone with lenses of shaly limestone | Marble, garnet skarn, garnet-hedenbergite skarn, hedenbergite-ilvaite skarn hedenbergite-pyroxmangite | Sphalerite, pyrite, and trace of galena, magnetite and chalcopyrite |

to the southern part of the mine where the fold limbs steepen. The two limbs are separated by a white marble zone through the fold axis. The dip of the beds on both limbs ranges from $15^{o}$ to $35^{o}$.

As shown in Figure 33, in the crestal region of the anticline alternating zones of marble, hedenbergite and ilvaite bearing skarns display more complex structural patterns. The eastern limb contains thick layers of nearly monomineralic green garnet skarn that alternate with numerous layers and lenses of marble, diopsidic hornfels, epidote, ilvaite and hedenbergite skarns. The western limb also contains alternating zones of banded skarns and marble. Quartz diorite sills of late Cretaceous age crop out on both limbs.

Rock at the New Jersey Zinc mine and adjacent area is highly fractured and faulted. Much of the fracturing preceded the metamorphism, others postdate the skarn rocks, but predate the dikes, and some are younger than the dikes. A few dikes were emplaced along fault zones. The walls of a few dikes are brecciated and these dikes contain abundant angular inclusions of the wallrock. Displacement along the faults or dikes is in general small and of little consequence in the mining operation. The major northeast trending fault which contains a quartz

latite porphyry dike has a left lateral displacement of between 3 and 15 meters. The northwest-trending fault that cuts the western limb of the anticline has not been determined, but is believed to be slight. These and other major fractures in the area acted as channelways for solutions during metamorphism. Intensive skarnization extends outward from the pluton for several hundred meters.

The extension of the zone of intense skarnization averages about 250 meters beyond the periphery of the stock. This probably increases with depth. It is probable that the stock also thickens with depth. The presence of isolated skarn bodies in sedimentary rock with no related fractures or intrusives at the surface tends to support that idea. A zone of intensive skarnization was mapped to the southeast of the stock (east of the Pewabic mine) at considerable distance from the intrusive (Plate 6).

The characteristics of major skarn rocks are given in the following pages.

Garnet

Garnet skarn is the most widespread variety of skarn in the mine. It forms at the contact between the carbonate country rock and the granodiorite stock. The greater bulk of the skarn consists of nearly monomineralic masses of garnet with minor quartz and calcite occurring interstitially

between garnet grains.

Several garnet grains from different intervals in the New Jersey Zinc mine were analyzed by means of an electron microprobe operated by Dr. G. S. Holden of the Colorado School of Mines. In general, the garnets are solid solutions of andradite and grossularite that consist of 80-90 percent andradite. Step traverses were made with the electron microprobe from core to rim of several grains which have both sectored cores and mantles that show repeated zoning. Calcium, iron, magnesium and aluminum values were measured. However, no distinct compositional changes were detected when the microprobe beam moved across zone boundaries except for some grains which have a slightly more grossularite-rich core. This may indicate that the birefringent zones do not represent compositional variation, but are rather a structural effect due to internal strain in the crystal.

In polarized light the garnet is yellow to light-brown, and isotropic to weakly birefringent. The grain sizes vary from 0.1 mm up to 1 cm. The garnet derived from argillaceous limestone is usually finer grained than that derived from more pure limestone.

The crystals are euhedral to subhedral, both dodecahedral and trapezohedral and show distinct repeated zones

of growth. Figure 34 shows garnet-rock composed mainly of large crystals of andradite with birefringent growth zones. Zoned and birefringent garnet has been reported in many papers. Zoning and polysynthetic twinning in anisotropic grandite garnet is mentioned by Morgan (1975) and Kennedy (1953). The example given by Kennedy indicates a 2V of approximately $90^{o}$ and a birefringence estimated at 0.005.

The minerals associated with garnet are quartz, calcite, hedenbergite and idocrase. Quartz and calcite occur in three different forms: (1) interstitial to garnet crystals, (2) very fine-grained inclusions in garnet and (3) veins which show crosscut garnet. Hedenbergite occurs as inclusions and as intergrowths with garnet. Inclusions of hedenbergite in the garnet crystals are fine-grained and display both sharp and irregular interfaces with enclosing garnet. This relationship indicates that the two minerals began to form at about the same time, but that garnet growth continued beyond that of hedenbergite.

An epidote-rich lens in the garnet skarn, just to the east of the anticline axis, in the New Jersey Zinc mine, contains intergrowths of epidote, garnet, quartz, calcite, scapolite, sphene, apatite and idocrase. However, formation of scapolite indicates the introduction of chlorine

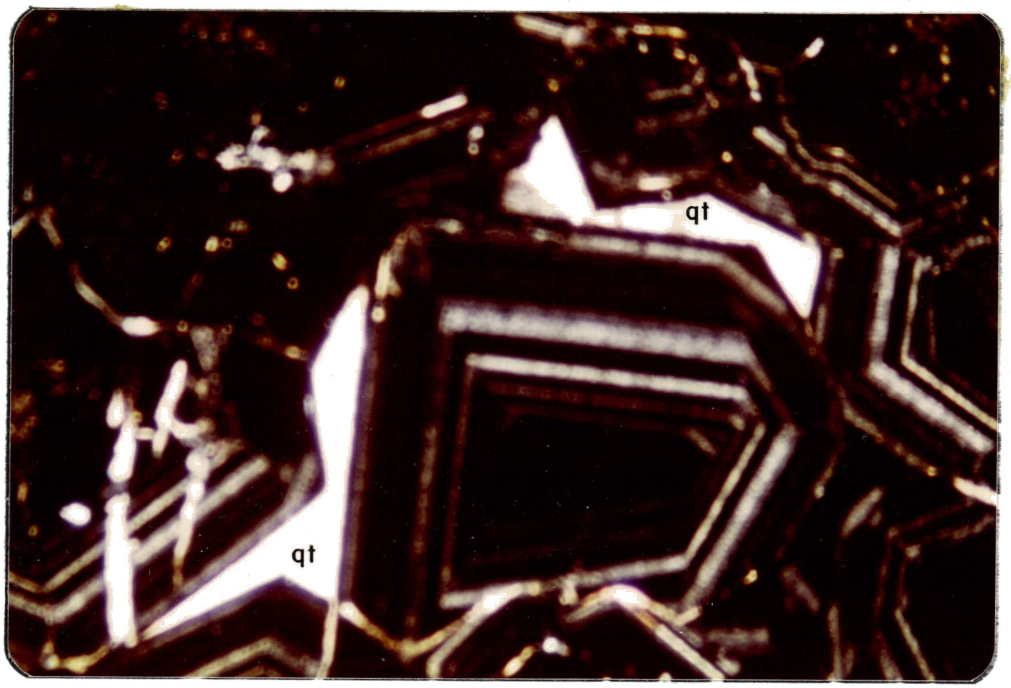


Figure 34. Garnet-rock, composed mainly of large crystals of zoned and birefringent andradite. Notice: the clear interstitial quartz(qt) and fine-grained inclusions of pyroxene (green). Location: eastern limb of the anticline, New Jersey Zinc mine. X nicols.

and fluorine into the system. The scapolite crystals are always idioblastic against other minerals.

Intensive chloritization of the garnet, epidote and scapolite occurred during retrograde metamorphism (Figure 35).

Sphene is a common product in epidote-garnet skarn derived from argillaceous limestone. It may owe its origin to minute rutile which occurs in argillaceous sediments.

Clinopyroxene

Diopside and salite occur in the lenticular bodies of hornfels within the garnet zone. Their characteristic and mineral association is like that mentioned at the Continental mine. However, discussion here is only concerned with the hedenbergite skarn.

Outward from the intrusive contact, garnet skarn grades into hedenbergite skarn. The contact between the two skarns is most commonly sharp, but is at some places gradational. As mentioned previously, hedenbergite appears to be an important host mineral for sphalerite and therefore the presence of hedenbergite in skarns may serve as an important guide to ore. In the massive zone of pyroxene skarn, the mineral assemblage is iron-manganese-rich, containing ferrosalite, hedenbergite, to johannsenite and

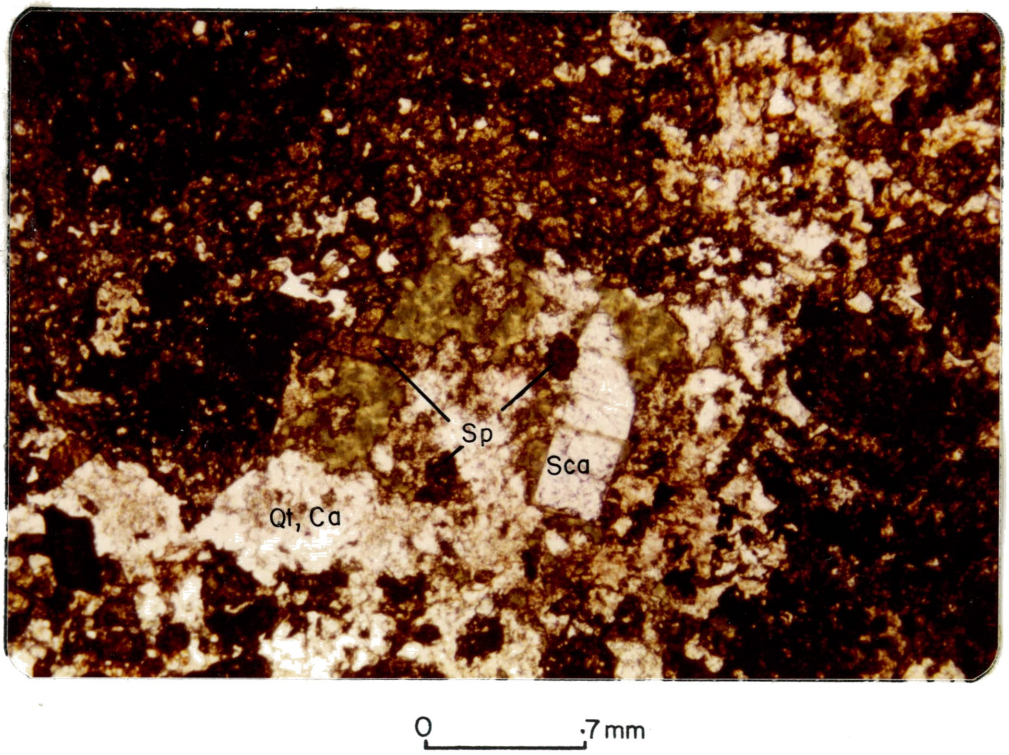


Figure 35. Granoblastic texture of epidote-garnet skarn showing the intergrowth of epidote (white to yellow), garnet (dark-brown), scapolite (sca), quartz-calcite (Qt, Ca), and sphene (sp). Chlorite (green) replacing epidote and garnet. Notice the chlorite forming in scapolite along cleavage plane. Location: eastern limb of the anticline, New Jersey Zinc mine. Plain light.

andradite of garnet group. Minerals of the manganese-bearing hedenbergite group were determined by x-ray diffraction analysis.

The crystals of the minerals in the monomineralic masses occur in various forms including prismatic aggregates, and randomly oriented blades, and radial fibers. Figure 36 shows hedenbergite mineral associated with high-grade sphalerite. The association of quartz and calcite, which are the only accessory minerals in the early monomineralic masses of hedenbergite, is more obvious under the microscope. Like the garnet skarn, quartz and calcite in pyroxene occur either as interstitial grains, inclusions in hedenbergite mineral, or in vein form.

For the most part, sphalerite replaced hedenbergite mainly at grain boundaries (Figure 37). However, some textural relations indicate intergrowth of the two minerals. The veins of sphalerite in the hedenbergite skarn are fairly abundant.

Intergrowth of manganhedenbergite, orthoclase, quartz, epidote and calcite is a typical characteristic texture in the region (Figure 38). Skarn of the manganhedenbergite-epidote-orthoclase-quartz facies is thought to be skarn of the higher-alkalinity facies, but the presence of hydrosilicate may indicate that their formation temperatures are

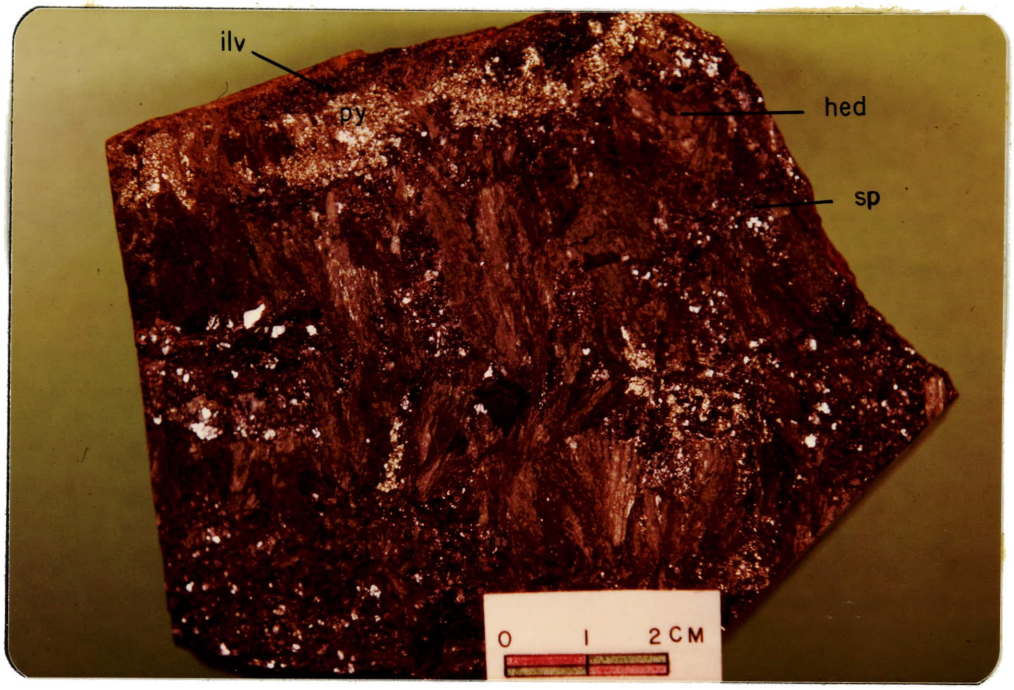


Figure 36. Hand specimen of hedenbergite-sphalerite skarn showing radial blades of hedenbergite (hed), massive sphalerite (sp), pyrite (py) and ilvaite (ilv). Notice: higher concentration of pyrite occurs in ilvaite zone. Location: crest of anticline, New Jersey mine.

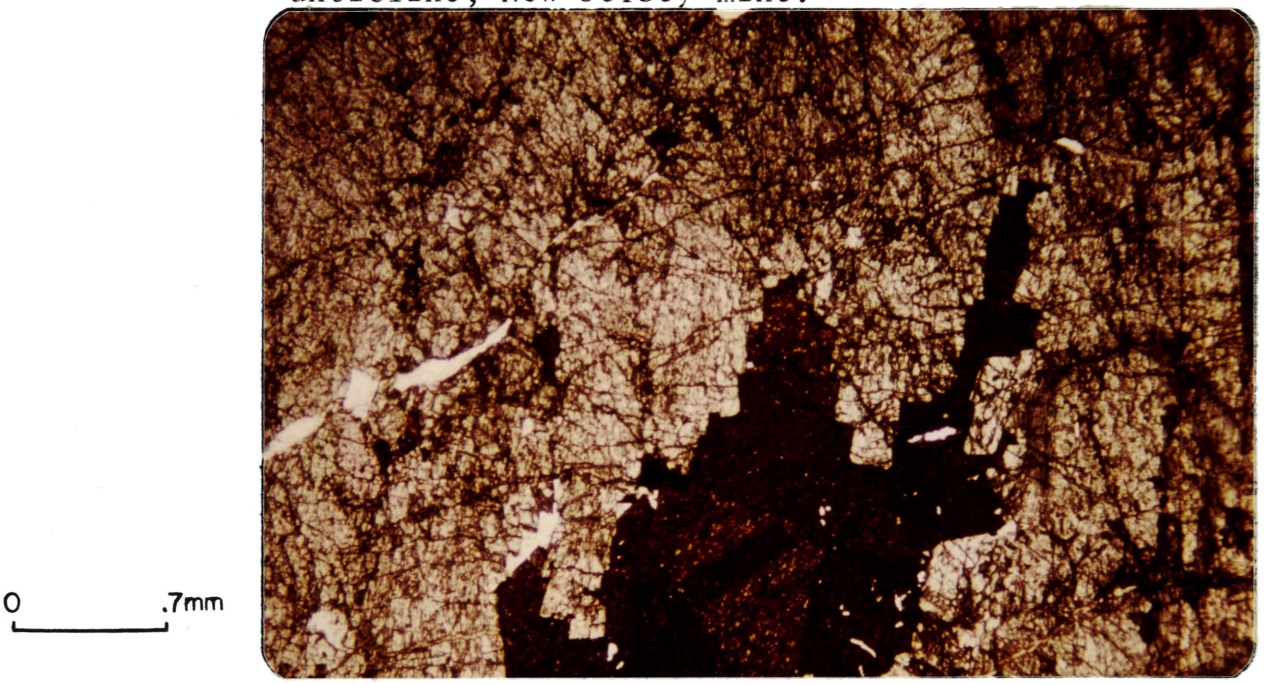


Figure 37. Photomicrograph of hedenbergite-sphalerite skarn showing coarse-grained crystals of hedenbergite (light-gray) replaced by sphalerite (yellow to dark brown). The white minerals are inclusions of quartz and calcite. Location: the same as figure 34. Plain light.

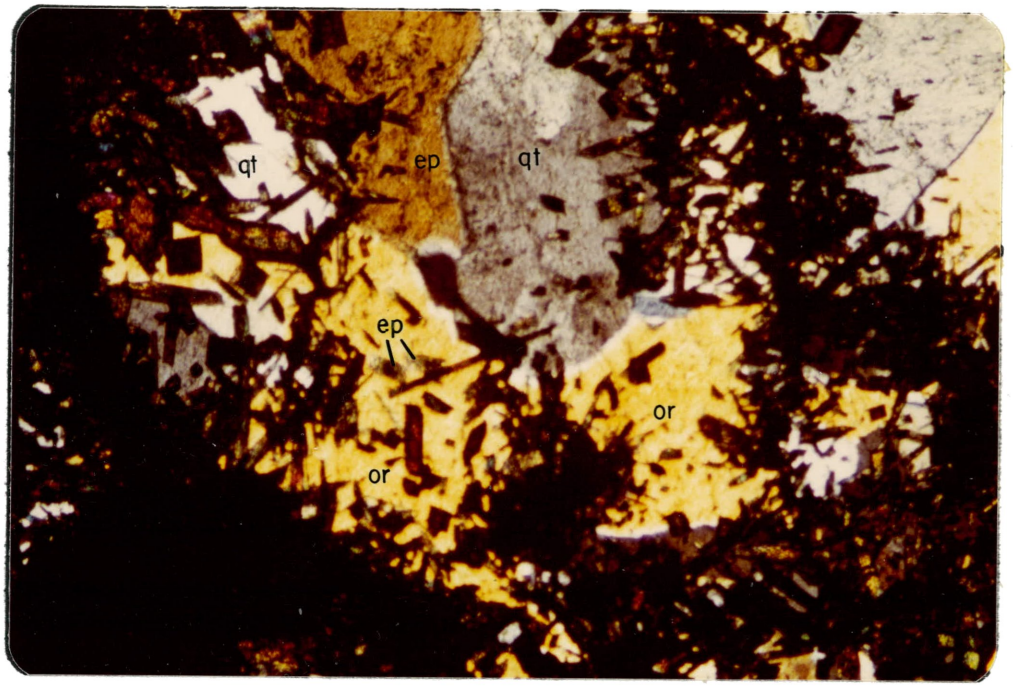


Figure 38. Hedenbergite-quartz-orthoclase-epidote skarn showing poikiloblastic orthoclase (or) and quartz (qt) enclose prisms and needles of manganhedenbergite. The yellowish-green minerals are epidote (ep). The dark area is aphanitic groundmass composed mainly of manganhedenbergite. Location: northwest part of the Annie Fox pit. X nicols.

not as high as the alkaline facies. However, this association may represent a low-temperature alkalinity facies (Dr. M. Brock, personal commun., 1979).

Iron and manganese in these silicates have possibly been derived from the granodiorite stock, which was also the source of the ore minerals. Goldschmidt (1911) has reported that the element iron was introduced as a volatile of chloride or fluoride complex and reacts with calcite.

$$Fe_2Cl_6 + 3CaCO_3 = Fe_2O_3 + 3CaCl_2 + 3CO_2$$

The released chloride would evolve into formation of scapolite. Scapolite is actually found in garnet-hedenbergite skarn. The occurrence of fluorite was not observed, but its presence is possible.

Epidote

The shale units everywhere around the southern margin of the stock are metasomatically replaced by epidote skarn. The marker bed of the Parting Shale at the base of the Oswaldo Formation is a typical example of epidotization of a shale unit. The endoskarn formed within the masses of the granodiorite stock at the contact with sedimentary rock is largely epidote.

In the epidote skarn, zoisite, clinozoisite and epidote frequently occur together, but the epidote is the

most abundant of the three. The epidote skarn derived from shale is always finer-grained than that formed in the igneous rock (Figures 39 and 40). Both rocks usually contain a large proportion of quartz in all samples. Quartz crystals poikilitically enclosed epidote grains (Figure 41). This is the characteristic feature of epidote derived from shale. The epidote rock of igneous origin shows intensive retrograde alteration. Crystals of epidote in this rock are replaced by chlorite, calcite, quartz and magnetite (Figure 40). Abundant disseminated magnetite occurs in the calcite replacing epidote. The grains of magnetite are always rimmed by fine-grained hematite.

Euhedral crystals of garnet, possibly of the grossular composition are fairly common in both the endoskarn and the exoskarn.

Ilvaite

Ilvaite is a common skarn mineral developed around the southern margin of the stock. It occurs in lenticular black masses, variable in thickness in the crest of the anticline at the New Jersey Zinc mine and at the El Paso mine (Figure 33 and Plates 4 and 6).

Intensive pyrite mineralization commonly accompanies ilvaite (Figure 42). Pyrite is always enclosed by ilvaite. Under the polarizing microscope, ilvaite is opaque, but in

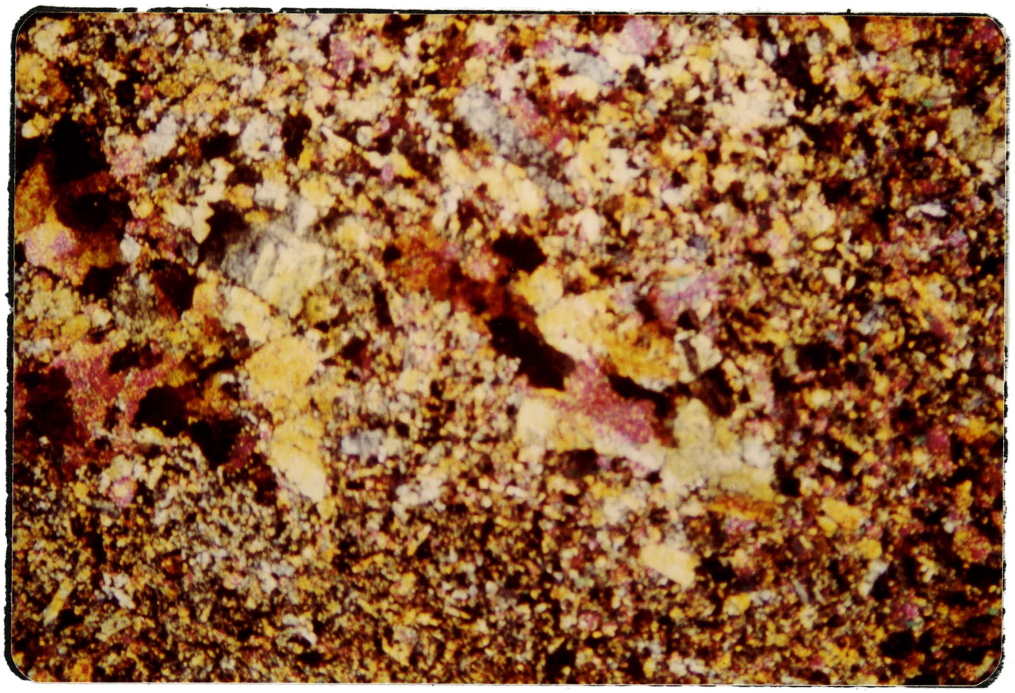


Figure 39. Epidote rock derived from metamorphosed shale showing fine- to medium-grained epidote. The fine-grained, white minerals are quartz. Location: Parting Shale, New Jersey mine. X nicols.

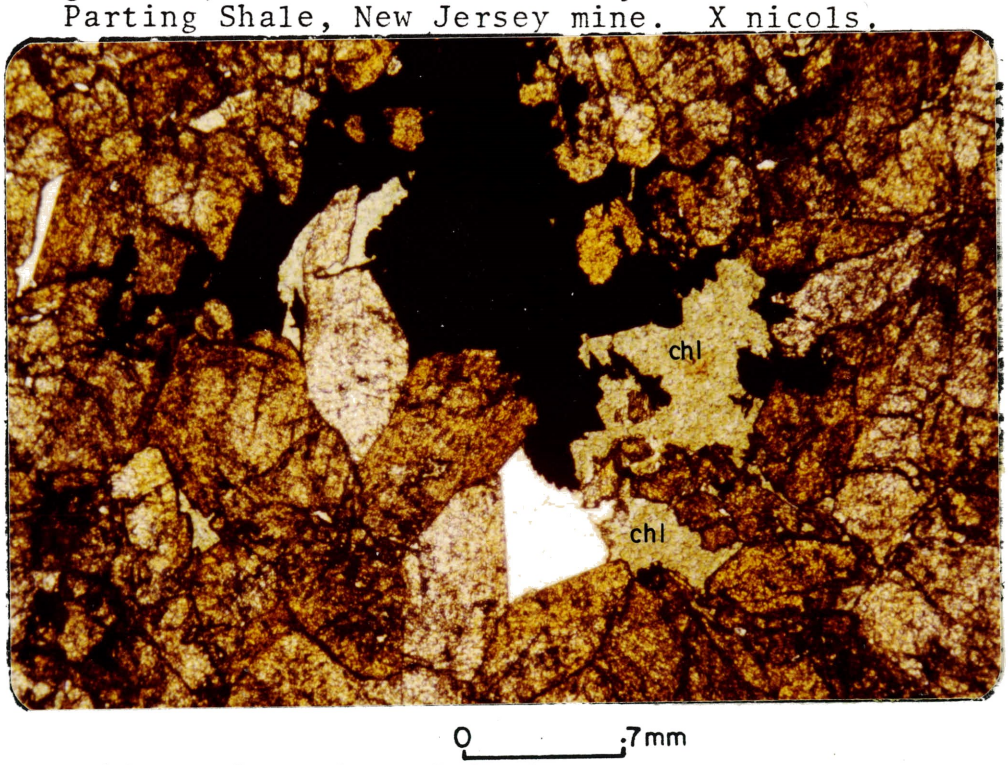


Figure 40. Epidote skarn formed in igneous rock showing coarse-grained epidote minerals. The white crystal is quartz. Notice: chlorite (chl) and magnetite (black) replacing epidote. Location: Epidotized dike, Annie Fox pit. Plain light.

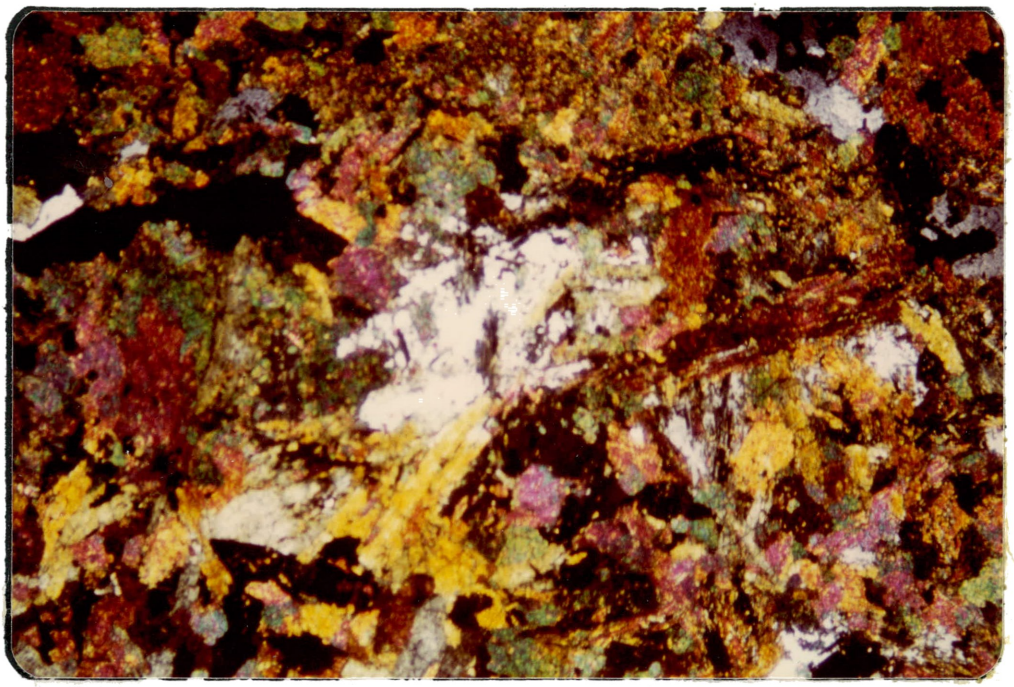


Figure 41. Epidote skarn derived from shale showing granoblastic quartz (white) poikilitically enclosing epidote. Notice: epidote inclusions are smaller than the granoblastic epidote in groundmass. Location: Parting Shale, New Jersey Zinc mine, X nicols.

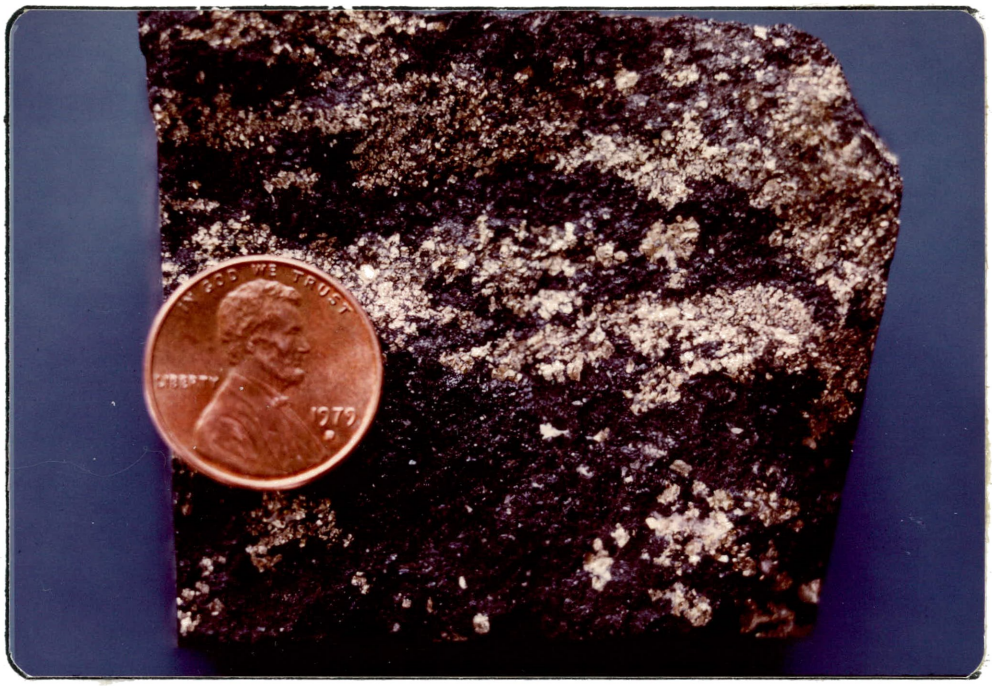


Figure 42. Hand specimen of ilvaite skarn showing ilvaite (black) and pyrite (light colored). Location: crest of anticline, New Jersey Zinc mine.

a very thin edge it is reddish-brown to orange. In polished section, the ilvaite shows variable birefringence from gray to blue with a deep-red interval reflection.

Ilvaite is commonly associated with hedenbergite, quartz and calcite. Inclusion of hedenbergite is fairly abundant in ilvaite. Pyroxene inclusions always show irregular outline, due to corrosion by the ilvaite. Therefore, this indicates that ilvaite was formed after hedenbergite. In addition to the ilvaite metasomatism, hedenbergite is frequently replaced by calcite and quartz.

One sample from the contact of ilvaite and sphalerite ore was studied under the microscope. In most of the thin section, the intergrowth of the two minerals is evident. However, further study is necessary to determine if the 2 minerals were always simultaneously precipitated.

Hornblende

In a small outcrop along the western contact of the stock with metasedimentary rocks (Plate 4), there is a strong amphibole-rich vein which crosscuts the epidote-diopside rock.

Among the amphibole group, hornblende is the predominant mineral. Trace amounts actinolite accompany the hornblende. Quartz crystals frequently occur both as inclusions in hornblende and as granoblastic mineral in the

groundmass (Figure 43). Plagioclase of intermediate composition ($An_{40}$) and some sphene accompany the amphibole locally. Occurrence of such an assemblage possibly is an indication of certain metasomatic transformations in which magmatic solution originated from the granodiorite stock seems to have been the sole agent.

Skarn Deposits at the Annie Fox Pit

The Annie Fox pit is a small open pit excavated in the skarn deposits to the south edge of the granodiorite stock (Plate 5). The skarn rocks in this area have similar features to those mentioned in the New Jersey Zinc mine, with some exceptions. Figure 44 and Table 8 show the geologic map and distribution of sedimentary and skarn rocks at the pit. To compare the geologic setting of the mine with that of the district see Figure 6.

A unique feature present in this area is the epidotization of a granodiorite dike. A petrographic description of this rock is given under the Epidote Zone, page 135. However, the contact between the stock and the dike is not exposed due to the mine dump (Figure 44). Therefore, the field relation between them is obscured. Fragments of fresh granodiorite rock were observed within the epidotized portion of the dike which probably represent inclusions of solidified wall-rock. It is not clear whether the

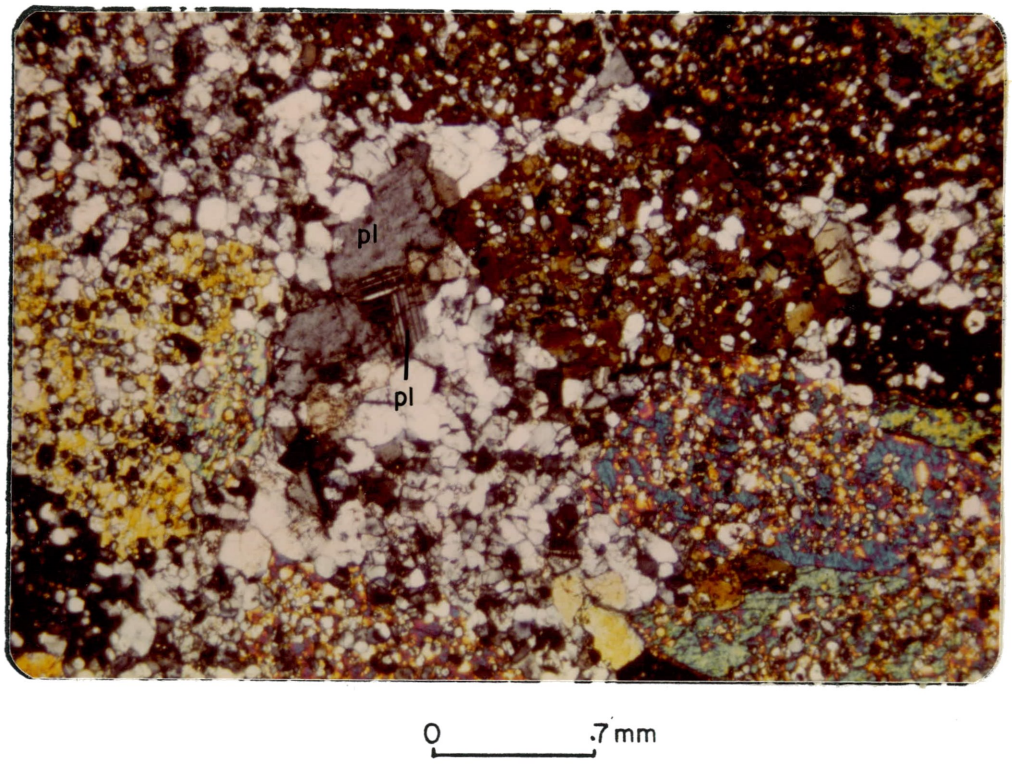


Figure 43. Photomicrograph of amphibole rock showing poikiloblastic hornblende (minerals with high birefringence), plagioclase (Pl) and quartz (white to gray minerals). Notice the quartz inclusions in the hornblende are smaller than quartz in the groundmass. Location: west contact of the granodiorite stock. X nicols.

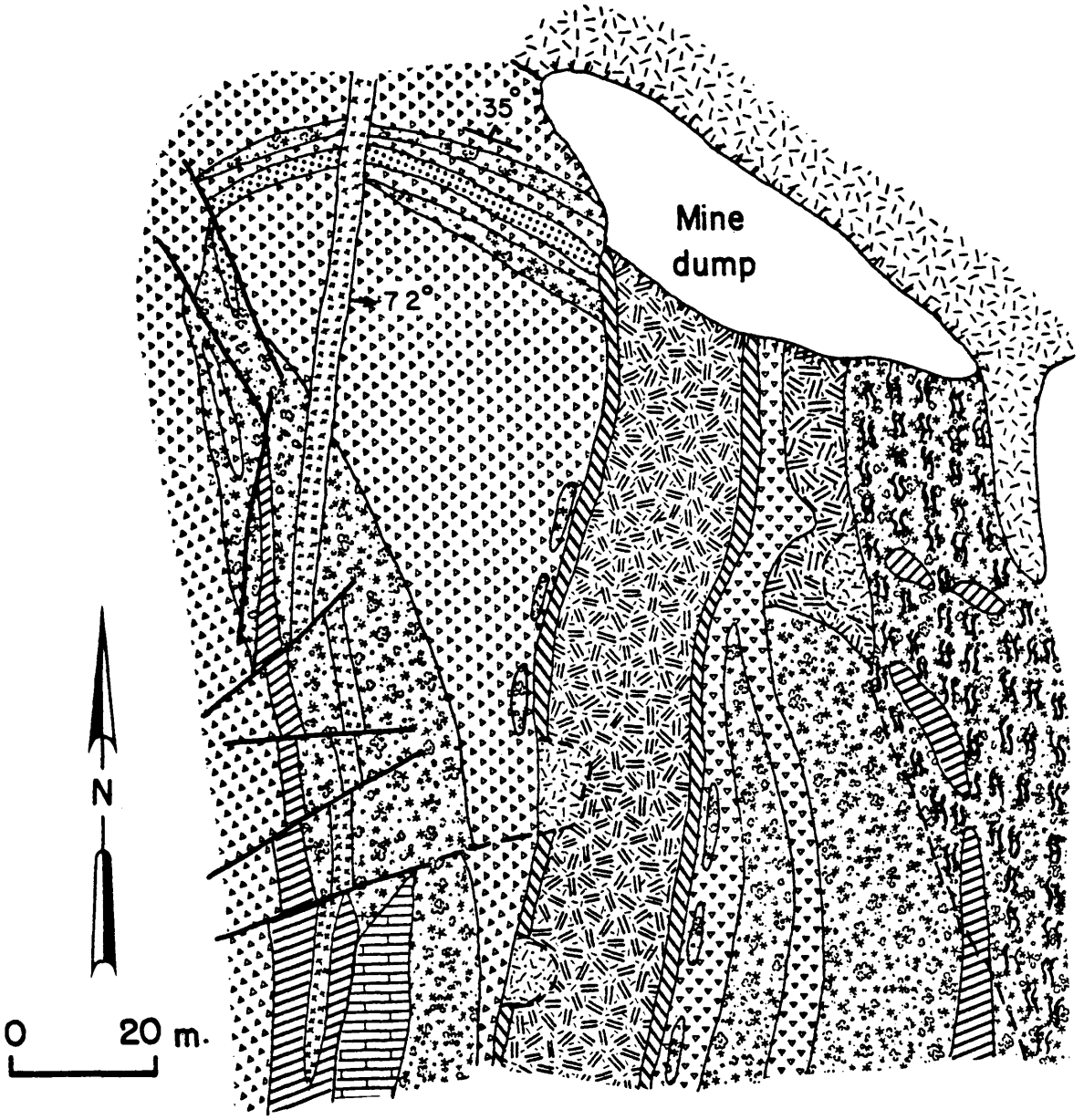


1. Granodiorite stock
2. Aplite dike
3. Garnet skarn with mineralization at the contact with pyroxene zone
4. Hedenbergite-johannsenite-orthoclase skarn, with pyrite and high grade sphalerite
5. Pyroxmangite-johannsenite-orthoclase-rhodonite skarn
6. Epidotized granodiorite dike
7. Unaltered granodiorite dike
8. Epidote skarn of originally shale unit
9. Garnet-epidote skarn
10. Calcitic marble
11. Fault
12. Crushed zone

Figure 44. Generalized diagram of alteration and metasomatic zoning in the Annie Fox pit.

Table 8. Ages and dominant lithologies of sedimentary and metasedimentary rocks and major ore minerals at the Annie Fox pit.

| Formation | Age | Lithology | | Hypogene Ore Minerals |
|---|---|---|---|---|
| | | Sedimentary rocks | Metamorphic rocks | |
| Oswaldo Formation | Upper and Middle Pennsylvanian | Limestone, argillaceous limestone, and silty limestone interbedded with siliceous shale and limy shale<br><br>DISCONFORMITY | Garnet skarn, garnet-hedenbergite skarn, pyroxmangite-hedenbergite-johannsenite-orthoclase, rhodonite skarn, marble, epidote-scapolite skarn, and garnet-diopside skarn. | Sphalerite, pyrite, galena, trace of chalcopyrite, magnetite and pyrrhotite |
| Lake Valley Limestone | Lower Mississippian | Upper part crinoidal limestone with nodules and lenses of chert. Lower part siliceous and marly limestone with lenses of shaly limestone | Marble, garnet skarn, garnet-hedenbergite skarn, hedenbergite-pyroxmangite-orthoclase-rhodonite skarn and spinel | Sphalerite, pyrite, galena and trace of chalcopyrite, magnetite and pyrrhotite |

epidotized dike is an apophysis of the stock or independent from it.

Johannsenite-pyroxmangite-orthoclase skarn

The walls of the Annie Fox pit display an intensive development of johannsenite and pyroxmangite skarns. The johannsenite rock in hand specimen is pale-brown and the crystals are randomly oriented in the forms of fine-grained fibrous needles and blades and commonly stained with pyrolusite and iron oxide on weathered surface.

The petrographic study revealed that johannsenite is always associated with hedenbergite, orthoclase and quartz. Fine-grained, shapeless epidote sometimes occurs as interstitial grains between the hedenbergite crystals. The prismatic and radial crystals of johannsenite and hedenbergite often occur as inclusions in orthoclase and quartz.

Hedenbergite skarn commonly contains numerous lenses of pyroxmangite-bearing skarn. On the weathered surface and along fractures, pyroxmangite rock is also coated with a very thin layer of pyrolusite and iron oxide. The rock is normally pale-pink on the fresh surface (Figure 45). Differentiation of pyroxmangite from other manganese-bearing silicates under the microscope is difficult. Therefore, x-ray diffraction analysis was used for this


Figure 45. Polished surface sample showing hedenbergite-johannsenite-orthoclase-quartz skarn (bottom, pale-brown), pyroxmangite-orthoclase-quartz-rhodonite skarn (middle, pale-pink), and calcitic marble (upper, white). Notice the intensive galena mineralization (fine-grained, black minerals). Variation of mineral paragenesis for each zone is shown in Figure 46. Location: to the west of the epidotized dike, Annie Fox pit.

purpose.

Pyroxmangite is colorless in thinsection. It is always associated with orthoclase, quartz, calcite and trace amounts of rhodonite. The granoblastic-polygonal orthoclase and quartz commonly contain inclusions of fine-grained prisms and blades of pyroxmangite.

A variety of yellow to yellowish-red, fine-grained crystals with characteristic lamellar twinning occurs in the pyroxmangite zone that may be rhodonite. Trace amounts of an unidentified mineral with negative optical sign were found in one thinsection. This mineral could be bustamite.

However, due to intensive oxidation of the rock and development of a dark-brown to black material, the crystal outline is obscured and differentiation of minerals becomes difficult. The prevalence of those two unidentified minerals elsewhere in the mine is not known.

The formation of pyroxmangite and associated minerals is possibly the result of replacement in the manganhedenbergite skarn. This idea is mainly based on the random distribution of irregular shaped masses of pyroxmangite embedded in manganhedenbergite skarn. This will be discussed later in detail under the structural characteristics of zonation.

Structural characteristics of Fe, Mn-bearing skarn

The increase in iron and introduction of manganese into the system during the acidic stage of skarnization causes a considerable change in the composition of pyroxene and the formation of iron-rich garnet (andradite) and such silicates as pyroxmangite. As a result, a sequence of skarns develops concurrently and provides zonation (Figures 45 and 46).

Zharikov (1970) pointed out that the development of such zonation indicates that all the constituents were completely mobile in their behavior during the process of formation. He also mentioned that the mobility series were $H_2O$, $CO_2$, $S(O_2)$, Na, K, Mn, Mg, Fe, Ca, Si, Al, and Ti. The sequence of evolution of skarns shown in the generalized section in Figure 46 was as follows:

↑
Calcitic marble
↑
Pyroxmangite-rhodonite skarn
↑
Manganhedenbergite-johannsenite skarn
(possibly several zones with different compositions)
↑
Andraditic skarn
(possibly alternating zones with different compositions)
↑
Granodiorite stock

The arrow shows the direction of transfer of constituents by the fluids.

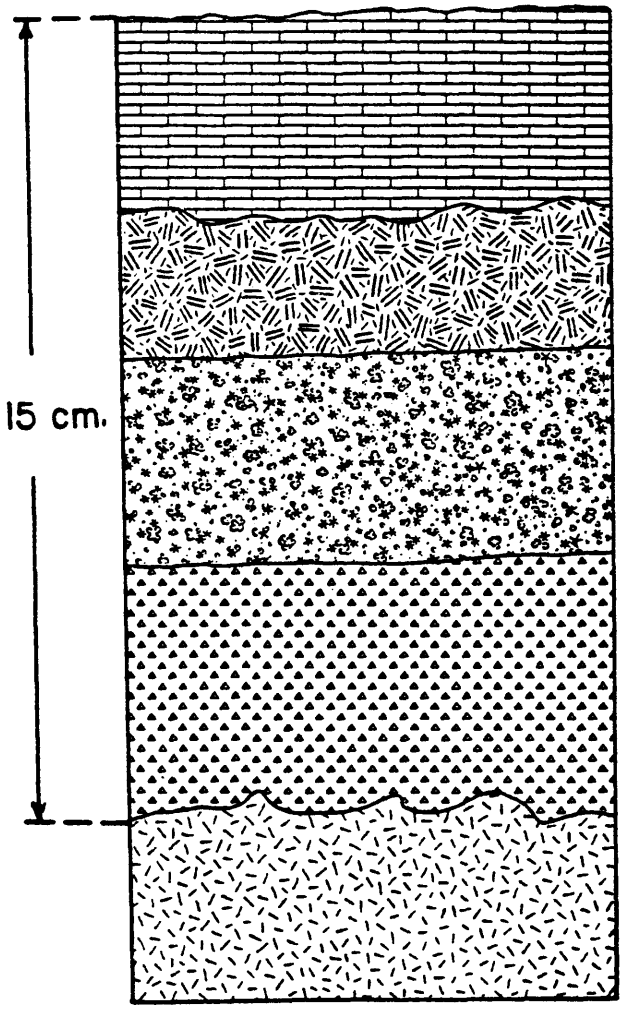


Figure 46. Generalized model of the metasomatic zoning of the limy skarns at the Annie Fox pit.

Detailed petrographic study, together with x-ray analysis, revealed the uniform compositions of minerals in each zone. Perhaps this is an important characteristic to be observed in such a sequence. As mentioned previously, the factors controlling the zonation are the changes in concentration and mobility of Fe, Mn, Mg, Na, K, etc. in the fluids, and $CO_2$ pressure.

Skarn Deposits at the Pewabic Mine

The Pewabic mine is a relatively large open pit and underground operation developed around the eastern and southeastern margins of the granodiorite stock at the contact with the equigranular facies (Plate 6, Figures 1 and 6). However, the mine is not operating at the present time. The principal ore produced was zinc.

Although the skarn deposits present in this area are very much similar to those at the New Jersey Zinc mine and the Annie Fox pit, the Pewabic mine was selected to complete the geologic mapping around the southern margin of the stock and particularly to study the mineralogy of some zones which are not present in other places in the region. Figure 47 and Table 9 show the geologic map, sedimentary and skarn rock distribution in the Pewabic mine and the immediate area. For the location of the mine within the region, compare Figure 47 with Plate 3 of Figure 6.

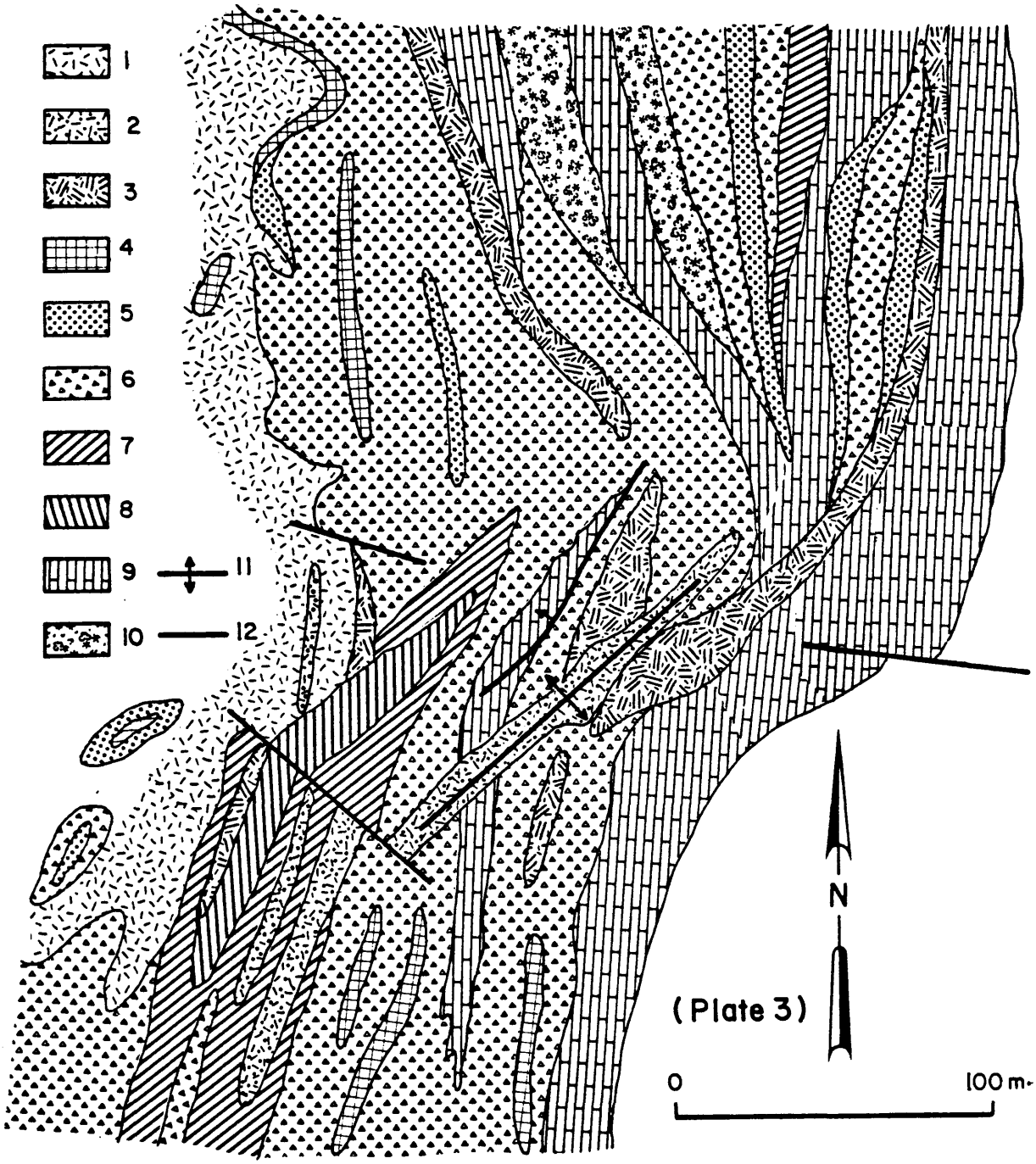


(1) Granodiorite stock, (2) Quartz latite dikes, (3) Hornblende-quartz diorite sills, (4) Epidote rock, (5) Pyroxene rock (6) Garnet skarn (mineralized), (7) Epidote-pyroxene rock, (8) Quartz-chlorite-muscovite-scapolite-garnet rock, (9) Calcitic marble, (10) Hedenbergite skarn (mineralized), (11) Axis of the anticline, and (12) Fault.

Figure 47. Generalized diagram of alteration and metasomatic zoning of skarn at the Pewabic mine.

Table 9. Ages and dominant lithologies of sedimentary and metasedimentary rocks and major ore minerals at the Pewabic mine.

| Formation | Age | Lithology | | Hypogene Ore Minerals |
|---|---|---|---|---|
| | | Sedimentary rocks | Metasomatic rocks | |
| Oswaldo Formation | Upper and Middle Pennsylvanian | Limestone, argillaceous and silty limestone, interbedded with siliceous shale and limy shale<br><br>DISCONFORMITY | Garnet-diopside skarn, garnet skarn, garnet-epidote skarn, garnet-hedenbergite skarn, marble, and epidote skarn | Sphalerite, trace of galena, chalcopyrite and magnetite and pyrite |
| Lake Valley Limestone | Lower Mississippian | Upper part crinoidal limestone with nodules and lenses of chert Lower part siliceous and marly limestone with lenses of shaly limestone | Marble, garnet skarn, garnet-hedenbergite skarn, hedenbergite-ilvaite skarn, garnet-diopside skarn | Sphalerite, trace of galena, chalcopyrite, magnetite, pyrite, and pyrrhotite |

The Pewabic mine area contains a small anticline which plunges gently to the south. Over part of its length the crest of the fold is occupied by a quartz latite porphyry dike. The dike is displaced by a fault with a general N45$^{o}$W trend.

Some irregular and discontinuous lenses of epidote skarn which formed inside the periphery of the granodiorite stock (Plate 6) have been classified as endoskarn. Part of this feature is shown in the upper left corner in Figure 47. The texture and general composition of this endoskarn is similar to that of the epidotized dike in the Annie Fox pit.

Variable sizes of xenoliths of the sedimentary wallrock were mapped within the equigranular facies of the stock along its southern boundary, the larger of which are shown on Plate 6 and Figure 47. These fragments are intensively metamorphosed to skarns with mineralogy similar to those beyond the margin of the stock. As far as genetic relation is concerned, the skarn derived from the xenoliths show relatively sharp contacts with the enclosing granodiorite. Fairly intensive magnetite mineralization was noted in a few xenoliths, but is an uncommon mineral in the exoskarn elsewhere in the southern area.

Chlorite-muscovite-quartz rock

Several lenticular bodies of metasomatized chlorite-muscovite-quartz rock of variable size are exposed at the Pewabic mine, embedded in garnet and diopside-epidote skarns (Figure 47 and Plate 6). The rock shows porphyroblastic texture with pseudomorphs of dark-green chlorite and magnetite embedded in a fine-grained, dark-green chlorite-rich groundmass.

Under the microscope, chlorite, muscovite, quartz and magnetite are seen to be the main constituents and include 80-90 percent of the rock volume (Figure 48). The accessory minerals in the order of abundance are scapolite, garnet and trace amounts of diopside and epidote. Colorless, light-red, and yellow muscovite occur in medium- to fine-grained, shreddy aggregates replacing other minerals. Commonly fine-grained muscovite has formed as pseudomorphs after feldspar.

Green to dark-green chlorite in masses and radiating fibrous aggregates have replaced biotite and hornblende (Figure 49). All biotite and hornblende grains have been completely replaced by chlorite pseudomorphically. The two chlorite-group minerals, clinochlore and pennine, were identified and are believed to have formed simultaneously. Chlorite is usually associated with fine-grained disseminated

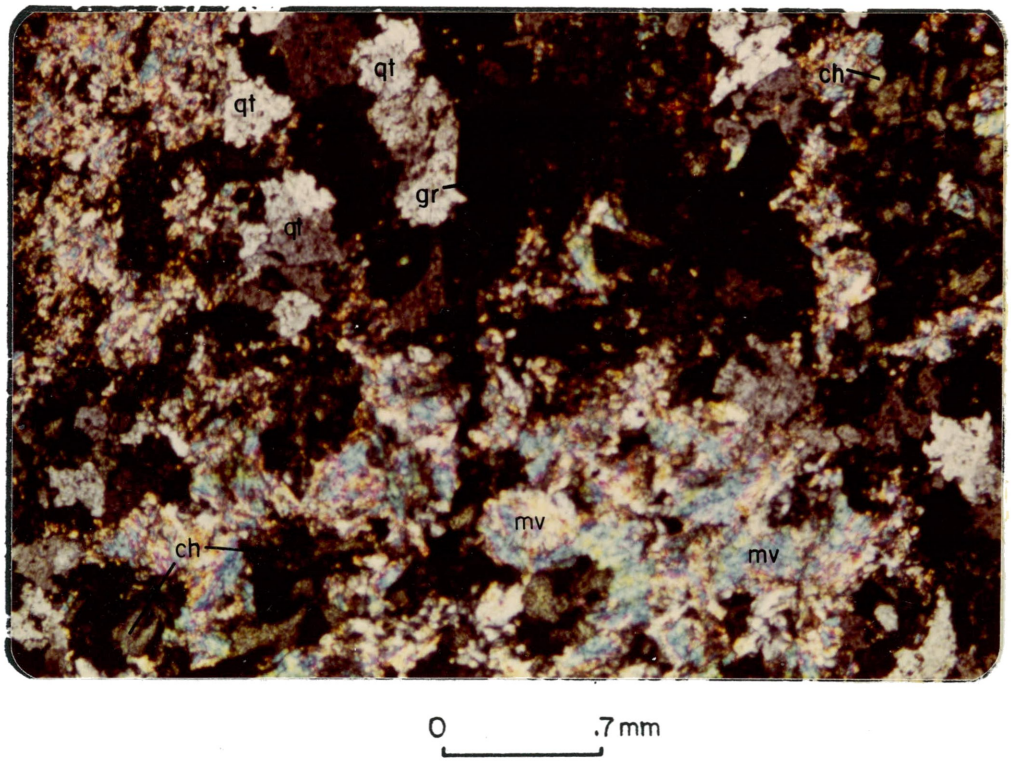


Figure 48. Photomicrograph of muscovite-chlorite-quartz rock showing granoblastic aggregates of muscovite (mv), chlorite (ch), quartz (qt) and dodecahedral grossularite (gr). The dark area is very fine-grained chlorite and magnetite. Location: Pewabic mine. X nicols.

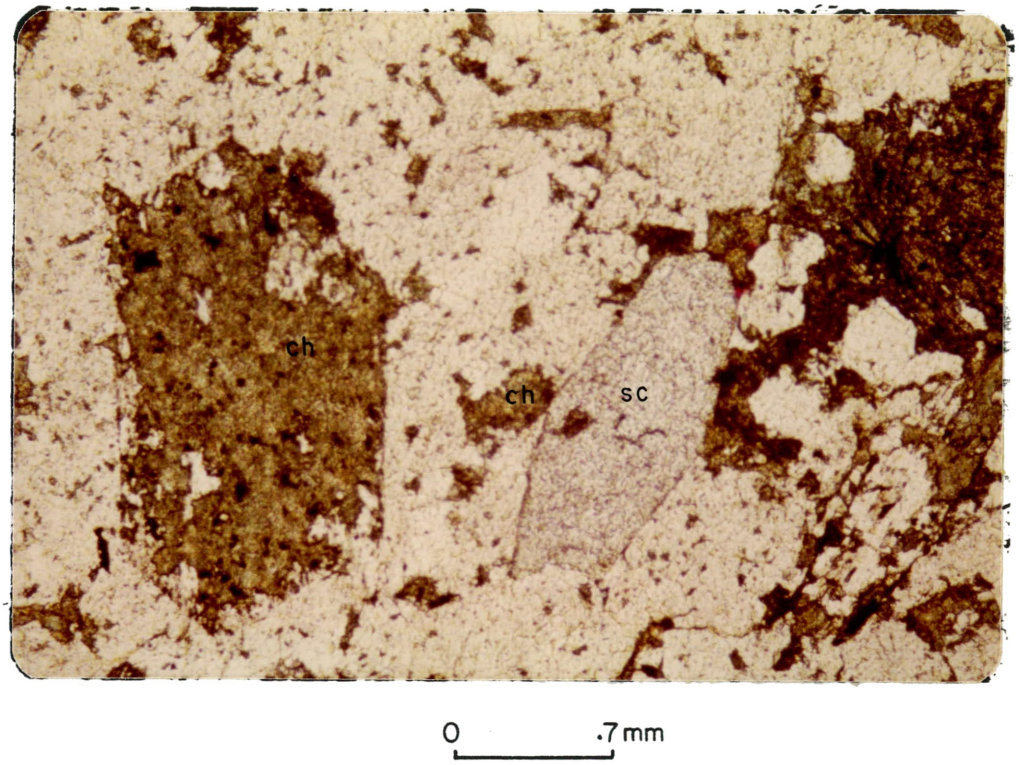


Figure 49. Photomicrograph of chlorite-muscovite-quartz-scapolite rock showing former phenocrysts of biotite and hornblende completely replaced by chlorite (ch) and magnetite (disseminated dark minerals). Euhedral mineral of scapolite (sc) is embedded in groundmass. The groundmass is composed of muscovite, quartz and very fine-grained chlorite. This photograph is of a different portion of the same sample as Figure 48. Plain light.

magnetite.

Quartz occurs in fine- to medium-grained, anhedral to subhedral crystals with irregular outline. It is 20-30 percent of the rock volume.

Trace amounts of fine- to medium-grained, anhedral to subhedral crystals of diopside and epidote are always associated with other minerals.

The pneumatolytic action of chloride is shown principally in the production of scapolite associated with chlorite and muscovite. The scapolite crystals are idioblastic against chlorite, muscovite and quartz (Figure 49).

Garnet occurs in colorless, isotropic and euhedral crystals. Most of the grains are six-sided, fine- to medium-grained. The crystal forms are dodecahedral and less commonly trapezohedral. No overgrowth zones were observed on garnet crystals in this rock.

The abundant muscovite and chlorite in this rock are pneumatolytic products. Textural and compositional relations of the chlorite-mucovite-quartz-scapolite-garnet rock may lead to the following conclusions:

Much sodium was removed from the rock during conversion of plagioclase to muscovite, but some was retained to form scapolite. Addition of potassium is reflected in the composition of muscovite.

It seems likely that the parent rock before metamorphism was an igneous rock of intermediate composition and hypidiomorphic texture as evidenced by the abundance of euhedral crystals of biotite, hornblende and feldspar plus subhedrons of quartz. The present rock is nearly completely composed of metamorphic and pneumatolytic minerals. It is likely that the hydration and other changes which converted biotite and hornblende to chlorite and magnetite, and the feldspars to muscovite, was not the result of high-temperature alteration. However, Dr. M. Brock (personal commun., 1979) suggested a moderate to low-temperature metamorphism of a hornblende-biotite-quartz diorite rock with addition of fluorine, chlorine and potassium.

## TEMPERATURE-PRESSURE CONDITIONS IN THE FORMATION OF MAGNESIAN AND LIMY SKARN

The maximum temperature reached during skarnization is limited by the temperature and the composition of the invading pluton. The zone in direct contact with the intrusive body is characterized by the highest temperature. Obviously, away from the intrusion the zones are marked by lower temperatures. The temperature of granitic magma is considered to be around 700$^{o}$ to 800$^{o}$C, of syenitic

magma about 900°C, and of gabbroic magma around 1200°C.

Jaeger (1957) studied the theoretical temperature gradients adjacent to intruding bodies. His calculation is based on the reasonable assumptions approximating natural conditions. Jaeger's data indicates that a tabular vertical sheet of granitic intrusion 2000 meters thick intruded at 800°C into country rock having a temperature of 100°C would crystallize at between 800° and 600°C and would elevate the temperature of adjacent wall rock to about 500° to 550°C. The temperature decreases rapidly outwards from the contact. This is based on the assumption that the heating of the country rock by the intrusion is due entirely to conductivity and that the heating by a transfer of volatile constituents can be neglected. However, the maximum temperature attained by the invaded rock would not be effected greatly by volatiles, but the rate of heat obtained within each zone must be a function of volatility. With time the temperature decreases and after the complete crystallization of the intrusion, the temperature at the contact is approximately 490°C.

Temperature-Pressure Conditions of Magnesian Skarn

Zharikov (1970), by using data from different authors, has drawn a diagram shown in Figure 50. With reasonable confidence, it is possible to interpret the paragenesis of

magnesian skarn and its restriction to magmatic contacts. Figure 50 is a summation of such data characterizing the temperature-pressure conditions in which the skarns are formed. The horizontal scale shows variation of pressure with the depth of abyssal, meso-abyssal and hypo-abyssal facies. The presently exposed level of the Hanover-Fierro stock may correspond to a hypo-abyssal depth. The following features are considered in this diagram:

(1) The liquidus-solidus curve for granitic intrusions (curves 3 and 4) is of general importance to this subject since the skarnization in the Hanover-Fierro region is related to the intrusion of the granodiorite stock.

(2) The dissociation curve for dolomite is curve 5. At temperatures somewhat higher than that of the dissociation of periclase, the following reaction takes place:

$$\text{dolomite} = \text{periclase} + \text{calcite} + CO_2$$

The equilibrium curve 5 is based on experimental data when the mole fraction of $CO_2$ = 1.0 determined by Harker and Tuttle (1955) and Metz (1967). In shallow contact metamorphism, the decomposition of dolomite to periclase + calcite becomes more probable at lower $P_f$. When the mole fraction of $CO_2$ = 1.0, the dissociation temperature is 820°C at 1000 bars, 760°C at 500 bars, and about 700°C at 250 bars (this corresponds to a depth of about 1 km).

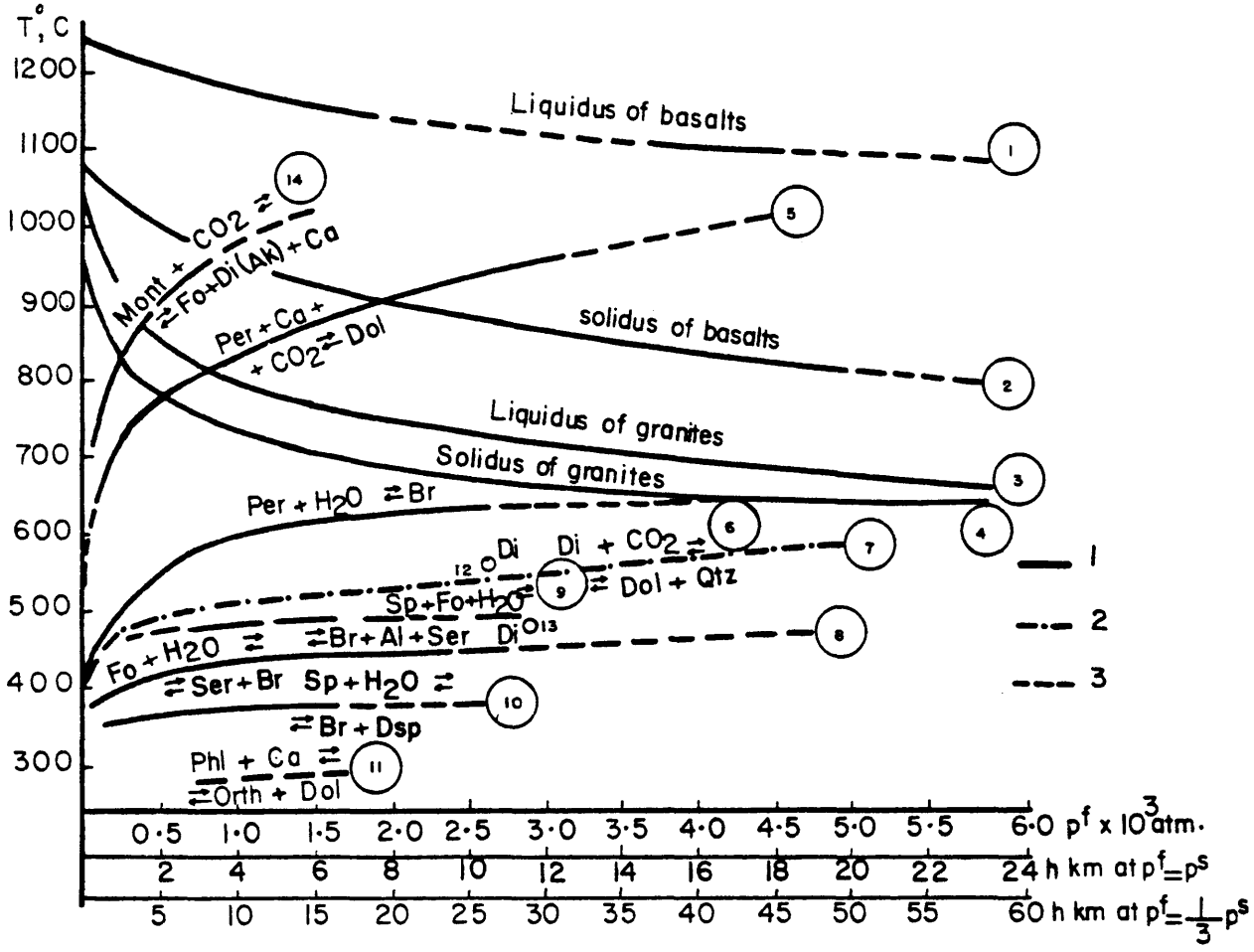


Figure 50. Summary T-P diagram of experimental data on formation conditions of magnesian skarn (from Zharikov and others, 1970)

Winkler (1974) mentioned that the dissociation of dolomite can take place at much lower temperature if $XCO_2$ of the fluid phase is very small (for example if some mechanism locally has diluted the liberated $CO_2$ with $H_2O$).

(3) The hydration of pericalse (curve 6).

$$\text{pericalse} + H_2O = \text{brucite}$$

At temperature below 620°C the periclase is not stable. After formation of periclase, it easily alters to brucite by circulating water. Therefore, most brucite marble such as that at the Continental mine does not contain periclase.

(4) Formation of diopside (curve 7). This equilibrium curve is based on experimental data given by Zharikov and the equilibrium points 12 and 13 for the formation of diopside from $CO_2$-saturated and $CO_2$-unsaturated solutions are obtained by Metz and Winkler (1963). Reaction

$$\text{dolomite} + \text{quartz} = \text{diopside} + CO_2$$

is represented by the diopside-bearing assemblage.

(5) Curve 8 shows the

$$\text{forsterite} + H_2O = \text{serpentine} + \text{brucite}$$

equilibrium condition. This indicates forsterite is not stable below 400°C.

(6) Curve 9 shows the

$$\text{spinel} + \text{forsterite} + H_2O = \text{brucite} + \text{Al serpentine},$$

curve 10 represents the

spinel + $H_2O$ = brucite + diaspore,

and curve 11 shows the equilibrium condition of

phlogopite + calcite = orthoclase + dolomite.

(7) Curve 14 is the equilibrium formation of

monticellite + $CO_2$ = forsterite + diopside + calcite, or

monticellite + $CO_2$ = forsterite + akermanite + calcite.

In general, the information in Figure 50 indicates that the temperature range for the formation of magnesian skarns may vary from 650° to 1000°C. This interpretation is based on the experimental data here cited.

Zharikov reported that the temperature formation of magnesian skarns at the contact with granitic intrusion ranges from 650° to 850°C. He also mentioned the hypo-abyssal facies with periclase representing higher temperatures than the periclase-free facies. However, there is no significant difference between the skarn with periclase and that of periclase-free facies at the Continental mine.

Based on the T-P conditions of stability of calcium silicates and other experimental data, magnesian skarns may form at depths ranging from 1-15 km to 30-40 km.

## Temperature-Pressure Conditions of Limy Skarn

The T-P diagram in Figure 51 is the same design which was prepared by Zharikov (1970). This diagram is used for the paragenesis in limy skarns and the information collected

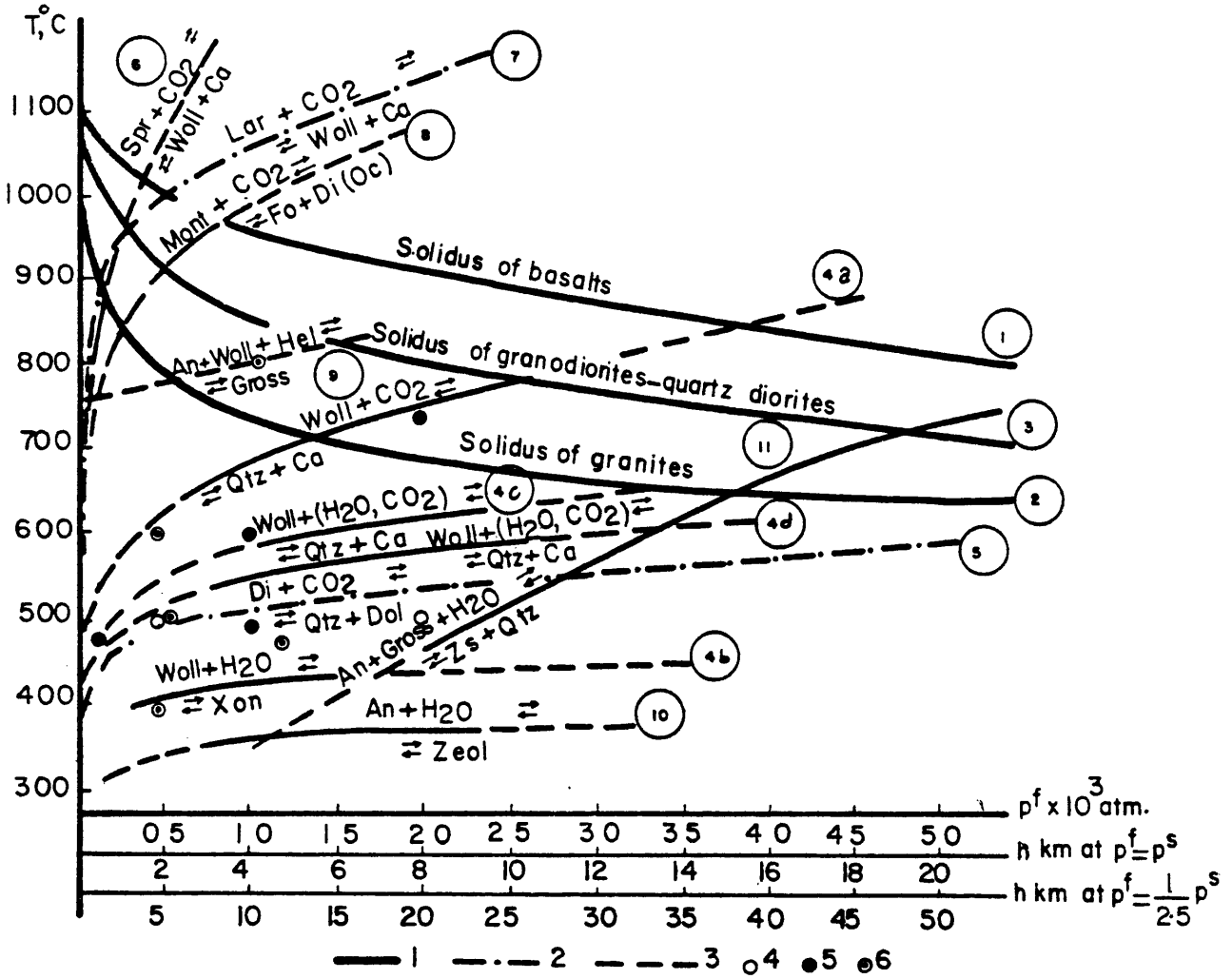


CURVES:
1 - experimental
2 - calculated
3 - presumptive

EXPERIMENTAL POINTS (SYNTHESIS)
4 - epidote
5 - garnet
6 - vesuvianite

Figure 51. Summary P-T diagram of experimental data characterizing formation conditions of limy skarn (from Zharikov and others, 1970).

is a summary of experimental data of the stability fields and the data on synthesis of the contactual and skarnal minerals. The following information is presented here:

(1) solidus temperature curves of water-saturated for basalt (curve 1) and for granite (curve 2). In addition to these curves, the diagram presents the solidus temperature curve for granodiorite-quartz diorite melt (curve 3).

(2) Curve 4a shows the equilibrium formation of

$$\text{quartz} + \text{calcite} = \text{wollastonite} + CO_2$$

As shown in the figure, very high temperature is required for calcite to react with quartz, but the carbonates dolomite and magnesite react with quartz at much lower temperature. In shallow contact metasomatism, quartz reacts with calcite at low $CO_2$-pressure. Wollastonite can form from decomposition of xonotlite in low-grade metamorphism. Curve 4b shows this equilibrium

$$\text{xonotlite} = \text{wollastonite} + H_2O$$

Curves 4c and 4d show the formation of wollastonite by reaction between quartz and calcite, at 0.25 and 0.1 $CO_2$ mole-fraction respectively in the gaseous phase. These are shown in the following reaction:

$$\text{quartz} + \text{calcite} = \text{wollastonite} + (H_2O,\ CO_2)$$

According to Zharikov's calculation, the equilibrium of

$$\text{diopside} + CO_2 = \text{quartz} + \text{dolomite}$$

is given by curve number 5.

(3) Tuttle and Harker have calculated the formation of silicates in a deep environment. Curve 6 is the equilibrium of

wollastonite + calcite = sparrite + $CO_2$

Curve 7 shows the equilibrium reaction of

wollastonite + calcite = larnite + $CO_2$

and curve 8 represents the equilibrium condition of

forsterite + diopside = monticellite + $CO_2$

(4) Curve 9 represents the formation condition of grossularite at very high temperature. Curves 10 and 11 show the lower limit of the temperature range of skarn formations.

Anorthite + $H_2O$ = zeolite

and

Anorthite + grossularite + $H_2O$ = zoisite + quartz

Determination of the depths at which limy skarns are formed is complicated, but Korzhinskii (1970) has mentioned that the upper limit could be drawn at 1-1.5 km. He also pointed out that the lower limit of the typical limy skarns is determined by stabilities of the characteristic calcium and aluminum silicates such as wollastonite, grossularite, and other minerals. Formation of limy skarns is strongly controlled by two unknown variables: the mole-fraction of carbon dioxide in the solution and the pressure related to the

fluid phase which is a part of the total pressure of the load. Based on the temperature below the solidus of granitic intrusion, and experimental data, together with the compositional relationships of coexisting scapolite and plagioclase, the optimum for the lower limit in which limy skarn can form could be at depths of about 15-16 km. However, this idea is tentative and mainly depends on geological and physico-chemical conditions.

The temperature range for the formation of limy skarn is variably between 350° and 1000°C. As shown in Figure 51, except for the formation of high-temperature grossularite-free stage, the main temperature range for limy skarns is between 800° and 400°C.

Skarnization is a process of decarbonatization. If carbon dioxide is retained in the system at the time of formation of skarn minerals, the $CO_2$ pressure gradually increases. Shoji (1970 and 1975) reported that andradite garnet is not stable in fluid containing high $CO_2$ pressure at approximately 400°C. Since the garnet is the most common skarn mineral in the Hanover-Fierro area, it must have been formed at moderate $CO_2$ pressures.

## GEOCHEMISTRY OF SKARN DEPOSITS

Analyses of 52 rock samples from various skarn zones at the Continental and New Jersey Zinc mines are presented in

Tables 10, 11, 12 and 13. Tables 10 and 11 show macroscopic description of each sample and the results of chemical compositions and trace element distribution of some samples is given in Tables 12 and 13.

One special case worthy of notice is that the low percentages of total oxide content in some samples is due to the lack of calculations of $H_2O$ and $CO_2$ in the sample. For example, some samples such as number 11 contain considerable amounts of epidote and other hydrosilicates which indicate high $H_2O$ content, or numbers 21, 23 and 41 samples are calcitic and dolomitic marbles and contain high percentages of $CO_2$ and some $H_2O$.

For the total digestion of rock, samples were treated with hydrofluoric, concentrated nitric and sulfuric acids. In determining the chemical composition, the amounts of MgO and $Na_2O$ were established by atomic absorption techniques while the rest of the oxides were identified by the x-ray fluorescence method. For all the samples iron is arbitrarily calculated as $Fe_2O_3$. The analysis would sum higher than total weight percent if an appreciable portion of the iron were present as $Fe^{+2}$.

In trace element analysis, a hot extraction technique was used and the samples were treated with concentrated nitric acid ($HNO_3$). Three blanks and three

duplicated samples were prepared for major and trace element data in order to obtain the accuracy and precision of the analyses. However, the error was within a limited, acceptable range.

Chemical compositions of clinopyroxene and garnet skarns from the Continental and New Jersey Zinc mines are given in Tables 12a and 12b. It is obvious that there is a sharp difference in the content of $Al_2O_3$, $Fe_2O_3$, MnO and $TiO_2$ when comparing the two mines. The samples from the Continental mine (Table 12a) contain higher $Al_2O_3$ and $TiO_2$ and significantly lower MnO than those from the New Jersey Zinc mine. MnO associated with ferrous iron occurs in high concentrations in the hedenbergitic pyroxene and possibly determines its reducing properties. The two components of $Fe_2O_3$ and $Al_2O_3$ occur in the garnets and garnet-diopside rocks in different proportions, but always in high total concentration, determine the oxidizing properties of garnet-diopside rock.

Alumina and ferric iron are considered together because aluminum does not contribute to reducing conditions in the presence of ore minerals, and these two components proxy for each other in the lime-iron garnet.

The pyroxene skarn at the Continental mine does not provide a suitable environment for the precipitation of sulfides.

The composition of pyroxene in this area ranges between diopside and salite. This type of skarn is one of the most common rocks at the Continental mine and it is localized by favorable structure at the contact with the granodiorite stock, but very little mineralization occurs in veinlets. The pyroxene in this case is very low in manganese (Table 12a). The ferrous iron in diopside and salite was produced in a weakly reducing environment and caused precipitation of small amounts of ore minerals.

The high content of MnO and ferrous iron in hedenbergite and johannsenite skarns at the New Jersey Zinc mine is paralleled by the high concentrations of sphalerite and galena, and low content of $Al_2O_3$ (Tables 12a and 12b). The highest concentration of ore minerals is always in the hedenbergite zone for the entire mineralized area to the south. It is supposed that the manganese plays the determining role in the precipitation of sphalerite and galena ores.

To test the hypothesis that oxides play the important role in the formation of sulfides, the manganese, zinc and lead contents were determined in samples with different concentrations of mineralization. For example, samples 30 and 35 from the New Jersey Zinc mine (Tables 12b and 13) contain high amounts of manganese. This increase is

ble 10. Macroscopic description of skarn rocks from the Continental pit selected for whole rock and trace element analyses.

| o. | Field No. | Sample Description |
|---|---|---|
| l | MYP3 | Diopside-quartz-feldspar rock, minor pyrite and chalcopyrite veinlets |
| 2 | MYP6 | Diopsidic hornfels in a fine-grained groundmass of quartz and feldspar (mainly plagioclase). |
| 3 | MYP16 | Garnet-clinopyroxene skarn with minor veinlets of pyrite and chalcopyrite |
| 4 | MYP20 | Porphyroblastic texture of diopside in an aphanitic groundmass of quartz and feldspar with veinlets of pyrite, epidote and quartz |
| 5 | MYP22 | Diopside-quartz-feldspar hornfels (equigranular texture) |
| 6 | MYP23 | Garnet-clinopyroxene hornfels |
| 7 | MYP28 | Clinopyroxene hornfels with nodules of epidote, veinlets of pyrite, amphiboles and epidote |
| 8 | MYP33 | Brown garnet with veinlets of quartz and calcite |
| 9 | MYP34 | Fine-grained brown garnet with disseminated very fine-grained chalcopyrite |
| 0 | MYP35 | Garnet-clinopyroxene skarn with disseminated chalcopyrite and pyrite in the garnet |
| 1 | MYP40 | Diopside-quartz-feldspar hornfels with nodules of epidote and veinlets of pyrite and chalcopyrite |
| 2 | MYP44 | Brown garnet with nodules of diopside and disseminated pyrite and chalcopyrite |
| 3 | MYP53 | Garnet skarn with disseminated clinopyroxene, veinlets of chalcopyrite, pyrite and magnetite |
| 4 | MYP63 | Garnet-clinopyroxene skarn with veinlets of pyrite and magnetite and trace chalcopyrite |
| 5 | MYP81 | Diopside-quartz-feldspar hornfels |
| 6 | MYP84 | Brown garnet includes 5% green garnet, with nodules and veins of epidote and diopside. Some chalcopyrite |

ble 10. (Continued)

| ab. o. | Field No. | Sample Description |
|---|---|---|
| 7 | MYP85 | Clinopyroxene hornfels with veinlets of pyrite and humatite |
| 8 | MYP89 | Diopside-quartz-feldspar hornfels with veinslets of pyrite and some chalcopyrite |
| 0 | MYP91 | Dolomitic marble with nodules and veins of magnesian skarn |
| 0 | MYP94 | Clinopyroxene hornfels with veinlets of pyrite |
| 1 | MYP95 | Dolomitic marble with spots of serpentine |
| 2 | MYP97 | Green to yellowish-green garnet |
| 3 | MYP100 | Calcitic marble |
| 4 | MYP102 | Green garnet with veins of quartz-calcite and zeolite |

le 11. Macroscopic description of skarn rocks from the New Jersey Zinc mine selected for whole rock and trace element analyses.

| b. . | Field No. | Sample Description |
|---|---|---|
| | MYS14 | Unaltered Percha Shale |
| | MYS15 | Oswaldo limestone (impure limestone) |
| | MYS16 | Hanover limestone (fairly pure crinoidal limestone) |
| | MYS19 | Epidote skarn from altered granodiorite at the contact with metasediments |
| | MYS25 | Green garnet skarn |
| | MYS26 | Hedenbergite skarn, minor sphalerite, quartz and calcite |
| 1 | MYS27 | Green garnet skarn |
| 2 | MYS28 | Unmineralized Parting Shale |
| 3 | MYS30 | Garnet-hedenbergite skarn |
| 4 | MYS31 | Recrystallized Oswaldo limestone |
| 5 | MYS33 | Garnet-hedenbergite skarn |
| 6 | MYS34 | Hedenbergite skarn with disseminated sphalerite |
| 7 | MYS38 | Garnet-hedenbergite skarn with pyrite veinlets |
| 8 | MYS39 | Epidote-garnet skarn |
| 9 | MYS45 | Green garnet with spots of clinopyroxene |
| 0 | MYS46 | Hedenbergite skarn with disseminated sphalerite |
| 1 | MYS47 | Calcitic marble between garnet and pyroxene zone |
| 2 | MYS49 | Hedenbergite skarn with small spots garnet |
| 3 | MYS59 | Clinopyroxene-epidote-quartz-feldspar skarn |
| 4 | MYS61 | Clinopyroxene-garnet-epidote skarn |
| 5 | MYS62 | Chlorite-mucovite-quartz-garnet-scapolite rock |
| 6 | MYS63 | Epidote skarn from altered granodiorite rock |

Table 11. (Continued)

| Lab. No. | Field No. | Sample Description |
|---|---|---|
| F | MYS64 | Pyroxmangite-rhodorite-orthoclase-quartz skarn with disseminated galena and sphalerite |
| B | MYS65 | Hedenbergite-johannsenite skarn with disseminated sphalerite and trace galena |
| D | MYS66 | Garnet-epidote-pyroxene skarn |
| D | MYS67 | Clinopyroxene-epidote skarn |
| 1 | MYS68 | Clinopyroxene-quartz-feldspar hornfels |

Table 12a. Major oxides (weight percent) from the Continental mine. Compare this table with the tables 10 and 11 for sample description. (N.D. = not determined)

| Oxide \ Sample No. | 3 | 8 | 10 | 11 | 14 | 21 | 23 |
|---|---|---|---|---|---|---|---|
| MgO | 3.7477 | 1.3492 | 2.8917 | 1.833 | 1.621 | 33.435 | 0.517 |
| $Al_2O_3$ | 11.1429 | 4.2314 | 9.8004 | 10.7576 | 1.933 | 0.234 | 0.082 |
| $SiO_2$ | 41.5511 | 36.7253 | 46.3426 | 53.397 | 44.64 | 2.98 | 0.156 |
| $P_2O_5$ | 0.1523 | 0.1485 | 0.2113 | 0.1863 | 0.18 | 0.190 | 0.064 |
| $SO_3$ | 0.6215 | 0.2127 | 1.0306 | 0.6642 | 0.196 | 0.181 | 0.09 |
| $K_2O$ | 0.0744 | 0.0300 | 0.0541 | 0.3711 | N.D. | 0.034 | N.D. |
| CaO | 23.037 | 28.7336 | 19.343 | 16.4146 | 24.52 | 41.005 | 77.96 |
| $TiO_2$ | 0.4061 | 0.2616 | 0.3813 | 0.5117 | 0.138 | 0.017 | N.D. |
| MnO | 0.8013 | 1.0492 | 0.8396 | 0.7012 | 0.63 | 0.334 | 0.157 |
| $Fe_2O_3$ | 17.6604 | 23.8509 | 14.299 | 10.893 | 23.57 | 3.635 | 0.429 |
| $Na_2O$ | 1.0512 | 0.4851 | 1.1185 | 1.739 | 0.202 | 0.62 | 0.283 |
| Total | 100.246 | 97.0780 | 96.3133 | 97.468 | 97.62 | 82.49 | 79.73 |

Table 12b. Major oxides (weight percent) from the New Jersey Zinc mine.

| Oxide \ Sample No. | 30 | 31 | 33 | 35 | 39 | 41 | |
|---|---|---|---|---|---|---|---|
| MgO | 2.515 | 0.104 | 0.79 | 5.184 | 1.35 | N.D. | |
| $Al_2O_3$ | 0.224 | 0.725 | 1.586 | 0.771 | 27.22 | 0.013 | |
| $SiO_2$ | 38.33 | 33.68 | 33.33 | 39.81 | 51.73 | 0.35 | |
| $P_2O_5$ | 0.113 | 0.06 | 0.051 | 0.08 | 0.15 | 0.04 | |
| $SO_3$ | 1.032 | 0.01 | 0.05 | 0.56 | 0.078 | 0.06 | |
| $K_2O$ | 0.0154 | N.D. | 0.02 | 0.02 | 2.36 | N.D. | |
| CaO | 21.22 | 25.88 | 30.54 | 26.62 | 0.62 | 78.92 | |
| $TiO_2$ | 0.009 | 0.012 | 0.033 | 0.016 | 1.5 | N.D. | |
| MnO | 19.43 | 0.75 | 1.46 | 4.05 | 0.05 | 0.23 | |
| $Fe_2O_3$ | 9.77 | 28.83 | 28.4 | 23.08 | 8.63 | 0.29 | |
| $Na_2O$ | 0.51 | 0.943 | 0.99 | 0.5 | 2.28 | 0.28 | |
| Total | 93.15 | 90.99 | 97.23 | 100.69 | 98.108 | 80.21 | |

Table 13. Chemical analyses of [illegible] for sample description.

| Element \ Sample No. | 1 | 2 | 3 | 4 | 5 | 6 | 7 | 8 | 9 | 10 | 11 | 12 |
|---|---|---|---|---|---|---|---|---|---|---|---|---|
| Zn | 36 | 26 | 20 | 12 | 18 | 34 | 16 | 126 | 64 | 54 | 65 | 74 |
| Cu | 2350 | 320 | 2700 | 310 | 233 | 4100 | 710 | 274 | 2200 | 6700 | 3200 | 980 |
| Fe | 8250 | 16100 | 13900 | 7800 | 8600 | 13300 | 12900 | 17200 | 15800 | 16400 | 16900 | 18800 |
| Mn | 107 | 173 | 272 | 187 | 148 | 296 | 125 | 959 | 628 | 330 | 337 | 956 |
| Pb | 13 | 18 | 9 | 8 | 8 | 40 | 9 | 36 | 11 | 17 | 18 | 19 |
| Ni | 24 | 18 | 16 | 12 | 11 | 17 | 32 | 19 | 18 | 20 | 24 | 13 |

| Element \ Sample No. | 13 | 14 | 15 | 16 | 17 | 18 | 19 | 20 | 21 | 22 | 23 | 24 |
|---|---|---|---|---|---|---|---|---|---|---|---|---|
| Zn | 95 | 46 | 21 | 39 | 19 | 48 | 111 | 20 | 5 | 19 | 91 | 201 |
| Cu | 5700 | 310 | 220 | 2800 | 49 | 2200 | 15 | 640 | 6 | 63 | 9 | 1900 |
| Fe | 14600 | 17500 | 6500 | 19700 | 6600 | 34000 | 1200 | 10700 | 100 | 14400 | 200 | 19700 |
| Mn | 459 | 966 | 153 | 598 | 126 | 200 | 1007 | 164 | 322 | 987 | 281 | 548 |
| Pb | 13 | 10 | 7 | 9 | 7 | 12 | 33 | 5 | 34 | 14 | 46 | 13 |
| Ni | 28 | 17 | 4 | 12 | 6 | 48 | 17 | 21 | 17 | 8 | 23 | 11 |

Table 13. (continued)

| Element \ Sample No. | 25 | 26 | 27 | 28 | 29 | 30 | 31 | 32 | 33 | 34 | 35 | 36 |
|---|---|---|---|---|---|---|---|---|---|---|---|---|
| Zn | 24 | 30 | 9 | 12 | 48 | 10400 | 16 | 84 | 12 | 6 | 7300 | 6300 |
| Cu | 180 | 17 | 6 | 69 | 5 | 24 | 5 | 6 | 6 | 4 | 7 | 78 |
| Fe | 20800 | 1800 | 400 | 6300 | 12100 | 4400 | 14700 | 26600 | 8200 | 300 | 6900 | 4300 |
| Mn | 193 | 65 | 62 | 126 | 995 | 41000 | 818 | 161 | 2210 | 54 | 11600 | 9800 |
| Pb | 12 | 31 | 43 | 14 | 12 | 7400 | 9 | 8 | 8 | 44 | 23 | 1900 |
| Ni | 42 | 22 | 21 | 5 | 4 | 6 | 4 | 43 | 7 | 23 | 7 | 3 |

| Element \ Sample No. | 37 | 38 | 39 | 40 | 41 | 42 | 43 | 44 | 45 | 46 | 47 | 48 |
|---|---|---|---|---|---|---|---|---|---|---|---|---|
| Zn | 400 | 146 | 127 | 33000 | 55 | 7700 | 1200 | 325 | 193 | 81 | 18400 | 6400 |
| Cu | 15 | 47 | 110 | 164 | 4 | 286 | 178 | 181 | 46 | 116 | 257 | 273 |
| Fe | 6000 | 7100 | 14400 | 6700 | 300 | 7300 | 8200 | 16300 | 38900 | 12100 | 4700 | 6200 |
| Mn | 1890 | 685 | 1960 | 20200 | 291 | 657 | 1295 | 1440 | 1077 | 679 | 19900 | 9200 |
| Pb | 18 | 25 | 16 | 5400 | 47 | 12 | 56 | 7 | 5 | 19 | 9600 | 258 |
| Ni | 13 | 10 | 10 | 9 | 24 | 6 | 25 | 16 | 11 | 9 | 8 | 4 |

accompanied by high concentrations of zinc and lead.

## METALLIZATION

The ore mineralization in the skarns of the Hanover-Fierro area may be classified in two major stages: (1) companion ores developed at the end of the alkaline stage as products of the ore-forming process and a joint action of the skarnization and (2) the imposed ores formed by metasomatic replacement in the previously formed calc-silicates. This stage of mineralization was accompanied by early stages of greisenization. The mechanism of ore mineralization at this stage is based mainly on the following: (1) the solubility of skarn silicates in acid solutions, and (2) decrease in the solubility of ore minerals.

### Primary Hypogene Mineralization

The primary ore minerals found in the skarn are: pyrrhotite, specularite, magnetite, pyrite, sphalerite, chalcopyrite, molybdenite, galena, bornite and chalcocite, roughly in that paragenetic order.

A brief description for each mineral is given in the following pages. For detailed information, including a paragenesis diagram, the reader is referred to the M.Sc. thesis by the writer (1977).

Pyrrhotite

Pyrrhotite is the least abundant sulfide mineral in the Continental mine. It is found disseminated in the serpentinized forsterite. A sample from the magnesian skarn at the southwest edge of the Continental pit in the Barringer fault zone, shows fairly abundant pyrrhotite mineralization. It appears brownish yellow with relatively high reflectivity. Pyrrhotite is associated with specularite, chalcopyrite, magnetite and pyrite. Commonly the pyrrhotite has been replaced by specularite and rimmed by chalcopyrite (Figure 52). This indicates the earlier crystallization of pyrrhotite.

High-temperature pyrrhotite (above 300°C, Ramdohr, 1969, p. 582) forms hexagonal crystals. Since pyrrhotite at the Continental mine forms in fault zones close to the intrusive contact, the temperature must have been very high and hexagonal pyrrhotite crystals can be expected. Fine-grained exsolved pyrite is common in pyrrhotite and possibly formed due to the following processes: At very high-temperature, pyrrhotite was able to dissolve high quantities of S and exsolved pyrite upon cooling.

Specularite

Specularite is minor iron-oxide in the Continental mine where observation of its paragenetic relations with

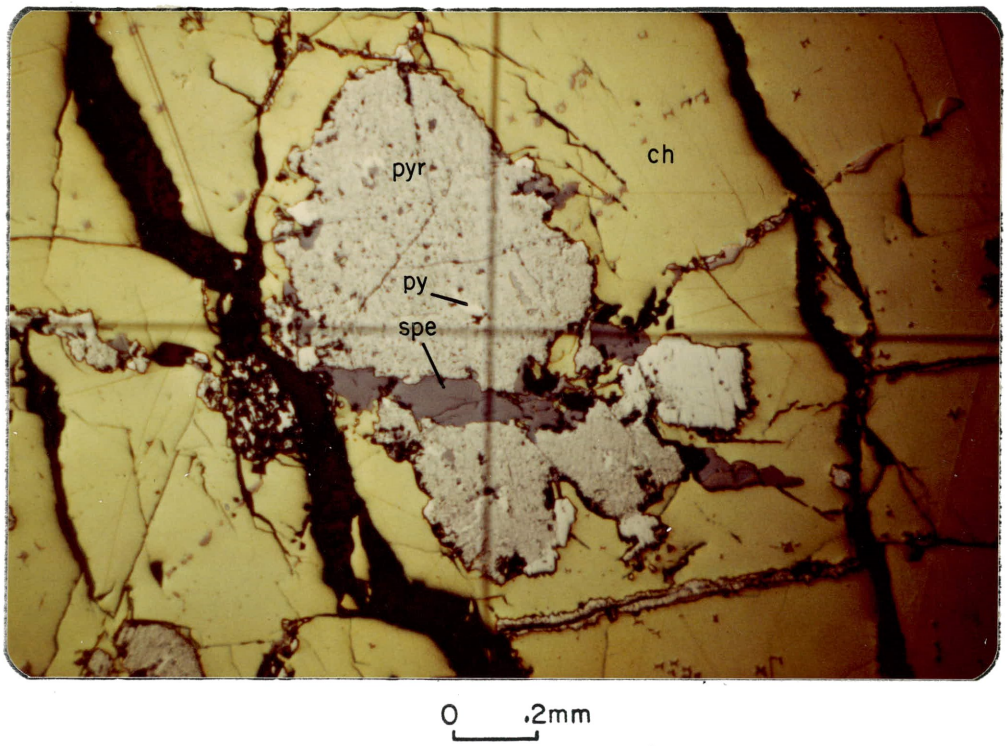


Figure 52. Pyrrhotite (pyr) is cut by specularite (spe) vein, and rimmed by chalcopyrite (ch). Note the pyrite (py) exsolved from pyrrhotite. Reflected light.

other ore minerals lead one to interpret the formation of specularite as having continued from the earliest stage of ore mineralization to the end. Where specularite is associated with sphalerite, strong embayment of specularite by sphalerite represents crystallization of specularite preceding that of sphalerite (Figure 53).

Magnetite

Magnetite is the only iron oxide in abundance in the study area. It occurs as massive ore interbedded with serpentine and magnesite in magnesian skarn and as disseminated deposits in the garnet of limy skarn. Over most of the area, magnetite was replaced by serpentine. The earliest coarse-grained magnetite formed prior to sepentinization of forsterite. The finer-grained magnetite is related to the period of serpentine deposition. However, serpentinization continued to form beyond the last stage of magnetite mineralization.

Although magnetite appears in the skarn almost everywhere, its abundance is controlled by temperature and fractures. Abundance decreases away from the intrusive contact and outward from the fractured zones.

Pyrite

Pyrite was deposited throughout the entire period of

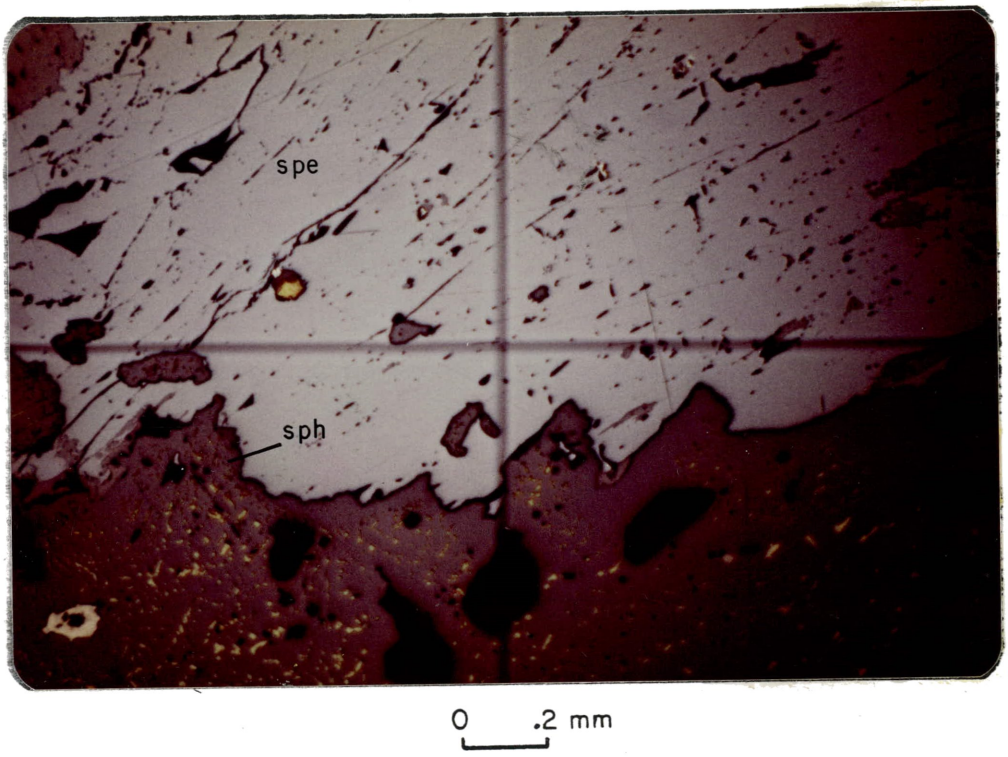


Figure 53. Specularite (spe) embayed by sphalerite (sph). Note exsolved chalcopyrite (yellow) in sphalerite. The dark minerals are dolomitic marble. Reflected light.

mineralization. The earliest pyrite formed as intergrowths with specular hematite. It is widespread in the skarn zone and in the adjacent upper Cretaceous Beartooth Quartzite and Colorado Formation. In the Hanover area pyrite is formed in hedenbergite and associates with sphalerite and ilvaite. Polished section studies show pyrite replaced by chalcopyrite along crystallographic planes. In most occurrences pyrite and chalcopyrite are associated together.

Sphalerite

Sphalerite shows a strong tendency for replacement in the garnet-marble zone of the Hanover Limestone at the Continental mine. It is commonly associated with chalcopyrite which has replaced pyrite and magnetite. Most of the sphalerite in the Continental mine is iron-rich and very black in hand specimen. This variety of sphalerite, mineralogically is called marmatite or christophite. Some sphalerite away from the contact of the intrusive is found as fracture filling and appears greenish, which is due to lower iron and higher zinc content.

The iron-rich sphalerite forms at higher temperatures. Most high-temperature sphalerites are associated with chalcopyrite and contain blebs of chalcopyrite. Oriented intergrowths of sphalerite and chalcopyrite are common in the Continental mine orebodies. This is possibly due

to solid solution at elevated temperatures and exsolution during falling temperatures (Ramdohr, 1969). Figures 54 and 55 represent several cases of sphalerite and chalcopyrite intergrowths as a result of solid solution and exsolution.

Figure 54 represents two stages of chalcopyrite and sphalerite crystallization. One is the exsolution texture showing exsolved particles of chalcopyrite from sphalerite, and the other is replacement of sphalerite by chalcopyrite along grain boundary. In the skarns around the southern margin of the stock, sphalerite always occurs in hedenbergite zone, at the contact of hedenbergite-garnet and hedenbergite marble zone. It is usually associated with low-grade galena. Disseminated chalcopyrite occasionally occurs with sphalerite. Intense galena mineralization accompanying sphalerite occurs in pyroxmangite and johannsenite skarns.

Chalcopyrite

Chalcopyrite, the major copper ore mineral, is present both as a disseminated crystal and as massive fracture fillings. It replaces garnet (Figure 56) and garnet-clinopyroxene with lesser amounts associated with sphalerite replacing marble. Considerable chalcopyrite has replaced specularite and massive magnetite in the magnesian

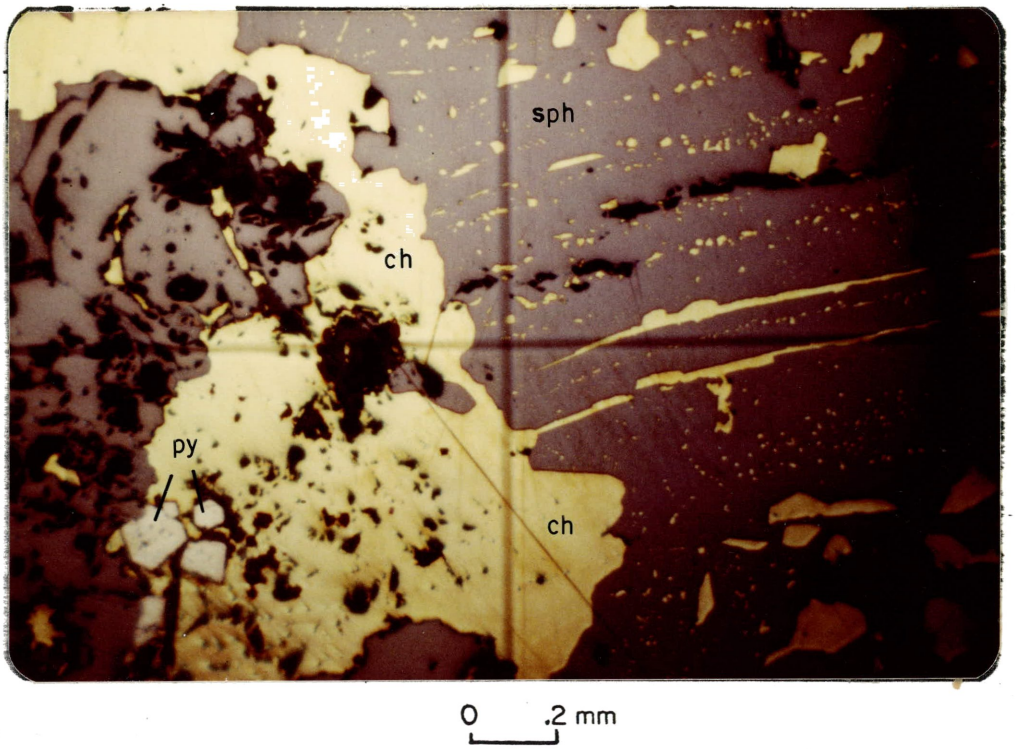


Figure 54. Chalcopyrite (ch) is embedded in sphalerite (sph) in the form of minute grains and blebs parallel to the cleavage of sphalerite. The white mineral is pyrite (py) replaced by chalcopyrite and sphalerite. Reflected light.

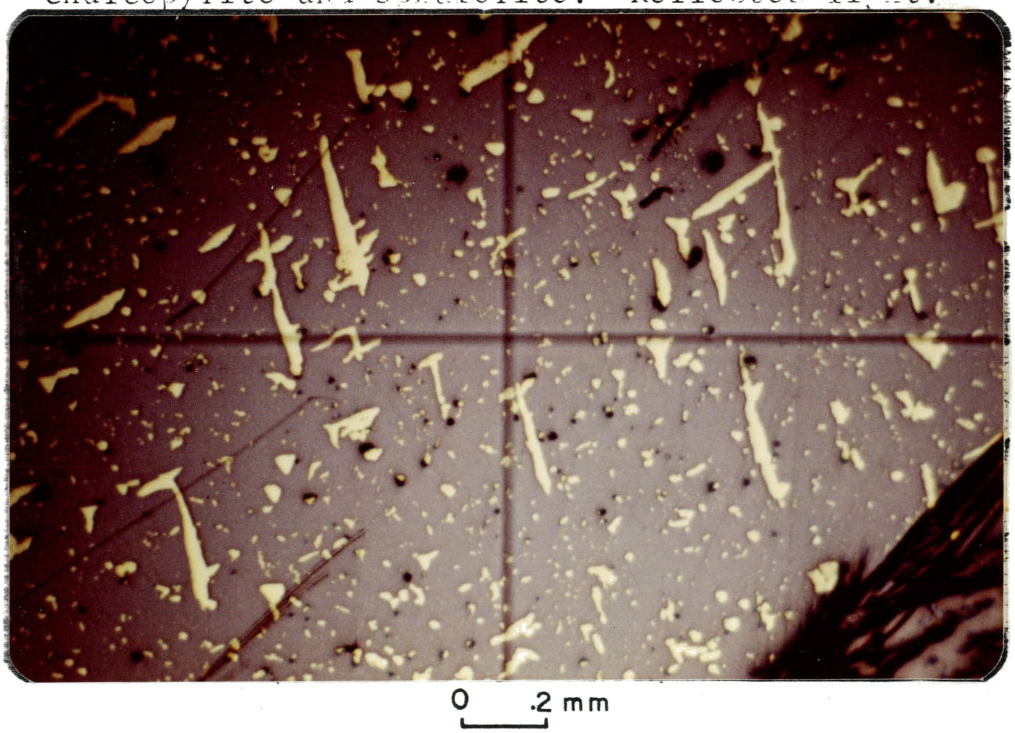


Figure 55. Chalcopyrite exsolution bodies (yellow), evenly distributed in sphalerite (gray). Reflected light.

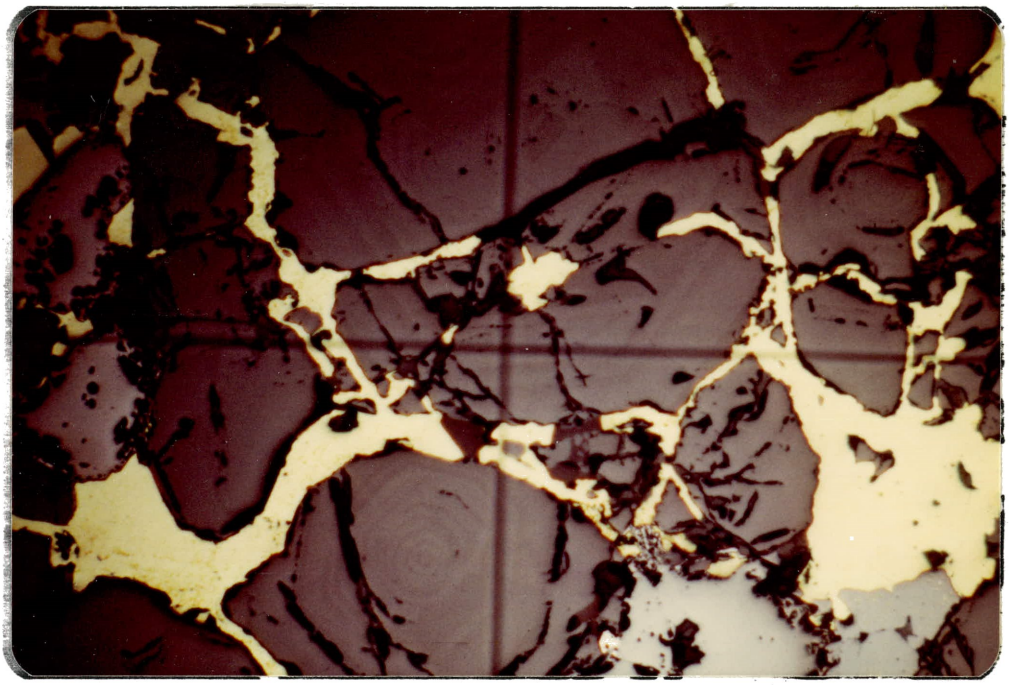


Figure 56. Chalcopyrite (yellow) replacing garnet (dark area) along grain boundaries. Reflected light.

skarns in some of the orebodies. Disseminated chalcopyrite has been observed in serpentine of magnesian skarn. Disseminated chalcopyrite in serpentine may indicate chalcopyrite was deposited before serpentinization of the forsterite. Deposition of chalcopyrite outside the major orebodies is strongly controlled by fracture and fissure systems.

The garnet of the hornfels zone in the upper part of the Syrena and Abo Formations is characterized by veinlets of fine-grained chalcopyrite commonly associated with disseminated bornite. The small size of the chalcopyrite grains probably is due to the low-temperature at the time of deposition.

Molybdenite

Molybdenite was found in the mafic igneous dikes and sills which intrude Paleozoic and Cretaceous metasediments and very minor amounts were found along fractures in skarn. The most favorable host rock is a diorite dike which has intruded the Fusselman dolomite; a second favorable host is the hornblende andesitic sills which intruded the Colorado Shale. These igneous rocks have been altered by the subsequent intrusion of the Hanover-Fierro stock. The diorite dike is locally

garnetized and has molybdenite mineralization along the fracture and joint planes. Elsewhere in the Continental mine, a trace of molybdenite was observed at the innermost part of the fracture zone.

No close association of molybdenite was observed with the other sulfides. Therefore, age relationships have not yet been determined. It may have formed during a relatively long interval of mineralization.

Bornite

Bornite occurs primarily as a primary hypogene copper sulfide in fracture and fissure systems. It very often occurs with pyrite and chalcopyrite and shows a color range from blue, green, greenish-blue, red to reddish-brown, and very commonly, pinkish. Several samples from different places showed bornite coating chalcopyrite and other sulfides. Pyrite is the most abundant sulfide present with the bornite. Only trace amounts of bornite occur as stringers cutting massive microbrecciated garnet and other silicates.

Chalcocite and digenite

Chalcocite and traces of digenite are the only other primary hypogene copper sulfides present in the Continental mine. Like bornite, significant amounts of chalcocite

were formed in fractures and along fault zones. Very rich chalcocite veins were observed in several fault zones throughout the Syrena, Abo, and Colorado Formations. Most of these veins are hydrothermal and the chalcocite is interbanded with quartz and pyrite in veins. The boundaries between the different veins are very sharp. Some quartz veins are cut by chalcocite. Occasionally there is some disseminated bornite in chalcocite, and very commonly chalcocite is coated with malachite. The hypogene solution containing chalcocite probably was formed above 78°C (Ramdohr, 1969, p. 438).

Chalcocite is very rarely present with digenite. They are disseminated in chrysocolla and malachite.

The other sulfides which have not yet been investigated are covellite and tetrahedrite. They may be present in the Continental mine as well.

Intensive galena mineralization occurs in a brecciated granitic dike, exposed to the northwest wall of the Continental pit. Trace amounts of molybdenite accompanies galena.

Supergene Enrichment

The presence of chrysocolla, malachite, azurite, native copper, tenorite, smithsonite, pyrolusite, chalcanthite,

epsomite, limonite, minor earthy hematite, montmorillonite, gypsum, and traces of chalcocite and bornite is characteristic of the secondary enrichment at the Continental and New Jersey Zinc mines. The following conditions were favorable for supergene enrichment.

(a) Copper occurred at higher levels in the Colorado Formation, probably as fissure and fracture filling. Most of the fracture and shear zones project down to the present pit level (Plate 1).

(b) The presence of carbonate either in the form of dissolved carbon dioxide in water or as carbonate rocks supplied the carbonate ion for the formation of malachite, azurite and smithsonite. The presence of these hydrous carbonates is the evidence of downward flow of impregnated solution. Chrysocolla, chalcanthite and epsomite also formed by this process.

(c) Abundant pyrite in fractures in the Colorado Formation, Beartooth Quartzite, Abo and Syrena Formations provided the sulfur for the formation of acids which dissolved the copper and other sulfides (in chemical weathering processes the metal ions go into solution, the oxidizing waters convert sulfide to a sulfate ion, and produce a

relatively acidic solution).

(d) Groundwater carried the copper to a considerable depth in the meteoric system.

Chrysocolla, malachite and azurite

Green to blue-green chrysocolla occurs in quite rich concentrations in crosscutting fractures and joints on the south side of the Continental pit. It is commonly associated with blebs and bands of malachite, disseminated chalcocite, and traces of disseminated digenite. Malachite and chrysocolla are the most common secondary ore minerals present in the Continental mine. Azurite is present filling small fractures and replacing primary copper sulfides.

Hematite and limonite

These two iron oxides are present as secondary concentrations along fault and shear zones in the upper benches of the present pit and elsewhere in the old pit sites.

Native copper

Native copper was observed as a very bright reddish material in the quartz monzonite breccia. The genesis of the native copper is not yet clear. Originally it may have been precipitated from hydrothermal solution as a result of oxidizing conditions, but it may have been secondary in origin.

Chalcocite, bornite and tenorite

Trace amounts of chalcocite and bornite may have formed as a result of supergene enrichment. Tenorite was observed in several samples from the Continental mine replaced primary sulfides.

Chalcanthite, epsomite, gypsum and montmorillonite

Chalcanthite and epsomite occur in the mine walls. Strong development of the two minerals was observed in the fault zone in both the underground and the open pit mines.

Abundant gypsum or selenite and montmorillonite occur along the Barringer fault zone where they are believed to be deposited from meteoric waters. These sulfates may have formed over a long period of time. In the Barringer fault zone gypsum is associated with silica, iron oxide, and clay minerals. Formation of associated minerals is likewise related to precipitation from subsurface water which caused cementation and hardening of altered rocks and fault materials, and produced surface silicification and oxidation.

Smithsonite and pyrolusite

Weathering and oxidation of sphalerite and manganese-bearing minerals in the Hanover area have produced a rela-

tively large variety of secondary minerals. Smithsonite in various colors is the most common supergene mineral. Abundant pyrolusite was found along with other oxides.

## SUMMARY AND CONCLUSIONS

The information presented in this investigation not only provides a better understanding of the genesis of skarn deposits, but also defines the most important geologic features and geochemical criteria that can be used in the search and evaluation of such deposits in a similar area.

### Structure

Most faults in the study area are of the high-angle normal type. Major fault zones comprise a network of subparallel faults which form a series of fault blocks and slivers. Fracture planes have been filled, in whole or in part, by from one to more than eight generations of greisen material.

Fractures and faults at the Continental mine and adjacent area provided the opportunity for infiltration of solutions. The intensity of metasomatism under such conditions is greater in more intensely fractured and brecciated rocks. The skarn rocks developed in the area are believed to have had much greater permeability than the enclosing

rocks. The ore deposits also are developed for the most part along bedding plane and near fractures by replacing skarn minerals. These features led the writer to suggest that the metasomatic replacement of rocks developed under conditions of maximum permeability of the country rocks. This permeability was greatly facilitated by the development of fault and fracture zones and of the breccias associated with such features. The intensity and statistical analysis of fractures are presented in Chapter 2 of this investigation, under the engineering section.

Skarnization is a process of decarbonatization. If carbon dioxide is retained in the system at the time of formation of skarn minerals, the $CO_2$ pressure gradually increases and reaches a condition where grandite garnet is no longer stable (Shoji, 1970 and 1975). This condition is not favorable for the formation of skarn. Since the grandite garnets are the most common skarn minerals in the area studied, the intensive fracture systems in this region served not only as channelways for solutions during metasomatism, but also the pathways for the release of excess carbon dioxide.

The relative competence of various rock units played an important role in the localization of skarn and ore minerals. Competent units deformed by fracturing, while

incompetent ones deformed mainly by plastic deformation and recrystallization. For example, marble units are essentially unmineralized, and show strong recrystallization effects. In contrast, garnet-skarn which is the only host rock for economic mineralization at the Continental mine is intensively deformed by microfractures which are visible only under a microscope. Fracturing in more competent rocks such as clinopyroxene-quartz-feldspar hornfels is different from that in garnet skarn. The hornfels always tends to form clean breaks rather than breccia.

The diffusional skarns of the Hanover-Fierro region show a close association in time and space with the intensively deformed zone at the contact with the sedimentary rock and the granodiorite stock.

Both magnesian and limy skarns, in fact, formed during tectonic deformation. The bimetasomatic skarns are localized in the zone of complex plastic deformation. The contact-infiltrational skarn are localized in fractured rocks.

Generally, the silicate minerals of high-temperature stage and ore minerals of lower-temperature stage were formed under high-stress conditions characterized by continuous renewal of shear-fractures accompanied by a long period of multistage mineralization.

Generally speaking, the skarn formation may be classified into two stages. The early stage is related to the formation of magnesian skarns associated with magnetite. The second stage, formation of limy skarn , followed the first one and partially overlapped it. Magnesian skarns are genetically classified into two groups: (1) high-temperature stage, characterized by alkaline composition of solutions, and (2) low-temperature stage formed in a more acidic solution.

Formation of limy skarns occurs under different regimes of the mobile constituents. Zharikov (1970) pointed out that the differences in skarnization conditions are recognized first by the alkali regime of the skarnizing solutions.

Considerable variation in the regimes of magnesium, manganese and iron of the entirely mobile constituents are characteristic aspects of limy skarns. The increase in iron content in limy skarn facies depends on the magnitudes of chemical potential of Mn, Mg, and Fe. Like the alkaline facies, the entities of iron facies differ among themselves at various temperatures. Korzhinskii (1970) mentioned that the paragenesis in limy skarns is significantly influenced by chemical potentials of magnesium and iron in the most common case.

There are four iron facies recognized in the skarns of the studied area: (1) wollastonitic, (2) diopsidic-salitic, (3) hedenbergetic, and (4) andraditic. The lower-temperature types of limy skarns are characterized by the absence of wollastonite and presence of pyroxmangite, followed by epidote and amphiboles skarns.

As far as the age relationships of skarnal facies are concerned, the following features are considered: the activity and chemical potential of iron increase progressively during skarnization. As a result, the iron content of skarn minerals increases and more ferruginous minerals succeed the low-iron ones. The progressive increase in the amount of iron in skarnal facies is believed to be the result of progressively increasing acidity of skarnizing solutions. This interpretation is based on the development of andradite garnet in skarns in the terminal stages of the process.

The replacement of carbonate rocks was accompanied by introduction of all constituents except for calcium and carbon dioxide. The mode of introduction of materials is varied. Silica, iron, magnesium, manganese and other components were brought in by the magmatic solutions originated from the granodiorite stock.

Silica is an introduced constituent in the majority

of cases, but in the original silty and cherty carbonate rocks, the silica was supplied at least in part by the parent rocks.

Calcium was contributed by limestone and dolomitic limestone.

Carbon dioxide was removed from the system.

Iron was introduced from the granodiorite stock.

Alumina was mainly redistributed in the shale units and went into formation of epidote and grossularite garnet. During postmagmatic alteration (greisenization) alumina was largely contributed by solutions.

Manganese was introduced from the stock. Development of iron-rich and manganese-bearing pyroxene around the southern margin of the stock may indicate that the equigranular facies of the stock was higher in manganese and iron.

Metallic Mineralization

It is believed that the mineralized solution of low-temperature alteration originated from a deep-seated source were responsible for the ore formations.

The early stage of ore mineralization was developed at the end of the alkaline stage. The ore forming process was accompanied by increasing acidity of the solutions. Korzhinskii (1970) and Zharikov (1970) have mentioned that

increasing acidity of the solutions provides cation replacement reactions in which the weaker cations ($Fe^{+2}$, $Fe^{+3}$, $Zn^{+2}$, $Pb^{+2}$ and others) take the place of the stronger ones ($Ca^{+2}$, $Mg^{+2}$, etc.).

The early-stage magnetite was accompanied by the formation of forsterite, but the highest grade magnetite was formed during the postmagmatic stage. The latter stage of magnetite mineralization during lower-temperature alteration was formed simultaneously with the formation of pyroxene, garnet, amphiboles and epidote veins. This was possibly accompanied by serpentinization of forsterite in the magnesian skarn.

Sulfide mineralization was the last of the ore-forming processes. As acidity of magmatic solutions increases, skarnization is succeeded by the deposition of magnetites and then by the formation of sulfide ores. Based on the experimental data by various authors, the temperature range of the sulfides following the alkaline stage may be estimated as $500^{o}C$, but most deposits formed between $250^{o}$ to $500^{o}C$. Magnetite usually forms in a wide temperature range which starts from early stages of high-temperature alteration and is continuous to the last stage of low-temperature processes.

The formation of imposed ore is accompanied by

greisenization. Based on Zharikov's (1970) interpretation, the processes of ore mineralization at this stage is based mainly on the following: (1) the solubility of skarn silicates in acid solution, and (2) decrease in the solubility of ore minerals.

He also mentioned that formation of massive magnetite and sulfides is possibly due to high-pressure crystallization of the ore minerals at the replacement front of the skarn. During ore formations, as the acid front passes, acidity of the solutions decreases and precipitation of the ore-forming and rock-forming minerals begins in the sequence of their increasing basicity.

Hydrothermal solutions act as buffers. Generation of $H^+$ by the oxidation of $H_2S$, $CH_4$ and $H_S^-$ becomes buffered by internal ore-fluid equilibria and wall-rock alteration. Toward the end of the ore mineralization, when the solution is fairly depleted of buffering material, the system becomes low in pH and calcite could dissolve. Later fluids somehow become more alkaline as calcite intensively forms in veins.

The following are the skarnal facies of ore minerals present in the Hanover-Fierro area:

1. Magnetite in magnesian skarn.
2. Magnetite in limy skarn (northern area).

3. Magnetite-specularite-pyrrhotite-pyrite-chalcopyrite in magnesian skarn.
4. Magnetite-specularite-sphalerite-chalcopyrite-pyrite-bornite in limy skarn (garnet and garnet-marble rock in the northern area).
5. Molybdenite in limy skarn (northern area).
6. Sphalerite in limy skarn (manganhedenbergite in the southern area).
7. Sphalerite-galena in limy skarn (manganhedenbergite and pyroxmangite in the southern area).
8. Sphalerite-galena-chalcopyrite-pyrrhotite in limy skarn (manganhedenbergite-pyroxmangite-garnet-marble in the southern area).
9. Sphalerite-magnetite (trace amounts) in limy skarn in the southern area.
10. Pyrite-sphalerite in limy skarn (ilvaite-hedenbergite).

Greisenization

Intensive distribution of veins of feldspar, quartz, calcite, epidote, amphibole and opaque minerals is a characteristic feature of greisenization. The initial stage of greisenization involved increasing acidic leaching accompanied by monomineral metasomatic formation.

Greisenization at the Continental mine is characterized by stockworks formed along a dense network of small scale

fractures. Although the introduction of metallic minerals during greisenization occurred toward the end of the system, the whole process was continued through a long period of time which began with crystallization first of silicates followed by opaque minerals and ended with the emplacement of post-mineralization quartz, feldspar, calcite, zeolite and chalcedony veins. The following assemblages are characteristic features of greisenization at the Continental mine: (1) amphiboles-epidote-quartz veins, (2) quartz-orthoclase-calcite veins, (3) epidote-magnetite-sulfide veins, (4) chlorite-quartz-calcite veins, (5) pyrite-quartz-chalcocite veins, (6) comb quartz-calcite veins, (7) calcite veins, (8) quartz-calcite-zeolite veins, (9) chalcedony veins and (10) dolomite veins.

Structural Control of Ore Deposits

The ore bodies in the Hanover-Fierro area are clearly a result of hypogene replacement of skarn minerals. The deposits are generally localized around the margin of the granodiorite stock and are strongly controlled by fractures. Distribution of mineralization is related not only to the distance from the intrusive and the intensity of hydrothermal solutions in the adjacent rocks, but also to the kind and amount of fracturing, the composition and permeability of the skarn. The preferred site for primary ore

deposition appears to have been within the skarn rocks along disconformable surfaces between formations. The most mineralized parts of the metasedimentary rocks are the Montoya-Fusselman Dolomite, the Lake Valley Limestone and the Oswaldo Formation. Three types of skarn minerals within these horizons are of particular interest from the exploration point of view: (1) the grandite garnets around the northern and northwestern margins of the granodiorite stock are the only important hosts to copper, iron and zinc ores, (2) the magnesian skarn on the northwest, west and northeast margins of the stock hosts the major magnetite orebodies, and (3) the manganhedenbergite and garnet skarns around the southern margin of the stock are basically the only important hosts for the zinc ore in that sector.

The close association of manganese with sphalerite and galena leads one to suggest that the Mn plays the determining role in the precipitation of zinc and lead ores. The transition between manganhedenbergite-garnet, manganhedenbergite-marble, and garnet-marble zones are again the preferred horizons of the zinc and lead mineralization at the New Jersey Zinc mine and other prospects around the southern margin of the stock (Figure 57).

The hornfels-type skarns that occur in the calcareous

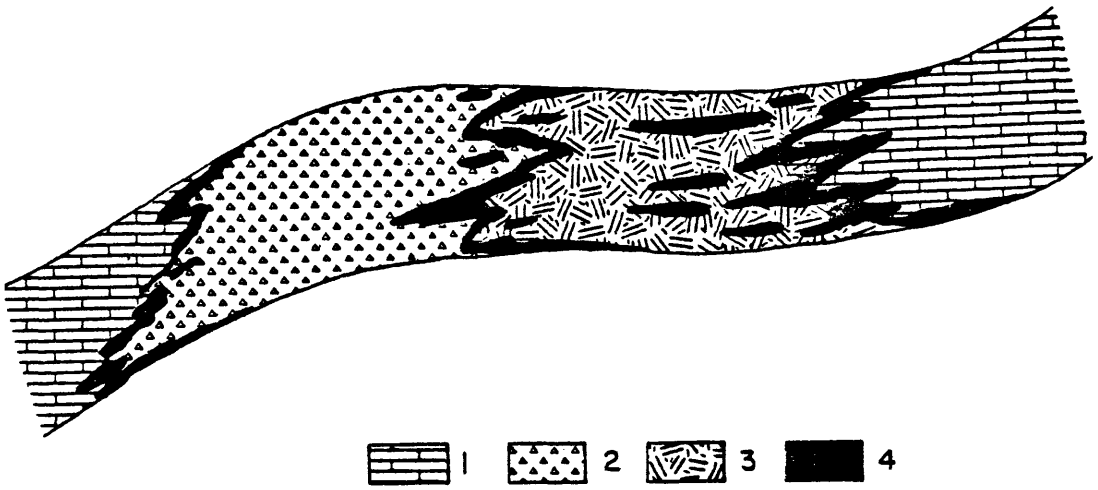


1. Marble
2. Garnet
3. Manganhedenbergite
4. Sphalerite

Figure 57. Generalized diagram showing location of zinc ore with respect to skarnal facies in the New Jersey Zinc mine.

shale and shaly limestone of the upper part of the Oswaldo Formation, Syrena and Abo Formations are believed to be partly aluminous and much more insoluble than the brecciated garnets in the more pure limestone of the lower Oswaldo Formation and the Lake Valley Limestone. The sulfide mineralization is restricted primarily to the silicate horizons which have the most solubility under the prevailing conditions. Wherever these silicates have been faulted and fractured, the intensity of mineralization is higher. Since the high-grade chalcopyrite mineralization favors a high-temperature zone of deposition, higher-grade copper deposits may occur deeper in the Continental underground mine.

An especially extensive deposit may exist to the southwest and west of the present Continental pit and in the area underlying Hermosa Mountain, judging from the mineralized fractures and the wide distribution of hypogene and supergene mineralization associated with the Barringer fault zone. A similar target is evident in the area underlying Hanover Mountain where a high-grade copper deposit was recently discovered.

# GEOTECHNICAL EVALUATION OF PIT SLOPE STABILITY AT THE CONTINENTAL MINE, FIERRO, NEW MEXICO

## INTRODUCTION

A simple, specific set of rules for achieving slope stability in open-pit mines is impossible to devise precisely. Each pit is located in a different environment of geologic structure and generally has its own unique mining programs. It must be assumed that, in each individual pit-slope design the value of capability in rock-slope design and stability of existing slopes cannot be compromised and the level of confidence in such investigations is not a hundred percent. This value can be obtained by using currently acceptable slope-mechanics fundamentals.

Essentially two groups of theories exist for calculation of stability: (a) zone failure or plastic flow theories which assume that material is in a state of failure at all points within the sliding mass, (b) line failure theories which assume that failure takes place by shear along a surface of planar or cylindrical shape. Such plane shear failures along rock discontinuities (faults and joints) are the most probable for the Continental pit, and calculations must recognize this mechanism if they

are to be meaningful.

During the past few years, there has been a universal acceptance of two fundamentals of rock-slope mechanics: (a) discontinuities control stability, and (b) failure criterion. Muller, 1964, presented an analysis of these conditions. Recognizing the Muller concepts, and their interdependency, there are two fundamental slope problems: (1) how to model the discontinuities, and (2) how to model the failure mechanics of the systems. Because of the complexity of these problems, the precise solutions are not available. Nevertheless, practical solutions which have been applied, permit slope mechanics to operate with a useful degree of confidence. Indeed, the concept of practical solutions in analysis of stability introduce the fact that slope mechanics is a science greatly dependent on the skill and perception of the investigators and the collection of all available pertinent data.

In Spring 1978, the Continental Mine mapping was studied by the writer and a quantity of applicable geologic data was collected in order to establish the geologic features that are critical in the evaluation of slope stability. The objective of this research was to obtain efficient and safe pit slopes and to refine the design process effecting slope stability.

## Physiography of the Continental Mine and Surrounding Area

The Continental mine of the UV Industries is a relatively small work-out open pit and underground mine operated by the company since 1968. The pit is cut in skarn rocks with three major fracture sets. It is roughly ellipsoid, 320 ft deep, with the major axis of 3000 ft and minor axis of 2000 ft, and with 40- and 50-degrees working slopes (see figures 58 and 59). An overall view of the pit is shown in figure 122.

The general environment can be classified as semi-arid. Based on the structural complexity, it is difficult to identify the exact groundwater table, but it often occurs at a depth of approximately 50-100 ft. Recharge is relatively slow. The higher groundwater level follows intensive rainfall during late July, August, and September. The presence of intensive fractures and underground workings have drained out most of the pit walls. Temperatures vary from winter lows of $20^{o}F$ to summer highs of $99^{o}F$.

## Role of Stability in Economic and Planning Consideration

The modern trend in mining appears to favor increasingly larger and deeper open-pits. Slope stability engineering is a practical design tool which can be used in the daily planning and operation of an open-pit mine.

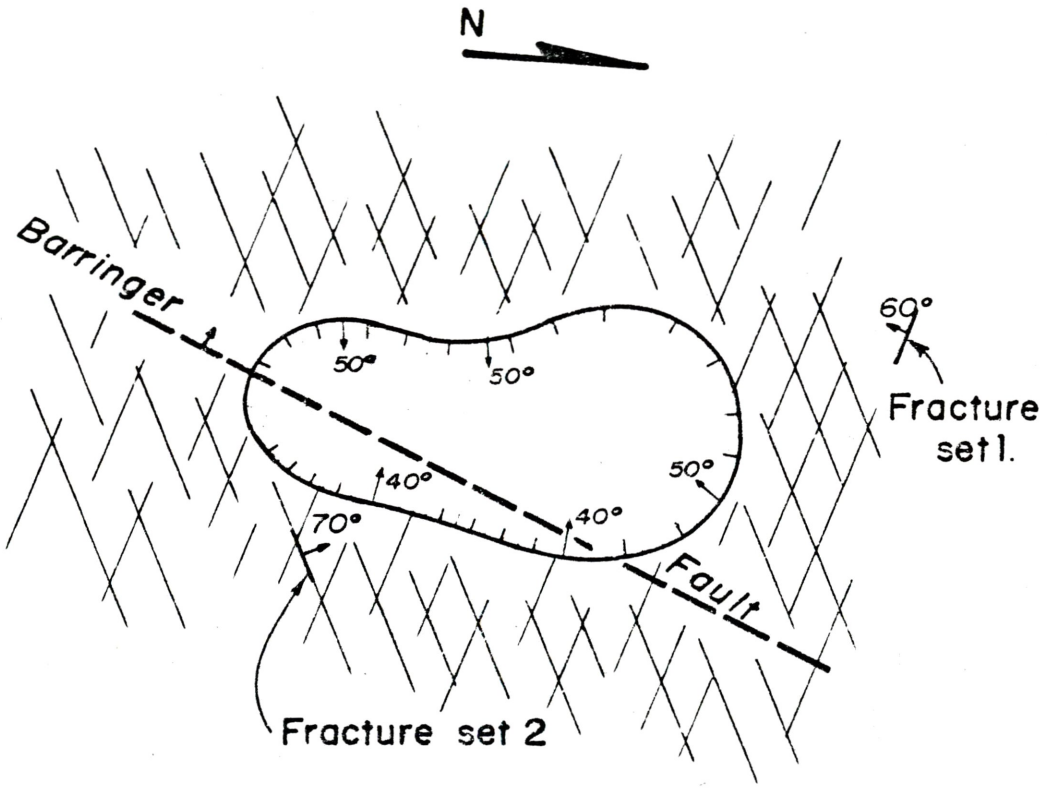


Figure 58. The Continental pit cut in rock with three major fracture sets.

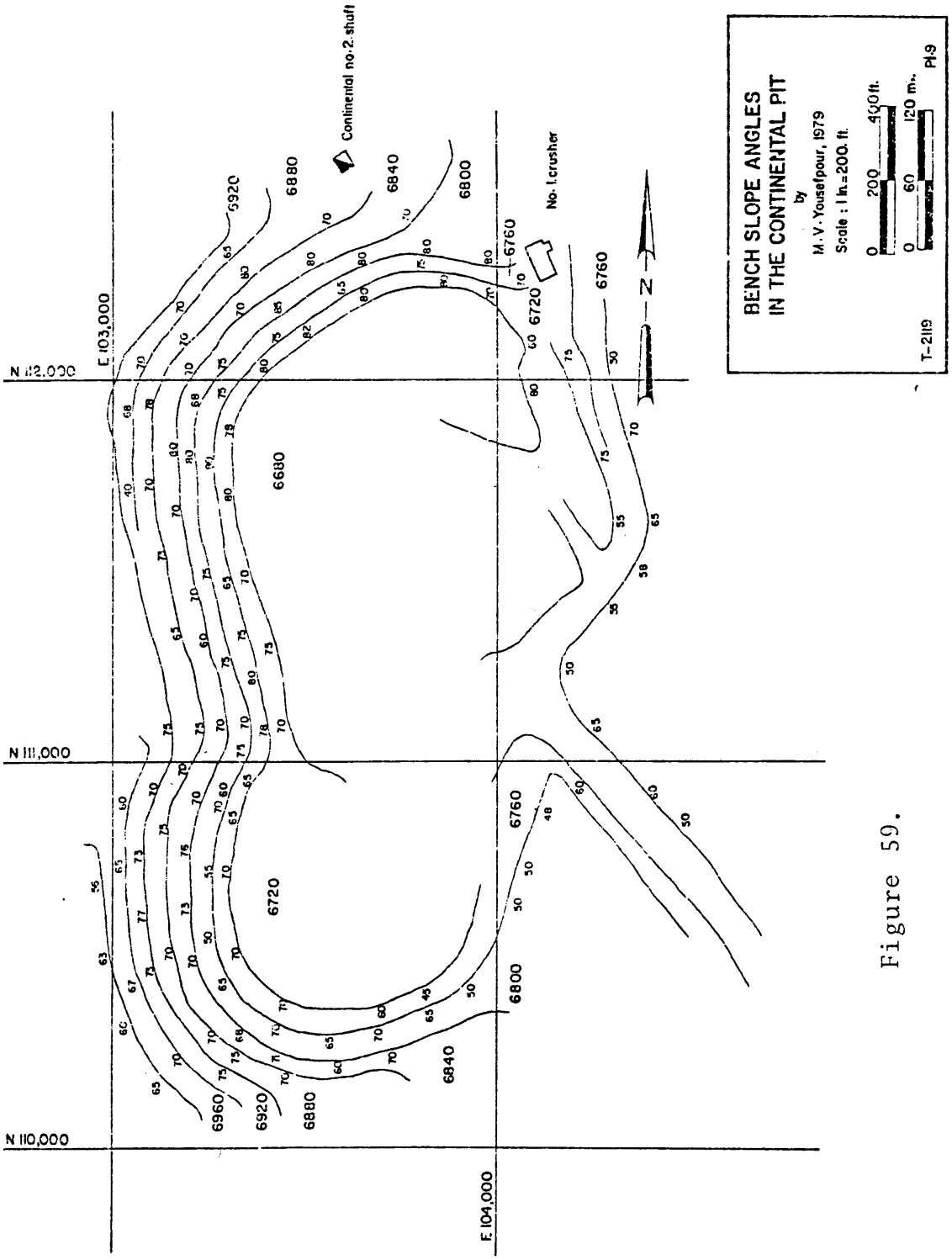
BENCH SLOPE ANGLES
IN THE CONTINENTAL PIT
by
M. V. Yousefpour, 1979
Scale : 1 in.=200. ft.
0 200 400ft.
0 60 120 m.
T-2119
Pl.9
Continental no.2 shaft
No. 1 crusher
N
E 103,000
E 104,000
N 112,000
N 111,000
N 110,000
6960
6920
6880
6840
6800
6760
6720
6680

Figure 59.

The principal aims of slope stability investigation are: 1) to improve the mining economics, and 2) to provide a safe operation.

The ultimate depth of a pit is a function of the slope angles which can be maintained for the life of the pit. The steeper the slope angle, the smaller the volume of overburden removed and the more favorable the economics. It is important to consider that this slope must also be secure against failure. The flatter the slope angle, the more secure against failure and the safer it will be (see Figure 60).

The cost of a totally stable slope is very high. However, a slope failure can be disastrous to life, damage machinery, and affect the economy by considerable volume of waste material to be removed.

A satisfactory compromise between these two conflicting requirements must be found in order to provide both economical and safe mining operations. In general, slope stability plays a minor part in daily operation, but it is the planning of the ultimate pit which is considered as a major role. This implies the complication of a time factor in slope stability analyses which should be correlated to the working life of the pit.

An optimum slope may have failures. Therefore, this

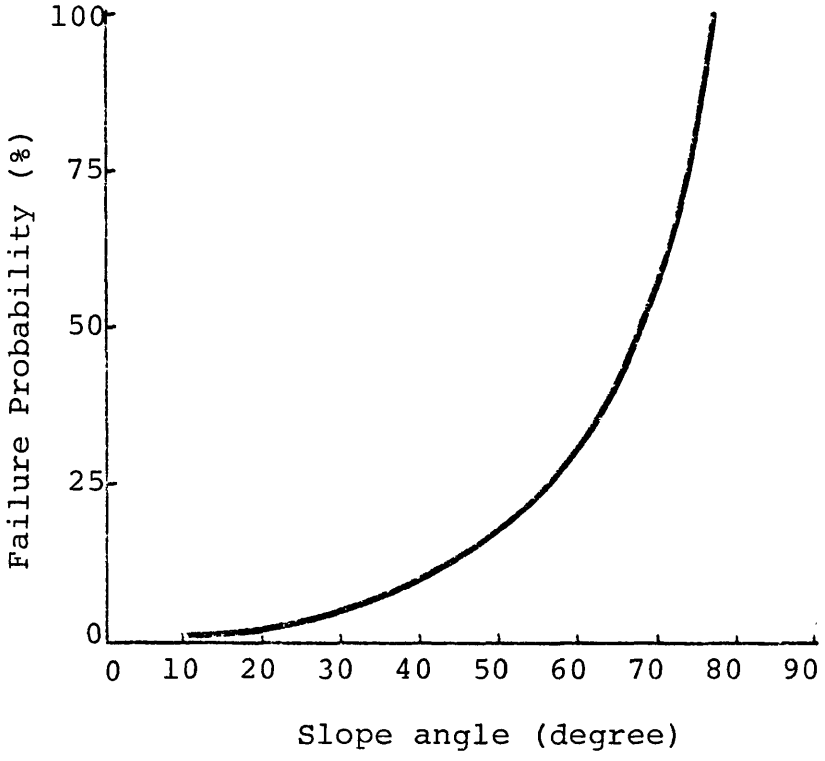


Figure 60. Example of failure probability as function of slope angle.

paper contains recommendations for ongoing investigations to assess and monitor the stability of particular slopes on the basis of the geological structures, groundwater conditions, and other controlling factors which occur in that specific slope. This would provide advance warning of major slope failures and permit engineering to minimize the natural conditions and overall cost of such disasters.

## DATA COLLECTION

### Site Investigation

The rocks of the Continental pit are structurally complex, containing extensive faults, joints and lithologic contacts (see Plates 1 and 2). These structures provide mechanical discontinuities and have lower strengths than unfractured rock.

In general, a rock mass with extensive discontinuities will fail at a lower applied stress than rock with less fractures. In particular cases, failure will typically occur along discontinuities which are adversely oriented to the pit wall and the applied stress. Therefore, the following questions were considered during fracture sampling:

1. What is the minimum number of fractures which must be sampled in order to achieve a valid model?
2. Which fractures are critically important and

must be emphasized during sampling?

3. What are the attitude limits of fracture sets?

The magnetic character of the orebody limits use of efficient fracture survey techniques. However, for better utilization the detail line sampling was preferred which is briefly described below.

Detail line sampling

Conventional geologic mapping was performed to determine rock types, locate major fractures, and determine structural domains. The detail line sampling consisted of stretching a 150-ft tape along the slope face and logging every visible fracture that intersected the tape.

The Continental pit is roughly ellipsoid and all sampled faces fall into what may be defined as the similar structural region. The detail line sampling was carried out all around the pit. Therefore, the lines had angular relationships of 0 to 90 degrees to the bearing of any one fracture set. Such a sampling is one of the most time-consuming techniques, but it contains the least operator bias. It is also most objective, and provides the maximum quantity of information and physical characteristics of each fracture. Particularly it was intended to record thickness, type of gouge materials, planarity and surface

roughness of each fracture.

Some of the fractures were wavy, and almost all of them were stained by iron oxide and filled with variable amounts of clay, calcite, quartz, epidote and some ore minerals.

Graphical Technique for Data Presentation

Over 2,600 fractures were observed and mapped during the pit site investigation. The majority of these fractures were reduced to an azimuthal strike (the strike defined as 90 degrees counter clockwise from the dip-direction) and listed on computer-compatible data sheets (see Appendix A).

A major part of the study evolved around equal-area net plotting of structural features. This statistical treatment proved to be a useful technique for evaluating and incorporating into geological data stability analysis. It is desirable to reduce fracture orientation data so that the numerical equivalent of an entire population can be visualized.

Graphical presentations include dip and strike histograms (see Appendix A), pole plots and density contour diagrams (see Appendix B and C) of the fracture data grouped as follows:

## Appendix B and C (Scatter and Contour Density Diagrams)

Figures 61 and 75, Quadrant N110,000-N111,000
257 poles at elevations 6920'-6960'

Figures 62 and 76, Quadrant N110,000-N111,000
159 poles at elevations 6840'-6880'

Figures 63 and 77, Quadrant N110,000-N111,000
95 poles at elevations 6760'-6800'

Figures 64 and 78, South edge of the pit
59 poles from Barringer-Zuniga fault zone

Figures 65 and 79, Quadrant N111,000-N111,750
115 poles at elevations 6880'-6920'

Figures 66 and 80, Quadrant N111,000-N111,750
174 poles at elevations 6800'-6840'

Figures 67 and 81, Quadrant N111,000-N111,750
94 poles at elevations 6720'-6760'

Figures 68 and 82, Quadrant N111,750-N112,750
166 poles at elevations 6880'-6920'

Figures 69 and 83, Quadrant N111,750-N112,750
179 poles at elevations 6800'-6840'

Figures 70 and 84, Quadrant N111,750-N112,750
125 poles at elevations 6720'-6760'

Figures 71 and 85, Quadrant E103,750-E104,500
174 poles at elevations 6680'-6760'

Figures 72 and 86, Quadrant N110,000-N111,000
569 poles at elevations 6760'-6960'

Figures 73 and 87, Quadrant N111,000-N111,750
383 poles at elevations 6720'-6920'

Figures 74 and 88, Quadrant N111,750-N112-750
470 poles at elevations 6720'-6920'

## Engineering Classification of Rock Masses

The physical properties of the rock masses vary from wall to wall, even over very short distances. Overall rock strength varies considerably due to presence of discontinuities and degree of alteration along discontinuities.

The attempt was to investigate individual homogeneous zones by detailed field observation, to distinguish them from each other. The homogeneous zones differ from one another in the mechanical properties of the rock masses. The mechanical behavior determines not only the strength properties, but also the type and direction of failure. This will be considered later in detail (page 274-285).

The rock masses have been grouped into five classes, as shown in Figure 89 and Plate 11 in the pocket. This classification is considered sufficient to provide a meaningful difference between groups in some important parameters characterizing the behavior of rock masses. More classes could be confusing to work with, while fewer classes may not provide sufficient distinctions.

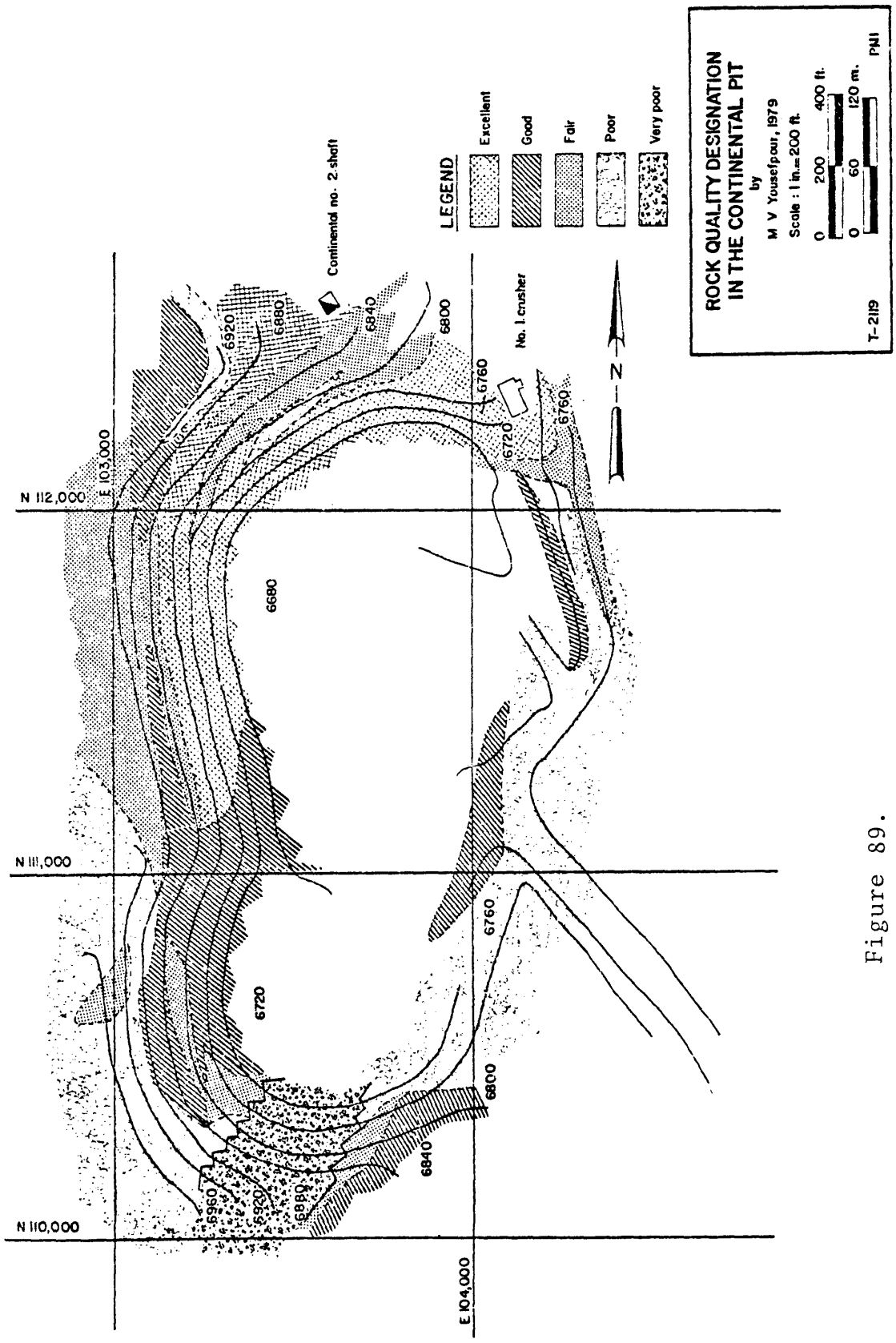
ROCK QUALITY DESIGNATION
IN THE CONTINENTAL PIT
by
M V Yousefpour, 1979
Scale : 1 in.=200 ft.
0 200 400 ft.
0 60 120 m.
PNI
T-2119
LEGEND
Excellent
Good
Fair
Poor
Very poor
N
Continental no. 2 shaft
No. 1 crusher
N 112,000
N 111,000
N 110,000
E 103,000
E 104,000
6920
6880
6840
6800
6760
6720
6680
6960

Figure 89.

| Classification Designation | Description |
|---|---|
| Excellent | Garnet skarn, and hornfels. The essential minerals are garnet and clinopyroxene. The accessories include quartz, calcite, epidote, feldspar, chalcopyrite, pyrite, magnetite, and sphalerite. The most alterable minerals are epidote, feldspar, chlorite and ore minerals. The rock is compact, relatively original state, solid and produces a ringing sound when struck with hammer. No visible sign of weathering. Rock fresh and crystals bright. It is traversed by important fractures which show some staining and oxidation with some clay filling. |
| Good | Garnet skarn, hornfels and recrystallized dolomite. The essential minerals are garnet, clinopyroxene, and dolomite. The accessory minerals include quartz calcite, epidote, chlorite, feldspar, chalcopyrite, pyrite, magnetite, and sphalerite. The most alterable minerals are ore minerals, chlorite, epidote and feldspar. The rock mass is relatively compact. Solid, producing a ringing sound when struck with hammer. The rock is fractured, penetrative weathering developed on fault and major joint surfaces. Fractures are discolored with oxide minerals and clay, but discoloration cannot extend more than 2 centimeters from fracture surface, except for major faults which are filled with clay materials. |
| Fair | Orthoquartzite and hornfels. The rock is solid and produces a dull and ringing sound when struck with hammer. The essential minerals are quartz in the Beartooth Quartzite, and clinopyroxene in hornfels. The accessories include garnet, calcite, quartz feldspar, epidote, chlorite and pyrite. The rock mass is intensively fractured. Wedge-shaped joints with approximate friction of less than 25 degrees in the Beartooth Quartzite and block joints with friction about 30 degrees in the hornfels zone. The Beartooth Quartzite |

| | |
|---|---|
| | breaks up into small angular fragments without any indication of chemical alteration. Discoloration is common in hornfels zone and extends through the greater part of the rock mass. Discontinuities are stained and contain a filling of calcite, quartz and clay minerals. |
| Poor | Serpentine and altered granodiorite in the east wall, siltstone and interbedded hornfels with altered pyroxene andesite dikes in the west and southwest walls. The rock is solid and produces a dull sound when struck with hammer. The essential minerals are antigorite, altered hornblende, biotite and feldspar in the east wall, and clinopyroxene in hornfels, pyroxene, hornblende and feldspar in intrusive dikes and quartz poorly cemented with calcite and mud in siltstone zone. The rock masses are completely shattered, slickensided, easily movable and displaceable. Weathering extends throughout the rock masses. The rocks have no luster. All materials except quartz are discolored. |
| Very Poor | Altered garnet skarn, hornfels and serpentine. Dull sound when struck with hammer. The rock mass has been extremely fractured. Mechanical fragmentation has transformed the rock mass into a suspension of clay particles. It is totally discolored and only fragments of the rock texture and structure are preserved. The external appearance is that of a soil. |

## Rock Weathering and Alteration

Metamorphic and igneous rocks of the Continental pit wall respond to different forms of weathering. Weathering of metamorphosed rocks produces a low shearing strength material, but tends not to produce spheroidal fragments in comparison with that of weathering product in igneous rocks. The hornfels is weathered along fractures by break-

down and eluviation of clay. Iron-oxide contents tend to hydrate to hydroxides and there is often migration of iron along fracture planes. In the upper benches of the west wall weathering is always intense at the surface (Figure 92), and decreases down the profile, but it persists along faults and joints to a much greater depth.

In general, the rock forming the upper 60 feet of the Continental pit is heavily oxidized. It is a relatively soft, porous material high in clay content. Below the oxidized zones is a hard garnet-clinopyroxene hornfels with thin layers of argillite along bedding plane faults. The contact marks a former water table and is the oxide-sulfide interface in the orebody.

Pyroxene andesite dikes are common igneous rock which crop out in the west and southwest walls of the Continental pit. The physical properties of these dikes play an important role in the slope stability of the pit. Therefore, it is worthwhile to include a brief description in the classification of the rock material, the state of weathering, the durability and the degree of decomposition.

Most of the pyroxene andesite dikes are thoroughly weathered and decomposed into spheroidal fragments. The fragments are distributed irregularly and individual spheres

are spaced ranging from a few centimeters to one foot. The spheroids themselves have a diameter of 3 centimeters to 8 inches. Figure 90 shows the relationships of the fragments in the partially weathered horizons. The reader is referred to the M.Sc. thesis (Yousefpour, 1977). The weathering profile is illustrated in Figure 91. In this illustration the approximate permeability and relative strength characteristics of each zone are described. The terminology of the profile was adopted from Patton and Deere, 1971. The contact between spheroid fragments is generally planar and indicates that joint planes have served as a starter. The fragments in the saprolite and more intense weathered zone are bounded by concave-convex concentric shells with various thicknesses from 7 centimeters to 2 inches.

The interior of the spheres is composed of fresh rock to relatively highly altered materials consisting of dark green to black phenocrysts of pyroxene, hornblende and feldspar and fine-grained green groundmass. The weathering produced surrounding the outer shells is a dark-brown clay which totally loses original texture. Any of the weathering products introduce low shearing strength, especially if accumulation is very high. They can be hazardous to foundations and excavations.

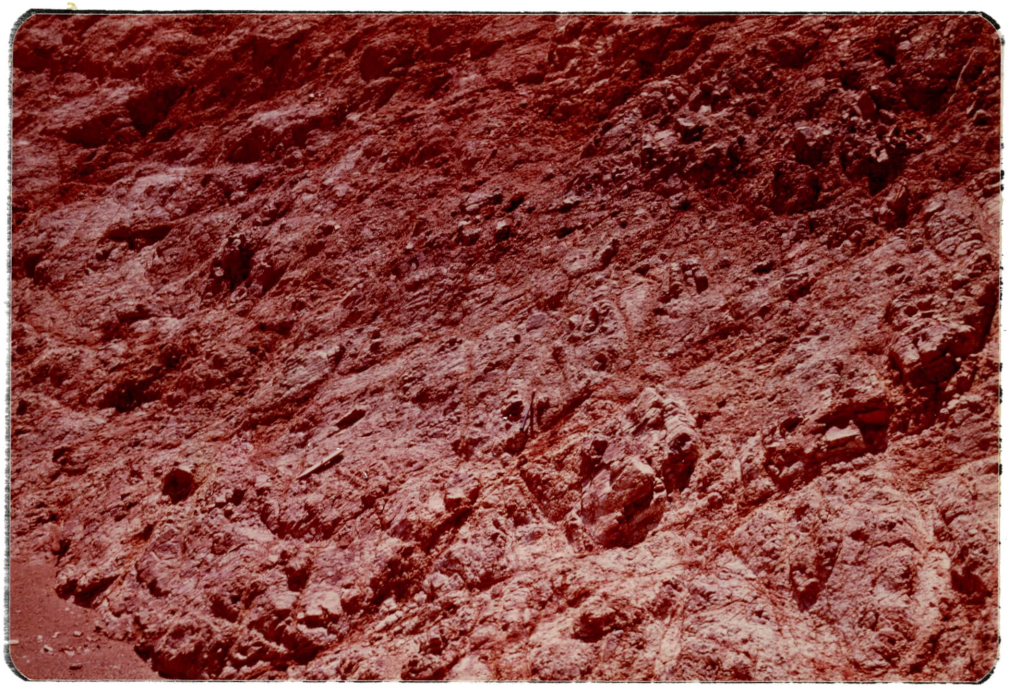

Figure 90. Pyroxene andesite dike showing the outcrop of the dike cut by open pit operation in the west side of the Continental pit. The fractures which control and contain the spheroidally weathered masses are obvious in the photograph. Notice the hammer for scale, near the center of the photograph.

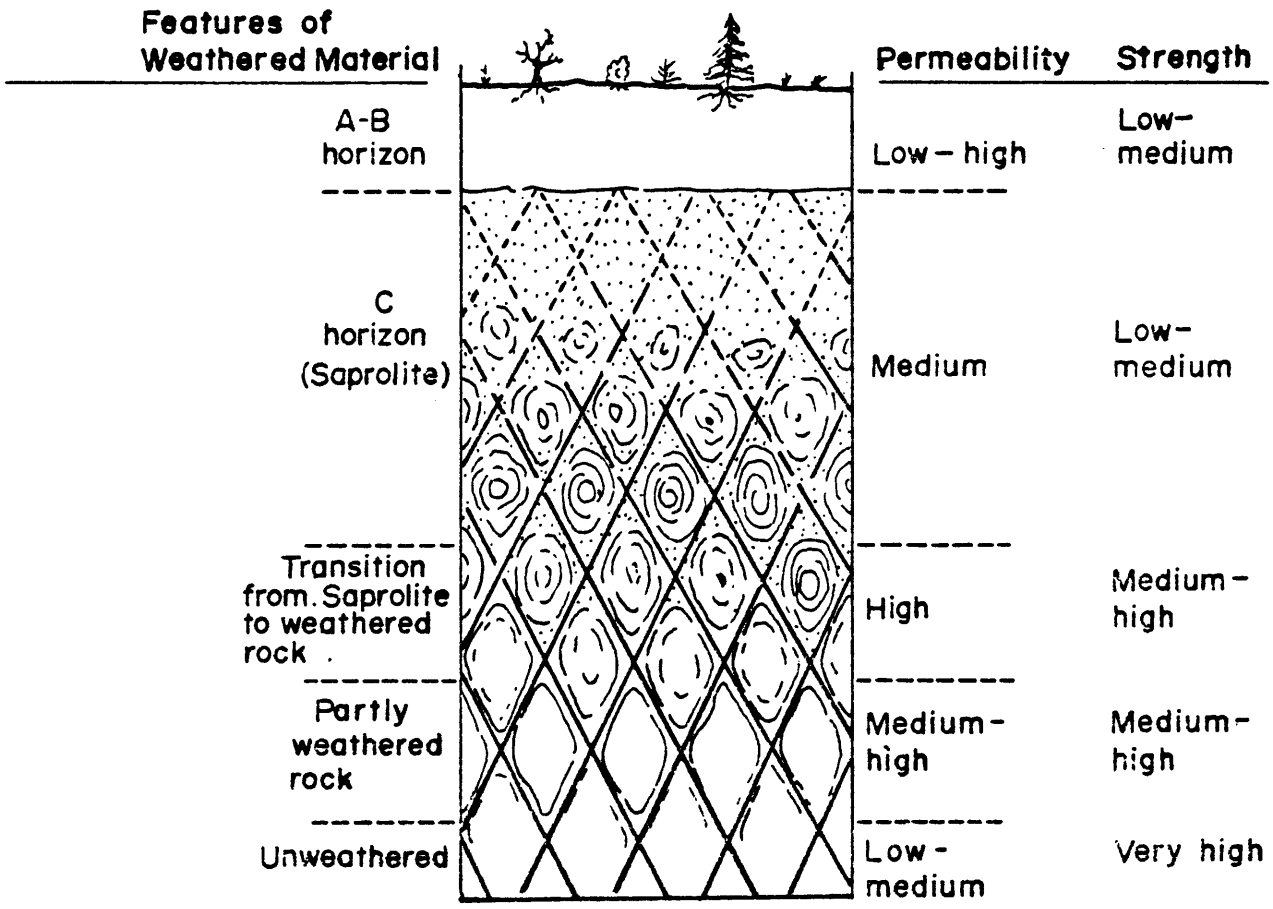


Figure 91. **Spheroidal weathering profile for mafic igneous rocks in the west wall of the pit** (modified from Patton and Deere, 1971).

The weathering products are the result of oxidation, carbonation and hydration of silicate minerals. By alteration of felsic and mafic minerals, soluble salts of K, Mg, Fe and Na are released. Free silica may be transported out of the weathering environment as well, but clay materials and detrital quartz grains will remain. The rock is gradually transformed into a saprolite (Figure 92) which resembles rock, but has the strength of a dense soil.

Basic Mechanics of a Sliding Block

The material properties which are most relevant to the discussion of slope stability are angle of friction, cohesion (resistance to shear), and the density of rock and soil masses (Hoek and Bray, 1977).

Essentially a generalization of the familiar Coulomb-Mohr envelope, the relationship between shear and normal stress for a typical rock surface or for a soil sample can be expressed as:

$$\tau = c + \sigma \text{ Tan } \phi \qquad (1)$$

where, $\tau$ is the shear stress required to cause sliding and increases with increasing normal stress, $\sigma$ is the normal stress on the sliding plane, and C is the cohesive strength. If the surface of plane failure is cemented or if it is

Figure 92. Highly weathered hornfels (Colorado Shale). Location: upper west and northwest walls of the pit. Notice the displacement of the Beartooth Quartzite (the resistant bed) by the fault.

rough, a finite value of shear stress is required to cause sliding when the normal stress is zero. $\phi$ is the angle of friction (the slope of the line relating shear to normal stress).

The simplest mechanical model for the problem of rock slope stability is illustrated in Figure 93. This consists of a rough, rigid block of rock sliding down along an inclined plane at an angle $\alpha$ under the influence of gravity. The weight of the block (W) acts vertically downwards as shown in the figure. $W\sin\alpha$ is the component of W which acts down the plane and tends to slide the block. $W\cos\alpha$ is the resolved part of W which acts across the plane and tends to stabilize the block. The shear stress per unit area inducing movement is given by

$$S = \frac{W}{A} \times \sin\alpha \qquad (2)$$

where A is the base area of the block.

The normal stress which acts across the sliding surface is

$$\sigma = \frac{W}{A} \times \cos\alpha \qquad (3)$$

Since the surface of the failure plane is rough, the normal stress induces a frictional resistance per unit area. Sliding or condition of limiting equilibrium occurs

when the shear stress equals the resistance, i.e.

$$S = R \tag{4}$$

where R is the shear force which resists sliding down the slope and is given by

$$R = cA + W \cos\alpha \times \tan\phi. \tag{5}$$

If the cohesion c = 0, the condition of limiting equilibrium defined by equation (4) can be simplified to

$$\alpha = \phi. \tag{6}$$

If the limiting equilibrium of the sliding block is reconsidered in terms of influence of water pressure, sliding will occur at an angle $\alpha$ given by

$$\tan\alpha = \left(1 - \frac{U}{W\cos\alpha}\right) \tan\phi \tag{7}$$

Where, U = UA, is water pressure or uplift force. The resistance to sliding is now

$$R = (W \cos\alpha - U) \tan\phi. \tag{8}$$

In the limiting equilibrium when the water pressure is equal to total normal pressure, the block becomes buoyant with no frictional resistance (Morgenstern, 1971). Therefore, water conditions may play an important role in slope

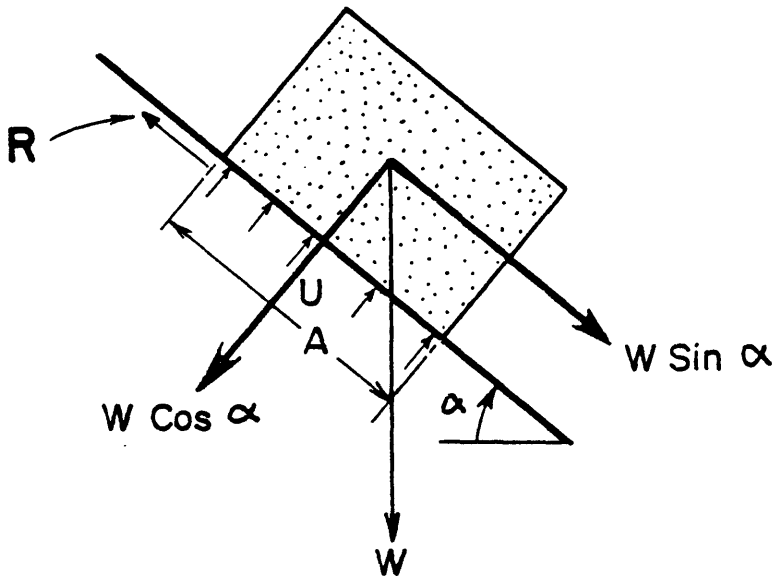


Figure 93. Mechanics of a sliding block.

stability.

## ROLE OF FRACTURES IN SLOPE STABILITY

### Oriented Plane and Zone of Weakness

Field observations permit the conclusion that the failure planes can form closely to pre-existing planes of discontinuities such as faults, shears and through-going joints. The strength along discontinuity surfaces has been altered and may be only a small fraction of the strength of the intact rock (Patton and Deere, 1971). Location and extent of these planes and intensively weathered zones have been indicated in detail (see Plates 1, 2 and 10 in the pocket).

### Variation in Strength Due to Irregularity Along Fractures

In a rock mass, the irregularities along a fault or joint surface create the difference between stability and failure of a mine slope (Patton and Deere, 1971). These authors have mentioned that the presence of irregular rock surfaces can result in the stability of different modes of failure along the same rock surface and, hence, different shear strength-normal stress relationships exist at different stress levels for the same rock surface.

Patton, 1966, has measured the average value of roughness angle (i) from photographs of bedding plane

traces in unstable limestone slopes. In his discussion, Patton found that in order to obtain reasonable agreement between field observations on the dip of unstable bedding planes and the sum of the angle "i" and the friction angle ($\phi$) it was necessary to measure only the first order irregularities of the surfaces. This is actually the major undulations on the bedding surfaces. The small irregularities such as ripples on the surface, have much higher "i" values and Patton called them the second order irregularities. This is shown in Figure 94, which is the actual trace of a bedding plane in limestone. The sketch is approximately 5 feet long.

The rougher the bedding plane trace, the steeper the angle of natural slope. Based on the field studies of natural slopes in sandstone and carbonate rocks, Patton has emphasized that the shear strength of their discontinuities is more closely associated with the smaller "i" values corresponding to those obtained from the larger first order irregularities.

The writer's experience in the Continental pit indicates that the surfaces of some discontinuities are highly irregular. Figure 95 shows breccia faults having thickness of 6 inches to 2 feet and strike similar to that of the bench face.

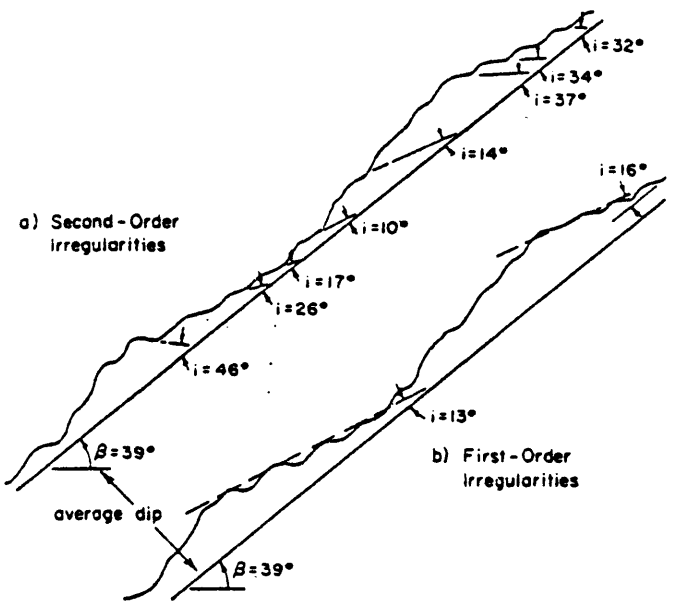


Figure 94. Measurement of first and second order irregularity angles on rough rock surfaces (after Patton, 1966).

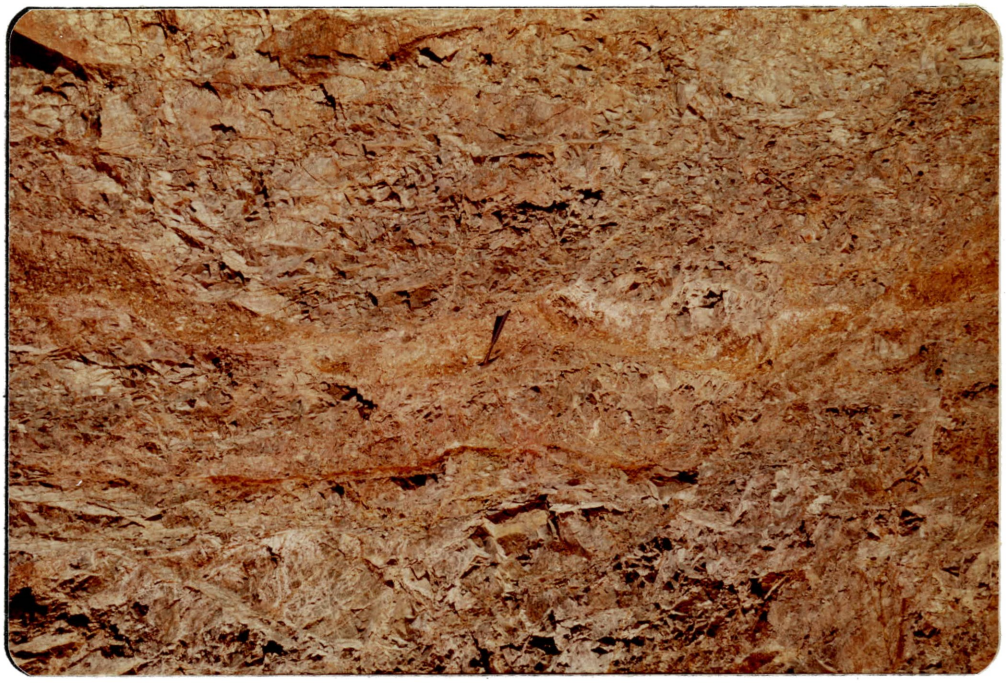

Figure 95. Breccia faults along bedding plane showing irregular surfaces. Location: upper Syrena Formation, north wall of the pit.

The Effects of Faults and Joints

The low residual strengths are associated along rock surfaces which have undergone considerable displacement particularly along uncemented fault or shear zones. This feature is significant in slope stability problems. Figure 96 shows a profile of several benches with an uncemented normal fault and two sets of joints. The normal fault and its parallel joint set both are unfavorably oriented fractures. In this particular example, the shearing strength along the joints will remain stable. However, when the pit is excavated deeper to expose the uncemented fault, the shearing strength at displacement would not be sufficient to resist the shearing stress, and as a result the slope will fail (compare this figure with the photograph in Figure 97).

The southwest wall of the pit is characterized by intensive intrusions of pyroxene andesite dikes along the previously faulted and sheared zones. This feature has significant influence on slope stability of this vicinity. The most important engineering properties of such a zone are shown in Figures 98 and 99. These include low permeability and low shear strength of the fault gouge, medium permeability and low to moderate shear strength of the zone between the fault gouges, and high permeability and

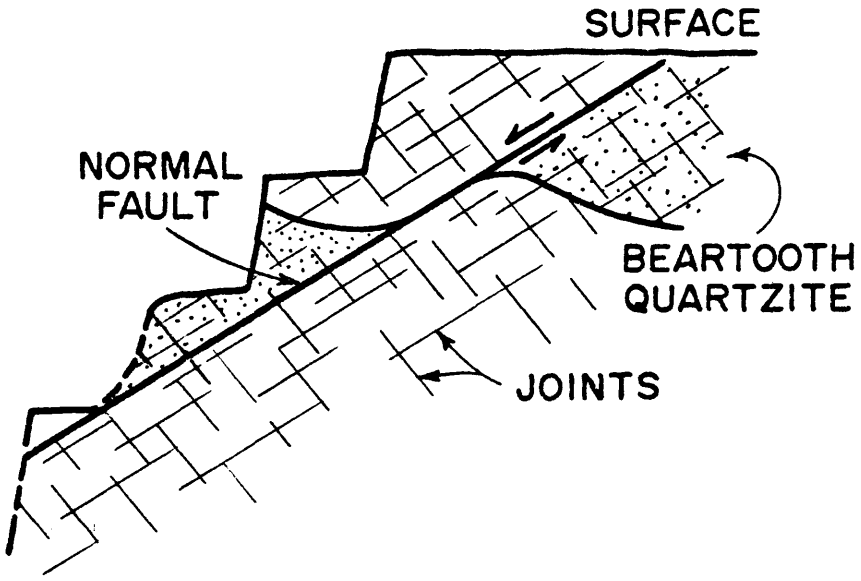


Figure 96. Significance of faults in slope stability problems in the west wall of the pit.

Figure 97. A typical wedge failure involving sliding along the line of intersection of normal fault and joint planes. Location: west wall of the pit.

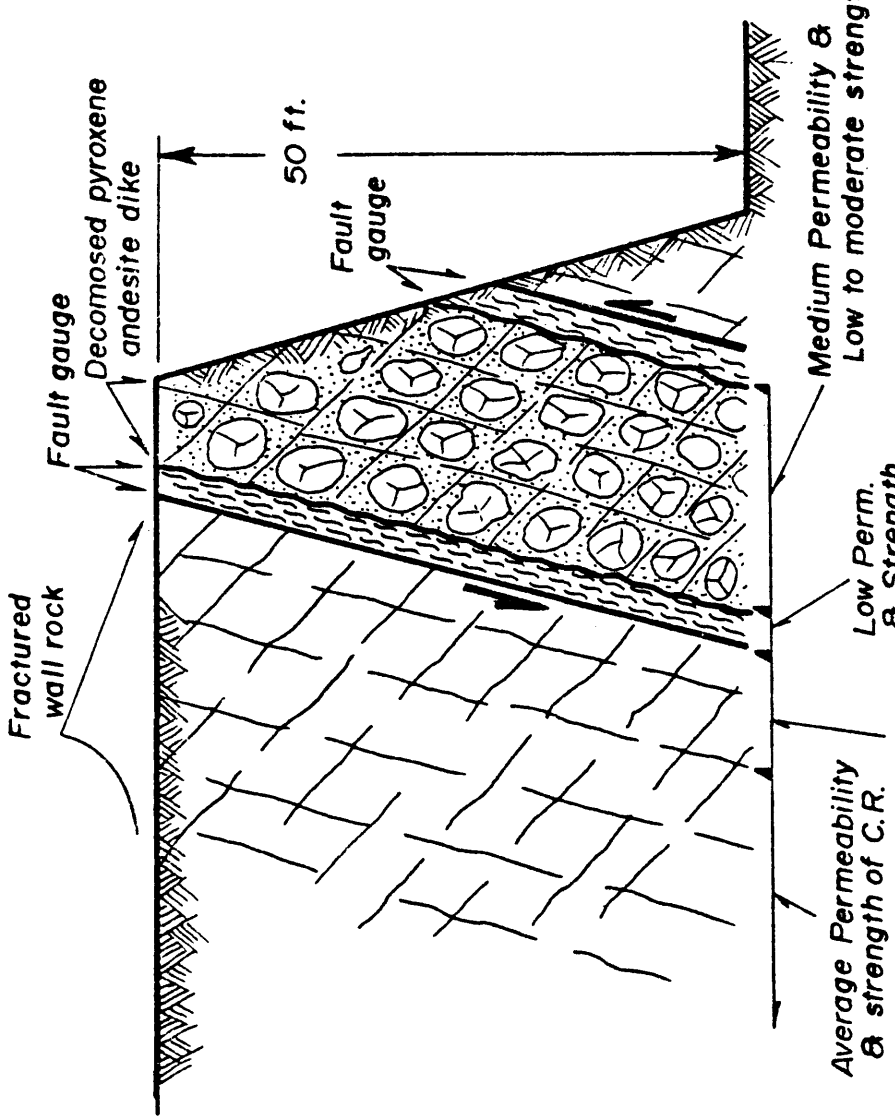


Figure 98. **Cross section of a pyroxene andesite dike, showing strength and permeability characteristics (Southwest wall of pit).**

Figure 99. Altered pyroxene andesite dike showing that the dike was intruded along a fault zone. Notice: intensive alteration along the fault plane (white zone), the rock on both hanging wall and footwall is highly altered. Location: southwest wall.

moderate strength of the rock adjacent to the fault compared with the country rock.

The effects of faults and through-going joints on a rock mass have been emphasized by Patton and Deere, 1971, as follows:

1. The area of influence of the structure increases and cohesion decreases.
2. By reducing friction and cohesion, the strength parameters approach to those of the residual strength.
3. The permeability first increases, and then decreases. The changing permeability reduces shearing strength along the fault.
4. When weathering and alteration is so high that production of various clay minerals, and oxide and sulfate materials reduces shearing resistance along the fault.

## KINEMATICAL CONSIDERATIONS AND TYPES OF FAILURES

Kinematic deals with the motion of a body without reference to the forces which move the body. In the case of rock masses, this implies the movement and modes of failure of the rock blocks and fracture surfaces.

The stability analysis of rock slope depends on accurate and representative descriptions of the pertinent

geologic structures existing in the field. A variety of literatures have been made in recent years to understand the geologic factors which affect the stability of rock slopes. In several instances, experience and the information from current research programs at the Continental mine led the writer to give a somewhat different emphasis to certain geologic factors.

The typical slope stability problem in the Continental pit can conveniently be grouped into four categories:

Type 1. Local wedge failures involving a single bench in the west wall of the pit.

Type 2. Failure in sheared and decomposed rock in the Barringer-Zuniga fault zone in the south wall of the pit which may involve several benches.

Type 3. Tension crack as an indicator of instability in the south wall of the pit.

Type 4. Plane failure in highly sheared and altered serpentine at the contact with granodiorite stock in the east and southeast walls of the pit.

These types of slope stability problems are illustrated in figures on the following pages.

Local Wedge Failures

Possible wedge failures of small rock masses along two or more fracture planes are illustrated in Figure 100 (compare this figure with Plate 2). As can be seen in this figure, a certain number of wedges can be formed by combining various pairs of discontinuities. As has been described by Pentz (1971), if n is the number of discontinuities, the total number of possible combinations would be

$$\frac{(nxn-1)}{2}$$

It has been shown in the figure that fortunately a large number of wedges would not fail due to their special geometry in relationship with the slope face. Those which show potential failures are almost impossible to eliminate completely without the use of excessively flat slopes or a costly slope-support system.

In the case of the Continental pit, if the west wall was overdesigned and probably too flat, such local failures would not occur. It is not recommended that the UV Industries should provide such a flat slope, because small failures like these would not create serious problems (this will be discussed later).

As far as field observation is concerned, it is

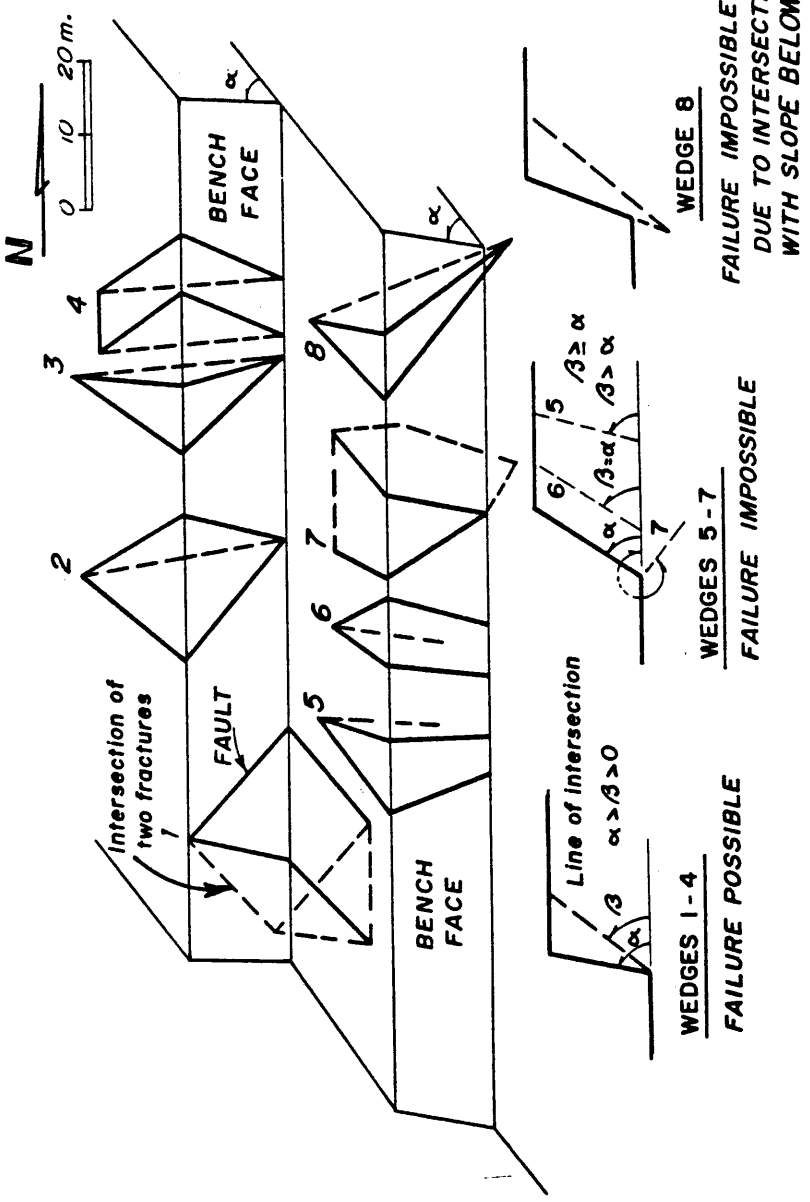


Figure 100. **Typical wedges produced by faults in the west wall.** (modified after Pentz, 1971).

impractical to analyze each individual block independently, but the combinations of members of each discontinuity set can be considered. In this case the kinematic discussion is particularly important. On the other hand, an individual block is sometimes considerably large and requires particular study as a single feature. In such a case, the stereographic projection permits a comprehensive discussion of force and moment equilibrium (this will be considered later in detail).

Block diagram (a) and plane view (b) of Figure 101 was prepared to analyze a typical wedge sliding in the west wall of the pit. The figure shows the line of intersection of discontinuities which gave rise to a potential failure mode of translation of rock blocks. Two planes remain simultaneously in contact as translation occurs parallel to the line of intersection. This situation is only possible if the line of intersection daylights into the free face. Under the gravity alone, the slide is possible only if the line of intersection is pointed downward at an angle greater than friction on the two planes (assuming no cohesion).

Goodman and Taylor (1967) have described that in more acute wedges, the line of intersection must plunge considerably steeper than friction angle for possible sliding.

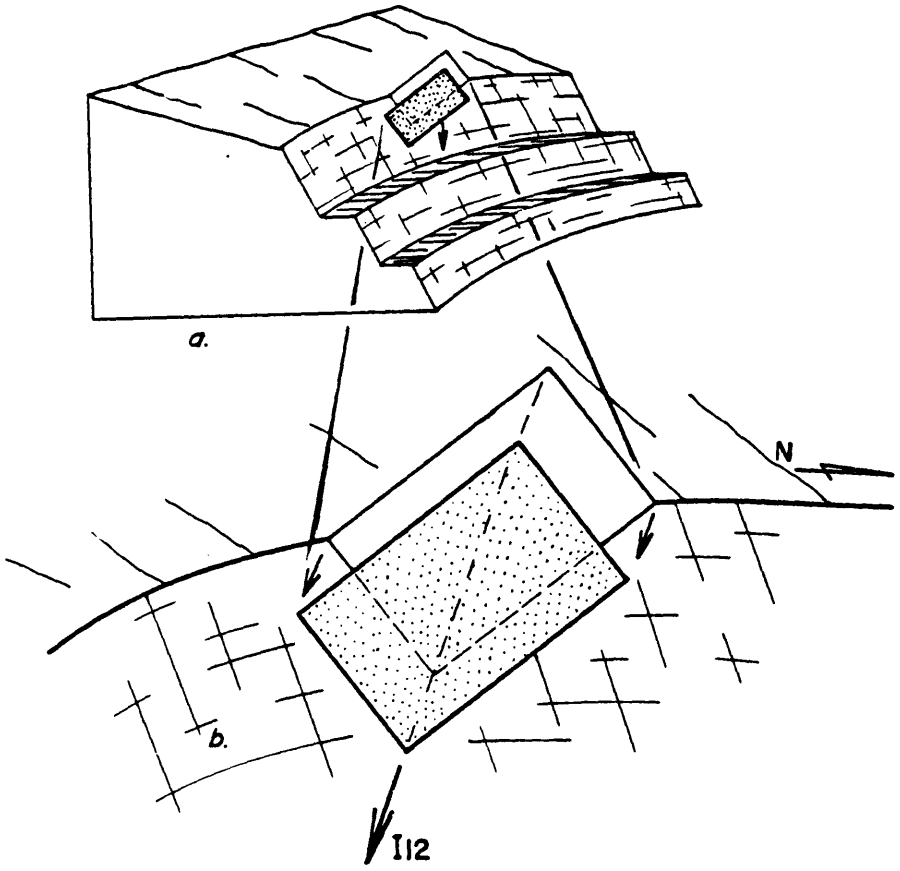


Figure 101. **Kinematics of a wedge sliding along the intersection of discontinuities.**

Based on the kinematic consideration, two important factors are responsible for the occurrence of a wedge sliding along the intersection of discontinuities:

1. The line of intersection must daylight into free space.
2. The plunge of intersection must be greater than friction angle.

As previously mentioned, wedge sliding is considered as a failure of slopes along discontinuities which strike across the slope crest and where sliding takes place along the line of intersection of two or more such planes. For better understanding of a wedge failure, it is necessary to point to more examples from the west wall of the pit. Figure 97 shows in the one case, the through-going normal fault with close association of joints. The fault daylighted in the lower bench and caused a wedge failure. This is actually shown in diagram of Figure 96 for the analytical treatment of this problem. In the other case, the wedge formed by a set of closely spaced planar discontinuities (Figure 102). In the latter case, the analytical treatment would still be related to the actual through-going planar features. However, to identify the dips and dip-directions and the locations of these planes permits useful practical interpretation.

Figure 102. Sets of intersecting normal faults and joint plane gave rise to the formation of wedge failures. Location: two different cases in the west wall of the pit.

These local failures are considered to extend a vertical distance of less than the height of one slope face. Such failures would not appreciably influence the overall mining operations for more than a few days at the most. The worst problem which may be presented by such a failure is that of hazard to men and equipment. The failure as illustrated in Figure 96, possibly has been involved fairly by the gradual separation of small loose blocks of rock and it is unlikely that it was dangerous to persons or equipment. On the other hand, the failure as shown in Figures 101 and 102 may have been involved in a relatively sudden fall of a single wedge which could have injured anyone working at the toe of the bench or damaged equipment during operations.

However, in the present-day mines, the cost of a single piece of equipment is extremely high and in this case a single local slope failure may change the entire economics of the mine operation.

In general, a good slope design will minimize small local failures. Nevertheless, it is not possible for many mining operations to eliminate all such failures. The best safety considerations in such cases would be continuous, close observation and monitoring of the pit slopes by regular mine survey personnel.

Failure in Sheared and Decomposed Rock of the Barringer-Zuniga Fault Zone

The existence of two regional faults (Barringer and Zuniga) and associated minor faults and through-going joints have led to the situation illustrated in the block diagram of Figure 103. This is actually a large-scale wedge failure which may become involved in the slide of the entire slope of the south wall. The present geologic condition is potentially much more hazardous than the local small wedge failures in the west wall.

The mine operators may have difficulty in detecting, and predicting failurewhere two adverse fracture sets are separated by a few hundreds of feet at the surface and where intensive alteration and weathering have made it hard to recognize the fracture sets. Detecting this significant structure and anticipating its future influence on mining operations is the result of careful geologic field work.

Hydrothermal alteration and weathering process on the rock in the Barringer-Zuniga fault zone and adjacent area have greatly reduced its strength, appreciably changed its deformability and permeability characteristics, and have developed a heterogeneous mass of residual soil, weathered rock, and unweathered rock.

The major components of soil material are clay minerals,

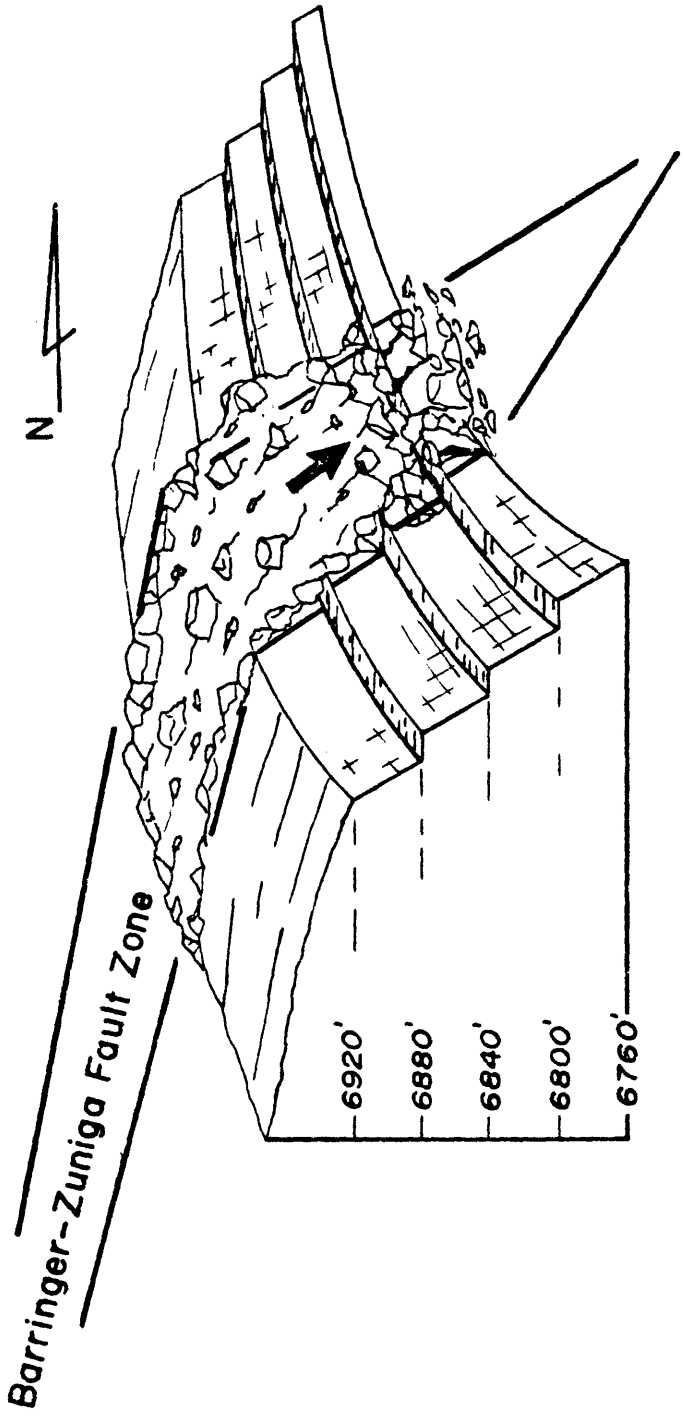


Figure 103. Failure in sheared and decomposed rock in the Barringer-Zuniga Fault Zone.

sand and hydrous sulfate, such as gypsum and chalcanthite. Formation of associated minerals is likewise related to precipitation and subsurface water which cause cementation and hardening of altered rock and fault materials and produce surface silicification and oxidation.

Such a zone often has a major influence on the groundwater flow and, therefore, may cause excess cleft and porewater pressures within and adjacent to the fault zone.

For the time being, the present condition shows little warning of slope failure, and may cause mine operators and workers to develop a false sense of security. The potential failure may appear when the line of intersection of two adverse discontinuities is exposed or daylighted into free face of a lower bench.

The other geometrical problem involving the south pitwall is the convex-pitward nose which has been developed by pit extension into the south wall. This nose distributes tangential stresses that may cause failure. It is strongly recommended that this nose should be avoided by straightening out the pit wall.

Such a zone indicates a potential failure problem. It may stop mining operation for a long period of time and change the economics of the entire operation. For these reasons it becomes so important to the investigator to

detect possible failure by locating the major through-going fractures and to anticipate such a failure before it occurs.

In order to understand the geologic conditions that could lead to rock slides and to attempt to clarify the origin of complex rock sliding, the use of stereographic projections as discussed on pages 274-285 is essential to obtain meaningful conclusions.

The south pitwall has an optimum slope angle of 65-80 degrees with an overall slope angle of 50 degrees (see Figure 59 and plate 9 in the pocket). For better safety conditions, the writer recommends that this slope should be flattened below the present 50-degrees overall slope design. A second recommendation is to initiate slope drainage in the face of the lower pit benches as an inexpensive method to drain some of the water. A drainage system is discussed on page 292.

Tension Crack as an Indicator of Instability

The writer has studied the petrology and mineralization in the Continental pit under his M.Sc. thesis in Summer 1976. There was no tension crack observed in the proposed pit at that time. Surprisingly, some of the tension cracks have been visible at the surface of the south pitwall during site investigation and surface monitoring in the Spring of 1978. The photograph in Figure 104 shows part of the tension crack.

Figure 104. Tension crack showing some part of a top tension crack in the foot-wall of the Barringer fault (south wall). Considerable horizontal and vertical movements have occurred. Looking west.

Hoek and Bray, 1977, have mentioned that some tension cracks have been observed in excavated rock slopes for several years, and in many cases do not appear to have any adverse influence in stability of the slope. However, it is worth while to consider how such a crack has been formed in the Continental mine and whether it can give rise to slope instability.

The above authors have reviewed a series of model studies on the failure of slopes in fractured rocks, and have come to conclusions that the tension crack was generated as a result of small shear movements within the rock mass. They have also pointed out that any individual movements are very small and would not cause such cracks, but their cumulative effect is a significant displacement of the slope surfaces and sufficient to cause separation of vertical joints behind the slope crest and to form tension cracks there. As a matter of fact, the presence of tension cracks in any rock slope is an important feature and indicates that shear failure was initiated within the rock mass.

In the case of the Continental pit, it is difficult to quantify the seriousness of a failure which may be initiated by the present tension crack since it is the start of a complex progressive failure process about which very

little is known. Nevertheless, the existence of this crack at the surface of the south pitwall, where it is associated with a large-scale wedge failure in the Barringer-Zuniga fault zone, should be taken as an indication of potential failure. This possibly signals the need for a detailed investigation into the stability of this portion of the slope.

Geometry of the slope with the tension crack

The failure which may occur in the south pitwall as a result of the tension crack, is actually a plane failure for the following reasons:

1. The crest of the benches in the south pitwall have an average trend of N75W, and 50 degree overall slope angle to the north. Thus, the tension crack at the surface is oriented approximately in the same direction (see Figure 105). Therefore, the plane on which sliding may occur is parallel to the slope face.
2. As shown in the same figure, the dip of the failure plane ($\alpha p$) is smaller than the dip of the slope face ($\alpha f$).
3. The dip of the failure plane ($\alpha p$) is greater than the friction angle ($\phi$). Based on the calculation

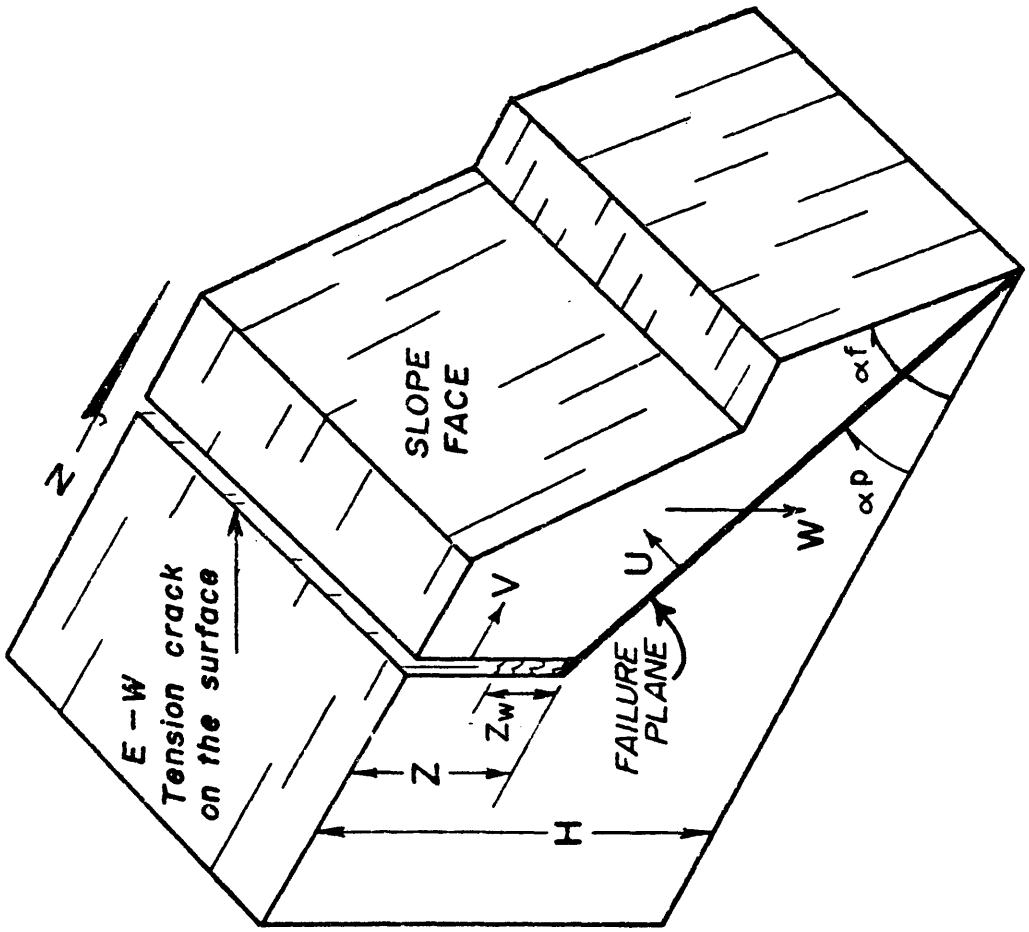


Figure 105. **Geometry of slope with tension crack on the surface in the south wall of the pit.** (Modified from Hoek and Bray, 1977).

which will be discussed later in this section, the αp equals 40 degrees, but the friction angle is considered to be 30 $\pm$ 5 degrees.

Inclination of failure plane

As previously mentioned, it has been found that the south pitwall is actually unstable for several reasons. Obviously, failure of a limited extent has already taken place in part of the slope in the Barringer-Zuniga fault zone. In addition, a suspicion of failure by presence of a tension crack on the footwall of the Barringer fault has been created. However, the decision on the effective and economical remedial measures is found to be necessary and it should be applied.

Figure 106 is the section through slope in the south pitwall. As can be seen in this figure, a 240-foot high slope has an overall slope angle of 50 degrees, and is made up from six 40-foot benches with average 70-degrees faces (see Figure 59). The slope is in faulted and shattered recrystallized dolomite, altered serpentine and garnet-clinopyroxene hornfels, quartzite and localized altered pyroxene andesite dikes. As it was considered on the preceding pages, the presence of intensive oxidation zones possibly indicates the existence of water pressure distribution.

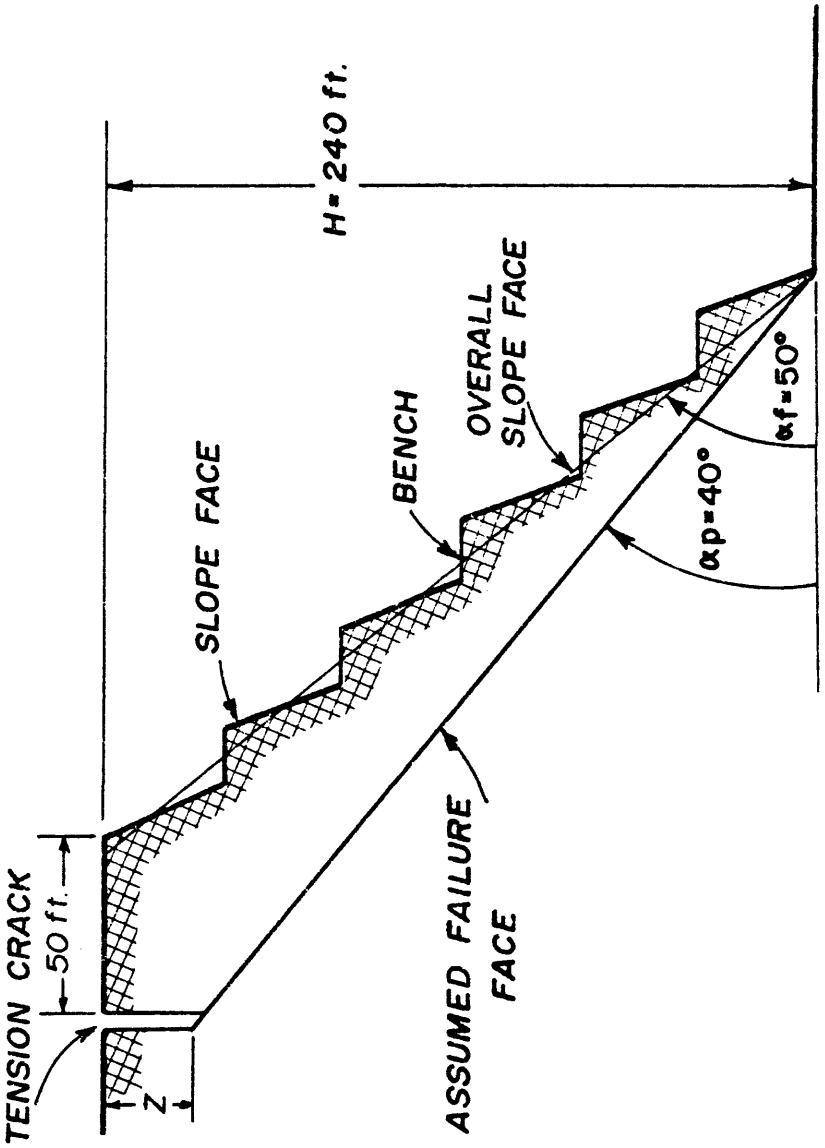


Figure 106. Section through slope in the south wall of the pit.

Figure 105 may suggest a question concerning the shape of the failure face. Hoek and Bray, 1977, have described how in a soil slope with a fairly flat slope face, the failure surface would have a circular or nearly circular shape. In a steep rock slope, the failure surface is relatively planar and for any slopes the inclination of such a plane can be found as

$$\alpha p = \tfrac{1}{2} (\alpha f + \phi) \qquad (9)$$

where, $\alpha p$ = angle of failure surface

$\alpha f$ = angle of slope face, and

$\phi$ = angle of friction.

Hoek and Bray have pointed out that if water is present in a tension crack, the inclination of the failure plane would be reduced by less than 10 percent. However, the equation (9) can be used to obtain the approximate critical failure plane inclination for the proposed slope.

Depth of tension crack

The previous analysis was based on which position of the tension crack is known from its visible trace at the surface. The depth actually can be established from the construction in Figure 107. The most probable position of the tension crack depth can be established as:

$$\frac{Z}{H} = 1 - \sqrt{\mathrm{Cot}\alpha_f \times \mathrm{Tan}\alpha_p} \quad . \qquad (10)$$

Hoek and Bray, 1977, have considered the equation (10) for dry conditions. Based on the field observation, the tension crack has occurred about 50 feet behind the crest of that slope (Figure 107), and it is safe to consider that this crack has occurred as a result of shear movement in a relatively dry slope. However, the above authors have concluded that the depth of a tension crack is independent of groundwater conditions and it can be calculated from the equation (10), by which it becomes approximately 39 feet vertically. At the present time, with this depth, it would not cause any failure, but we must keep in mind that it will deepen gradually and indicate the onset of instability.

Graphical analysis of stability

Good background information on the behavior of the failing mass, its size, shape, and structural control is essential. Figures 105 and 107 examine the possible mechanics involved in the failure. The following conditions have been considered in this analysis:

1. The strikes of both sliding surface and the tension crack are parallel to the slope face (approximately N75$^{o}$W), and the tension carck projects to a depth of 39 feet.
2. The tension crack occurs about 50 feet behind the slope face. It is vertical and is saturated

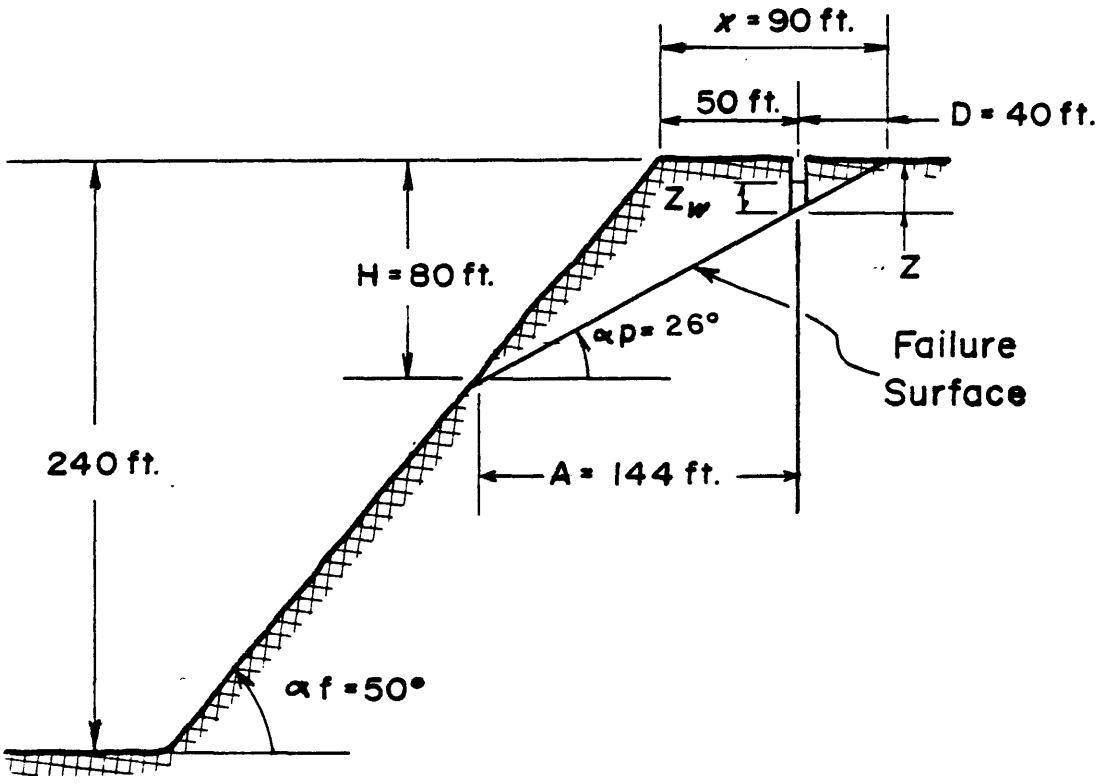


ure 107. **Geometry of possible slope failure in the south wall of the pit.** (Modified from Hoek and Bary, 1977.

with water during heavy rainfall to a depth $Z_w$ (Figure 106).

3. Water enters the sliding surface along the base of the tension crack and seeps along the sliding surface and escapes at atmospheric pressure where the sliding surface daylights into free face. A feeling for the direction and magnitude of the movement is essential to determine which area will slide first and what tonnage is involved.
4. The weight of the sliding block (W), the uplift force of water pressure on the sliding surface (U), and horizontal water pressure in the tension crack (V), all act through the center of the sliding mass (Hoek and Bray, 1977). This means there are no moments which would tend to cause rotation of the block and failure is by sliding only.
5. Under the mechanics of a sliding block, on the preceding pages, it has been considered that the shear strength of the sliding surface is defined by cohesion c and friction angle $\phi$ in the equation $\tau = c + \sigma \text{Tan}\phi$. It is assumed that the surface of the failure plane is rough, having a curvilinear shear strength curve.

In this case, the factor of safety as given by Hoek and Bray, can be expressed by the ratio of total force resisting sliding to the total force tending to induce sliding:

$$F = \frac{cA(W\text{Cos}\alpha p - U - V\text{XSin}\alpha p)\ \text{Tan}\phi}{W\text{Sin}\alpha_p + VX\ \text{Cos}\alpha_p} \qquad (11)$$

Where, from Figures 105 and 107

Base area of the block: $A = (H-Z) \times \text{Cos}\alpha_p$

Uplift water pressure : $U = \frac{1}{2}\ \gamma_w \times Z_w \times A$

Horizontal water pressure in tension crack: $V = \frac{1}{2}\ \gamma_w \times Z_w^2$

where, $_w$ = the unit weight of water.

Assuming a rock density of 160 $lb/ft^3$ and a water density of 62.4 $lb/ft^3$, the weight of the sliding block in Figure 105 can be calculated as:

$$W = \frac{1}{2}\ \gamma(HX - DZ) \qquad (12)$$

where, $\gamma$ = the unit weight of rock.

By knowing W, V, and U, it is possible to establish the force diagram and to determine the approximate shear strength. This has been plotted in Figure 108. Because the proposed block is not in limiting equilibrium condition yet, it can be concluded that the friction angle probably is $30 \pm 5$ degrees. This range of friction angles

and related cohesive strengths in Figure 108 are used to determine the stability of overall slope in the south pitwall.

Assuming a friction angle of 30 degrees with the overall slope angle of 50 degrees, the factor of safety can be determined. It is suggested that a 50-degree slope is unstable under the saturated conditions prevailing after heavy rainfall.

The drainage of the slope or the control of surface water which can enter the top of the tension crack is essential. This will be considered later under drainage system. Since it cannot be guaranteed that drainage could be fully effective, it is recommended that the slope should be flattened to 40 degrees.

Plane Failures

As far as the geometric of a failure is concerned, a plane failure is comparatively absent or very rare in the west and north pitwalls. The geometrical conditions which are required to produce such a failure are developed only in the east wall and again in the south wall. The plane failure in the south pitwall as a tension crack will be discussed later. The present section deals with the failure in the east pitwall.

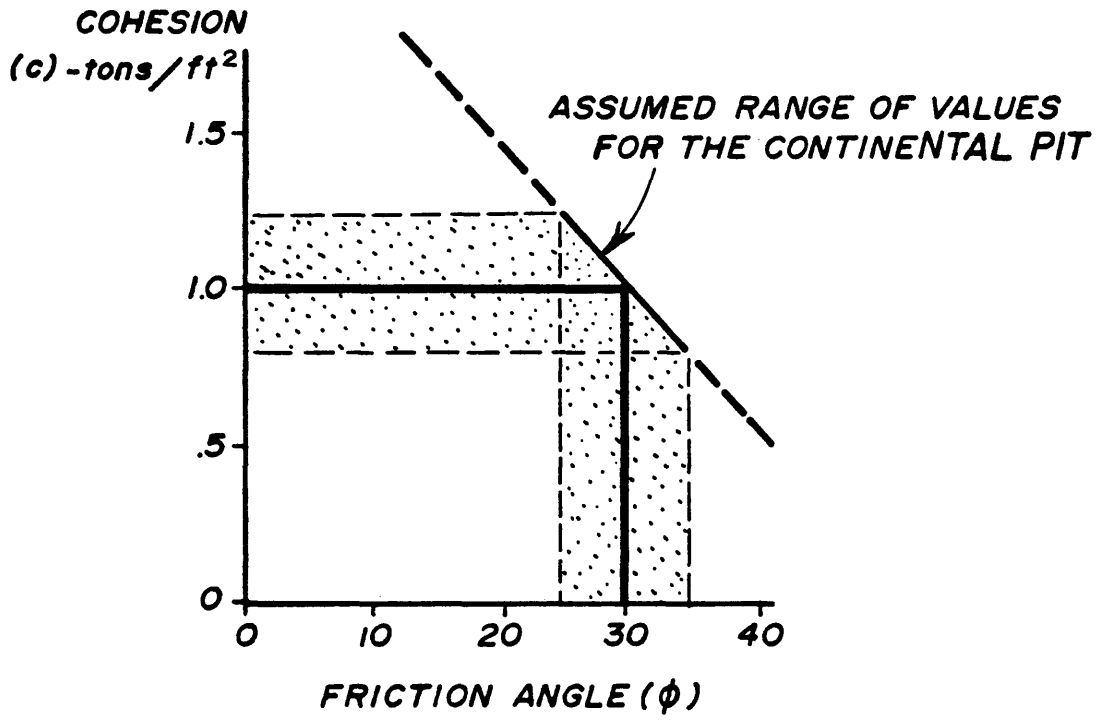


Figure 108. **Determination of shear strength.**
*(Modified from Hoek & Bray, 1977)*

This portion of the pit is extremely sheared and altered. It is localized at the contact of granodiorite intrusive with altered serpentine. The alteration was produced as the result of hydrothermal solutions originated from the intrusive. The original dolomite interbedded with thin layers of shale was altered to forsterite. In the later stage of hydrothermal activity the whole mass has been replaced by serpentine, a rock of very low cohesive strength. Such a low quality rock is developed throughout the east and southeast walls of the pit.

There are many important points to be considered in the mechanical interpretation of the failure mode of the east and southeast pitwalls, and it is particularly useful to demonstrate the sensitivity of the wall slopes to changes in shear strength and groundwater conditions.

As in the south and southwest pitwalls, there is enough evidence at hand of groundwater in and around the eastern portion of the pit. All water seeps observed in the pit-wall have been mapped and described. The groundwater control will be described later under separate coverage.

Slickensides as an important factor in rock strength is a very common linear feature and occurs everywhere in open pit and underground mines. They are most commonly observed at the contact of the granodiorite intrusive with

invaded sedimentary rocks. In the east wall of the pit, numerous slickensides are uniformly oriented in the north and northeast directions and dipping to the west and northwest into the pit. The photograph in Figure 109 is an example of this linear feature. As a matter of fact, they show all variations between pure dip and pure strike slip in a small scale.

In fact, most of the slip surfaces in serpentine are highly polished and show definite evidence of frictional heating. Slickensides are also developed in fault gouge on bedding planes and on the surfaces of extension fracture filling when subjected to the appropriate stress field.

Development of such surfaces reduces the friction angle and decreases the cohesive strength of the rock. The influence of cohesive strength, angle of friction, and groundwater conditions in relationship with slope height and slope angle for a particular slope such as that of the east wall of the Continental pit can be summarized as follows:

1. A decrease in the cohesive strength causes a decrease in the safe height of steep slopes.
2. A reduction in the angle of friction results in a decrease in the safe angle of slopes.

Figure 109. Uniformly oriented slickensides in the serpentine zone (east wall). Looking to the east.

3. An increase in cleft and pore-water pressures causes a general reduction in the stability of slopes.

In this portion of the pit, the planes on which sliding may occur generally strike parallel or nearly parallel to the slope face.

General characteristics of plane failure in the east pitwall

The conditions which provide plane failures in the east pitwall can be summarized in the following items:

1. The planes on which sliding may occur strike north and northeast (parallel or nearly parallel to the slope face) (see Figure 59).
2. The optimum slope angles vary between 48 and 65 degrees with an overall slope angle of 40 degrees (see Figures 58 and 59). The failure plane daylights in the slope face. This means that its dip is smaller than the dip of the slope face, i.e. $\alpha_f > \alpha_p$.
3. The plunge of intersection of two sets of discontinuities is greater than the friction angle of this plane, i.e. $\alpha_p > \phi$ (see Figure 100).

As mentioned previously, this wall contains very weak rock which has been classified as poor quality. It

is hard rock, slickensided and wet, and failures are anticipated at the present design angle of 40 degrees. The writer strongly recommends this wall should be flattened to about 30 degrees, or so. The recommended angle should both allow provision for haulage and provide a flat enough slope so that if any failure occurs, it can be handled without much problem.

## STRUCTURAL EVALUATION OF SLOPE STABILITY

### Introduction

The dominant role of geologic discontinuities in rock slope has already been emphasized. This section deals with the stereographic projection of adequate set of geologic data. But the question is, what is an adequate set of data? What type of geologic data and how much detailed data must be analyzed in order to be able to evaluate the stability of the proposed slope?

For slopes which are not critical, there is little need for data collection (Hoek and Bray, 1977). Indeed, the critical slopes can only be defined if there is sufficient data and information available for their stability evaluation. This requirement has been carried out in two stages:

1. The site investigation and preliminary geologic

data collection from surface mapping.

2. Analysis of this data has permitted establishment of a critical geologic pattern, related to the proposed pit slopes and assessed probability of failure developing.

This presentation has been prepared in a way which can be interpreted by others who may be involved in the later stability analysis at the Continental mine, or one who may be brought in to check the results of these interpretations.

The graphs on the following pages are presented to identify slopes in which unfavorable discontinuities exist and to mark those slopes in which failure would be critical at any stage of the mining operation.

Before discussing the plotting techniques, the writer would like to comment on the question of sample bias. It has become a common practice to reduce fracture data in order to apply Terzaghi's (1965) equations to correct the effects of sample line bearing on the number of fractures sampled by an unbiased operator. The basis for the correction is that joint traces are sampled on a plane surface and, therefore, the number of intercepts is a direct function of the angle between the fracture and the surface.

The first criticism of the plan was that unequal

directions of sample line would introduce bias errors. For instance, if most of the slope cuts were trending N-S, the sampler would record proportionally few N-S fractures which were nearly parallel to the line of sampling. The most frequent recordings to represent equal density of fractures of all strikes, would be those fractures intersecting the line of sampling at a right angle or nearly so.

Beside geometric problems, there are other factors related to fracture sampling at the Continental mine. One factor is the size, frequency, and spacing of the fractures being recorded. The third factor is the roughness of the fracture surface. The author's experience at the Continental mine indicates that some surfaces are highly irregular, presumably as a result of close spacing of fractured elements, and rock breakage due to blasting.

The most frequent fractures were recorded at some degree inclined to a nearly vertical angle to the slope face. In effect, the sampler's bias counteracts the mathematical bias to some unimportant degree. Therefore, it has been decided to present the data as sampled, with no corrections.

## The Equal-Area Projection

As mentioned previously on the preceding pages, all

data were reduced to an azimuthal strike and listed on computer-compatible data sheets. They are presented in Appendix A with dip and strike histograms.

The orientations of fracture planes in space are plotted in terms of their poles on the equal-area net. The net represents a plan view of a 2-degree, intervals-graduated lower hemisphere. The poles represent the projections of lines normal to the fracture planes. The pole of a horizontal plane would plot at the center of the net and that of a vertical plane would plot on the circumference. The initial plots of poles are presented in Appendix B.

After plotting the poles, the Denness curvilinear cell counting method was used for the evaluation of the statistical density. The Denness counting method was used because of very close concentrations of poles to the circumference of the net. In Denness (1972) the reference sphere is divided into 100 squares. The density evaluation was obtained by counting over the prescribed grid the number of poles which fall in one square, the area of which is 1 percent of the entire reference sphere. These values are then contoured and spatial patterns of anomalous density are presented in Appendix C.

## Stereoplots of Structural Conditions and Evaluation of Potential Slope Problems

The slopes of the Continental pit are associated with different geologic structures. It is the purpose of stereographic projection to recognize the potential stability problems. Examining the pole plots indicates that some of the structural patterns should be watched.

The stereoplot diagrams given in the figures of the following pages show the appearance of typical pole plots of geologic structural conditions. In assessing stability, the orientation of the cutting face of the slope must be plotted to identify the daylighting portion of the lower hemisphere. In preparing these diagrams, a 50-degree overall slope angle is considered for south, west, and north walls, while a 30-degree slope angle is considered for the east wall. The average friction angle of the discontinuity surfaces in the rock mass is considered to be 30 degrees.

The diagrams, as given here, have been simplified for the sake of clarity. In this topical plotting, a number of significant pole concentrations have been presented. Furthermore, it was possible to identify those which represent potential failure planes and to eliminate those which represent structural and are unlikely to be involved in

slope failures. Fortunately, most fractures are of this type. In order to be able to establish such a diagram, the following data are required.

1. The great circle representing the slope face.
2. The pole concentration representing fracture density (they are indicated with numbers in the figures of the following pages).
3. Great circle representing the plane corresponding to center of pole concentration (this is shown with dashed lines in the figures).
4. Pole to great circle of item 3, representing line of intersection (for example $I_{12}$ means pole to great circle passing through plane 1 and 2).
5. The friction circle.

Sliding can only occur along the line of intersection and, hence, this line must "daylight" in the slope face. This means the plunge of the line of intersection must be less than the dip of the slope face. Under gravity alone, sliding is possible only if the intersection of discontinuities is pointed downward at an angle which overcomes friction on the planes (Goodman, 1976).

Figures 114 and 115 show that the south and east slopes are potentially unstable when the points defining the line of intersection of two planes fall within the

area included between the great circle of the slope face and circle of friction (shaded area). From the two figures it can be seen that the most dangerous combinations of discontinuities are those represented by the pole concentrations numbered 1 and 2 in Figure 115 and 1, 2 and 4 in Figure 114. The intersection of other pole concentrations in this figure and all other figures from the west and north walls fall outside the critical area and are unlikely to give rise to instability, at least at present pit design.

The pole concentration numbered 1, in Figure 111 from north and northwest slopes, falls within the critical area. As shown in this figure, there are strong fracture sets oriented northeast and northwest, which dip into the pit at relatively low angle. The friction angle on these surfaces is less than the dip angle of intersection lines, and, hence, down-dip sliding may occur whenever the rock loosens up enough to yield free blocks.

However, this test has been carried out to identify critical discontinuities. A more detailed analysis would be necessary in order to determine the factor of safety of the slope.

A contour plan of the Continental open pit mine is presented in Figure 116 and Plate 8 in the pocket. The simplified contoured stereoplots of available structural

data are superimposed on this plan. The overlay is aligned in the dip direction of each portion of the slope as indicated in the figure. Two distinct structural areas, A and B, have been identified and the boundary between the two regions is shown by the dashed line.

Figure 116 and Plate 8 show that the western and northern portion of the pit (structural area A), is likely to be stable at the present slope of 50 degrees. The rock in this portion of the pit is that of excellent, good and fair qualities (see Figure 89 and Plate 11 in the pocket), and relatively free of major adverse fracture sets.

The high-grade orebody is controlled stratigraphically over this area. Based on the geometric relationship between pit wall and the orebody, the west and north walls should be as steep as possible. But any design in this region should provide a wide catch berm just below the Beartooth Quartzite, as this unit is characterized by intensive wedge-shaped joints with low friction and exhibits a strong tendency to break up. This unit has been classified as fair quality rock. Alternatively, if it becomes necessary, this portion of the pit wall could be used as a haul road location with steep faces above and below the haul road.

On the other hand, the eastern and southern portion

of the pit (structural area B) contains a number of potential slope problems. As discussed previously, plane failure is possible in the east wall. Wedge failure associated with a tension crack is of potential instability in the south wall. Indication of failure problem in Figure 116 and Plate 8 would suggest that serious consideration should be given to flattening these slopes.

The south wall has a combination of structurally controlled slope failures such as wedge failure, tension crack and convex nose. Realignment of this slope is not recommended since its cost would be too high, but flattening of the slope and drainage would greatly reduce failure problems.

Groundwater Control

Water in the Beartooth Quartzite and fracture zones in the Continental pit plays an important role on the stability of the pit slopes. The mine survey personnel may make the mistake of thinking that the slope surfaces are completely dry and yet there is water behind the slopes of the Continental pit such as in the south, southwest, and east slopes. Figure 117 shows intense oxidized zones and represents where water seeps into the ground. It must be remembered that it is water pressure and not rate of flow which is responsible for instability in slopes. It has

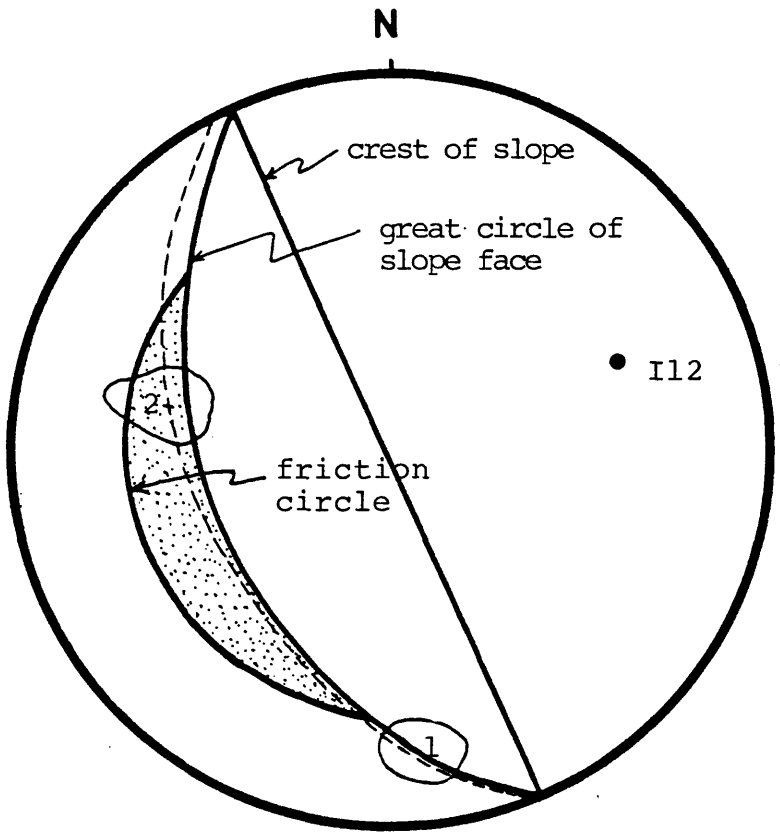


Figure 110. Representation of two sets of fractures by their poles and determination of the line of intersection of the sets by the pole of great circle (north and northeast part of the pit).

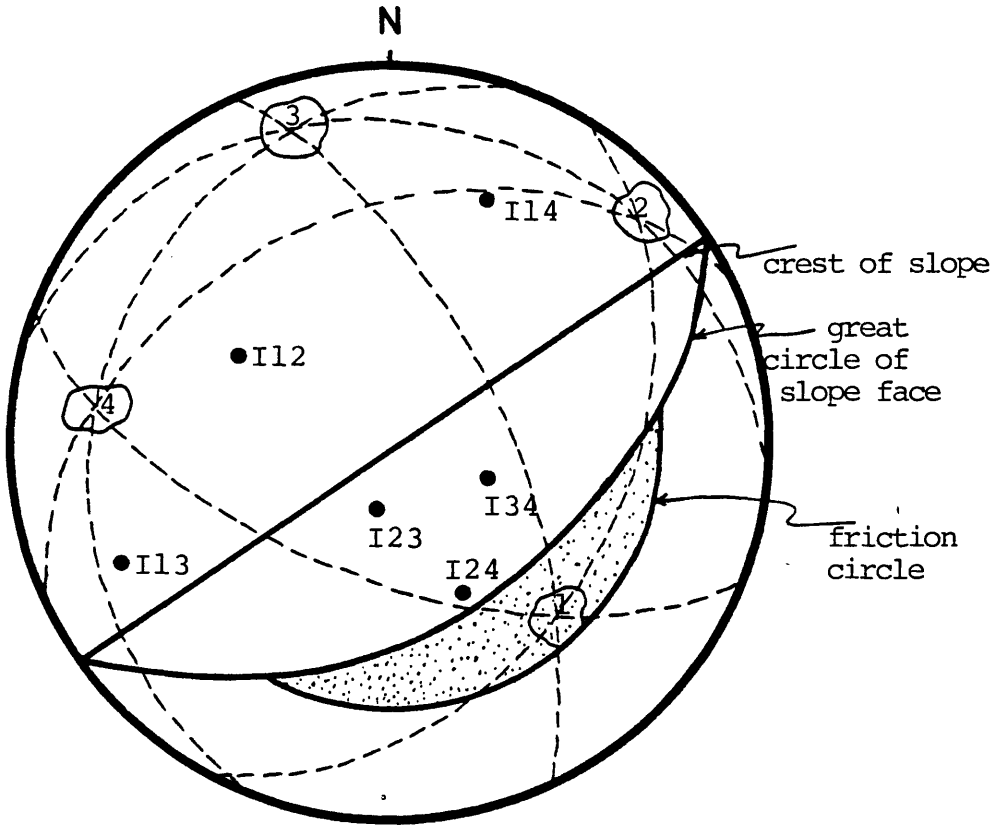


Figure 111. Representation of four sets of fractures by their poles and determination of the line of intersection of the sets by the pole of great circle (northwest part of the pit).

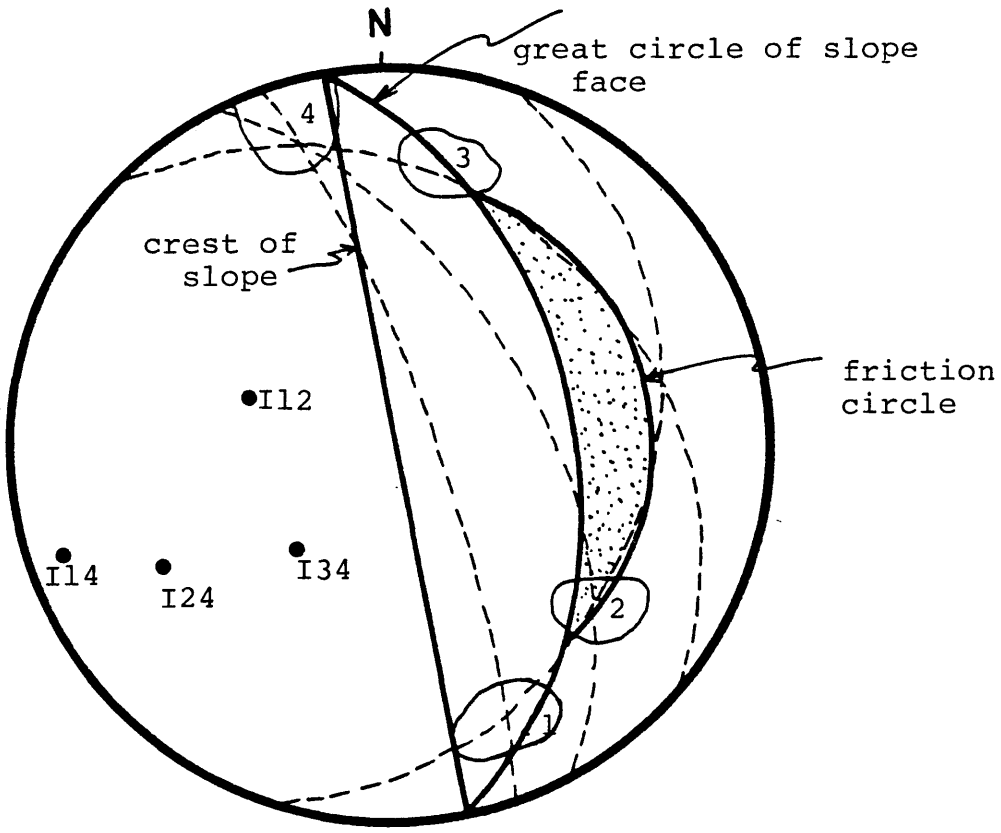


Figure 112. Representation of four sets of fractures by their poles and determination of the intersection of the sets by the pole of great circle (midwest side of the pit).

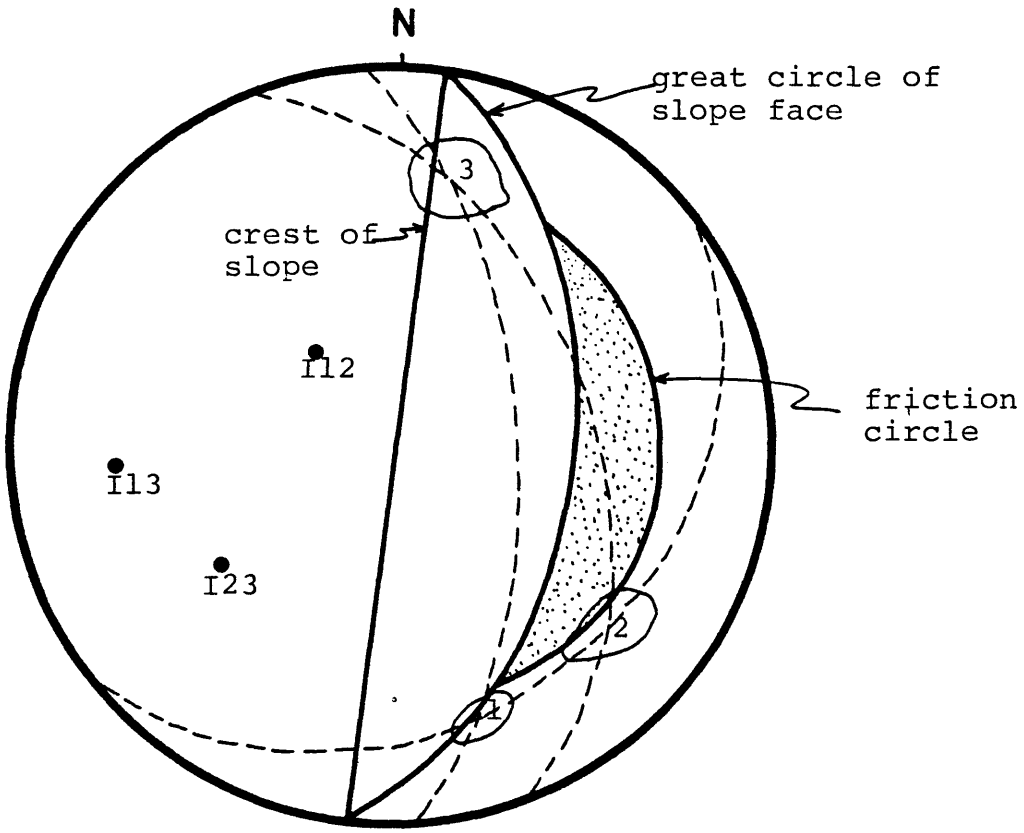


Figure 113. Representation of three sets of fractures by their poles and determination of the line of intersection of the sets by the pole of the great circle (upper southwest part of the pit).

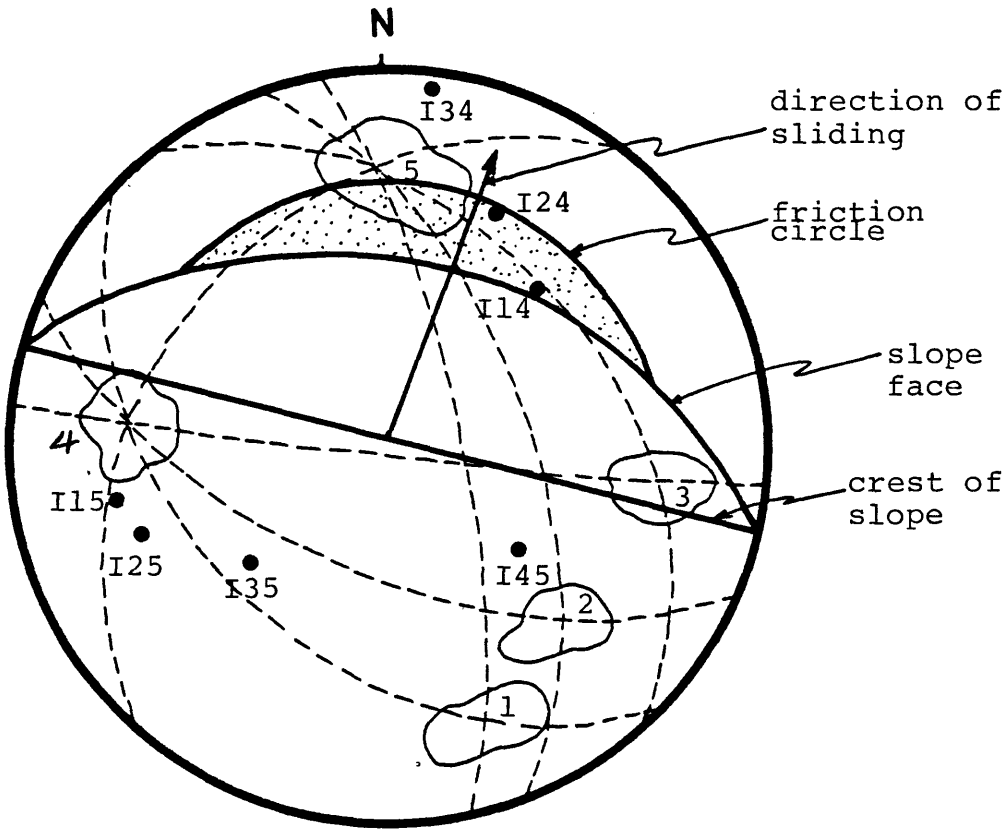


Figure 114. Evaluation of slope stability in the south wall of the pit. (Wedge failure possible along intersection lines I14 and I24).

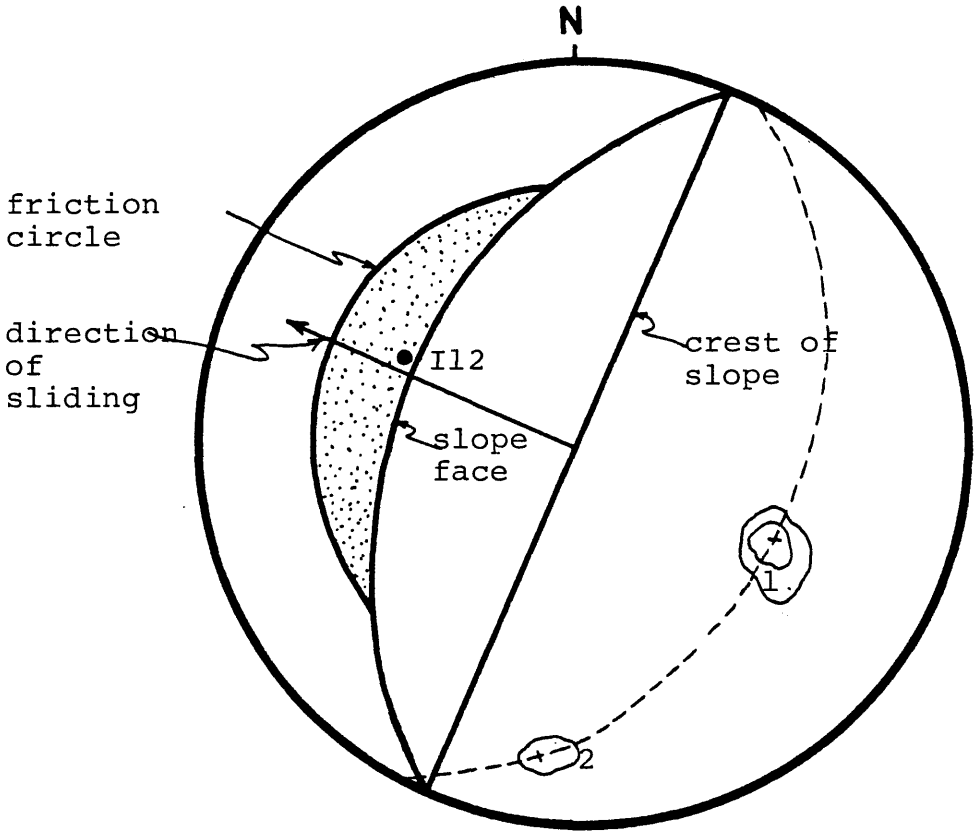


Figure 115. Potential sliding is assumed along the intersection line I12 in highly fractured serpentine and altered granodiorite in the east wall of the pit.

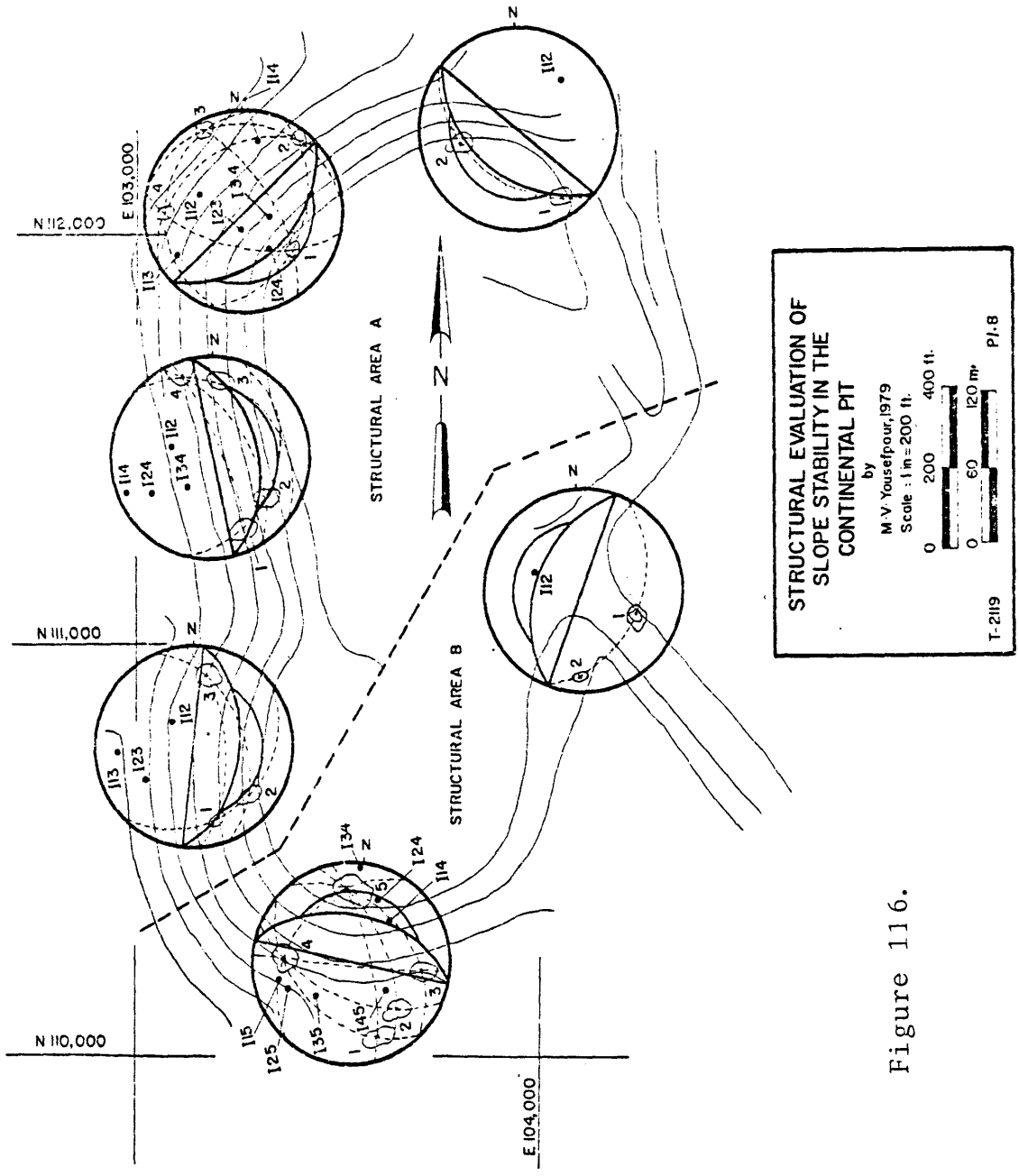
N 112,000
E 103,000
N 111,000
N 110,000
E 104,000
STRUCTURAL AREA A
STRUCTURAL AREA B
N
STRUCTURAL EVALUATION OF SLOPE STABILITY IN THE CONTINENTAL PIT
by
M.V. Yousefpour, 1979
Scale : 1 in = 200 ft.
0 200 400 ft.
0 60 120 m
T-2119
Pl.8

Figure 116.

Figure 117. Intensive oxidation and formation of clay minerals indicate water seeps along fault. Location: Barringer fault zone, south wall.

been reported that water is standing in many of the development drill holes. In fact, a more detailed program is needed to define the standing water levels in all open drill holes around the pit and to record any information on wet holes.

Water pressure reduces the stability of the slopes by reducing the shear strength of potential failure surface. It has been considered previously that the effect of water pressure in tension cracks reduces stability by increasing uplift force, which in turn decreases the normal force acting across the failure surface.

The rock at the Continental mine is anisotropic. Directional variation of permeability is controlled mainly by oriented discontinuities, particularly faults and through-going joints. Because of the preferred orientations of discontinuities, an anisotropic variation of permeability represents the hydraulic properties of the rock. It is reasonable to neglect the permeability of intact rocks such as garnet skarn and hornfels of the Oswaldo and Syrene Formations. It is the secondary permeability controls water inflow.

Distribution of discontinuities is known in detail. Variation of fracture continuities, aperture opening, surface roughness, water seepage and other characteristics

of discontinuities in rock mass were mapped and emphasized during site investigations. Fissure apertures will open substantially at high pressure and cause a large apparent increase in permeability.

Stereographic projection indicates two major sets of discontinuities in the west wall. One set strikes northwest and the other is oriented to the northeast. This systematic orientation of rock discontinuities facilitates the choice of the directions of maximum and minimum flows.

The pattern of groundwater flow with major fractures has been established and is shown in Figure 118 and Plate 10 in the pocket.

Local topography also has an essential role in controlling groundwater movement and water pressure distribution. Clearly, precipitation in the large catchment area of the pit is an essential source of groundwater as suggested from the geographic location of the Continental mine, where the pit has been excavated on the east and southeast side of the Hermosa Mountain. The stability of upper weathered zone can appreciably influence the entire south and southwest slopes. The geographic position is included to emphasize the fact that groundwater can and does travel a considerable distance from the Hermosa Mountain and adjacent area through fracture and fault zones

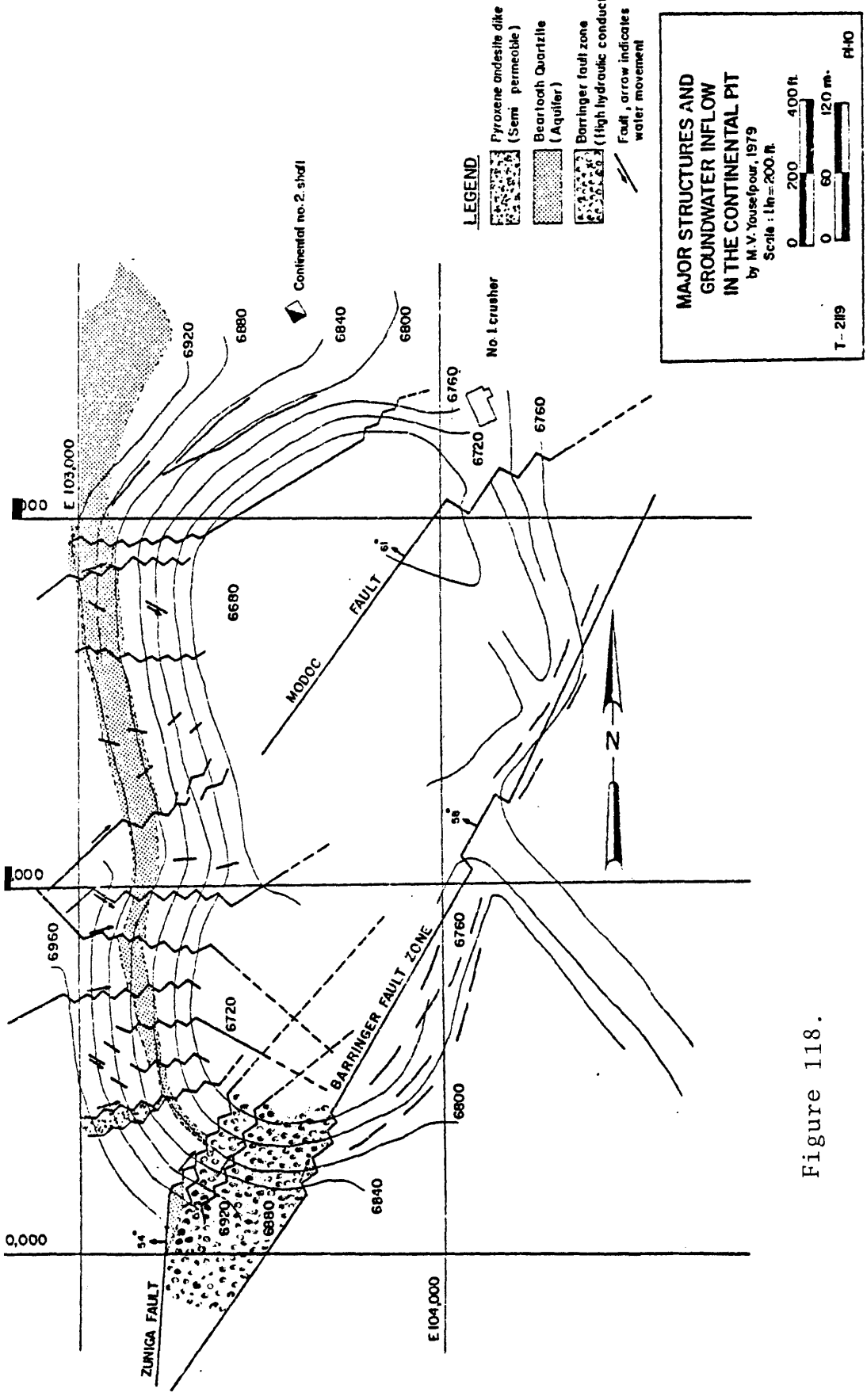
MAJOR STRUCTURES AND
GROUNDWATER INFLOW
IN THE CONTINENTAL PIT
by M.V. Yousefpour, 1979
Scale : 1 in = 200 ft.
0 200 400 ft.
0 60 120 m.
T-2119
A-10
LEGEND
Pyroxene andesite dike (Semi permeable)
Beartooth Quartzite (Aquifer)
Barringer fault zone (High hydraulic conductive)
Fault, arrow indicates water movement
Continental no. 2 shaft
No. 1 crusher
MODOC FAULT
BARRINGER FAULT ZONE
ZUNIGA FAULT
N
E 103,000
E 104,000
6920
6880
6840
6800
6760
6720
6680
6960
61°
58°
54°

Figure 118.

in the rock mass into the pit area.

The distribution of water pressure very commonly is controled by degree of fracturing and continuity of these fractures. The Beartooth Quartzite acts as a regional aquifer. The Barringer-Zuniga fault zone in the south and east walls, the frequent intrusions of pyroxene andesite dikes along the previously faulted and fractured zones in the southwest wall, and breccia faults in the west and northwest walls, are of particular consideration. Figure 119 shows through-going faults in the southwest wall. Obviously, the hydraulic conductivity of such zones would be high as compared with other parts of rock mass.

Since the movement of groundwater is concentrated in open fissures and channels, it is difficult to identify the exact nature of the water table, but it can be determined by means of piezometers. In the simplest form the water table below which the ground is saturated is a fairly horizontal plane. In a succession of layers of diverse permeability such as that of the Continental pit, there may be multiple water tables. When permeability is irregular or discontinuous, the water table is similarly erratic (Morgenstern, 1971).

The writer recommends drilling drainage holes in the south slope to reduce the water content in the Barringer-

Figure 119. Major fault and minor fractures with intensive oxidation along the fracture planes due to water seep. Location: southwest wall.

Zuniga fault zone and other critical areas associated with tension crack.

Drainage system

The south pitwall shows obvious sign of instability. It was considered previously that the rock in this area is highly fractured and altered and its strength properties reduced. The rock mass will still possess its maximum strength by reducing water pressure if drainage is anticipated. Since both underground and open pit operations are carried out, drainage can contribute to the stability of the present open pit.

Four different methods of drainage have been recommended by Hoek and Sharp (1970). The modified diagram of these methods is shown in Figure 120. These include:

1. Vertical boreholes drilled from surface
2. Drainage drift excavated in the rock mass behind the slope face with or without a substantial vertical borehole excavated from the drift.
3. Horizontal or nearly horizontal holes drilled from the slope face.
4. Surface drainage channel.

The advantages of vertical boreholes are:

a. They would not interfere with operation of the face.

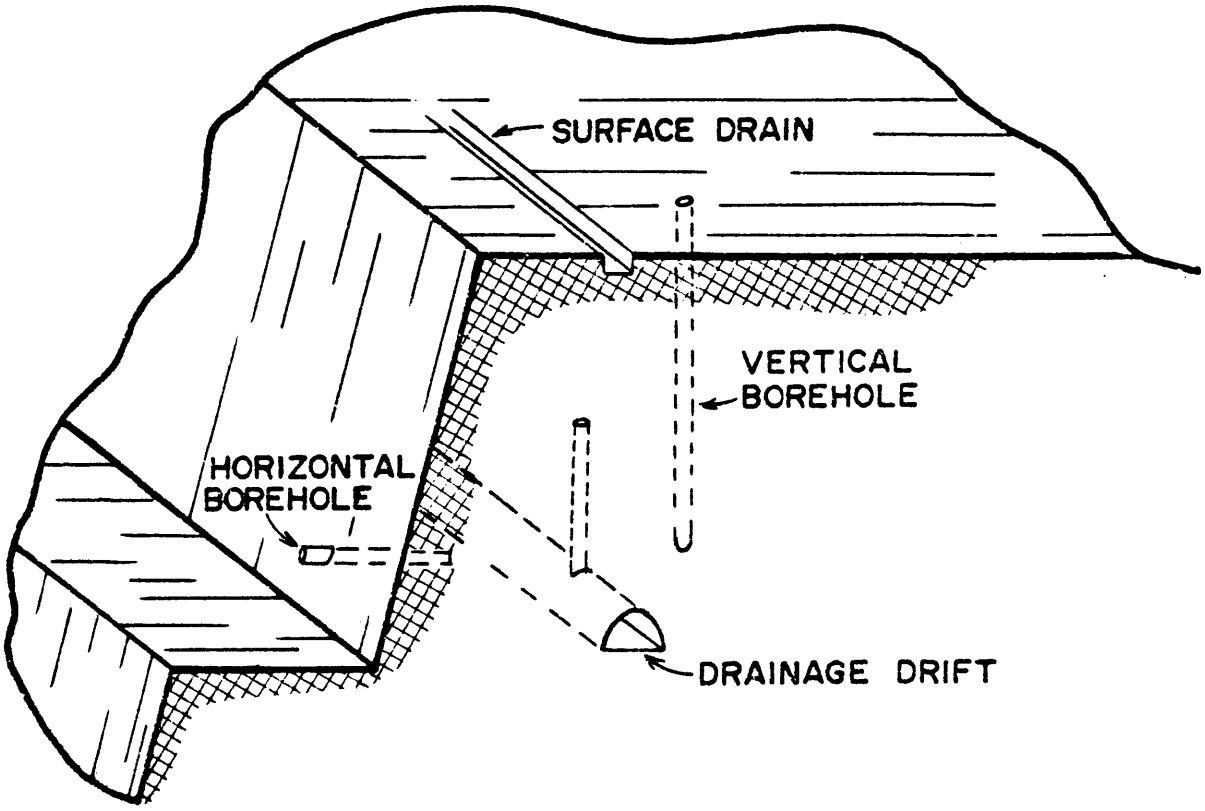


Figure 120. **Slope drainage system** (modified from Hoek and Sharp, 1970).

b. Any exploration or development boreholes in the vicinity can be used for drainage purposes if suitable pumping service is available.

The depth of the holes should be sufficient to contain all the material in the altered zone. In other words, it should be drilled to a depth equal to that of the pit. Since this particular vicinity of the pit has relatively uniform permeability, the holes can be spaced approximately 50 feet apart. This is based on the theoretical experience obtained by Hoek and Sharp. The diameter of the holes can vary from 3-6 inches.

The cost of excavation of a drainage drift could be very high. For this reason and others, such as the particular structure involved in the south wall, this method is not recommended.

In the case of horizontal boreholes, they should be drilled at the toe of the lower bench. The length, space and diameter of these holes would be very much like that of the vertical boreholes. This method is the most convenient one to be carried out and hence it would have a lower cost and provide reasonably effective drainage.

Surface drainage also has been recommended by several authors, but it would be difficult to have the control of surface water, at the Continental mine, since most of the

water entering the pit, travels through a large catchment area surrounding the west side of the pit. Nevertheless, as much surface control as possible should be applied. The tension crack in this region is a major problem because during heavy rainfall, water drains into the ground through the crack.

It is recommended to fill the tension crack and grade the surface. After the tension crack has been filled, it would be efficient to cover the area surrounding the crack with thick plastic material to prevent water infiltration. The other solution would be to drill closely spaced horizontal boreholes from the face to intersect the tension crack near its base.

Effects of Blasting

One major problem which arises in open pit mining is that the material which should be dept stable is disturbed when it is subjected to high seismic shocks caused by blasting.

A fundamental economic requirement is to minimize the cost of any necessary process. In order to achieve the lowest overall cost of processes such as drilling, breaking, loading, transporting and crushing, it is necessary to provide well fragmented rock. This relationship is shown in Figure 121, which was taken from Harries and Mercer, 1975.

However, the primary objectives are generally to avoid overbreak and to eliminate back damage. Blasting can be improved to cut down wall damage by the three following methods:

1. To reduce the amount of charge per delay to a minimum. The optimum loading per delay can best be achieved by experimentation.
2. To use presplitting on the final walls. This is basically a creation of a fracture between the blast and the final wall by shooting a series of decoupled charges in closely spaced holes.
3. To use a buffer zone between the presplit and the main bench shots. This consists of a series of holes more closely spaced than the main blast holes, and blasted sequentially between the presplit and the main shot.

The effects of blasting on the Continental mine operation was evaluated by means of dilation of fractures exposed in the bench faces and by backbreak along bench crest. Skarn rock always make a good wall. The condition of the rock in the slopes is very good. Except for a few observations, generally the joints remain tight and, hence, mucking operating has cleaned loose material from the slopes very well.

In spite of the general good condition of the slopes, there have been a few locations observed in the south, west and north walls, which have been affected by blasting. The tension crack in the south wall seems to have been formed by blasting the overburden of the extension pit into the south wall. There is also some evidence for noticeable opening on joints and small backbreaks on the west and north slopes. Some of these features may constitute a hazard to men and equipment at working times.

Some controlled blasting has been achieved mainly in the slope to the west of Number 1 crusher, where a raise is being driven from underground. However, more control is recommended, particularly the north slope.

## RECOMMENDATIONS

### Data Collection

Data collection is one of the most time-consuming approaches in slope stability investigation. The writer recommends that UV Industries provide a program for logging engineering characteristics of drill core prior to splitting for various purposes. This particularly should be anticipated for all drill core from areas in which future development is considered. To photograph all

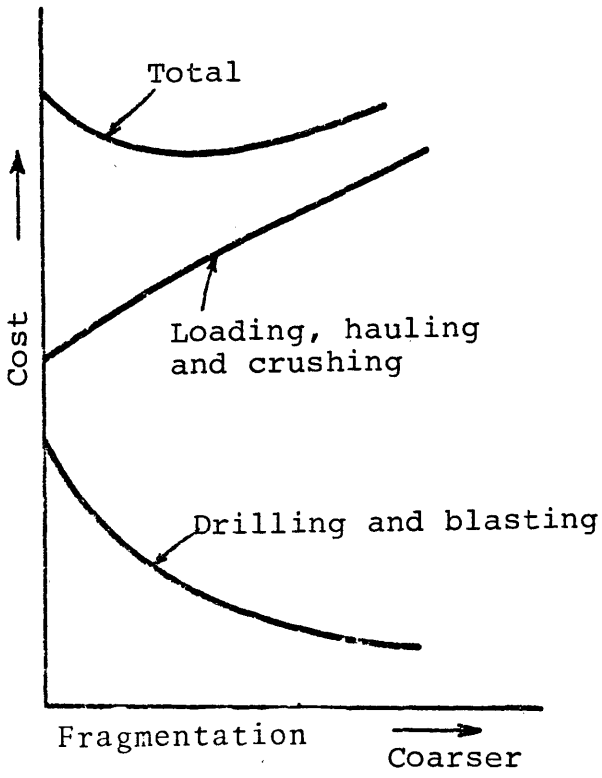


Figure 121. Effect of fragmentation on the cost of drilling, blasting, loading, transporting and crushing in an open pit operation. (From Harries and Mercer, 1975.)

fresh drill core is highly recommended. This will permit logging of the core even if the core itself is no longer available.

Pit Monitoring

A general view of the Continental pit is shown in Figure 122.

Safety considerations require close observation and monitoring of the pit and adjacent slopes by company staff during and following excavation. Regular mine survey personnel often recognize the geologic conditions leading to failure at any early stage. The area around the pit requiring monitoring can be listed in the order of priority, as follows:

1. Barringer-Zuniga fault zone in the south pitwall.
2. Tension crack zone above south slope.
3. General coverage of east and southeast slopes.
4. Southwest wall.
5. General coverage of west and northwest walls.

Noses

There are several benches which have left convex pitwards in the west wall. This area is intensively fractured. The Modoc fault and associated fractures leave a wedge which can fail if the rock strength is overcome. This actually

distributes tangential stresses and causes potential failure problem. Another nose has recently been developed in the south slope by extension of the pit into the south wall. It is strongly recommended that these noses should be avoided and removed.

Slope Angles

Figure 59 and Plate 9 show bench slope angles around the pit. South, west and north walls have bench slope angles of 60-80 degrees and an overall slope angle of 50 degrees. The east and southeast walls have bench slopes of 50-65 degrees with an overall working slope of 40 degrees.

Very high-grade ore has been left on the northeast, north and west walls. The geometry of the orebody suggests that considerable ore will be recovered through steepening of these walls. The overall slope angle of the west pitwall can be as steep as 70 degrees. This will permit mining of the orebody by catch berms and road, but it must be remembered any design in the west section should provide a wide catch berm right below the Beartooth Quartzite. If a haul road is required along the west slope, a steep face should be provided above and below the haul road.

The south slope does not seem to be stable at present design. Considering that several problems exist in

this portion, a 40-degree or less overall slope angle is recommended.

Similar to the south wall, the east slope is almost entirely in the Barringer fault zone which dips to the west and northwest at about 58 degrees. This slope shows strong tendency to plane failure and it is not stable under the present design. The east wall should be flattened to about 30 degrees to provide a flat enough slope.
In addition, it would allow safe conditions for haulage.
Based on the geotechnical information and the experience from site investigation, the following slope configuration is recommended:

| | | |
|---|---|---|
| West and north walls | : | overall slope angle of 60 degrees |
| South wall | : | overall slope angle of 40 degrees or less |
| East wall | : | overall slope angle of 30 degrees. |

Groundwater

During site investigation, all water seeps were noted and have been mapped. Based on this information, there is enough evidence at hand of water pressure in the catchment area of the pit, particularly in the south, southwest and east areas. A surveillance program should be continued and oriented towards collection of data. This data should

include any increase or decrease in groundwater inflow. The most useful information can be collected from blast holes and any other primary drilling during development. The writer recommends that a drainage program should be anticipated for the south wall in particular.

Figure 122. The Continental pit (looking west).

# APPENDIX A

## HISTOGRAMS AND LISTING OF CONTINENTAL MINE FRACTURE DATA

QUADRANT N110,000-N111,000
All data at elevations 6920-6960

| Sequence Number | Strike Azimuth | Dip Angle |
|---|---|---|
| 1 | 222 | 50 |
| 2 | 222 | 60 |
| 3 | 222 | 65 |
| 4 | 222 | 70 |
| 5 | 222 | 55 |
| 6 | 222 | 60 |
| 7 | 222 | 65 |
| 8 | 100 | 40 |
| 9 | 100 | 50 |
| 10 | 45 | 37 |
| 11 | 65 | 45 |
| 12 | 65 | 40 |
| 13 | 65 | 50 |
| 14 | 63 | 48 |
| 15 | 180 | 45 |
| 16 | 60 | 50 |
| 17 | 81 | 60 |
| 18 | 210 | 45 |
| 19 | 210 | 50 |
| 20 | 60 | 55 |
| 21 | 81 | 60 |
| 22 | 65 | 50 |
| 23 | 200 | 40 |
| 24 | 200 | 30 |
| 25 | 200 | 35 |
| 26 | 85 | 45 |
| 27 | 85 | 50 |
| 28 | 85 | 45 |
| 29 | 66 | 50 |
| 30 | 66 | 55 |
| 31 | 66 | 50 |
| 32 | 66 | 50 |
| 33 | 66 | 55 |
| 34 | 66 | 50 |
| 35 | 66 | 50 |
| 36 | 245 | 50 |
| 37 | 245 | 55 |
| 38 | 245 | 55 |
| 39 | 245 | 50 |
| 40 | 245 | 55 |
| 41 | 89 | 49 |
| 42 | 83 | 50 |
| 43 | 87 | 51 |

| Sequence Number | Strike Azimuth | Dip Angle |
|---|---|---|
| 44 | 87 | 47 |
| 45 | 87 | 55 |
| 46 | 99 | 57 |
| 47 | 285 | 57 |
| 48 | 88 | 47 |
| 49 | 88 | 52 |
| 50 | 88 | 64 |
| 51 | 88 | 60 |
| 52 | 88 | 54 |
| 53 | 88 | 53 |
| 54 | 88 | 55 |
| 55 | 88 | 65 |
| 56 | 88 | 60 |
| 57 | 107 | 56 |
| 58 | 96 | 55 |
| 59 | 90 | 60 |
| 60 | 261 | 90 |
| 61 | 261 | 90 |
| 62 | 82 | 62 |
| 63 | 105 | 50 |
| 64 | 97 | 60 |
| 65 | 93 | 62 |
| 66 | 97 | 60 |
| 67 | 115 | 53 |
| 68 | 106 | 46 |
| 69 | 109 | 52 |
| 70 | 109 | 55 |
| 71 | 109 | 62 |
| 72 | 109 | 60 |
| 73 | 278 | 85 |
| 74 | 278 | 85 |
| 75 | 117 | 52 |
| 76 | 111 | 53 |
| 77 | 90 | 61 |
| 78 | 101 | 58 |
| 79 | 101 | 60 |
| 80 | 101 | 61 |
| 81 | 101 | 62 |
| 82 | 101 | 55 |
| 83 | 101 | 52 |
| 84 | 107 | 56 |
| 85 | 107 | 52 |
| 86 | 107 | 63 |
| 87 | 99 | 55 |
| 88 | 99 | 55 |
| 89 | 99 | 60 |
| 90 | 254 | 55 |

| Sequence Number | Strike Azimuth | Dip Angle |
|---|---|---|
| 91 | 254 | 60 |
| 92 | 254 | 58 |
| 93 | 254 | 62 |
| 94 | 84 | 90 |
| 95 | 84 | 90 |
| 96 | 84 | 58 |
| 97 | 97 | 75 |
| 98 | 123 | 50 |
| 99 | 123 | 55 |
| 100 | 253 | 68 |
| 101 | 253 | 65 |
| 102 | 253 | 67 |
| 103 | 253 | 64 |
| 104 | 253 | 66 |
| 105 | 76 | 90 |
| 106 | 96 | 90 |
| 107 | 96 | 90 |
| 108 | 87 | 56 |
| 109 | 87 | 65 |
| 110 | 270 | 89 |
| 111 | 277 | 90 |
| 112 | 275 | 88 |
| 113 | 270 | 75 |
| 114 | 271 | 88 |
| 115 | 270 | 85 |
| 116 | 271 | 90 |
| 117 | 265 | 85 |
| 118 | 247 | 88 |
| 119 | 82 | 78 |
| 120 | 101 | 80 |
| 121 | 104 | 50 |
| 122 | 218 | 52 |
| 123 | 208 | 55 |
| 124 | 67 | 56 |
| 125 | 67 | 55 |
| 126 | 67 | 56 |
| 127 | 67 | 55 |
| 128 | 202 | 52 |
| 129 | 60 | 56 |
| 130 | 60 | 46 |
| 131 | 60 | 52 |
| 132 | 60 | 56 |
| 133 | 60 | 52 |
| 134 | 60 | 51 |
| 135 | 60 | 50 |
| 136 | 70 | 55 |

| Sequence Number | Strike Azimuth | Dip Angle |
|---|---|---|
| 137 | 70 | 52 |
| 138 | 218 | 52 |
| 139 | 223 | 52 |
| 140 | 223 | 50 |
| 141 | 223 | 48 |
| 142 | 223 | 50 |
| 143 | 260 | 60 |
| 144 | 64 | 75 |
| 145 | 64 | 75 |
| 146 | 205 | 55 |
| 147 | 260 | 55 |
| 148 | 90 | 52 |
| 149 | 63 | 82 |
| 150 | 66 | 62 |
| 151 | 78 | 70 |
| 152 | 76 | 66 |
| 153 | 227 | 55 |
| 154 | 227 | 40 |
| 155 | 227 | 52 |
| 156 | 227 | 55 |
| 157 | 335 | 62 |
| 158 | 224 | 55 |
| 159 | 260 | 69 |
| 160 | 74 | 68 |
| 161 | 74 | 66 |
| 162 | 74 | 68 |
| 163 | 74 | 68 |
| 164 | 74 | 65 |
| 165 | 74 | 64 |
| 166 | 70 | 65 |
| 167 | 74 | 65 |
| 168 | 73 | 68 |
| 169 | 87 | 63 |
| 170 | 87 | 60 |
| 171 | 87 | 60 |
| 172 | 87 | 51 |
| 173 | 80 | 55 |
| 174 | 85 | 50 |
| 175 | 87 | 52 |
| 176 | 83 | 56 |
| 177 | 87 | 59 |
| 178 | 78 | 60 |
| 179 | 84 | 52 |
| 180 | 89 | 63 |
| 181 | 82 | 58 |
| 182 | 87 | 62 |

| Sequence Number | Strike Azimuth | Dip Angle |
|---|---|---|
| 183 | 97 | 55 |
| 184 | 90 | 60 |
| 185 | 95 | 65 |
| 186 | 93 | 66 |
| 187 | 97 | 50 |
| 188 | 92 | 62 |
| 189 | 252 | 88 |
| 190 | 250 | 89 |
| 191 | 232 | 90 |
| 192 | 240 | 90 |
| 193 | 244 | 62 |
| 194 | 254 | 62 |
| 195 | 257 | 60 |
| 196 | 91 | 72 |
| 197 | 80 | 90 |
| 198 | 264 | 65 |
| 199 | 238 | 65 |
| 200 | 237 | 60 |
| 201 | 240 | 62 |
| 202 | 236 | 56 |
| 203 | 89 | 49 |
| 204 | 92 | 50 |
| 205 | 264 | 65 |
| 206 | 90 | 62 |
| 207 | 85 | 62 |
| 208 | 95 | 60 |
| 209 | 90 | 55 |
| 210 | 91 | 58 |
| 211 | 89 | 60 |
| 212 | 90 | 62 |
| 213 | 85 | 65 |
| 214 | 87 | 60 |
| 215 | 83 | 65 |
| 216 | 82 | 62 |
| 217 | 80 | 62 |
| 218 | 83 | 65 |
| 219 | 87 | 65 |
| 220 | 80 | 62 |
| 221 | 246 | 62 |
| 222 | 240 | 62 |
| 223 | 245 | 63 |
| 224 | 87 | 55 |
| 225 | 80 | 58 |
| 226 | 84 | 59 |
| 227 | 82 | 60 |
| 228 | 90 | 62 |

| Sequence Number | Strike Azimuth | Dip Angle |
|---|---|---|
| 229 | 97 | 63 |
| 230 | 87 | 55 |
| 231 | 85 | 58 |
| 232 | 86 | 60 |
| 233 | 257 | 60 |
| 234 | 255 | 62 |
| 235 | 250 | 65 |
| 236 | 252 | 65 |
| 237 | 254 | 63 |
| 238 | 260 | 52 |
| 239 | 100 | 60 |
| 240 | 110 | 59 |
| 241 | 105 | 60 |
| 242 | 254 | 65 |
| 243 | 270 | 74 |
| 244 | 237 | 62 |
| 245 | 266 | 62 |
| 246 | 264 | 65 |
| 247 | 260 | 67 |
| 248 | 102 | 58 |
| 249 | 100 | 65 |
| 250 | 105 | 62 |
| 251 | 102 | 55 |
| 252 | 115 | 56 |
| 253 | 90 | 70 |
| 254 | 91 | 71 |
| 255 | 279 | 58 |
| 256 | 80 | 72 |
| 257 | 42 | 54 |

QUADRANT N110,000-N111,000
All data at elevations 6920-6960

STRIKE HISTOGRAM

| Azimuth | Number | Percentage | *....*....*....*....*....*....*....*....*....*.... |
|---|---|---|---|
| 0 | 1 | 0.4 | 0 |
| 10 | 0 | 0.4 | 0 |
| 20 | 4 | 1.9 | 011 |
| 30 | 4 | 3.5 | 011 |
| 40 | 15 | 9.3 | 0111111 |
| 50 | 6 | 11.7 | 011 |
| 60 | 21 | 19.8 | 011111111 |
| 70 | 51 | 39.7 | 01111111111111111111 |
| 80 | 39 | 54.9 | 011111111111111 |
| 90 | 61 | 78.6 | 0111111111111111111111111 |
| 100 | 34 | 91.8 | 011111111111111 |
| 110 | 15 | 97.7 | 0111111 |
| 120 | 5 | 99.6 | 011 |
| 130 | 0 | 99.6 | 0 |
| 140 | 0 | 99.6 | 0 |
| 150 | 0 | 99.6 | 0 |
| 160 | 0 | 100.0 | 0 |
| 170 | 0 | 100.0 | 0 |
| 180 | 0 | 100.0 | 0 |
| | | | *....*....*....*....*....*....*....*....*....*.... |
| | TOTAL | 257 | 0 5 10 15 20 25 30 3 40 45 50,/ |

Percent of Observations

## DIP HISTOGRAM

| Dip | Number | Percentage | *....*....*....*....*....*....*....*....*....*.... |
|---|---|---|---|
| 0 | 0 | 0.0 | 0 |
| 5 | 0 | 0.0 | 0 |
| 10 | 0 | 0.0 | 0 |
| 15 | 0 | 0.0 | 0 |
| 20 | 0 | 0.0 | 0 |
| 25 | 0 | 0.0 | 0 |
| 30 | 1 | 0.4 | 0 |
| 35 | 2 | 1.2 | 01 |
| 40 | 4 | 2.7 | 011 |
| 45 | 9 | 6.2 | 01111 |
| 50 | 48 | 24.9 | 0111111111111111111 |
| 55 | 48 | 43.6 | 0111111111111111111 |
| 60 | 67 | 69.6 | 01111111111111111111111111 |
| 65 | 36 | 83.7 | 011111111111111 |
| 70 | 12 | 88.3 | 011111 |
| 75 | 5 | 90.3 | 011 |
| 80 | 3 | 91.4 | 01 |
| 85 | 4 | 93.0 | 011 |
| 90 | 18 | 100.0 | 01111111 |
| | | | *....*....*....*....*....*....*....*....*....*.... |
| | TOTAL | 257 | 0 5 10 15 20 25 30 3 40 45 50,/ |

Percent of Observations

QUADRANT N110,000-N111,000
All data at elevations 6840-6880

| Sequence Number | Strike Azimuth | Dip Angle |
|---|---|---|
| 1 | 42 | 54 |
| 2 | 60 | 48 |
| 3 | 65 | 54 |
| 4 | 62 | 53 |
| 5 | 61 | 62 |
| 6 | 72 | 40 |
| 7 | 70 | 55 |
| 8 | 60 | 58 |
| 9 | 76 | 63 |
| 10 | 72 | 62 |
| 11 | 77 | 60 |
| 12 | 62 | 65 |
| 13 | 90 | 56 |
| 14 | 80 | 65 |
| 15 | 79 | 65 |
| 16 | 200 | 52 |
| 17 | 195 | 50 |
| 18 | 224 | 62 |
| 19 | 220 | 60 |
| 20 | 214 | 65 |
| 21 | 210 | 58 |
| 22 | 214 | 55 |
| 23 | 200 | 54 |
| 24 | 222 | 60 |
| 25 | 220 | 62 |
| 26 | 223 | 62 |
| 27 | 224 | 67 |
| 28 | 230 | 65 |
| 29 | 60 | 62 |
| 30 | 82 | 65 |
| 31 | 76 | 65 |
| 32 | 90 | 68 |
| 33 | 87 | 70 |
| 34 | 93 | 57 |
| 35 | 78 | 69 |
| 36 | 240 | 55 |
| 37 | 244 | 60 |
| 38 | 80 | 68 |
| 39 | 100 | 58 |
| 40 | 262 | 56 |
| 41 | 93 | 62 |

| Sequence Number | Strike Azimuth | Dip Angle |
|---|---|---|
| 42 | 313 | 61 |
| 43 | 94 | 68 |
| 44 | 90 | 71 |
| 45 | 96 | 67 |
| 46 | 98 | 67 |
| 47 | 89 | 59 |
| 48 | 251 | 58 |
| 49 | 250 | 59 |
| 50 | 255 | 60 |
| 51 | 90 | 58 |
| 52 | 85 | 60 |
| 53 | 80 | 65 |
| 54 | 88 | 66 |
| 55 | 254 | 55 |
| 56 | 250 | 58 |
| 57 | 254 | 52 |
| 58 | 249 | 58 |
| 59 | 257 | 61 |
| 60 | 90 | 58 |
| 61 | 92 | 60 |
| 62 | 88 | 57 |
| 63 | 92 | 62 |
| 64 | 93 | 55 |
| 65 | 98 | 58 |
| 66 | 97 | 60 |
| 67 | 98 | 58 |
| 68 | 89 | 58 |
| 69 | 95 | 60 |
| 70 | 80 | 61 |
| 71 | 144 | 55 |
| 72 | 232 | 58 |
| 73 | 253 | 60 |
| 74 | 235 | 55 |
| 75 | 262 | 70 |
| 76 | 98 | 70 |
| 77 | 108 | 48 |
| 78 | 105 | 51 |
| 79 | 97 | 58 |
| 80 | 100 | 62 |
| 81 | 102 | 59 |
| 82 | 101 | 50 |
| 83 | 95 | 67 |
| 84 | 104 | 49 |
| 85 | 98 | 60 |

| Sequence Number | Strike Azimuth | Dip Angle |
|---|---|---|
| 86 | 100 | 68 |
| 87 | 85 | 69 |
| 88 | 94 | 68 |
| 89 | 96 | 67 |
| 90 | 263 | 55 |
| 91 | 260 | 58 |
| 92 | 269 | 85 |
| 93 | 93 | 67 |
| 94 | 191 | 70 |
| 95 | 50 | 61 |
| 96 | 70 | 57 |
| 97 | 224 | 48 |
| 98 | 227 | 55 |
| 99 | 58 | 60 |
| 100 | 98 | 40 |
| 101 | 98 | 37 |
| 102 | 60 | 88 |
| 103 | 70 | 70 |
| 104 | 245 | 70 |
| 105 | 250 | 68 |
| 106 | 268 | 68 |
| 107 | 84 | 53 |
| 108 | 85 | 50 |
| 109 | 102 | 55 |
| 110 | 100 | 66 |
| 111 | 113 | 40 |
| 112 | 115 | 37 |
| 113 | 110 | 40 |
| 114 | 100 | 62 |
| 115 | 261 | 60 |
| 116 | 104 | 54 |
| 117 | 97 | 57 |
| 118 | 99 | 62 |
| 119 | 95 | 70 |
| 120 | 87 | 71 |
| 121 | 85 | 66 |
| 122 | 77 | 75 |
| 123 | 245 | 52 |
| 124 | 222 | 45 |
| 125 | 97 | 70 |
| 126 | 249 | 70 |
| 127 | 266 | 80 |
| 128 | 102 | 62 |
| 129 | 100 | 59 |
| 130 | 88 | 60 |

| Sequence Number | Strike Azimuth | Dip Angle |
|---|---|---|
| 131 | 89 | 56 |
| 132 | 85 | 59 |
| 133 | 90 | 65 |
| 134 | 89 | 68 |
| 135 | 108 | 68 |
| 136 | 77 | 85 |
| 137 | 260 | 68 |
| 138 | 99 | 62 |
| 139 | 100 | 59 |
| 140 | 85 | 60 |
| 141 | 95 | 62 |
| 142 | 91 | 64 |
| 143 | 100 | 60 |
| 144 | 107 | 60 |
| 145 | 105 | 61 |
| 146 | 97 | 59 |
| 147 | 245 | 56 |
| 148 | 98 | 60 |
| 149 | 99 | 59 |
| 150 | 92 | 72 |
| 151 | 117 | 70 |
| 152 | 278 | 70 |
| 153 | 100 | 68 |
| 154 | 127 | 61 |
| 155 | 102 | 72 |
| 156 | 293 | 58 |
| 157 | 114 | 60 |
| 158 | 107 | 72 |
| 159 | 108 | 65 |

QUADRANT N110,000-N111,000
All data at elevations 6840-6880

STRIKE HISTOGRAM

| Azimuth | Number | Percentage | *....*....*....*....*....*....*....*....*....*.... |
|---|---|---|---|
| 0 | 0 | 0.0 | 0 |
| 10 | 1 | 0.6 | 01 |
| 20 | 3 | 2.5 | 011 |
| 30 | 3 | 4.4 | 011 |
| 40 | 9 | 10.1 | 0111111 |
| 50 | 4 | 12.6 | 0111 |
| 60 | 11 | 19.5 | 01111111 |
| 70 | 18 | 30.8 | 011111111111 |
| 80 | 21 | 44.0 | 0111111111111 |
| 90 | 34 | 65.4 | 01111111111111111111 |
| 100 | 39 | 89.9 | 011111111111111111111111 |
| 110 | 11 | 96.9 | 01111111 |
| 120 | 2 | 98.1 | 01 |
| 130 | 2 | 99.4 | 01 |
| 140 | 1 | 100.0 | 01 |
| 150 | 0 | 100.0 | 0 |
| 160 | 0 | 100.0 | 0 |
| 170 | 0 | 100.0 | 0 |
| 180 | 0 | 100.0 | 0 |
| | | | *....*....*....*....*....*....*....*....*....*.... |
| | TOTAL | 159 | 0 5 10 15 20 25 30 3 40 45 50,/ |

Percent of Observations

## DIP HISTOGRAM

| Azimuth | Number | Percentage | *....*....*....*....*....*....*....*....*....*.... |
|---|---|---|---|
| 0 | 0 | 0.0 | 0 |
| 5 | 0 | 0.0 | 0 |
| 10 | 0 | 0.0 | 0 |
| 15 | 0 | 0.0 | 0 |
| 20 | 0 | 0.0 | 0 |
| 25 | 0 | 0.0 | 0 |
| 30 | 0 | 0.0 | 0 |
| 35 | 2 | 1.3 | 01 |
| 40 | 4 | 3.8 | 0111 |
| 45 | 1 | 4.4 | 01 |
| 50 | 11 | 11.3 | 01111111 |
| 55 | 24 | 26.4 | 011111111111111 |
| 60 | 62 | 65.4 | 01111111111111111111111111111111111111 |
| 65 | 21 | 78.6 | 011111111111 |
| 70 | 29 | 96.9 | 0111111111111111111 |
| 75 | 1 | 97.5 | 01 |
| 80 | 1 | 98.1 | 01 |
| 85 | 2 | 99.4 | 01 |
| 90 | 1 | 100.0 | 01 |
| | | | *....*....*....*....*....*....*....*....*....*.... |
| | TOTAL | 159 | 0 5 10 15 20 25 30 3 40 45 50,/ |

Percent of Observations

QUADRANT N110,000-N111,000
All data at elevations 6760-6800

| Sequence Number | Strike Azimuth | Dip Angle |
|---|---|---|
| 1 | 183 | 55 |
| 2 | 82 | 62 |
| 3 | 235 | 55 |
| 4 | 93 | 55 |
| 5 | 106 | 56 |
| 6 | 100 | 60 |
| 7 | 220 | 55 |
| 8 | 95 | 54 |
| 9 | 119 | 39 |
| 10 | 92 | 60 |
| 11 | 247 | 56 |
| 12 | 80 | 62 |
| 13 | 88 | 60 |
| 14 | 82 | 62 |
| 15 | 263 | 55 |
| 16 | 90 | 60 |
| 17 | 86 | 59 |
| 18 | 288 | 63 |
| 19 | 81 | 62 |
| 20 | 88 | 65 |
| 21 | 84 | 68 |
| 22 | 100 | 70 |
| 23 | 95 | 70 |
| 24 | 273 | 60 |
| 25 | 95 | 59 |
| 26 | 85 | 90 |
| 27 | 94 | 73 |
| 28 | 88 | 73 |
| 29 | 30 | 82 |
| 30 | 85 | 80 |
| 31 | 284 | 62 |
| 32 | 296 | 65 |
| 33 | 118 | 65 |
| 34 | 117 | 68 |
| 35 | 110 | 66 |
| 36 | 290 | 68 |
| 37 | 295 | 65 |
| 38 | 100 | 60 |
| 39 | 188 | 44 |
| 40 | 212 | 39 |
| 41 | 249 | 85 |
| 42 | 103 | 45 |
| 43 | 117 | 40 |
| 44 | 130 | 44 |
| 45 | 261 | 78 |

| Sequence Number | Strike Azimuth | Dip Angle |
|---|---|---|
| 46 | 259 | 70 |
| 47 | 274 | 68 |
| 48 | 90 | 60 |
| 49 | 88 | 90 |
| 50 | 140 | 60 |
| 51 | 265 | 66 |
| 51 | 90 | 67 |
| 53 | 121 | 48 |
| 54 | 105 | 52 |
| 55 | 253 | 58 |
| 56 | 266 | 70 |
| 57 | 85 | 70 |
| 58 | 92 | 54 |
| 59 | 117 | 57 |
| 60 | 110 | 54 |
| 61 | 266 | 59 |
| 62 | 118 | 46 |
| 63 | 85 | 65 |
| 64 | 97 | 80 |
| 65 | 92 | 88 |
| 66 | 94 | 81 |
| 67 | 283 | 90 |
| 68 | 113 | 85 |
| 69 | 104 | 79 |
| 70 | 100 | 85 |
| 71 | 85 | 90 |
| 72 | 87 | 85 |
| 73 | 93 | 88 |
| 74 | 81 | 85 |
| 75 | 112 | 78 |
| 76 | 105 | 82 |
| 77 | 65 | 60 |
| 78 | 50 | 62 |
| 79 | 65 | 75 |
| 80 | 80 | 80 |
| 81 | 72 | 78 |
| 82 | 70 | 76 |
| 83 | 220 | 80 |
| 84 | 222 | 90 |
| 85 | 230 | 88 |
| 86 | 215 | 78 |
| 87 | 218 | 65 |
| 88 | 202 | 60 |
| 89 | 195 | 50 |
| 90 | 200 | 45 |
| 91 | 242 | 70 |
| 92 | 82 | 80 |
| 93 | 70 | 83 |
| 94 | 80 | 78 |
| 95 | 50 | 80 |

QUADRANT N110,000-N111,000
All data at elevations 6760-6800

STRIKE HISTOGRAM

| Azimuth | Number | Percentage | *....*....*....*....*....*....*....*....*....*.... |
|---|---|---|---|
| 0 | 1 | 1.1 | 01 |
| 10 | 1 | 2.1 | 01 |
| 20 | 3 | 5.3 | 0111 |
| 30 | 2 | 7.4 | 011 |
| 40 | 5 | 12.6 | 011111 |
| 50 | 3 | 15.8 | 0111 |
| 60 | 2 | 17.9 | 011 |
| 70 | 8 | 26.3 | 011111111 |
| 80 | 12 | 38.9 | 01111111111111 |
| 90 | 26 | 66.3 | 01111111111111111111111111 |
| 100 | 12 | 78.9 | 01111111111111 |
| 110 | 9 | 88.4 | 0111111111 |
| 120 | 9 | 97.9 | 0111111111 |
| 130 | 1 | 98.9 | 01 |
| 140 | 1 | 100.0 | 01 |
| 150 | 0 | 100.0 | |
| 160 | 0 | 100.0 | |
| 170 | 0 | 100.0 | |
| 180 | 0 | 100.0 | |
| | | | *....*....*....*....*....*....*....*....*....*.... |
| | TOTAL | 95 | 0 5 10 15 20 25 30 3 40 45 50,/ |

Percent of Observations

QUADRANT N110,000-N111,000
All data at elevations 6760-6800

DIP HISTOGRAM

| Azimuth | Number | Percentage | *....*....*....*....*....*....*....*....*....*.... |
|---|---|---|---|
| 0 | 0 | 0.0 | 0 |
| 5 | 0 | 0.0 | 0 |
| 10 | 0 | 0.0 | 0 |
| 15 | 0 | 0.0 | 0 |
| 20 | 0 | 0.0 | 0 |
| 25 | 0 | 0.0 | 0 |
| 30 | 0 | 0.0 | 0 |
| 35 | 0 | 0.0 | 0 |
| 40 | 3 | 3.2 | 0111 |
| 45 | 5 | 8.4 | 011111 |
| 50 | 3 | 11.6 | 0111 |
| 55 | 11 | 23.2 | 01111111111111 |
| 60 | 20 | 44.2 | 01111111111111111111 |
| 65 | 10 | 54.7 | 011111111111 |
| 70 | 10 | 65.3 | 011111111111 |
| 75 | 4 | 69.5 | 01111 |
| 80 | 15 | 85.3 | 01111111111111111 |
| 85 | 6 | 91.6 | 0111111 |
| 90 | 8 | 100.0 | 011111111 |
| | | | *....*....*....*....*....*....*....*....*....*.... |
| | TOTAL | 95 | 0 5 10 15 20 25 30 3 40 45 50,/ |

Percent of Observations

SOUTH EDGE OF PIT
All data from Barringer Fault Zone

| Sequence Number | Strike Azimuth | Dip Angle |
|---|---|---|
| 1 | 180 | 70 |
| 2 | 20 | 68 |
| 3 | 10 | 70 |
| 4 | 200 | 65 |
| 5 | 210 | 72 |
| 6 | 7 | 57 |
| 7 | 195 | 64 |
| 8 | 185 | 65 |
| 9 | 10 | 72 |
| 10 | 182 | 71 |
| 11 | 183 | 67 |
| 12 | 182 | 55 |
| 13 | 360 | 49 |
| 14 | 358 | 45 |
| 15 | 2 | 50 |
| 16 | 345 | 55 |
| 17 | 8 | 54 |
| 18 | 15 | 61 |
| 19 | 195 | 65 |
| 20 | 190 | 52 |
| 21 | 16 | 64 |
| 22 | 50 | 63 |
| 23 | 10 | 68 |
| 24 | 195 | 72 |
| 25 | 225 | 61 |
| 26 | 183 | 56 |
| 27 | 185 | 56 |
| 28 | 200 | 58 |
| 29 | 360 | 60 |
| 30 | 192 | 71 |
| 31 | 306 | 57 |
| 32 | 195 | 58 |
| 33 | 185 | 56 |
| 34 | 195 | 72 |
| 35 | 200 | 63 |
| 36 | 182 | 49 |
| 37 | 190 | 56 |
| 38 | 45 | 78 |
| 39 | 13 | 58 |
| 40 | 193 | 58 |

| Sequence Number | Strike Azimuth | Dip Angle |
|---|---|---|
| 41 | 195 | 60 |
| 42 | 210 | 70 |
| 43 | 185 | 64 |
| 44 | 188 | 62 |
| 45 | 360 | 68 |
| 46 | 198 | 58 |
| 47 | 192 | 55 |
| 48 | 190 | 60 |
| 49 | 200 | 58 |
| 50 | 198 | 62 |
| 51 | 205 | 58 |
| 52 | 208 | 60 |
| 53 | 190 | 70 |
| 54 | 198 | 72 |
| 55 | 195 | 58 |
| 56 | 200 | 60 |
| 57 | 195 | 57 |
| 58 | 190 | 63 |
| 59 | 192 | 65 |

SOUTH EDGE OF PIT
All data from Barringer Fault Zone

STRIKE HISTOGRAM

| Azimuth | Number | Percentage | *....*....*....*....*....*....*....*....*....*.... |
|---|---|---|---|
| 0 | 7 | 11.9 | 0111111111111 |
| 10 | 20 | 45.8 | 01111111111111111111111111111111111 |
| 20 | 19 | 78.0 | 0111111111111111111111111111111 |
| 30 | 4 | 84.7 | 01111111 |
| 40 | 0 | 84.7 | 0 |
| 50 | 3 | 89.8 | 011111 |
| 60 | 0 | 89.8 | 0 |
| 70 | 0 | 89.8 | 0 |
| 80 | 0 | 89.8 | 0 |
| 90 | 0 | 89.8 | 0 |
| 100 | 0 | 89.8 | 0 |
| 110 | 0 | 89.8 | 0 |
| 120 | 0 | 89.8 | 0 |
| 130 | 1 | 91.5 | 011 |
| 140 | 0 | 91.5 | 0 |
| 150 | 0 | 91.5 | 0 |
| 160 | 0 | 91.5 | 0 |
| 170 | 1 | 93.2 | 011 |
| 180 | 4 | 100.0 | 01111111 |
| | | | *....*....*....*....*....*....*....*....*....*.... |
| | TOTAL | 59 | 0 5 10 15 20 25 30 3 40 45 50,/ |

Percent of Observations

SOUTH EDGE OF PIT
All data from Barringer Fault Zone

DIP HISTOGRAM

| Azimuth | Number | Percentage | *....*....*....*....*....*....*....*....*....*....*.... |
|---|---|---|---|
| 0 | 0 | 0.0 | 0 |
| 5 | 0 | 0.0 | 0 |
| 10 | 0 | 0.0 | 0 |
| 15 | 0 | 0.0 | 0 |
| 20 | 0 | 0.0 | 0 |
| 25 | 0 | 0.0 | 0 |
| 30 | 0 | 0.0 | 0 |
| 35 | 0 | 0.0 | 0 |
| 40 | 0 | 0.0 | 0 |
| 45 | 1 | 1.7 | 011 |
| 50 | 4 | 8.5 | 01111111 |
| 55 | 11 | 27.1 | 01111111111111111111 |
| 60 | 17 | 55.9 | 011111111111111111111111111111111 |
| 65 | 11 | 74.6 | 01111111111111111111 |
| 70 | 14 | 98.3 | 011111111111111111111111111 |
| 75 | 0 | 98.3 | 0 |
| 80 | 1 | 100.0 | 011 |
| 85 | 0 | 100.0 | 0 |
| 90 | 0 | 100.0 | 0 |
| | | | *....*....*....*....*....*....*....*....*....*....*.... |
| | TOTAL | 59 | 0 5 10 20 25 30 3 40 45 50,/ |

Percent of Observations

QUADRANT N111,000-N111,750
All data at elevations 6880-6920

| Sequence Number | Strike Azimuth | Dip Angle |
|---|---|---|
| 1 | 88 | 52 |
| 2 | 79 | 60 |
| 3 | 100 | 58 |
| 4 | 92 | 60 |
| 5 | 98 | 65 |
| 6 | 7 | 46 |
| 7 | 198 | 46 |
| 8 | 183 | 45 |
| 9 | 189 | 43 |
| 10 | 183 | 42 |
| 11 | 84 | 65 |
| 12 | 235 | 65 |
| 13 | 220 | 54 |
| 14 | 80 | 72 |
| 15 | 60 | 90 |
| 16 | 260 | 67 |
| 17 | 74 | 64 |
| 18 | 248 | 59 |
| 19 | 70 | 72 |
| 20 | 90 | 62 |
| 21 | 70 | 64 |
| 22 | 255 | 68 |
| 23 | 80 | 49 |
| 24 | 60 | 75 |
| 25 | 241 | 80 |
| 26 | 225 | 82 |
| 27 | 70 | 61 |
| 28 | 71 | 88 |
| 29 | 80 | 60 |
| 30 | 250 | 88 |
| 31 | 71 | 87 |
| 32 | 74 | 75 |
| 33 | 257 | 67 |
| 34 | 70 | 75 |
| 35 | 71 | 78 |
| 36 | 266 | 72 |
| 37 | 280 | 82 |
| 38 | 73 | 90 |
| 39 | 95 | 90 |
| 40 | 288 | 60 |
| 41 | 74 | 83 |
| 42 | 110 | 90 |

| Sequence Number | Strike Azimuth | Dip Angle |
|---|---|---|
| 43 | 75 | 64 |
| 44 | 80 | 90 |
| 45 | 98 | 60 |
| 46 | 98 | 65 |
| 47 | 80 | 68 |
| 48 | 84 | 70 |
| 49 | 100 | 70 |
| 50 | 105 | 75 |
| 51 | 100 | 68 |
| 52 | 110 | 76 |
| 53 | 105 | 62 |
| 54 | 112 | 60 |
| 55 | 105 | 85 |
| 56 | 82 | 76 |
| 57 | 85 | 68 |
| 58 | 88 | 68 |
| 59 | 267 | 70 |
| 60 | 248 | 57 |
| 61 | 258 | 76 |
| 62 | 80 | 72 |
| 63 | 86 | 65 |
| 64 | 88 | 75 |
| 65 | 256 | 75 |
| 66 | 87 | 70 |
| 67 | 80 | 78 |
| 68 | 85 | 66 |
| 69 | 98 | 70 |
| 70 | 275 | 70 |
| 71 | 80 | 82 |
| 72 | 265 | 62 |
| 73 | 88 | 90 |
| 74 | 82 | 90 |
| 75 | 257 | 76 |
| 76 | 251 | 75 |
| 77 | 250 | 70 |
| 78 | 255 | 75 |
| 79 | 70 | 65 |
| 80 | 75 | 75 |
| 81 | 256 | 67 |
| 82 | 90 | 90 |
| 83 | 65 | 72 |
| 84 | 86 | 90 |
| 85 | 265 | 74 |
| 86 | 260 | 75 |
| 87 | 70 | 64 |
| 88 | 93 | 90 |

| Sequence Number | Strike Azimuth | Dip Angle |
|---|---|---|
| 89 | 82 | 70 |
| 90 | 220 | 63 |
| 91 | 60 | 85 |
| 92 | 70 | 90 |
| 93 | 245 | 69 |
| 94 | 75 | 69 |
| 95 | 100 | 68 |
| 96 | 115 | 65 |
| 97 | 226 | 66 |
| 98 | 280 | 88 |
| 99 | 80 | 90 |
| 100 | 280 | 85 |
| 101 | 73 | 90 |
| 102 | 70 | 85 |
| 103 | 80 | 89 |
| 104 | 228 | 55 |
| 105 | 220 | 58 |
| 106 | 240 | 52 |
| 107 | 235 | 58 |
| 108 | 86 | 90 |
| 109 | 79 | 90 |
| 110 | 279 | 87 |
| 111 | 259 | 90 |
| 112 | 242 | 72 |
| 113 | 240 | 59 |
| 114 | 74 | 90 |
| 115 | 98 | 90 |

QUADRANT N111,000-N111,750
All data at elevations 6880-6920

STRIKE HISTOGRAM

| Azimuth | Number | Percentage | *....*....*....*....*....*....*....*....*....*.... |
|---|---|---|---|
| 0 | 2 | 1.7 | 011 |
| 10 | 2 | 3.5 | 011 |
| 20 | 1 | 4.3 | 01 |
| 30 | 0 | 4.3 | 0 |
| 40 | 3 | 710 | 0111 |
| 50 | 3 | 9.6 | 0111 |
| 60 | 9 | 17.4 | 01111111111111111111 |
| 70 | 24 | 38.3 | 011111111111111111111111111 |
| 80 | 30 | 64.3 | 01111111111111111 |
| 90 | 18 | 80.0 | 011111111111111 |
| 100 | 15 | 93.0 | 0111111 |
| 110 | 7 | 99.1 | 01 |
| 120 | 1 | 100.0 | 0 |
| 130 | 0 | 100.0 | 0 |
| 140 | 0 | 100.0 | 0 |
| 150 | 0 | 100.0 | 0 |
| 160 | 0 | 100.0 | 0 |
| 170 | 0 | 100.0 | 0 |
| 180 | 0 | 100.0 | 0 |
| | TOTAL | 115 | *....*....*....*....*....*....*....*....*....*.... |
| | | | 0 5 10 15 20 25 30 3 40 45 50,/ |

Percent of Observations

# DIP HISTOGRAM

| Azimuth | Number | Percentage | *....*....*....*....*....*....*....*....*....*....* |
|---|---|---|---|
| 0 | 0 | 0.0 | 0 |
| 5 | 0 | 0.0 | 0 |
| 10 | 0 | 0.0 | 0 |
| 15 | 0 | 0.0 | 0 |
| 20 | 0 | 0.0 | 0 |
| 25 | 0 | 0.0 | 0 |
| 30 | 0 | 0.0 | 0 |
| 35 | 0 | 0.0 | 0 |
| 40 | 1 | 0.9 | 01 |
| 45 | 4 | 4.3 | 0111 |
| 50 | 3 | 7.0 | 0111 |
| 55 | 3 | 9.6 | 0111 |
| 60 | 15 | 22.6 | 01111111111111 |
| 65 | 17 | 37.4 | 011111111111111 |
| 70 | 22 | 56.5 | 0111111111111111111 |
| 75 | 15 | 69.6 | 01111111111111 |
| 80 | 6 | 74.8 | 011111 |
| 85 | 7 | 80.9 | 0111111 |
| 90 | 22 | 100.0 | 0111111111111111111 |
| | | | *....*....*....*....*....*....*....*....*....*....* |
| | TOTAL | 115 | 0 5 10 15 20 25 30 3 40 45 50,/ |

Percent of Observations

QUADRANT N111,000-N111,750
All data at elevations 6800-6840

| Sequence Number | Strike Azimuth | Dip Angle |
|---|---|---|
| 1 | 88 | 79 |
| 2 | 105 | 70 |
| 3 | 281 | 70 |
| 4 | 105 | 90 |
| 5 | 120 | 55 |
| 6 | 121 | 60 |
| 7 | 125 | 62 |
| 8 | 86 | 84 |
| 9 | 106 | 90 |
| 10 | 84 | 84 |
| 11 | 91 | 76 |
| 12 | 93 | 85 |
| 13 | 280 | 85 |
| 14 | 92 | 79 |
| 15 | 93 | 71 |
| 16 | 77 | 79 |
| 17 | 244 | 45 |
| 18 | 100 | 68 |
| 19 | 226 | 55 |
| 20 | 250 | 60 |
| 21 | 244 | 55 |
| 22 | 250 | 45 |
| 23 | 95 | 68 |
| 24 | 240 | 58 |
| 25 | 92 | 78 |
| 26 | 90 | 76 |
| 27 | 91 | 65 |
| 28 | 79 | 79 |
| 29 | 77 | 80 |
| 30 | 253 | 80 |
| 31 | 89 | 90 |
| 32 | 78 | 90 |
| 33 | 90 | 58 |
| 34 | 73 | 85 |
| 35 | 265 | 85 |
| 36 | 244 | 60 |
| 37 | 70 | 60 |
| 38 | 100 | 55 |
| 39 | 82 | 72 |
| 40 | 225 | 45 |
| 41 | 70 | 85 |
| 42 | 263 | 82 |

| Sequence Number | Strike Azimuth | Dip Angle |
|---|---|---|
| 43 | 74 | 71 |
| 44 | 62 | 80 |
| 45 | 240 | 56 |
| 46 | 245 | 62 |
| 47 | 235 | 60 |
| 48 | 246 | 61 |
| 49 | 70 | 68 |
| 50 | 75 | 62 |
| 51 | 70 | 70 |
| 52 | 245 | 70 |
| 53 | 252 | 61 |
| 54 | 220 | 64 |
| 55 | 219 | 60 |
| 56 | 77 | 62 |
| 57 | 82 | 72 |
| 58 | 232 | 58 |
| 59 | 232 | 60 |
| 60 | 230 | 65 |
| 61 | 235 | 68 |
| 62 | 215 | 70 |
| 63 | 68 | 78 |
| 64 | 215 | 57 |
| 65 | 224 | 72 |
| 66 | 250 | 70 |
| 67 | 91 | 73 |
| 68 | 80 | 81 |
| 69 | 251 | 66 |
| 70 | 250 | 62 |
| 71 | 223 | 47 |
| 72 | 77 | 73 |
| 73 | 74 | 83 |
| 74 | 82 | 85 |
| 75 | 264 | 59 |
| 76 | 283 | 78 |
| 77 | 70 | 72 |
| 78 | 68 | 76 |
| 79 | 264 | 60 |
| 80 | 266 | 61 |
| 81 | 88 | 59 |
| 82 | 78 | 60 |
| 83 | 266 | 60 |
| 84 | 259 | 63 |
| 85 | 80 | 72 |
| 86 | 74 | 85 |
| 87 | 285 | 85 |
| 88 | 115 | 70 |

| Sequence Number | Strike Azimuth | Dip Angle |
|---|---|---|
| 89 | 133 | 52 |
| 90 | 97 | 88 |
| 91 | 100 | 78 |
| 92 | 310 | 85 |
| 93 | 295 | 75 |
| 94 | 280 | 80 |
| 95 | 279 | 80 |
| 96 | 105 | 79 |
| 97 | 295 | 85 |
| 98 | 80 | 70 |
| 99 | 72 | 83 |
| 100 | 84 | 70 |
| 101 | 86 | 74 |
| 102 | 80 | 73 |
| 103 | 248 | 55 |
| 104 | 240 | 48 |
| 105 | 83 | 73 |
| 106 | 88 | 75 |
| 107 | 255 | 65 |
| 108 | 67 | 75 |
| 109 | 215 | 71 |
| 110 | 273 | 87 |
| 111 | 228 | 60 |
| 112 | 220 | 58 |
| 113 | 225 | 60 |
| 114 | 218 | 57 |
| 115 | 215 | 58 |
| 116 | 85 | 64 |
| 117 | 104 | 48 |
| 118 | 268 | 66 |
| 119 | 72 | 75 |
| 120 | 117 | 72 |
| 121 | 286 | 80 |
| 122 | 74 | 75 |
| 123 | 263 | 82 |
| 124 | 244 | 70 |
| 125 | 248 | 75 |
| 126 | 240 | 83 |
| 127 | 76 | 78 |
| 128 | 74 | 69 |
| 129 | 82 | 67 |
| 130 | 70 | 82 |
| 131 | 84 | 76 |
| 132 | 263 | 69 |
| 133 | 224 | 70 |
| 134 | 73 | 83 |

| Sequence Number | Strike Azimuth | Dip Angle |
|---|---|---|
| 135 | 82 | 78 |
| 136 | 243 | 79 |
| 137 | 224 | 74 |
| 138 | 67 | 80 |
| 139 | 79 | 84 |
| 140 | 241 | 67 |
| 141 | 221 | 78 |
| 142 | 230 | 68 |
| 143 | 62 | 88 |
| 144 | 50 | 85 |
| 145 | 60 | 90 |
| 146 | 70 | 75 |
| 147 | 295 | 85 |
| 148 | 68 | 74 |
| 149 | 80 | 82 |
| 150 | 62 | 75 |
| 151 | 70 | 80 |
| 152 | 226 | 55 |
| 153 | 254 | 60 |
| 154 | 230 | 54 |
| 155 | 227 | 50 |
| 156 | 205 | 58 |
| 157 | 246 | 59 |
| 158 | 240 | 57 |
| 159 | 241 | 60 |
| 160 | 70 | 82 |
| 161 | 65 | 83 |
| 162 | 60 | 76 |
| 163 | 78 | 61 |
| 164 | 242 | 62 |
| 165 | 250 | 63 |
| 166 | 242 | 60 |
| 167 | 238 | 61 |
| 168 | 68 | 80 |
| 169 | 228 | 67 |
| 170 | 236 | 70 |
| 171 | 240 | 75 |
| 172 | 68 | 85 |
| 173 | 64 | 90 |
| 174 | 69 | 82 |

QUADRANT N111,000-N111,750
All data at elevations 6800-6840

STRIKE HISTOGRAM

| Azimuth | Number | Percentage | *....*....*....*....*....*....*....*....*....*.... |
|---|---|---|---|
| 0 | 0 | 0.0 | 0 |
| 10 | 0 | 0.0 | 0 |
| 20 | 0 | 0.0 | 0 |
| 30 | 1 | 0.6 | 01 |
| 40 | 13 | 8.0 | 01111111 |
| 50 | 13 | 15.5 | 01111111 |
| 60 | 25 | 29.9 | 0111111111111111 |
| 70 | 42 | 54.0 | 01111111111111111111111111 |
| 80 | 32 | 72.4 | 01111111111111111 |
| 90 | 21 | 84.5 | 0111111111111 |
| 100 | 11 | 90.8 | 0111111 |
| 110 | 6 | 94.3 | 0111 |
| 120 | 7 | 98.3 | 01111 |
| 130 | 3 | 100.0 | 011 |
| 140 | 0 | 100.0 | 0 |
| 150 | 0 | 100.0 | 0 |
| 160 | 0 | 100.0 | 0 |
| 170 | 0 | 100.0 | 0 |
| 180 | 0 | 100.0 | 0 |
| | TOTAL | 174 | *....*....*....*....*....*....*....*....*....*.... |
| | | | 0 5 10 15 20 25 30 3 40 45 50,/ |

Percent of Observations

DIP HISTOGRAM

| Azimuth | Number | Percentage | *....*....*....*....*....*....*....*....*....*.... |
|---|---|---|---|
| 0 | 0 | 0.0 | 0 |
| 5 | 0 | 0.0 | 0 |
| 10 | 0 | 0.0 | 0 |
| 15 | 0 | 0.0 | 0 |
| 20 | 0 | 0.0 | 0 |
| 25 | 0 | 0.0 | 0 |
| 30 | 0 | 0.0 | 0 |
| 35 | 0 | 0.0 | 0 |
| 40 | 0 | 0.0 | 0 |
| 45 | 4 | 2.3 | 011 |
| 50 | 4 | 4.6 | 011 |
| 55 | 11 | 10.9 | 0111111 |
| 60 | 35 | 31.0 | 01111111111111111111 |
| 65 | 23 | 37.9 | 01111111 |
| 70 | 28 | 54.0 | 011111111111111111 |
| 75 | 21 | 66.1 | 0111111111111 |
| 80 | 29 | 82.8 | 011111111111111111 |
| 85 | 22 | 95.4 | 0111111111111 |
| 90 | 8 | 100.0 | 011111 |
| | TOTAL | 174 | *....*....*....*....*....*....*....*....*....*.... |
| | | | 0 5 10 15 20 25 30 3 40 45 50,/ |

Percent of Observations

QUADRANT N111,000-N111,750
All data at elevations 6720-6760

| Sequence Number | Strike Azimuth | Dip Angle |
|---|---|---|
| 1 | 60 | 88 |
| 2 | 253 | 62 |
| 3 | 187 | 65 |
| 4 | 60 | 79 |
| 5 | 66 | 80 |
| 6 | 70 | 78 |
| 7 | 58 | 83 |
| 8 | 202 | 54 |
| 9 | 200 | 58 |
| 10 | 58 | 67 |
| 11 | 60 | 65 |
| 12 | 75 | 60 |
| 13 | 70 | 62 |
| 14 | 214 | 58 |
| 15 | 68 | 75 |
| 16 | 250 | 75 |
| 17 | 280 | 85 |
| 18 | 250 | 85 |
| 19 | 50 | 65 |
| 20 | 62 | 64 |
| 21 | 65 | 80 |
| 22 | 58 | 81 |
| 23 | 60 | 70 |
| 24 | 187 | 49 |
| 25 | 60 | 67 |
| 26 | 215 | 59 |
| 27 | 210 | 60 |
| 28 | 58 | 85 |
| 29 | 60 | 78 |
| 30 | 55 | 76 |
| 31 | 216 | 59 |
| 32 | 220 | 60 |
| 33 | 218 | 61 |
| 34 | 50 | 81 |
| 35 | 213 | 69 |
| 36 | 225 | 66 |
| 37 | 215 | 60 |
| 38 | 208 | 58 |
| 39 | 68 | 75 |
| 40 | 63 | 72 |
| 41 | 226 | 65 |
| 42 | 230 | 68 |
| 43 | 218 | 70 |
| 44 | 235 | 75 |
| 45 | 60 | 85 |

| Sequence Number | Strike Azimuth | Dip Angle |
|---|---|---|
| 46 | 69 | 64 |
| 47 | 58 | 65 |
| 48 | 70 | 70 |
| 49 | 60 | 75 |
| 50 | 220 | 59 |
| 51 | 207 | 60 |
| 52 | 244 | 62 |
| 53 | 247 | 73 |
| 54 | 240 | 74 |
| 55 | 217 | 60 |
| 56 | 227 | 58 |
| 57 | 60 | 90 |
| 58 | 242 | 89 |
| 59 | 68 | 85 |
| 60 | 240 | 87 |
| 61 | 248 | 75 |
| 62 | 70 | 90 |
| 63 | 188 | 60 |
| 64 | 58 | 90 |
| 65 | 250 | 72 |
| 66 | 240 | 65 |
| 67 | 205 | 68 |
| 68 | 237 | 79 |
| 69 | 76 | 90 |
| 70 | 60 | 85 |
| 71 | 68 | 90 |
| 72 | 232 | 61 |
| 73 | 218 | 70 |
| 74 | 59 | 75 |
| 75 | 112 | 70 |
| 76 | 227 | 75 |
| 77 | 230 | 58 |
| 78 | 190 | 45 |
| 79 | 60 | 88 |
| 80 | 50 | 85 |
| 81 | 243 | 75 |
| 82 | 70 | 78 |
| 83 | 100 | 55 |
| 84 | 107 | 65 |
| 85 | 98 | 60 |
| 86 | 118 | 60 |
| 87 | 100 | 65 |
| 88 | 103 | 58 |
| 89 | 98 | 55 |
| 90 | 225 | 48 |
| 91 | 80 | 82 |
| 92 | 110 | 90 |
| 93 | 70 | 90 |
| 94 | 223 | 63 |

QUADRANT N111,000-N111,750
All data at elevations 6720-6760

STRIKE HISTOGRAM

| Azimuth | Number | Percentage | |
|---|---|---|---|
| | | | *....*....*....*....*....*....*....*....*....*.... |
| 0 | 0 | 0.0 | 0 |
| 10 | 4 | 4.3 | 01111 |
| 20 | 2 | 6.4 | 011 |
| 30 | 6 | 12.8 | 0111111 |
| 40 | 10 | 23.4 | 011111111111 |
| 50 | 11 | 35.1 | 011111111111 |
| 60 | 29 | 66.0 | 01111111111111111111111111111111 |
| 70 | 19 | 86.2 | 0111111111111111111 |
| 80 | 3 | 89.4 | 0111 |
| 90 | 0 | 89.4 | 0 |
| 100 | 6 | 95.7 | 0111111 |
| 110 | 3 | 98.9 | 0111 |
| 120 | 1 | 100.0 | 0 |
| 130 | 0 | 100.0 | 0 |
| 140 | 0 | 100.0 | 0 |
| 150 | 0 | 100.0 | 0 |
| 160 | 0 | 100.0 | 0 |
| 170 | 0 | 100.0 | 0 |
| 180 | 0 | 100.0 | 0 |
| | | | *....*....*....*....*....*....*....*....*....*.... |
| | TOTAL | 94 | 0 5 10 15 20 25 30 3 40 45 50,/ |

Percent of Observations

# DIP HISTOGRAM

| Azimuth | Number | Percentage | |
|---|---|---|---|
| | | | *....*....*....*....*....*....*....*....*....*.... |
| 0 | 0 | 0.0 | 0 |
| 5 | 0 | 0.0 | 0 |
| 10 | 0 | 0.0 | 0 |
| 15 | 0 | 0.0 | 0 |
| 20 | 0 | 0.0 | 0 |
| 25 | 0 | 0.0 | 0 |
| 30 | 0 | 0.0 | 0 |
| 35 | 0 | 0.0 | 0 |
| 40 | 0 | 0.0 | 0 |
| 45 | 1 | 1.1 | 01 |
| 50 | 2 | 3.2 | 011 |
| 55 | 3 | 6.4 | 0111 |
| 60 | 23 | 30.9 | 01111111111111111111111 |
| 65 | 14 | 45.7 | 0111111111111111 |
| 70 | 10 | 56.4 | 011111111111 |
| 75 | 12 | 69.1 | 0111111111111 |
| 80 | 10 | 79.8 | 011111111111 |
| 85 | 9 | 89.4 | 01111111111 |
| 90 | 10 | 100.0 | 011111111111 |
| | | | *....*....*....*....*....*....*....*....*....*.... |
| | TOTAL | 94 | 0 5 10 15 20 25 30 3 40 45 50,/ |

Percent of Observations

QUADRANT N111,750-N112,750
All data at elevations 6880-6920

| Sequence Number | Strike Azimuth | Dip Angle |
|---|---|---|
| 1 | 330 | 78 |
| 2 | 326 | 83 |
| 3 | 92 | 90 |
| 4 | 126 | 52 |
| 5 | 300 | 66 |
| 6 | 314 | 83 |
| 7 | 220 | 45 |
| 8 | 75 | 68 |
| 9 | 240 | 38 |
| 10 | 220 | 35 |
| 11 | 310 | 62 |
| 12 | 330 | 62 |
| 13 | 120 | 68 |
| 14 | 136 | 82 |
| 15 | 321 | 72 |
| 16 | 140 | 90 |
| 17 | 139 | 50 |
| 18 | 20 | 36 |
| 19 | 255 | 77 |
| 20 | 145 | 44 |
| 21 | 75 | 90 |
| 22 | 70 | 90 |
| 23 | 50 | 88 |
| 24 | 54 | 80 |
| 25 | 60 | 85 |
| 26 | 70 | 90 |
| 27 | 80 | 90 |
| 28 | 68 | 85 |
| 29 | 60 | 80 |
| 30 | 70 | 67 |
| 31 | 74 | 68 |
| 32 | 69 | 90 |
| 33 | 65 | 65 |
| 34 | 100 | 64 |
| 35 | 307 | 51 |
| 36 | 305 | 72 |
| 37 | 84 | 90 |
| 38 | 80 | 90 |
| 39 | 313 | 50 |
| 40 | 350 | 78 |
| 41 | 50 | 88 |
| 42 | 48 | 84 |

| Sequence Number | Strike Azimuth | Dip Angle |
|---|---|---|
| 43 | 50 | 88 |
| 44 | 197 | 62 |
| 45 | 209 | 58 |
| 46 | 207 | 70 |
| 47 | 200 | 70 |
| 48 | 115 | 42 |
| 49 | 321 | 56 |
| 50 | 207 | 60 |
| 51 | 20 | 85 |
| 52 | 25 | 82 |
| 53 | 24 | 85 |
| 54 | 18 | 82 |
| 55 | 72 | 72 |
| 56 | 250 | 65 |
| 57 | 82 | 68 |
| 58 | 230 | 58 |
| 59 | 225 | 42 |
| 60 | 101 | 90 |
| 61 | 100 | 59 |
| 62 | 75 | 67 |
| 63 | 100 | 61 |
| 64 | 80 | 82 |
| 65 | 227 | 60 |
| 66 | 261 | 78 |
| 67 | 223 | 56 |
| 68 | 80 | 78 |
| 69 | 75 | 78 |
| 70 | 210 | 50 |
| 71 | 85 | 79 |
| 72 | 110 | 60 |
| 73 | 105 | 59 |
| 74 | 216 | 55 |
| 75 | 110 | 56 |
| 76 | 112 | 57 |
| 77 | 105 | 62 |
| 78 | 100 | 59 |
| 79 | 320 | 72 |
| 80 | 130 | 52 |
| 81 | 20 | 60 |
| 82 | 123 | 64 |
| 83 | 131 | 59 |
| 84 | 130 | 55 |
| 85 | 120 | 52 |
| 86 | 132 | 55 |
| 87 | 120 | 52 |
| 88 | 230 | 49 |

| Sequence Number | Strike Azimuth | Dip Angle |
|---|---|---|
| 89 | 229 | 45 |
| 90 | 228 | 46 |
| 91 | 225 | 48 |
| 92 | 220 | 49 |
| 93 | 240 | 45 |
| 94 | 271 | 64 |
| 95 | 287 | 84 |
| 96 | 212 | 45 |
| 97 | 220 | 45 |
| 98 | 212 | 44 |
| 99 | 230 | 47 |
| 100 | 132 | 55 |
| 101 | 286 | 84 |
| 102 | 105 | 88 |
| 103 | 120 | 57 |
| 104 | 104 | 60 |
| 105 | 280 | 85 |
| 106 | 50 | 55 |
| 107 | 218 | 48 |
| 108 | 215 | 44 |
| 109 | 218 | 50 |
| 110 | 220 | 60 |
| 111 | 215 | 55 |
| 112 | 298 | 62 |
| 113 | 160 | 50 |
| 114 | 138 | 56 |
| 115 | 175 | 48 |
| 116 | 172 | 55 |
| 117 | 215 | 47 |
| 118 | 210 | 50 |
| 119 | 320 | 58 |
| 120 | 295 | 63 |
| 121 | 140 | 60 |
| 122 | 275 | 57 |
| 123 | 220 | 45 |
| 124 | 210 | 48 |
| 125 | 25 | 64 |
| 126 | 273 | 55 |
| 127 | 146 | 90 |
| 128 | 120 | 79 |
| 129 | 207 | 50 |
| 130 | 325 | 83 |
| 131 | 317 | 85 |
| 132 | 170 | 50 |

| Sequence Number | Strike Azimuth | Dip Angle |
|---|---|---|
| 133 | 309 | 45 |
| 134 | 140 | 64 |
| 135 | 135 | 86 |
| 136 | 295 | 69 |
| 137 | 138 | 90 |
| 138 | 225 | 49 |
| 139 | 227 | 50 |
| 140 | 230 | 55 |
| 141 | 140 | 81 |
| 142 | 145 | 77 |
| 143 | 133 | 79 |
| 144 | 345 | 80 |
| 145 | 140 | 90 |
| 146 | 296 | 72 |
| 147 | 135 | 90 |
| 148 | 300 | 72 |
| 149 | 217 | 81 |
| 150 | 242 | 73 |
| 151 | 245 | 80 |
| 152 | 205 | 77 |
| 153 | 200 | 78 |
| 154 | 210 | 75 |
| 155 | 210 | 75 |
| 156 | 205 | 67 |
| 157 | 210 | 60 |
| 158 | 187 | 53 |
| 159 | 35 | 83 |
| 160 | 37 | 77 |
| 161 | 20 | 90 |
| 162 | 35 | 81 |
| 163 | 30 | 75 |
| 164 | 37 | 80 |
| 165 | 33 | 70 |
| 166 | 30 | 75 |

QUADRANT N111,750-112,750
All data at elevations 6880-6920

STRIKE HISTOGRAM

| Azimuth | Number | Percentage | *....*....*....*....*....*....*....*....*....*.... |
|---|---|---|---|
| 0 | 1 | 0.6 | 01 |
| 10 | 1 | 1.2 | 01 |
| 20 | 9 | 6.6 | 011111 |
| 30 | 19 | 18.1 | 011111111111 |
| 40 | 18 | 28.9 | 011111111111 |
| 50 | 17 | 39.2 | 011111111111 |
| 60 | 5 | 42.2 | 0111 |
| 70 | 10 | 48.2 | 0111111 |
| 80 | 12 | 55.4 | 01111111 |
| 90 | 4 | 57.8 | 011 |
| 100 | 8 | 62.7 | 011111 |
| 110 | 8 | 67.5 | 011111 |
| 120 | 13 | 75.3 | 011111111 |
| 130 | 13 | 83.1 | 011111111 |
| 140 | 16 | 92.8 | 011111111111 |
| 150 | 7 | 97.0 | 01111 |
| 160 | 1 | 97.6 | 01 |
| 170 | 4 | 100.0 | 011 |
| 180 | 0 | 100.0 | 0 |
| | | | *....*....*....*....*....*....*....*....*....*.... |
| | TOTAL | 166 | 0 5 10 15 20 25 30 3 40 45 50,/ |

Percent of Observations

# DIP HISTOGRAM

| Azimuth | Number | Percentage | *....*....*....*....*....*....*....*....*....*.... |
|---|---|---|---|
| 0 | 0 | 0.0 | 0 |
| 5 | 0 | 0.0 | 0 |
| 10 | 0 | 0.0 | 0 |
| 15 | 0 | 0.0 | 0 |
| 20 | 0 | 0.0 | 0 |
| 25 | 0 | 0.0 | 0 |
| 30 | 0 | 0.0 | 0 |
| 35 | 2 | 1.2 | 01 |
| 40 | 3 | 3.0 | 011 |
| 45 | 13 | 10.8 | 011111111 |
| 50 | 21 | 23.5 | 01111111111111 |
| 55 | 17 | 33.7 | 01111111111 |
| 60 | 21 | 46.4 | 01111111111111 |
| 65 | 12 | 53.6 | 01111111 |
| 70 | 14 | 62.0 | 011111111 |
| 75 | 9 | 67.5 | 011111 |
| 80 | 21 | 80.1 | 01111111111111 |
| 85 | 14 | 88.6 | 011111111 |
| 90 | 19 | 100.0 | 011111111111 |
| | | | *....*....*....*....*....*....*....*....*....*.... |
| | TOTAL | 166 | 0 5 10 15 20 25 30 3 40 45 50,/ |

Percent of Observations

QUADRANT N111,750-N112,750
All data at elevations 6800-6840

| Sequence Number | Strike Azimuth | Dip Angle |
|---|---|---|
| 1 | 226 | 50 |
| 2 | 80 | 72 |
| 3 | 95 | 60 |
| 4 | 100 | 59 |
| 5 | 254 | 61 |
| 6 | 242 | 59 |
| 7 | 86 | 90 |
| 8 | 100 | 75 |
| 9 | 230 | 75 |
| 10 | 90 | 90 |
| 11 | 235 | 72 |
| 12 | 237 | 60 |
| 13 | 220 | 57 |
| 14 | 211 | 60 |
| 15 | 70 | 90 |
| 16 | 95 | 57 |
| 17 | 100 | 81 |
| 18 | 98 | 76 |
| 19 | 94 | 90 |
| 20 | 85 | 90 |
| 21 | 80 | 90 |
| 22 | 270 | 88 |
| 23 | 74 | 90 |
| 24 | 257 | 70 |
| 25 | 220 | 46 |
| 26 | 120 | 55 |
| 27 | 120 | 47 |
| 28 | 140 | 68 |
| 29 | 135 | 65 |
| 30 | 130 | 59 |
| 31 | 135 | 60 |
| 32 | 118 | 72 |
| 33 | 120 | 70 |
| 34 | 225 | 46 |
| 35 | 132 | 46 |
| 36 | 262 | 42 |
| 37 | 110 | 55 |
| 38 | 115 | 72 |
| 39 | 274 | 68 |
| 40 | 228 | 48 |
| 41 | 220 | 50 |
| 42 | 230 | 55 |

| Sequence Number | Strike Azimuth | Dip Angle |
|---|---|---|
| 43 | 120 | 90 |
| 44 | 128 | 57 |
| 45 | 291 | 61 |
| 46 | 170 | 58 |
| 47 | 297 | 68 |
| 48 | 230 | 56 |
| 49 | 232 | 50 |
| 50 | 294 | 61 |
| 51 | 257 | 57 |
| 52 | 255 | 60 |
| 53 | 303 | 82 |
| 54 | 140 | 68 |
| 55 | 303 | 80 |
| 56 | 140 | 68 |
| 57 | 303 | 80 |
| 58 | 140 | 68 |
| 59 | 280 | 64 |
| 60 | 285 | 60 |
| 61 | 280 | 65 |
| 62 | 325 | 69 |
| 63 | 240 | 43 |
| 64 | 235 | 44 |
| 65 | 330 | 71 |
| 66 | 343 | 74 |
| 67 | 183 | 72 |
| 68 | 187 | 74 |
| 69 | 185 | 59 |
| 70 | 190 | 58 |
| 71 | 195 | 50 |
| 72 | 234 | 52 |
| 73 | 250 | 49 |
| 74 | 238 | 48 |
| 75 | 140 | 58 |
| 76 | 175 | 61 |
| 77 | 70 | 51 |
| 78 | 233 | 44 |
| 79 | 225 | 48 |
| 80 | 230 | 70 |
| 81 | 92 | 90 |
| 82 | 80 | 90 |
| 83 | 70 | 86 |
| 84 | 238 | 62 |
| 85 | 230 | 63 |
| 86 | 240 | 65 |
| 87 | 219 | 65 |
| 88 | 225 | 66 |

| Sequence Number | Strike Azimuth | Dip Angle |
|---|---|---|
| 89 | 68 | 90 |
| 90 | 72 | 70 |
| 91 | 248 | 70 |
| 92 | 258 | 64 |
| 93 | 250 | 70 |
| 94 | 236 | 64 |
| 95 | 246 | 70 |
| 96 | 246 | 68 |
| 97 | 62 | 70 |
| 98 | 79 | 61 |
| 99 | 44 | 90 |
| 100 | 254 | 84 |
| 101 | 66 | 90 |
| 102 | 205 | 64 |
| 103 | 100 | 75 |
| 104 | 264 | 75 |
| 105 | 83 | 90 |
| 106 | 120 | 70 |
| 107 | 125 | 65 |
| 108 | 130 | 60 |
| 109 | 120 | 90 |
| 110 | 220 | 67 |
| 111 | 218 | 70 |
| 112 | 207 | 55 |
| 113 | 235 | 56 |
| 114 | 230 | 55 |
| 115 | 273 | 80 |
| 116 | 108 | 90 |
| 117 | 225 | 57 |
| 118 | 116 | 76 |
| 119 | 304 | 88 |
| 120 | 42 | 85 |
| 121 | 40 | 90 |
| 122 | 38 | 90 |
| 123 | 280 | 60 |
| 124 | 315 | 70 |
| 125 | 310 | 75 |
| 126 | 130 | 90 |
| 127 | 302 | 70 |
| 128 | 305 | 80 |
| 129 | 310 | 85 |
| 130 | 148 | 90 |
| 131 | 135 | 90 |
| 132 | 329 | 82 |

| Sequence Number | Strike Azimuth | Dip Angle |
|---|---|---|
| 133 | 120 | 90 |
| 134 | 320 | 85 |
| 135 | 305 | 70 |
| 136 | 330 | 80 |
| 137 | 130 | 90 |
| 138 | 300 | 85 |
| 139 | 224 | 44 |
| 140 | 225 | 46 |
| 141 | 120 | 57 |
| 142 | 125 | 60 |
| 143 | 109 | 80 |
| 144 | 125 | 82 |
| 145 | 183 | 55 |
| 146 | 185 | 60 |
| 147 | 190 | 85 |
| 148 | 230 | 55 |
| 149 | 7 | 56 |
| 150 | 14 | 60 |
| 151 | 20 | 79 |
| 152 | 19 | 80 |
| 153 | 15 | 55 |
| 154 | 20 | 65 |
| 155 | 25 | 60 |
| 156 | 18 | 70 |
| 157 | 27 | 75 |
| 158 | 25 | 60 |
| 159 | 30 | 65 |
| 160 | 10 | 80 |
| 161 | 5 | 72 |
| 162 | 226 | 47 |
| 163 | 246 | 46 |
| 164 | 248 | 45 |
| 165 | 248 | 35 |
| 166 | 247 | 48 |
| 167 | 233 | 50 |
| 168 | 272 | 50 |
| 169 | 47 | 72 |
| 170 | 340 | 61 |
| 171 | 260 | 50 |
| 172 | 243 | 45 |
| 173 | 240 | 48 |
| 174 | 242 | 47 |
| 175 | 178 | 72 |
| 176 | 315 | 65 |
| 177 | 237 | 50 |
| 178 | 204 | 43 |
| 179 | 208 | 45 |

QUADRANT N111,750-N112,750
All data at elevations 6800-6840

STRIKE HISTOGRAM

| Azimuth | Number | Percentage | *....*....*....*....*....*....*....*....*.... |
|---|---|---|---|
| 0 | 4 | 2.2 | 011 |
| 10 | 9 | 7.3 | 011111 |
| 20 | 7 | 11.2 | 01111 |
| 30 | 8 | 15.6 | 01111 |
| 40 | 11 | 21.8 | 0111111 |
| 50 | 20 | 33.0 | 011111111111 |
| 60 | 15 | 41.3 | 011111111 |
| 70 | 18 | 51.4 | 01111111111 |
| 80 | 12 | 58.1 | 01111111 |
| 90 | 9 | 63.1 | 011111 |
| 100 | 10 | 68.7 | 0111111 |
| 110 | 6 | 72.1 | 0111 |
| 120 | 18 | 82.1 | 01111111111 |
| 130 | 13 | 89.4 | 01111111 |
| 140 | 11 | 95.5 | 0111111 |
| 150 | 5 | 98.3 | 0111 |
| 160 | 2 | 99.4 | 01 |
| 170 | 1 | 100.0 | 01 |
| 180 | 0 | 100.0 | 0 |
| | | | *....*....*....*....*....*....*....*....*.... |
| | TOTAL | 179 | 0 5 10 15 20 25 30 3 45 50,/ |

Percent of Observations

## DIP HISTOGRAM

| Azimuth | Number | Percentage | *....*....*....*....*....*....*....*....*....*....* |
|---|---|---|---|
| 0 | 0 | 0.0 | 0 |
| 5 | 0 | 0.0 | 0 |
| 10 | 0 | 0.0 | 0 |
| 15 | 0 | 0.0 | 0 |
| 20 | 0 | 0.0 | 0 |
| 25 | 0 | 0.0 | 0 |
| 30 | 0 | 0.0 | 0 |
| 35 | 1 | 0.6 | 01 |
| 40 | 1 | 1.1 | 01 |
| 45 | 16 | 10.1 | 0111111111 |
| 50 | 16 | 19.0 | 0111111111 |
| 55 | 17 | 28.5 | 0111111111 |
| 60 | 27 | 43.6 | 011111111111111 |
| 65 | 15 | 52.0 | 011111111 |
| 70 | 31 | 69.3 | 0111111111111111 |
| 75 | 10 | 74.9 | 0111111 |
| 80 | 13 | 82.1 | 01111111 |
| 85 | 7 | 86.0 | 01111 |
| 90 | 25 | 100.0 | 011111111111111 |
| | | | *....*....*....*....*....*....*....*....*....*....* |
| | TOTAL | 179 | 0 5 10 15 20 25 30 3 40 45 50,/ |

Percent of Observations

QUADRANT N111,750-N112,750
All data at elevations 6720-6760

| Sequence Number | Strike Azimuth | Dip Angle |
|---|---|---|
| 1 | 247 | 63 |
| 2 | 214 | 60 |
| 3 | 228 | 59 |
| 4 | 264 | 85 |
| 5 | 250 | 85 |
| 6 | 58 | 90 |
| 7 | 240 | 70 |
| 8 | 245 | 75 |
| 9 | 238 | 60 |
| 10 | 82 | 85 |
| 11 | 320 | 75 |
| 12 | 318 | 70 |
| 13 | 236 | 62 |
| 14 | 74 | 83 |
| 15 | 222 | 69 |
| 16 | 245 | 70 |
| 17 | 260 | 70 |
| 18 | 242 | 66 |
| 19 | 110 | 75 |
| 20 | 116 | 78 |
| 21 | 100 | 90 |
| 22 | 235 | 60 |
| 23 | 243 | 72 |
| 24 | 205 | 55 |
| 25 | 140 | 57 |
| 26 | 135 | 60 |
| 27 | 138 | 65 |
| 28 | 120 | 85 |
| 29 | 202 | 58 |
| 30 | 132 | 90 |
| 31 | 100 | 90 |
| 32 | 130 | 90 |
| 33 | 140 | 67 |
| 34 | 285 | 75 |
| 35 | 142 | 60 |
| 36 | 173 | 58 |
| 37 | 15 | 56 |
| 38 | 330 | 75 |
| 39 | 325 | 85 |
| 40 | 315 | 80 |
| 41 | 298 | 85 |
| 42 | 302 | 70 |

| Sequence Number | Strike Azimuth | Dip Angle |
|---|---|---|
| 43 | 7 | 73 |
| 44 | 10 | 73 |
| 45 | 330 | 70 |
| 46 | 327 | 65 |
| 47 | 185 | 68 |
| 48 | 132 | 90 |
| 49 | 15 | 75 |
| 50 | 10 | 75 |
| 51 | 162 | 90 |
| 52 | 10 | 66 |
| 53 | 7 | 63 |
| 54 | 65 | 90 |
| 55 | 360 | 70 |
| 56 | 200 | 85 |
| 57 | 95 | 90 |
| 58 | 72 | 60 |
| 59 | 75 | 65 |
| 60 | 68 | 70 |
| 61 | 230 | 55 |
| 62 | 220 | 60 |
| 63 | 230 | 62 |
| 64 | 235 | 79 |
| 65 | 233 | 79 |
| 66 | 240 | 79 |
| 67 | 85 | 60 |
| 68 | 92 | 60 |
| 69 | 221 | 62 |
| 70 | 237 | 70 |
| 71 | 268 | 74 |
| 72 | 245 | 85 |
| 73 | 160 | 70 |
| 74 | 58 | 90 |
| 75 | 220 | 70 |
| 76 | 178 | 65 |
| 77 | 310 | 85 |
| 78 | 303 | 79 |
| 79 | 4 | 62 |
| 80 | 160 | 90 |
| 81 | 160 | 59 |
| 82 | 175 | 60 |
| 83 | 180 | 65 |
| 84 | 5 | 70 |
| 85 | 8 | 90 |
| 86 | 250 | 86 |
| 87 | 5 | 70 |
| 88 | 3 | 60 |

| Sequence Number | Strike Azimuth | Dip Angle |
|---|---|---|
| 89 | 10 | 60 |
| 90 | 15 | 65 |
| 91 | 198 | 60 |
| 92 | 2 | 75 |
| 93 | 6 | 73 |
| 94 | 25 | 69 |
| 95 | 30 | 72 |
| 96 | 35 | 74 |
| 97 | 240 | 64 |
| 98 | 80 | 68 |
| 99 | 68 | 70 |
| 100 | 248 | 70 |
| 101 | 80 | 56 |
| 102 | 110 | 60 |
| 103 | 62 | 90 |
| 104 | 50 | 90 |
| 105 | 45 | 90 |
| 106 | 40 | 90 |
| 107 | 240 | 80 |
| 108 | 292 | 85 |
| 109 | 145 | 86 |
| 110 | 238 | 84 |
| 111 | 132 | 90 |
| 112 | 20 | 90 |
| 113 | 13 | 80 |
| 114 | 17 | 68 |
| 115 | 8 | 70 |
| 116 | 35 | 63 |
| 117 | 230 | 78 |
| 118 | 220 | 80 |
| 119 | 200 | 85 |
| 120 | 215 | 33 |
| 121 | 205 | 70 |
| 122 | 200 | 65 |
| 123 | 260 | 68 |
| 124 | 70 | 80 |
| 125 | 195 | 77 |

QUADRANT N111,750-N112,750
All data at elevations 6720-6760

STRIKE HISTOGRAM

| Azimuth | Number | Percentage | *....*....*....*....*....*....*....*....*....*.... |
|---|---|---|---|
| 0 | 7 | 5.6 | 0111111 |
| 10 | 13 | 16.0 | 01111111111 |
| 20 | 11 | 24.8 | 0111111111 |
| 30 | 5 | 28.8 | 01111 |
| 40 | 9 | 36.0 | 01111111 |
| 50 | 7 | 41.6 | 0111111 |
| 60 | 15 | 53.6 | 011111111111 |
| 70 | 13 | 64.0 | 01111111111 |
| 80 | 7 | 69.6 | 0111111 |
| 90 | 3 | 72.0 | 011 |
| 100 | 3 | 74.4 | 011 |
| 110 | 4 | 77.6 | 0111 |
| 120 | 5 | 81.6 | 01111 |
| 130 | 5 | 85.6 | 01111 |
| 140 | 8 | 92.0 | 0111111 |
| 150 | 5 | 96.0 | 01111 |
| 160 | 4 | 99.2 | 0111 |
| 170 | 0 | 99.2 | 0 |
| 180 | 1 | 100.0 | 01 |
| | | | *....*....*....*....*....*....*....*....*....*.... |
| | TOTAL | 125 | 0 5 10 15 20 25 30 3 40 45 50,/ |

Percent of Observations

DIP HISTOGRAM

| Azimuth | Number | Percentage | *....*....*....*....*....*....*....*....*....*....*....* |
|---|---|---|---|
| 0 | 0 | 0.0 | 0 |
| 5 | 0 | 0.0 | 0 |
| 10 | 0 | 0.0 | 0 |
| 15 | 0 | 0.0 | 0 |
| 20 | 0 | 0.0 | 0 |
| 25 | 0 | 0.0 | 0 |
| 30 | 0 | 0.0 | 0 |
| 35 | 0 | 0.0 | 0 |
| 40 | 0 | 0.0 | 0 |
| 45 | 0 | 0.0 | 0 |
| 50 | 0 | 0.0 | 0 |
| 55 | 5 | 4.0 | 01111 |
| 60 | 22 | 21.6 | 0111111111111111111 |
| 65 | 14 | 32.8 | 01111111111 |
| 70 | 25 | 52.8 | 0111111111111111111111 |
| 75 | 14 | 64.0 | 01111111111 |
| 80 | 11 | 72.8 | 0111111111 |
| 85 | 16 | 85.6 | 01111111111111 |
| 90 | 18 | 100.0 | 01111111111111 |
| | | | *....*....*....*....*....*....*....*....*....*....*....* |
| | TOTAL | 125 | 0 5 10 15 20 25 30 3 40 45 50,/ |

Percent of Observations

QUADRANT E103,750-E104,500
All data at elevations 6680-6760

| Sequence Number | Strike Azimuth | Dip Angle |
|---|---|---|
| 1 | 7 | 67 |
| 2 | 15 | 85 |
| 3 | 200 | 83 |
| 4 | 210 | 82 |
| 5 | 218 | 80 |
| 6 | 18 | 90 |
| 7 | 200 | 83 |
| 8 | 25 | 90 |
| 9 | 257 | 56 |
| 10 | 225 | 75 |
| 11 | 8 | 90 |
| 12 | 15 | 90 |
| 13 | 3 | 78 |
| 14 | 10 | 80 |
| 15 | 190 | 80 |
| 16 | 190 | 85 |
| 17 | 195 | 75 |
| 18 | 180 | 90 |
| 19 | 210 | 73 |
| 20 | 222 | 69 |
| 21 | 220 | 52 |
| 22 | 218 | 80 |
| 23 | 175 | 80 |
| 24 | 5 | 67 |
| 25 | 213 | 83 |
| 26 | 218 | 85 |
| 27 | 215 | 70 |
| 28 | 340 | 56 |
| 29 | 20 | 82 |
| 30 | 220 | 84 |
| 31 | 183 | 60 |
| 32 | 17 | 78 |
| 33 | 20 | 82 |
| 34 | 200 | 72 |
| 35 | 193 | 68 |
| 36 | 27 | 80 |
| 37 | 17 | 76 |
| 38 | 262 | 65 |
| 39 | 256 | 78 |
| 40 | 282 | 52 |
| 41 | 265 | 56 |
| 42 | 290 | 58 |

| Sequence Number | Strike Azimuth | Dip Angle |
|---|---|---|
| 43 | 257 | 62 |
| 44 | 261 | 60 |
| 45 | 298 | 57 |
| 46 | 290 | 70 |
| 47 | 294 | 60 |
| 48 | 284 | 75 |
| 49 | 80 | 90 |
| 50 | 264 | 84 |
| 51 | 270 | 71 |
| 52 | 82 | 90 |
| 53 | 260 | 80 |
| 54 | 280 | 72 |
| 55 | 268 | 85 |
| 56 | 70 | 88 |
| 57 | 273 | 77 |
| 58 | 258 | 85 |
| 59 | 260 | 78 |
| 60 | 50 | 68 |
| 61 | 265 | 62 |
| 62 | 23 | 65 |
| 63 | 290 | 75 |
| 64 | 287 | 78 |
| 65 | 278 | 83 |
| 66 | 79 | 86 |
| 67 | 105 | 72 |
| 68 | 293 | 68 |
| 69 | 286 | 50 |
| 70 | 267 | 60 |
| 71 | 285 | 56 |
| 72 | 295 | 57 |
| 73 | 300 | 60 |
| 74 | 290 | 60 |
| 75 | 295 | 56 |
| 76 | 267 | 57 |
| 77 | 266 | 60 |
| 78 | 187 | 63 |
| 79 | 197 | 57 |
| 80 | 7 | 56 |
| 81 | 189 | 59 |
| 82 | 198 | 55 |
| 83 | 70 | 90 |
| 84 | 85 | 85 |
| 85 | 272 | 70 |
| 86 | 270 | 60 |
| 87 | 264 | 62 |
| 88 | 275 | 78 |

| Sequence Number | Strike Azimuth | Dip Angle |
|---|---|---|
| 89 | 270 | 77 |
| 80 | 268 | 84 |
| 91 | 278 | 65 |
| 92 | 273 | 60 |
| 93 | 260 | 65 |
| 94 | 265 | 54 |
| 95 | 262 | 60 |
| 96 | 250 | 64 |
| 97 | 248 | 59 |
| 98 | 254 | 60 |
| 99 | 274 | 65 |
| 100 | 292 | 62 |
| 101 | 270 | 72 |
| 102 | 94 | 90 |
| 103 | 263 | 90 |
| 104 | 268 | 70 |
| 105 | 265 | 70 |
| 106 | 253 | 68 |
| 107 | 266 | 67 |
| 108 | 40 | 66 |
| 109 | 253 | 80 |
| 110 | 293 | 85 |
| 111 | 17 | 54 |
| 112 | 7 | 56 |
| 113 | 82 | 90 |
| 114 | 80 | 90 |
| 115 | 248 | 85 |
| 116 | 80 | 90 |
| 117 | 62 | 90 |
| 118 | 68 | 58 |
| 119 | 337 | 50 |
| 120 | 5 | 54 |
| 121 | 70 | 90 |
| 122 | 65 | 90 |
| 123 | 80 | 45 |
| 124 | 86 | 60 |
| 125 | 8 | 52 |
| 126 | 9 | 60 |
| 127 | 10 | 52 |
| 128 | 2 | 56 |
| 129 | 5 | 61 |
| 130 | 5 | 53 |
| 131 | 7 | 57 |
| 132 | 9 | 53 |

| Sequence Number | Strike Azimuth | Dip Angle |
|---|---|---|
| 133 | 180 | 48 |
| 134 | 5 | 45 |
| 135 | 12 | 45 |
| 136 | 8 | 50 |
| 137 | 268 | 62 |
| 138 | 260 | 71 |
| 139 | 270 | 70 |
| 140 | 265 | 75 |
| 141 | 250 | 72 |
| 142 | 268 | 76 |
| 143 | 257 | 60 |
| 144 | 264 | 78 |
| 145 | 260 | 60 |
| 146 | 75 | 86 |
| 147 | 70 | 75 |
| 148 | 260 | 85 |
| 149 | 85 | 90 |
| 150 | 247 | 70 |
| 151 | 248 | 65 |
| 152 | 47 | 86 |
| 153 | 270 | 69 |
| 154 | 264 | 62 |
| 155 | 70 | 90 |
| 156 | 80 | 90 |
| 157 | 102 | 90 |
| 158 | 48 | 90 |
| 159 | 260 | 86 |
| 160 | 260 | 85 |
| 161 | 252 | 72 |
| 162 | 20 | 57 |
| 163 | 251 | 88 |
| 164 | 60 | 90 |
| 165 | 67 | 90 |
| 166 | 254 | 83 |
| 167 | 245 | 79 |
| 168 | 63 | 58 |
| 169 | 245 | 59 |
| 170 | 290 | 58 |
| 171 | 280 | 78 |
| 172 | 260 | 90 |
| 173 | 262 | 65 |
| 174 | 17 | 48 |

QUADRANT E103,750-E104,500
All data at elevations 6680-6760

STRIKE HISTOGRAM

| Azimuth | Number | Percentage | |
|---|---|---|---|
| | | | *....*....*....*....*....*....*....*....*....*....* |
| 0 | 6 | 3.4 | 0111 |
| 10 | 22 | 16.1 | 01111111111111 |
| 20 | 17 | 25.9 | 011111111111 |
| 30 | 5 | 28.7 | 0111 |
| 40 | 8 | 33.3 | 011111 |
| 50 | 4 | 35.6 | 011 |
| 60 | 3 | 37.4 | 011 |
| 70 | 22 | 50.0 | 01111111111111 |
| 80 | 32 | 68.4 | 01111111111111111111 |
| 90 | 28 | 84.5 | 01111111111111111 |
| 100 | 8 | 89.1 | 011111 |
| 110 | 13 | 96.6 | 01111111 |
| 120 | 4 | 98.9 | 011 |
| 130 | 0 | 98.9 | 0 |
| 140 | 0 | 98.9 | 0 |
| 150 | 0 | 98.9 | 0 |
| 160 | 2 | 100.0 | 01 |
| 170 | 0 | 100.0 | 0 |
| 180 | 0 | 100.0 | 0 |
| | | | *....*....*....*....*....*....*....*....*....*....* |
| | TOTAL | 174 | 0 5 10 15 20 25 30 3 40 45 50,/ |

Percent of Observations

DIP HISTOGRAM

| Azimuth | Number | Percentage | *....*....*....*....*....*....*....*....*....*....* |
|---|---|---|---|
| 0 | 0 | 0.0 | 0 |
| 5 | 0 | 0.0 | 0 |
| 10 | 0 | 0.0 | 0 |
| 15 | 0 | 0.0 | 0 |
| 20 | 0 | 0.0 | 0 |
| 25 | 0 | 0.0 | 0 |
| 30 | 0 | 0.0 | 0 |
| 35 | 0 | 0.0 | 0 |
| 40 | 0 | 0.0 | 0 |
| 45 | 3 | 1.7 | 011 |
| 50 | 9 | 6.9 | 011111 |
| 55 | 20 | 18.4 | 011111111111 |
| 60 | 29 | 35.1 | 01111111111111111 |
| 65 | 13 | 42.5 | 01111111 |
| 70 | 21 | 54.6 | 0111111111111 |
| 75 | 11 | 60.9 | 0111111 |
| 80 | 20 | 72.4 | 011111111111 |
| 85 | 22 | 85.1 | 0111111111111 |
| 90 | 26 | 100.0 | 01111111111111111 |
| | | | *....*....*....*....*....*....*....*....*....*....* |
| | TOTAL | 174 | 0 5 10 15 20 25 30 3 40 45 50,/ |

Percent of Observations

# APPENDIX B

SCATTER DIAGRAMS OF FRACTURE DATA

SCHMIDT EQUAL-AREA NET

LOWER HEMISPHERE

257 ORIGINAL POLES

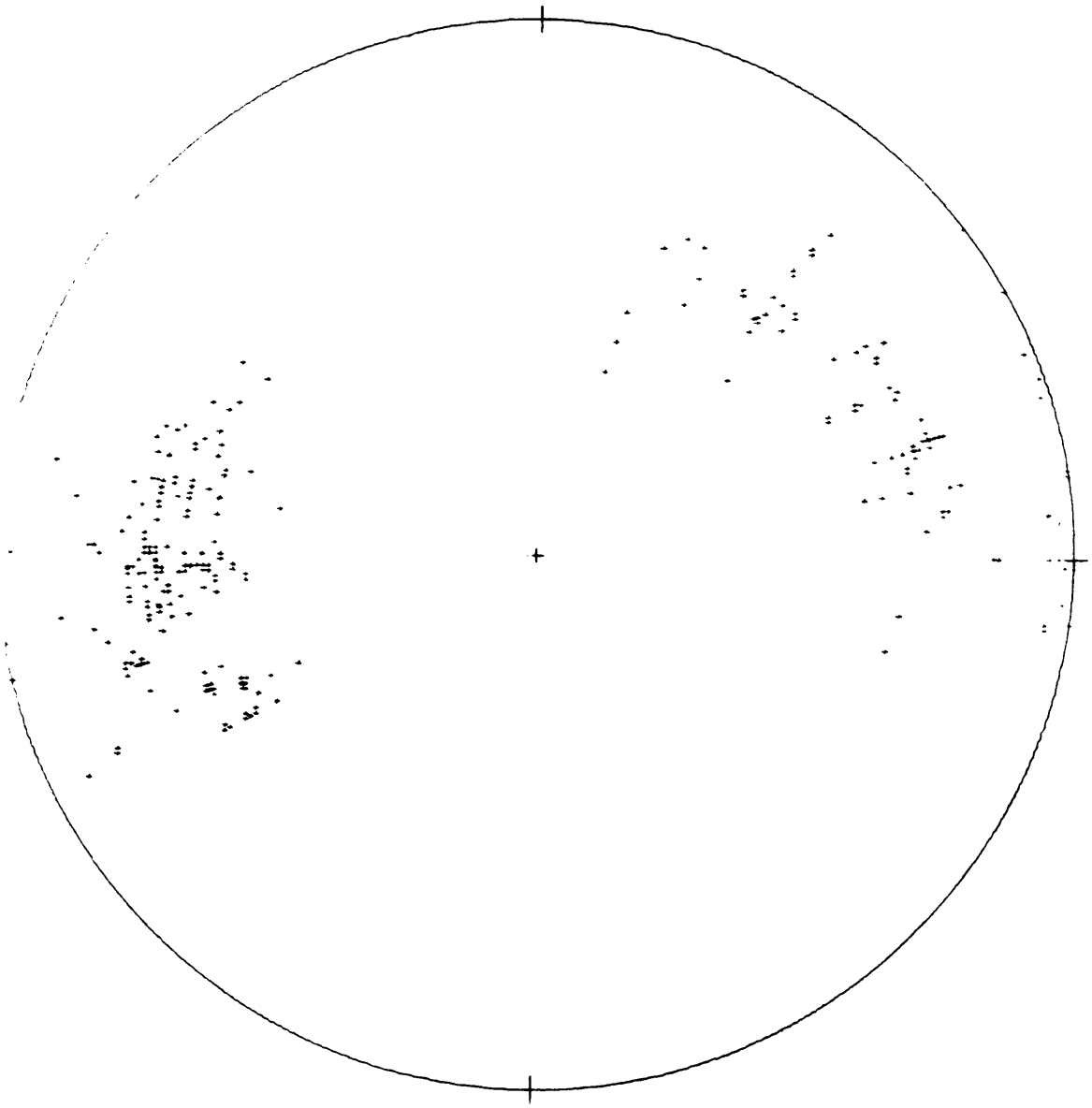

Figure 61. Quadrant N110,000 - N111,000
All data at elevations 6920 - 6960.

159 ORIGINAL POLES

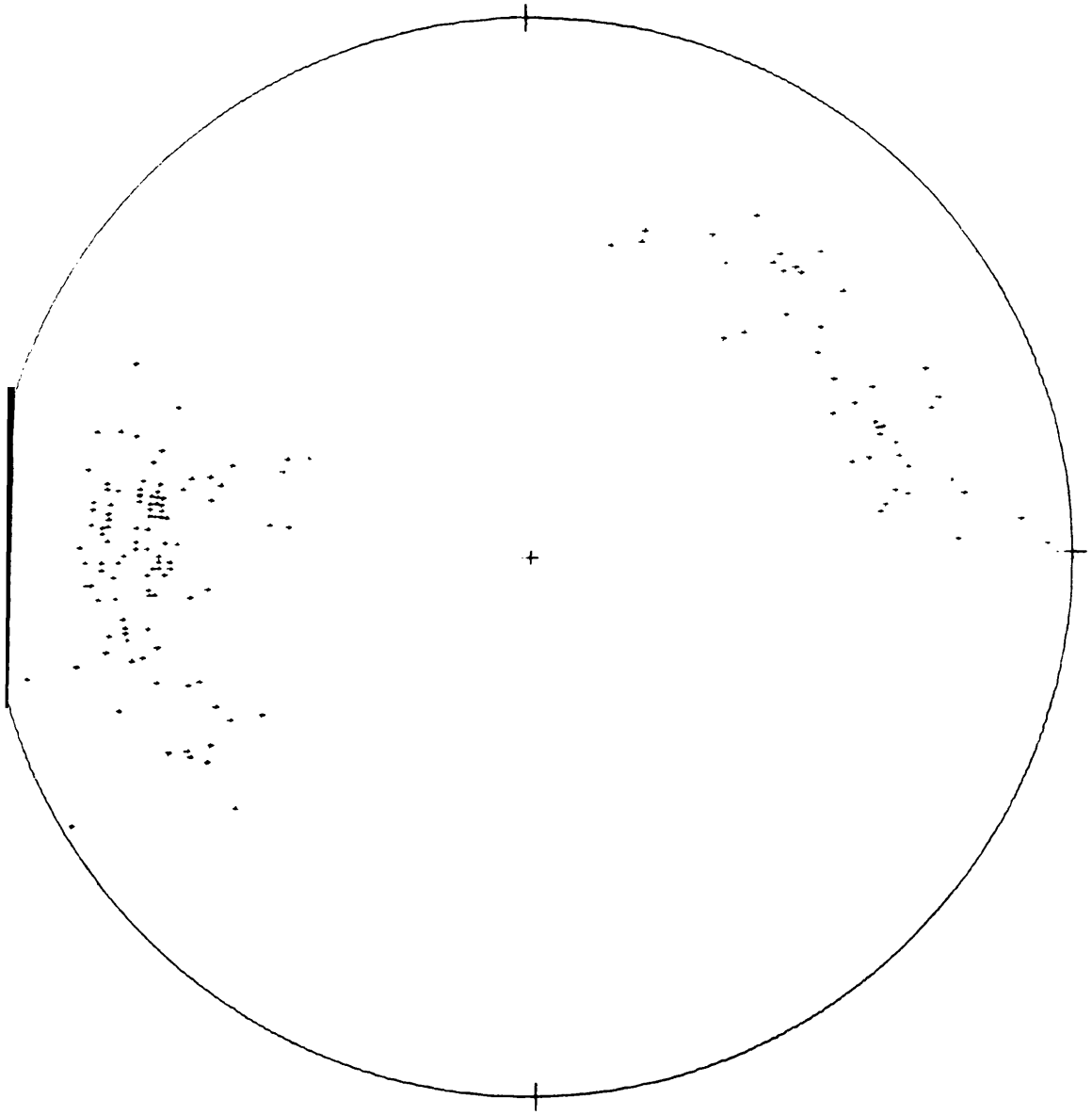

Figure 62. Quadrant N110,000 - N1111,000
All data at elevations 6840 - 6880

95 ORIGINAL POLES

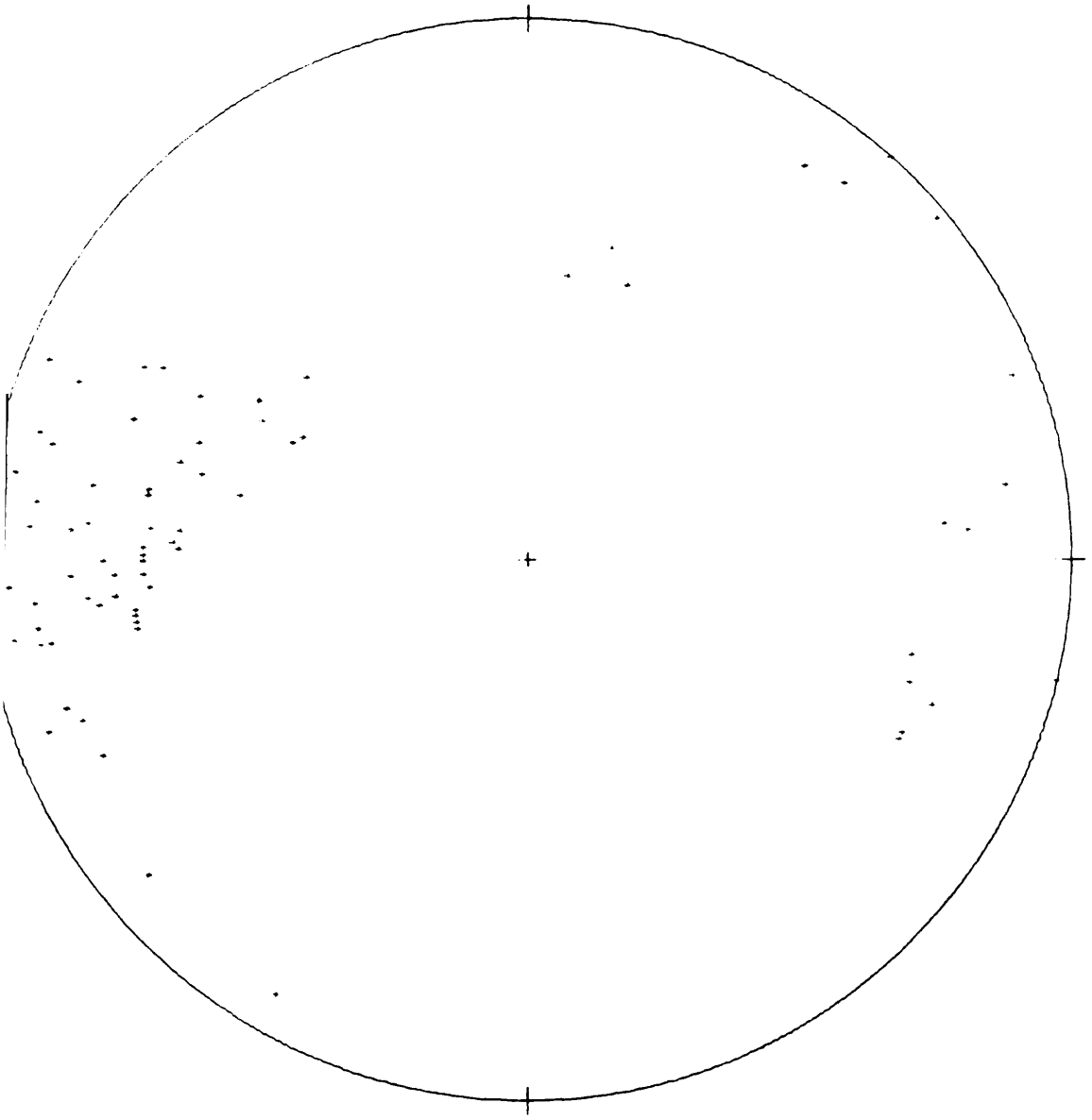

Figure 63. Quadrant N110,000 - N111,000
All data at elevations 6760 - 6800

59 ORIGINAL POLES

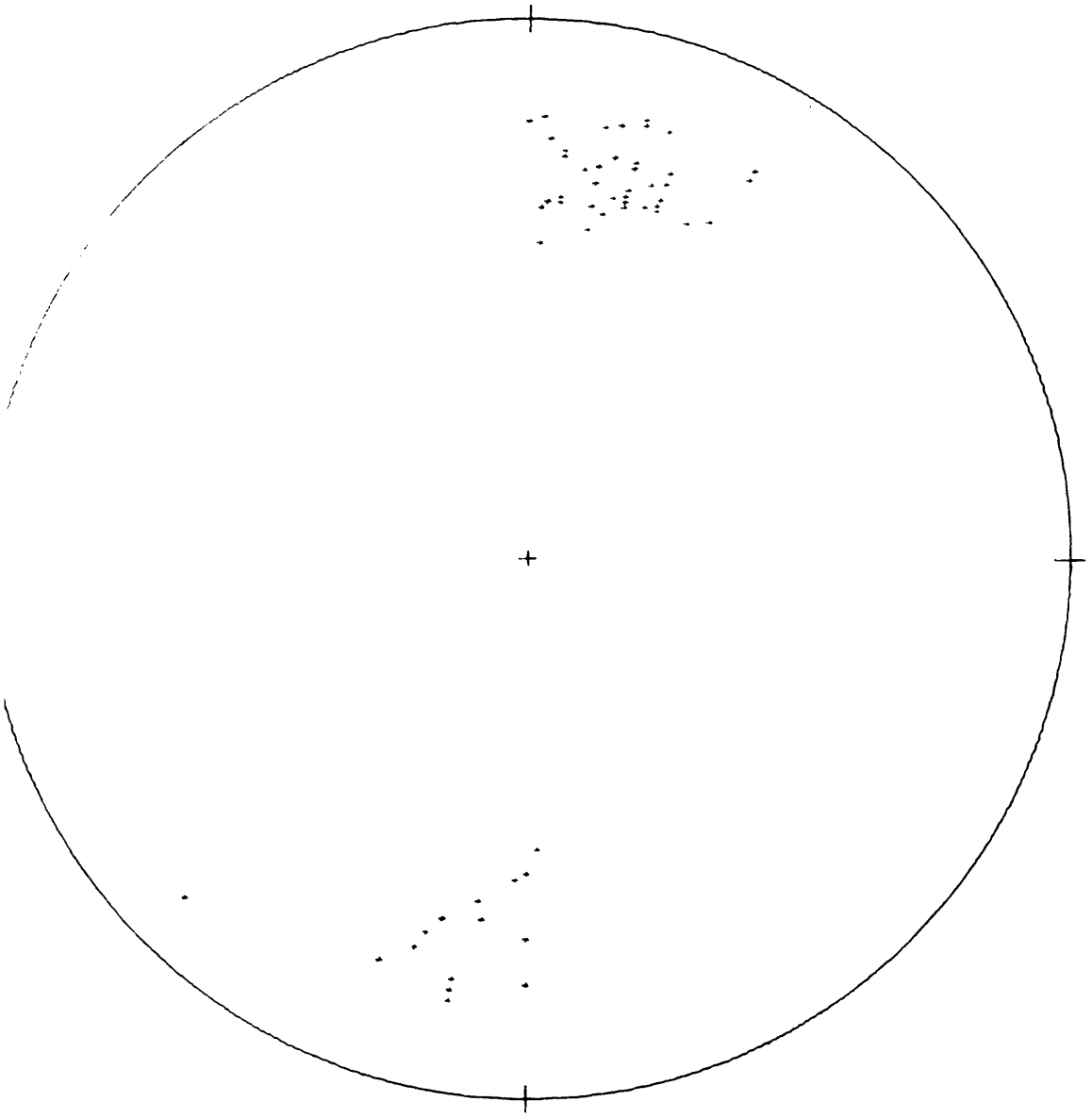

Figure 64. South edge of the pit
All data from Barringer fault zone

115 ORIGINAL POLES

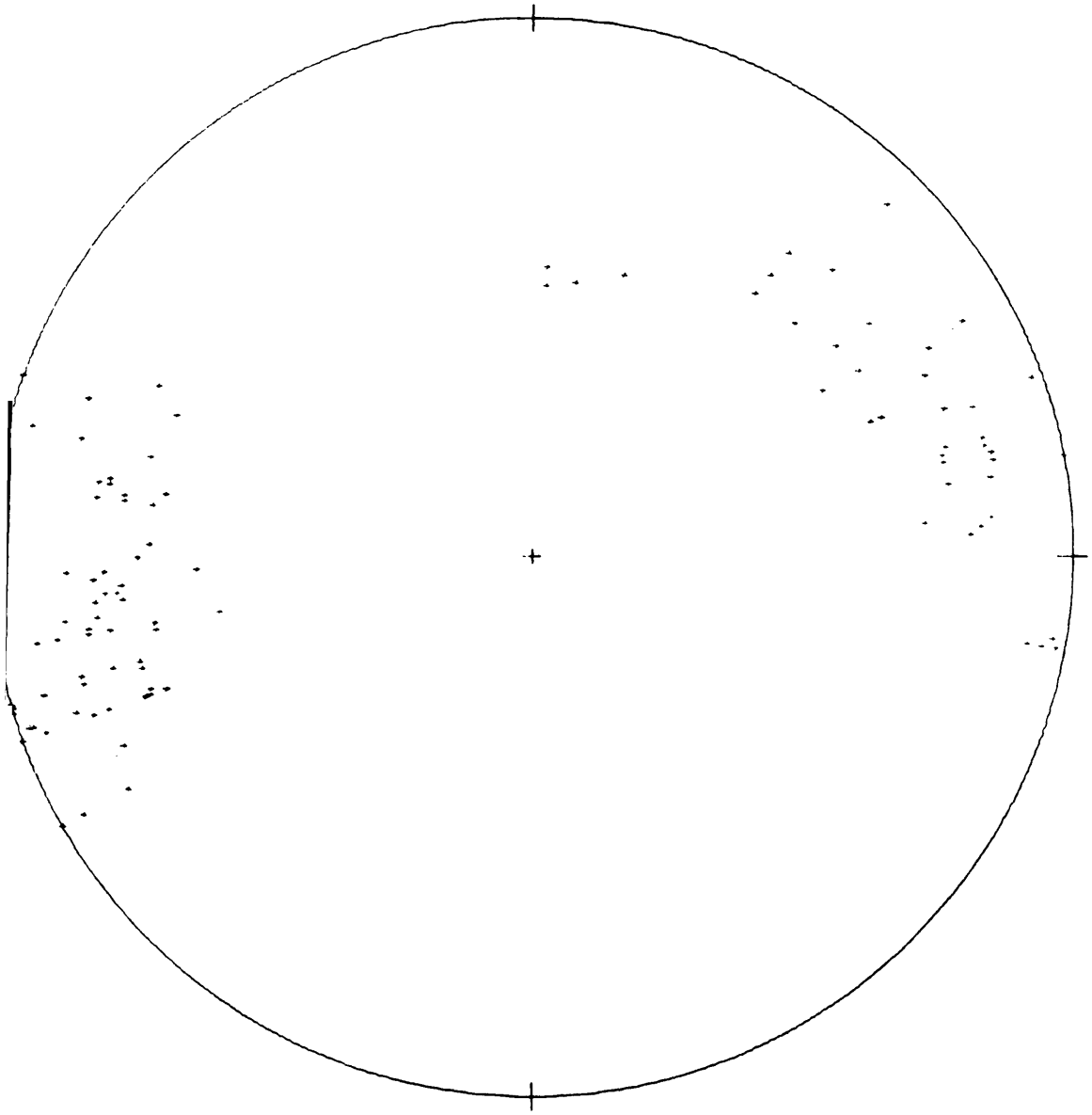

Figure 65. Quadrant N111,000 - N111,750
All data at elevations 6880 - 6920

174 ORIGINAL POLES

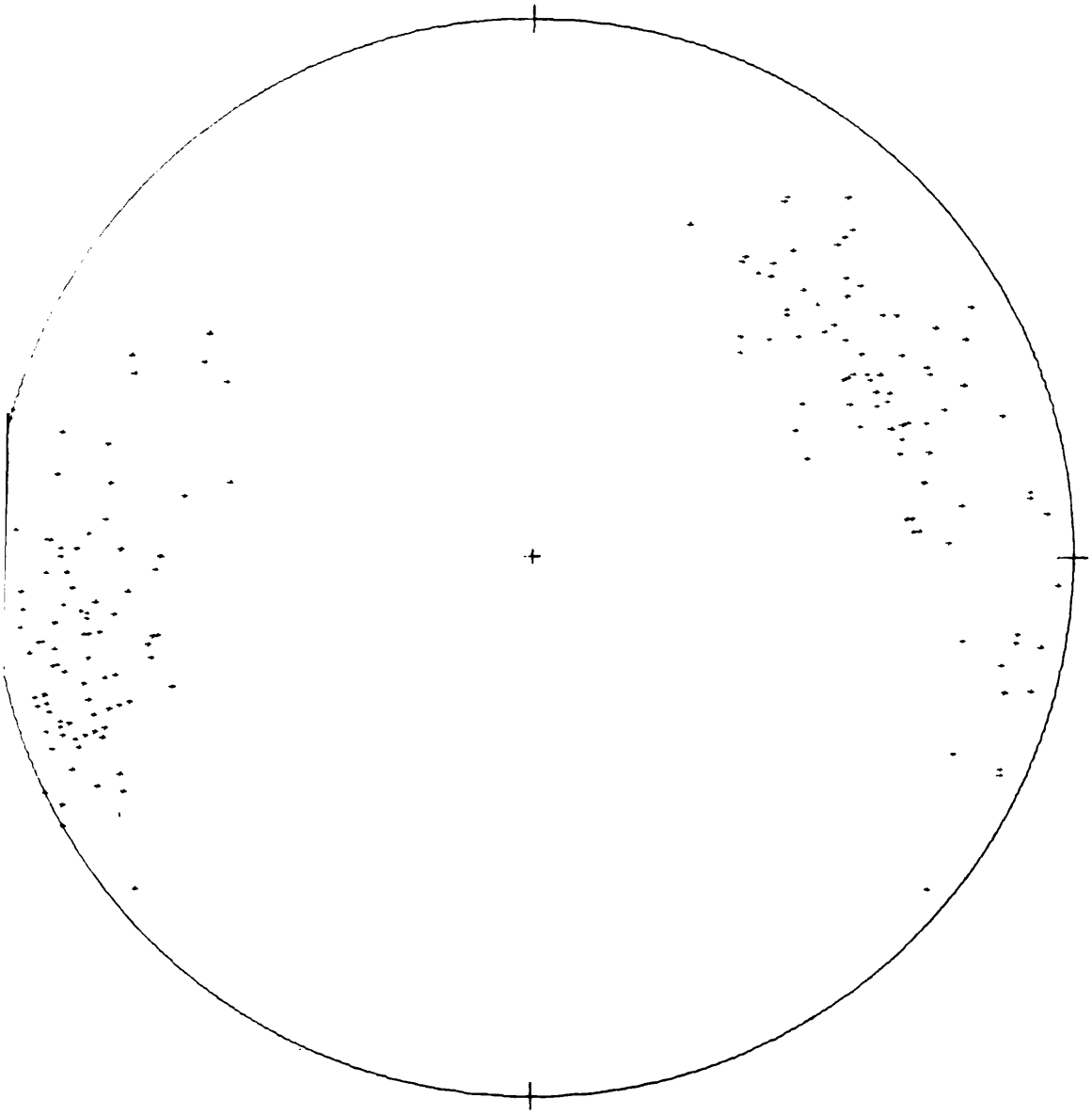

Figure 66.Quadrant N111,000 - 111,750
All data at elevations 6800 - 6840

94 ORIGINAL POLES

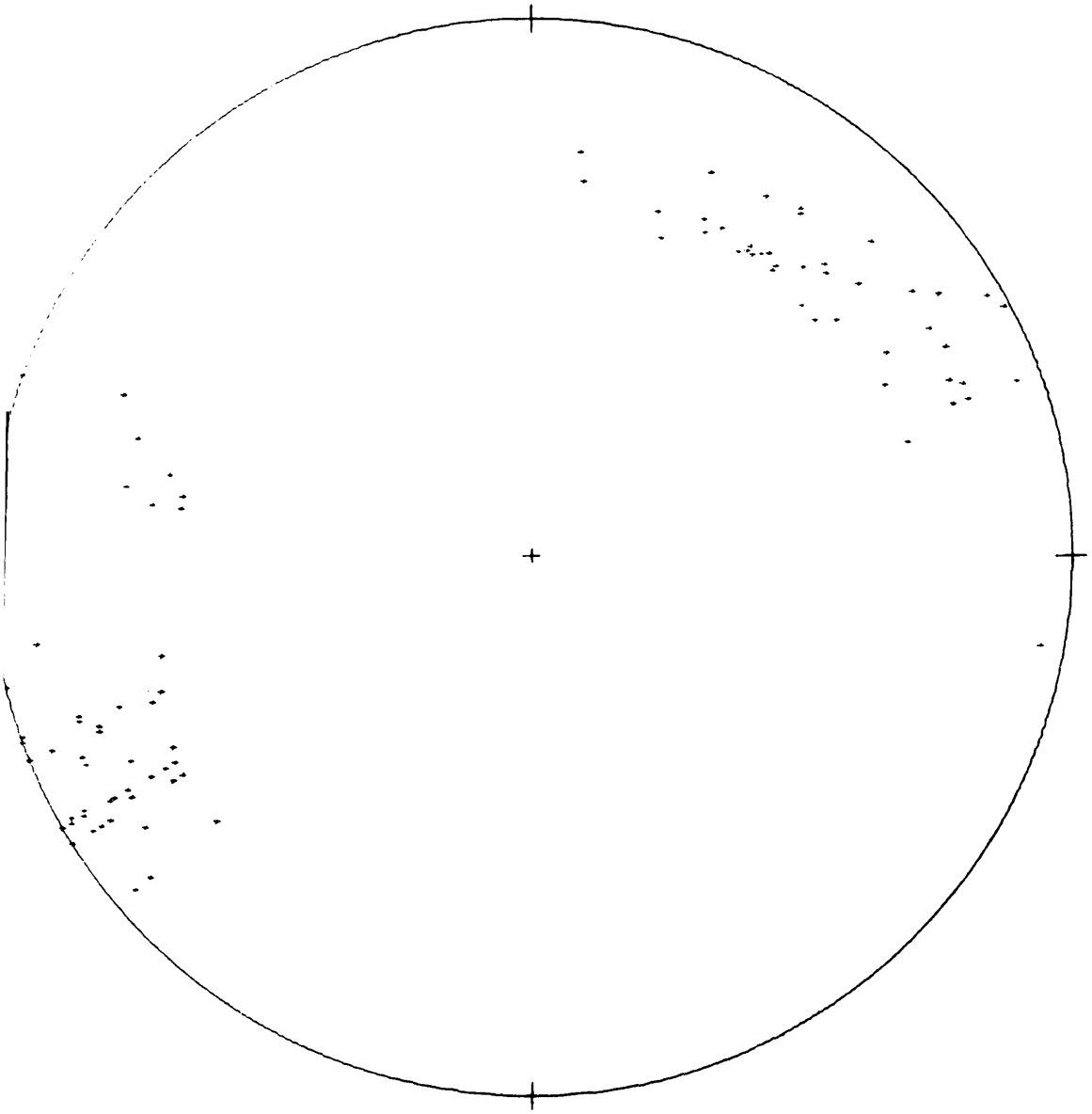

Figure 67. Quadrant N111,000 - N111,750
All data at elevations 6720 - 6760

166 ORIGINAL POLES

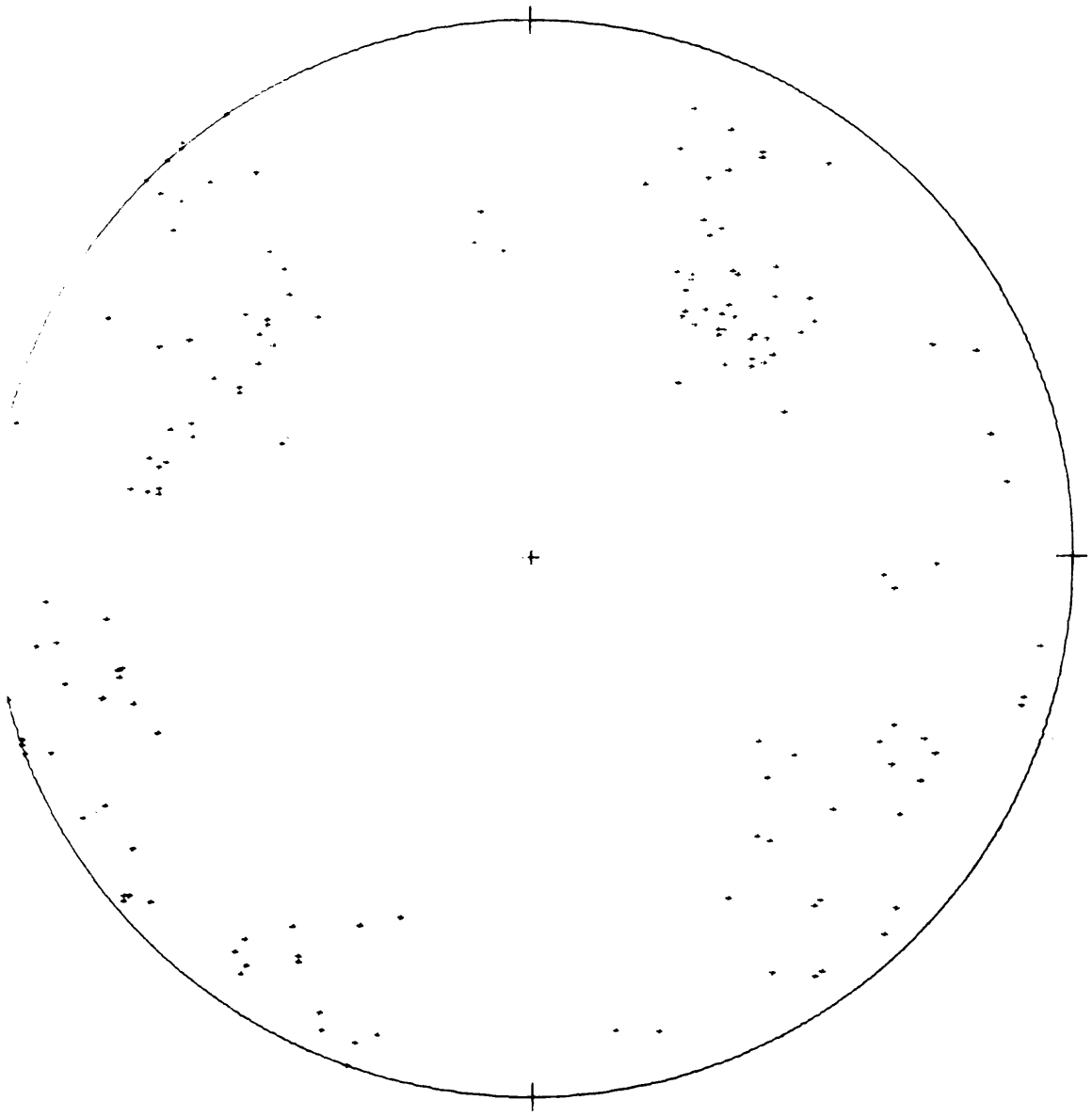

Figure 68. Quadrant N111,750 - N112,750
All data at elevations 6880 - 6920

179 ORIGINAL POLES

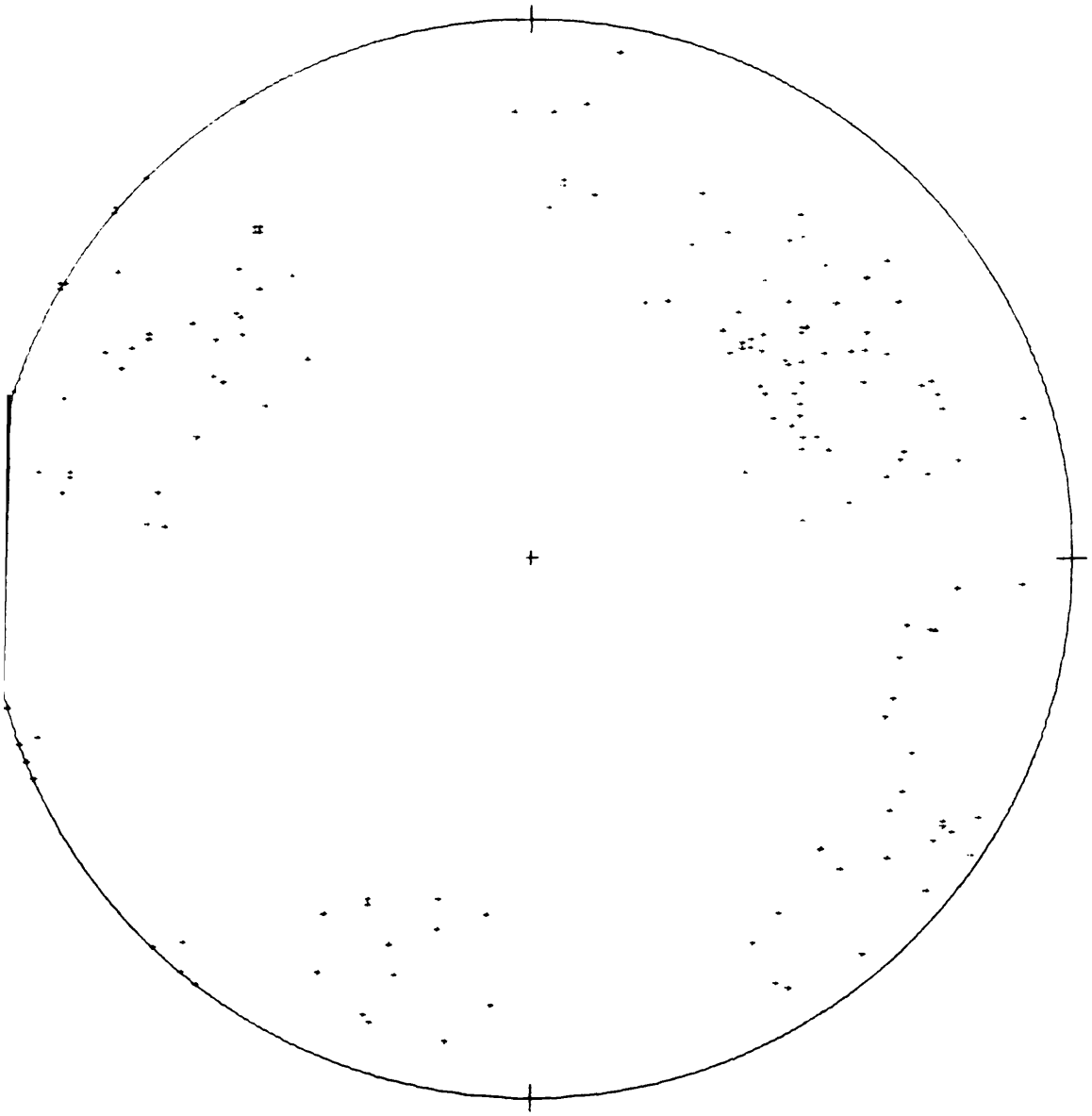

Figure 69. Quadrant N111,750 - N112,750
All data at elevations 6800 - 6840

125 ORIGINAL POLES

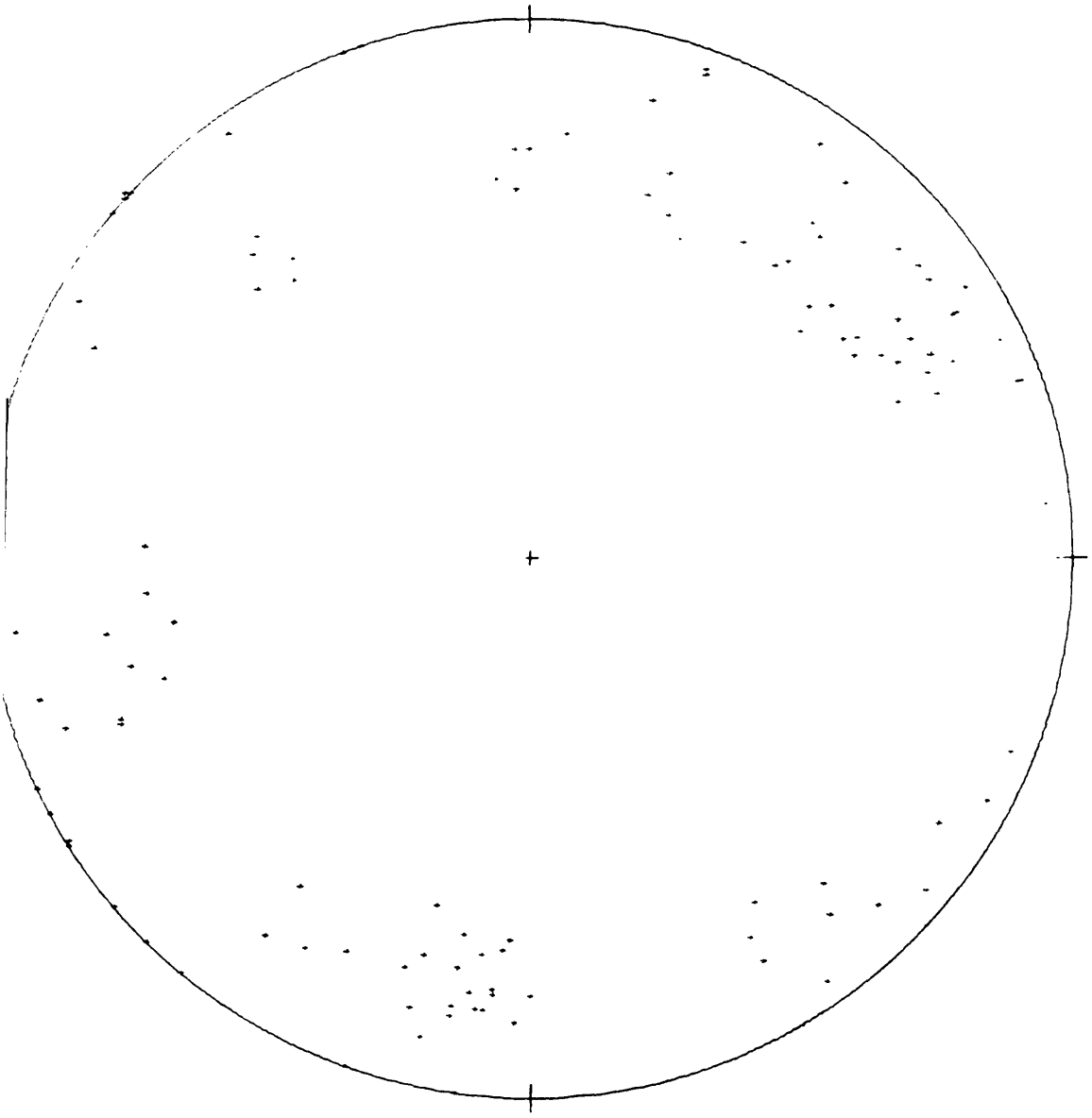

Figure 70. Quadrant N111,750 - N112,750
All data at elevations 6720 - 6760

174 ORIGINAL POLES

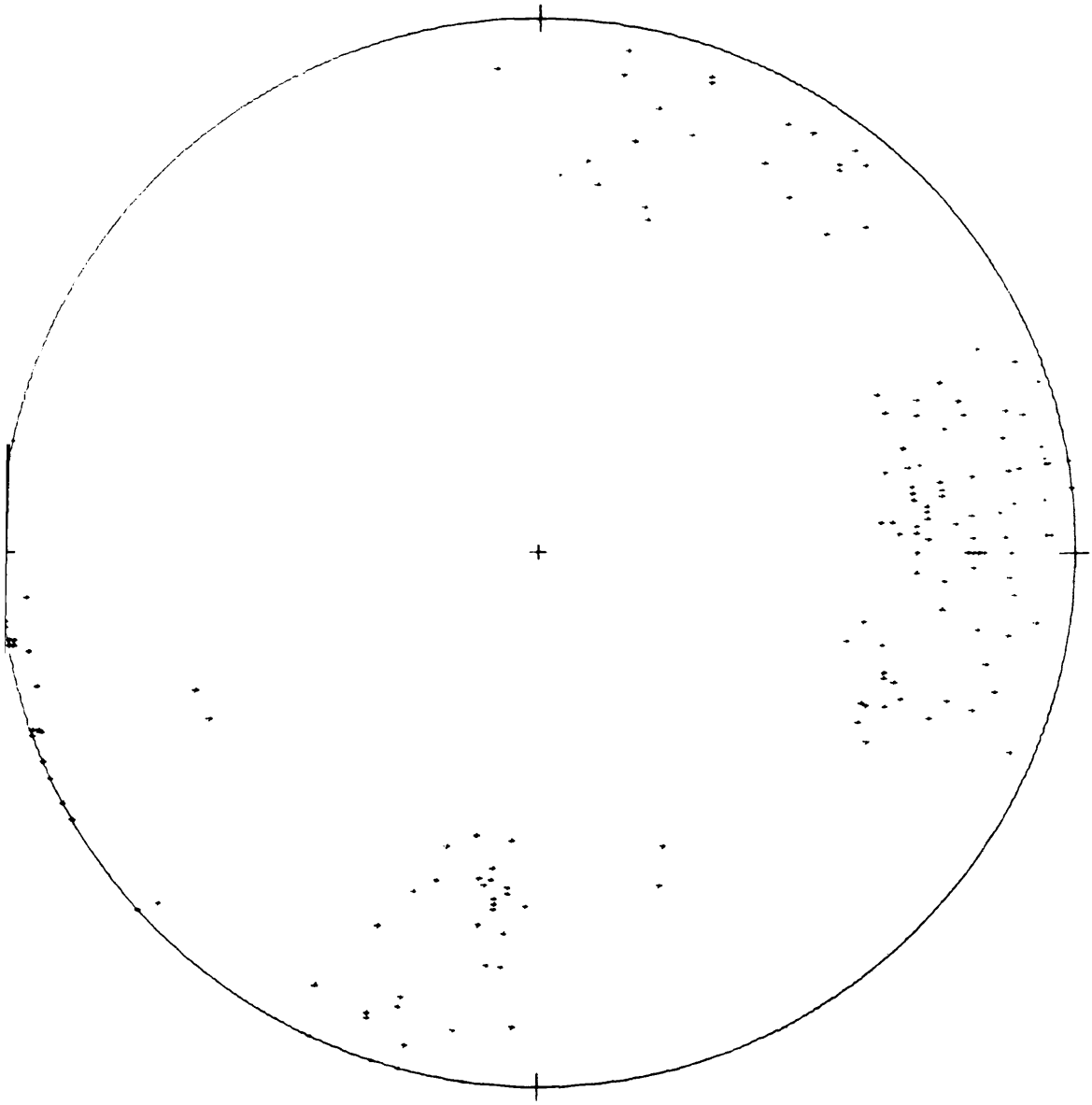

Figure 71. Quadrant E103,750 - E104,500
All data at elevations 6680 - 6760

569 ORIGINAL POLES

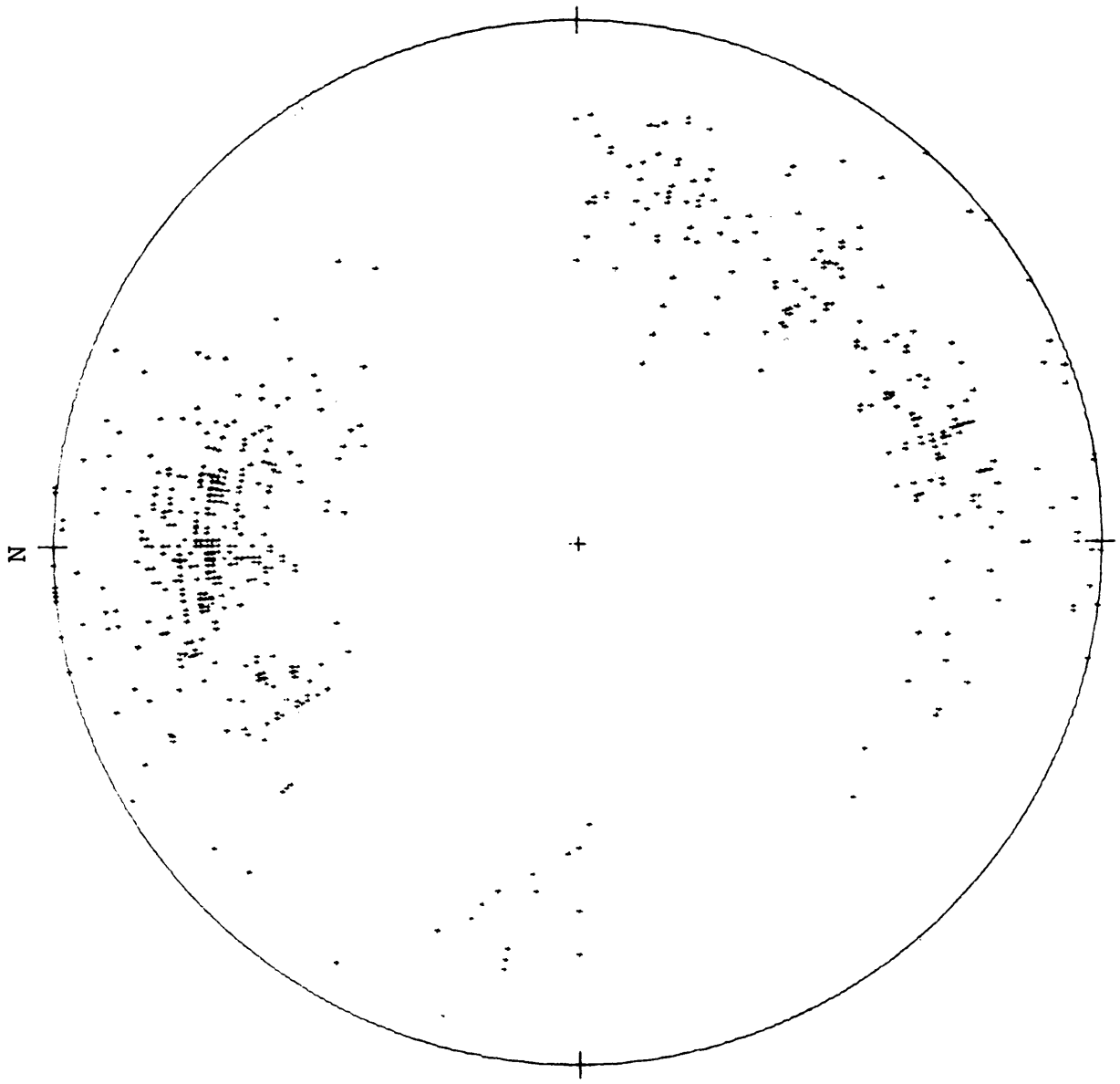


Figure 72. Quadrant N110,000 - N111,000
All data at elevations 6760 - 6960

383 ORIGINAL POLES

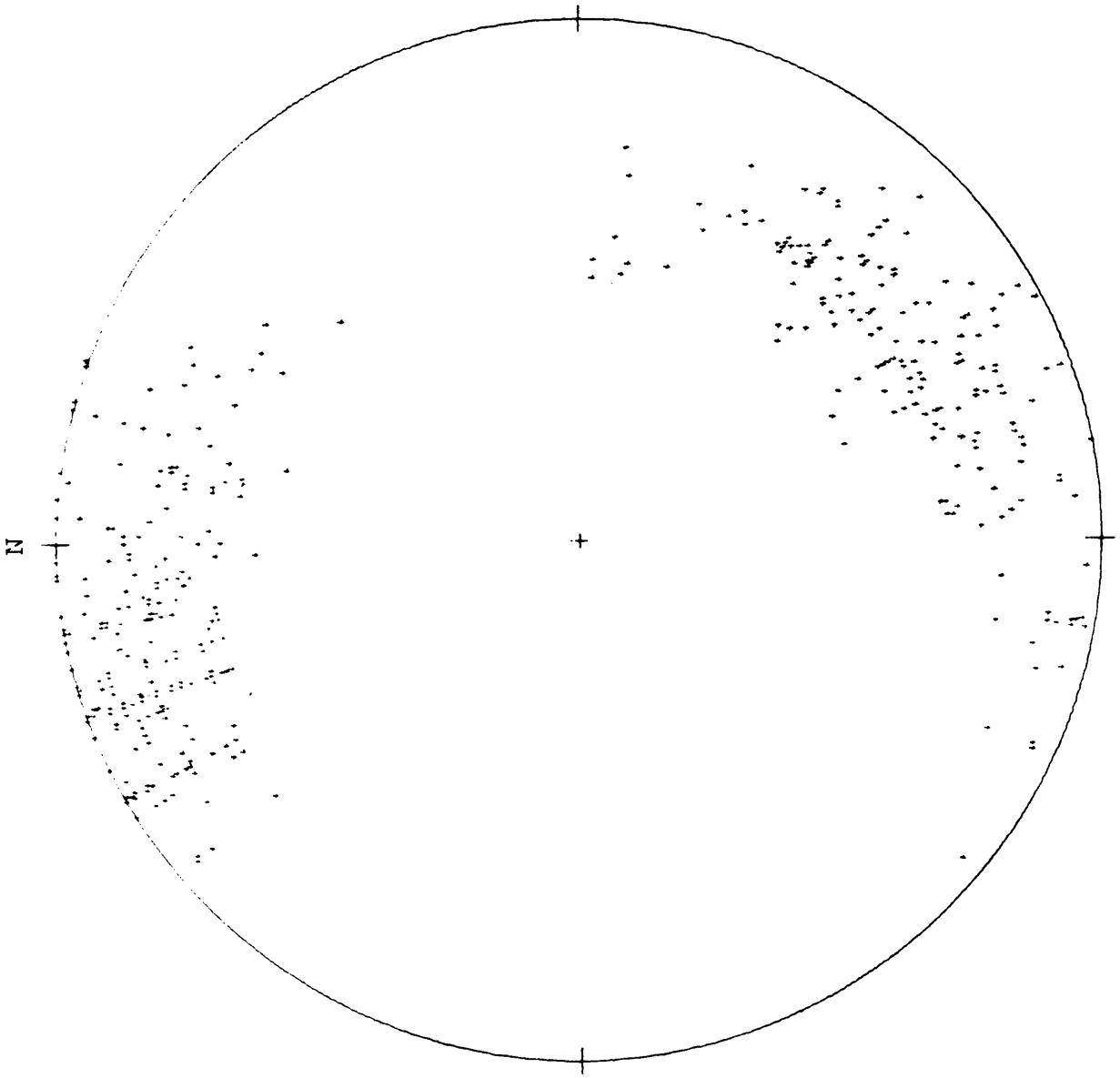


Figure 73. Quadrant N111,000 - N111,750
All data at elevations 6720 - 6920

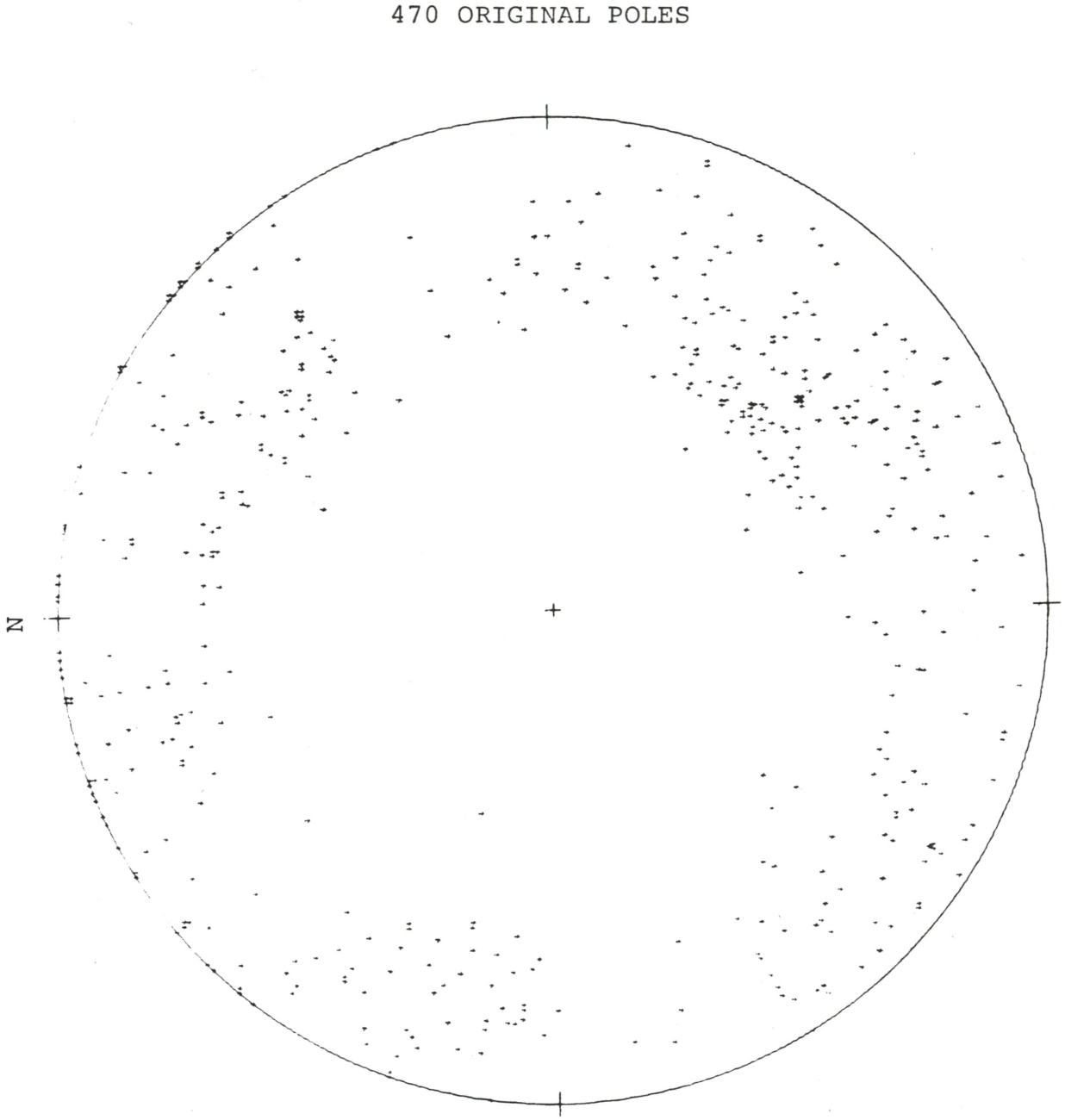


Figure 74. Quadrant N111,750 - N112,750
All data at elevations 6720 - 6920

# APPENDIX C

CONTOURED ORIENTATION DIAGRAMS OF FRACTURE DATA

SCHMIDT EQUAL-AREA NET

LOWER HEMISPHERE

Figure 75. Quadrant N110,000 - N111,000
All data at elevations 6920 - 6960

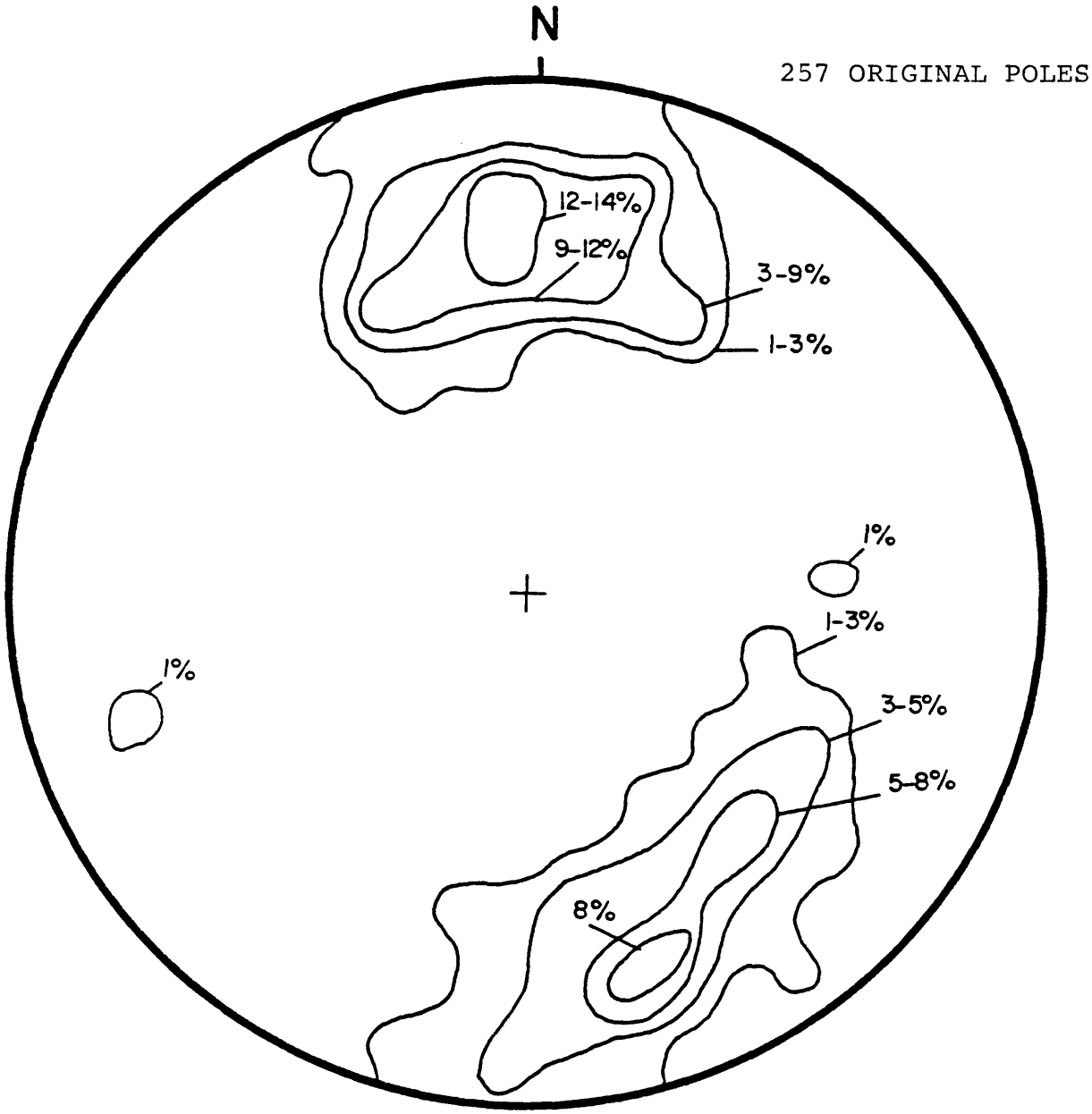

Figure 76. Quadrant N110,000 - N111,000
All data at elevations 6840 - 6880

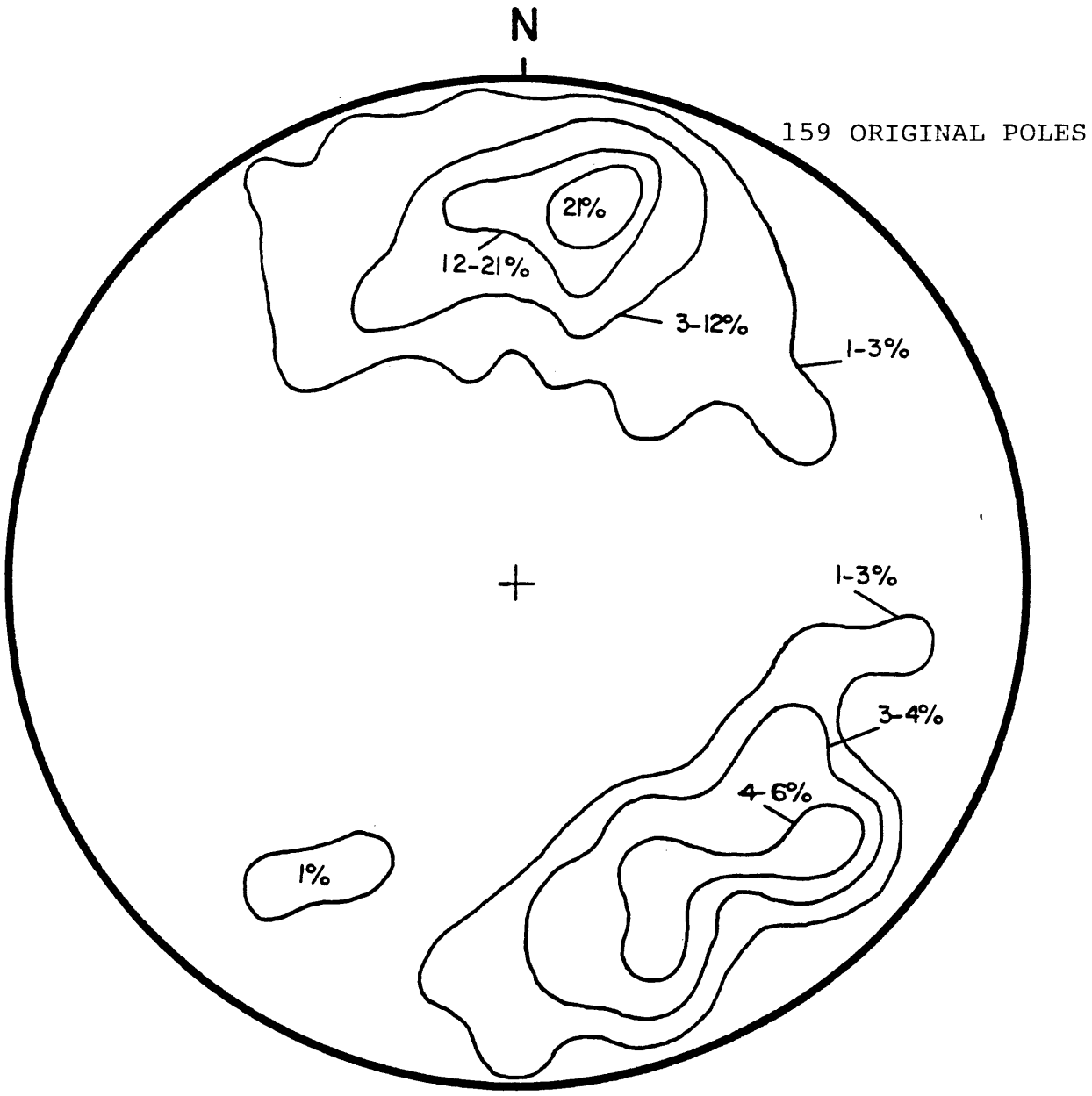

Figure 77. Quadrant N110,000 - N111,000
All data at elevations 6760 - 6800

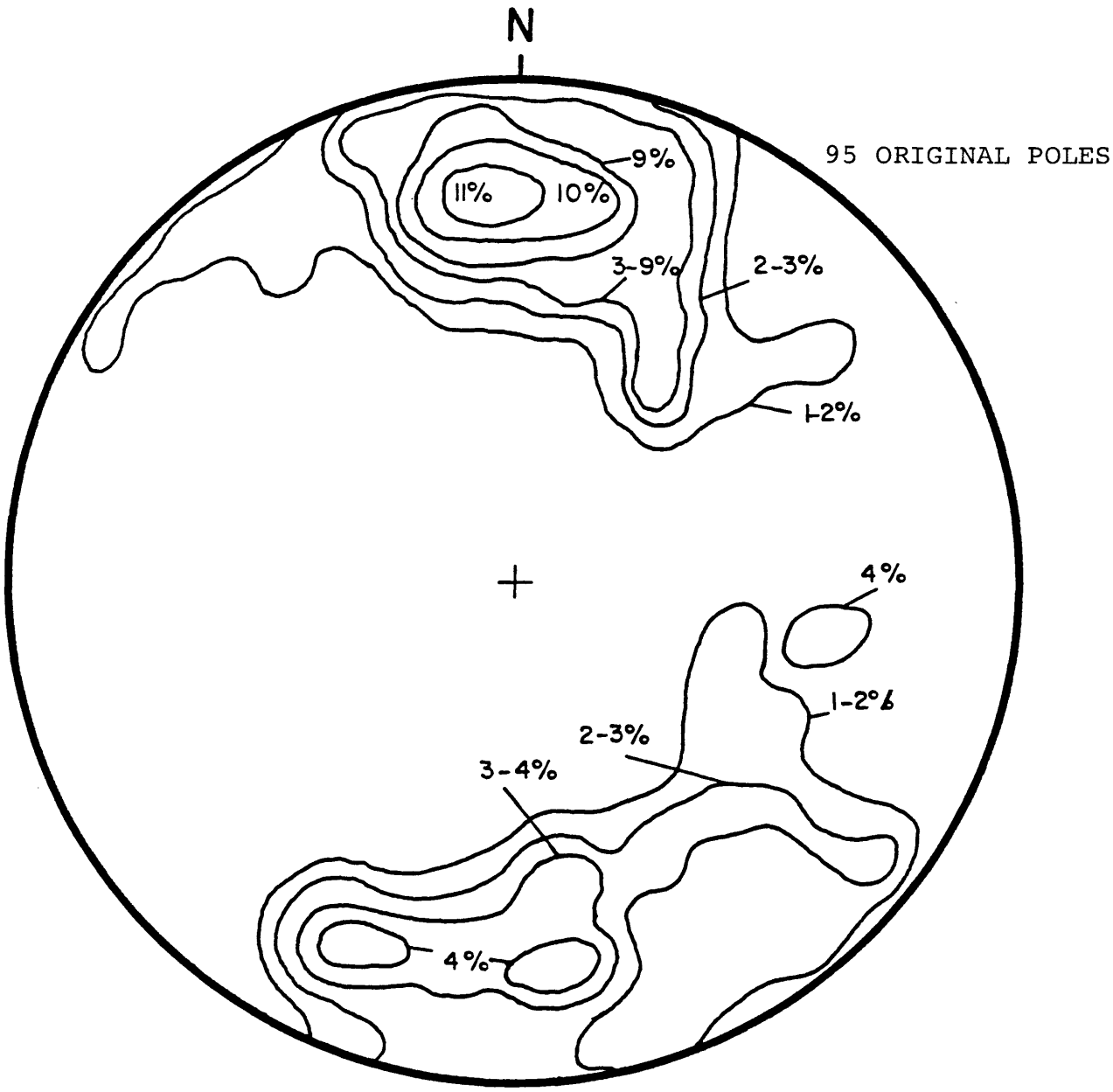

Figure 78. South edge of the pit
All data from Barringer fault zone

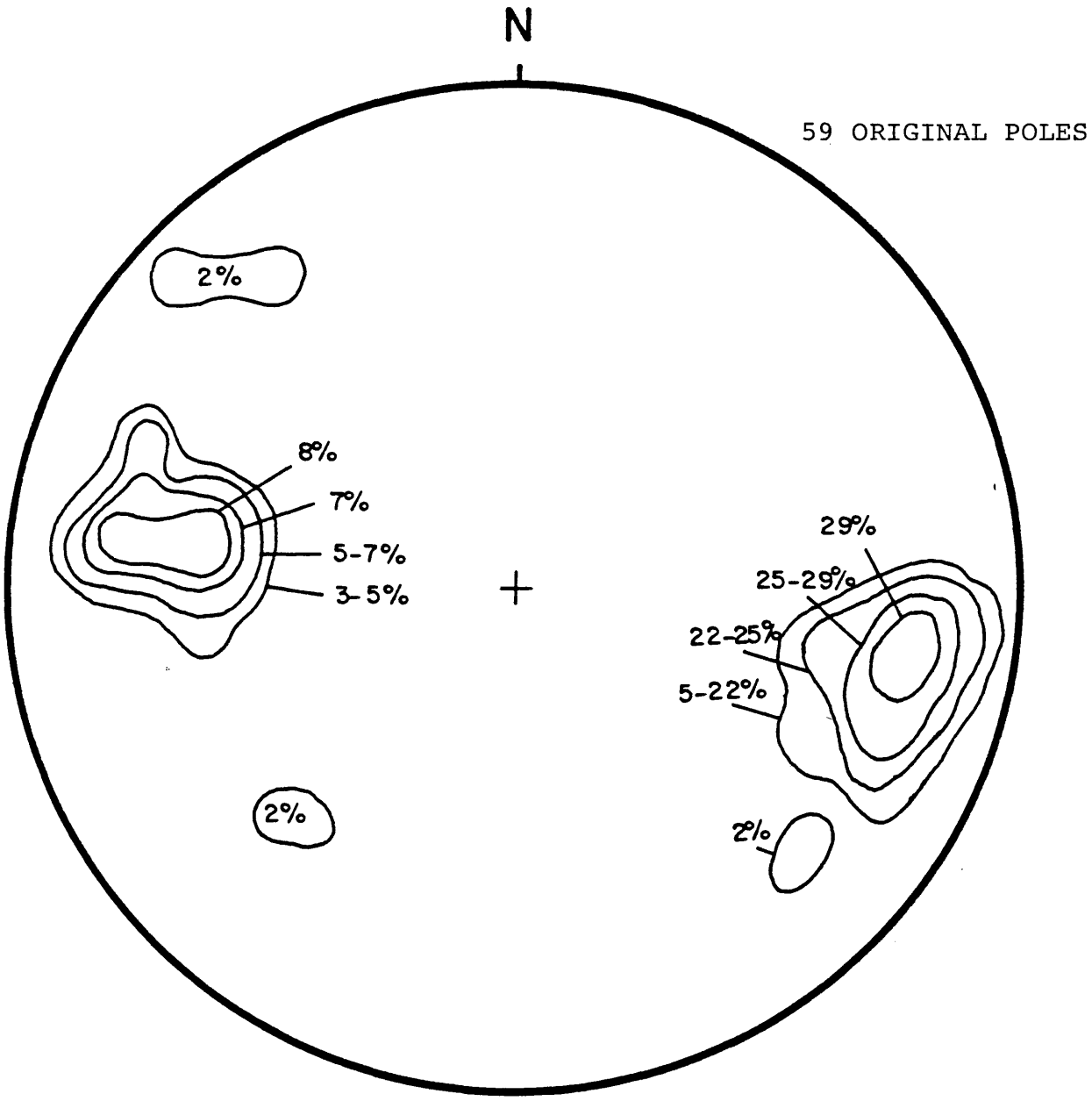

Figure 79. Quadrant N111,000 - N111,750
All data at elevations 6880 - 6920

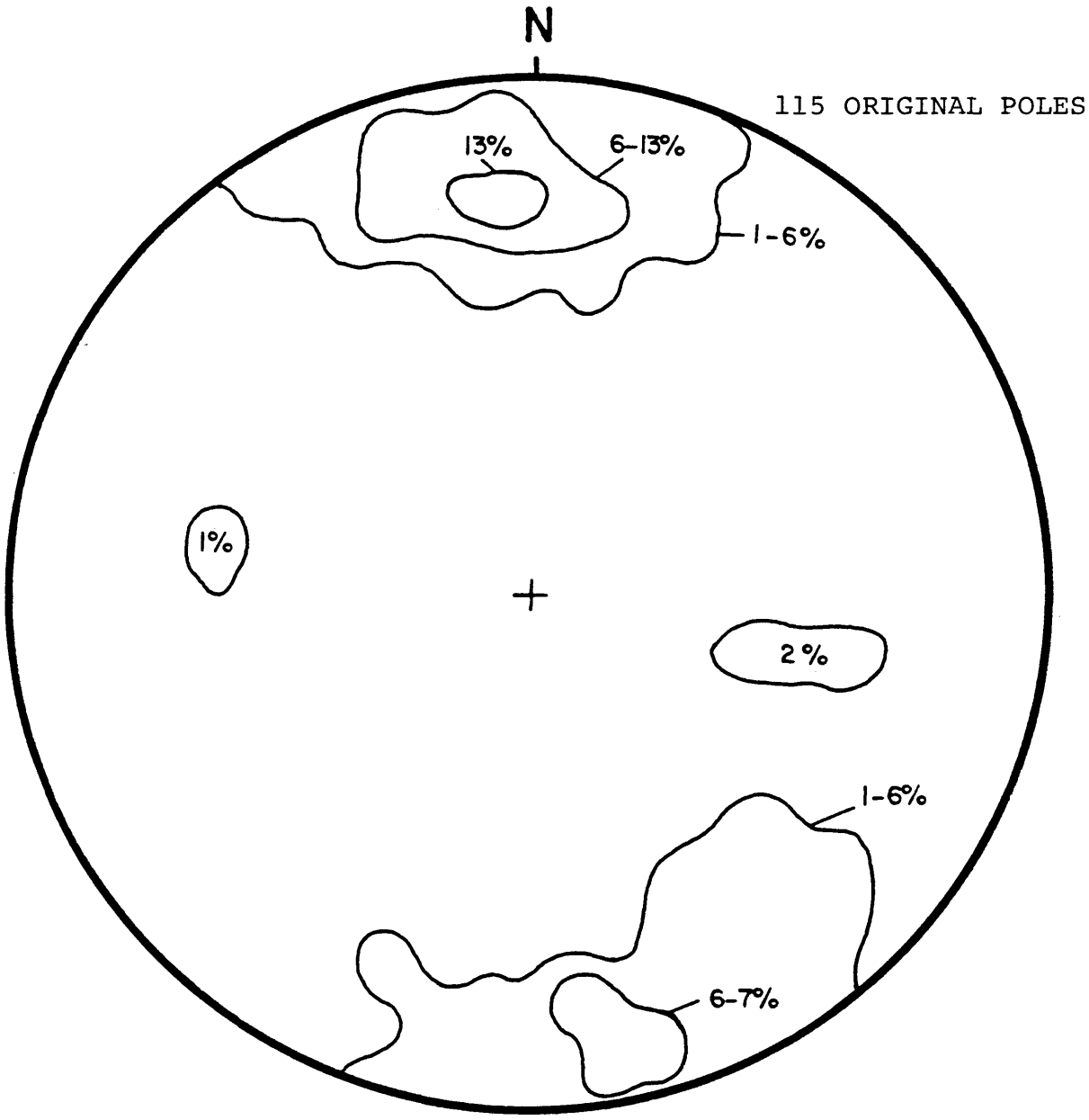

Figure 80. Quadrant N111,000 - N111,750
All data at elevations 6800 - 6840

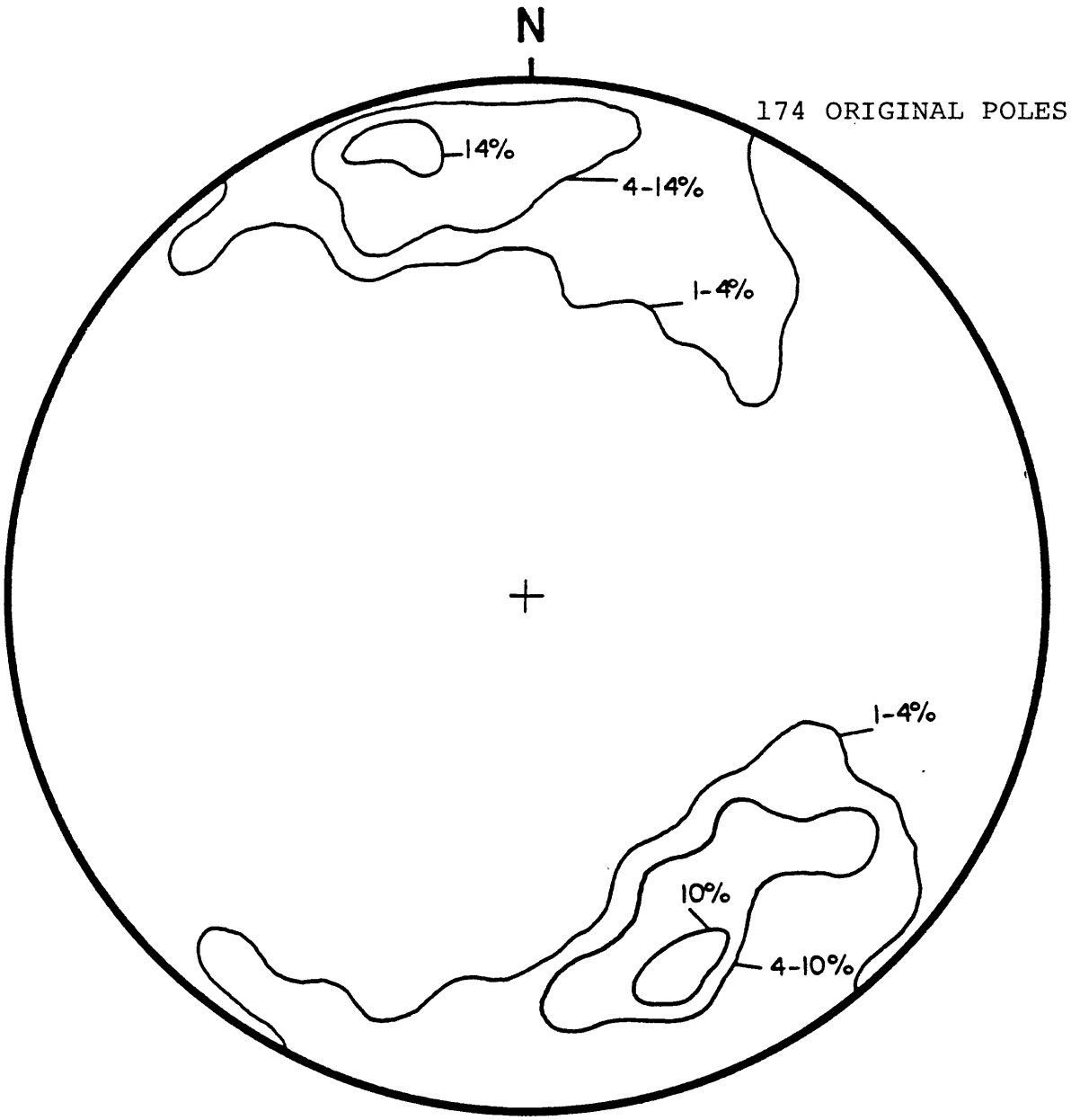

Figure 81. Quadrant N111,000 - N111,750
All data at elevations 6720 - 6760

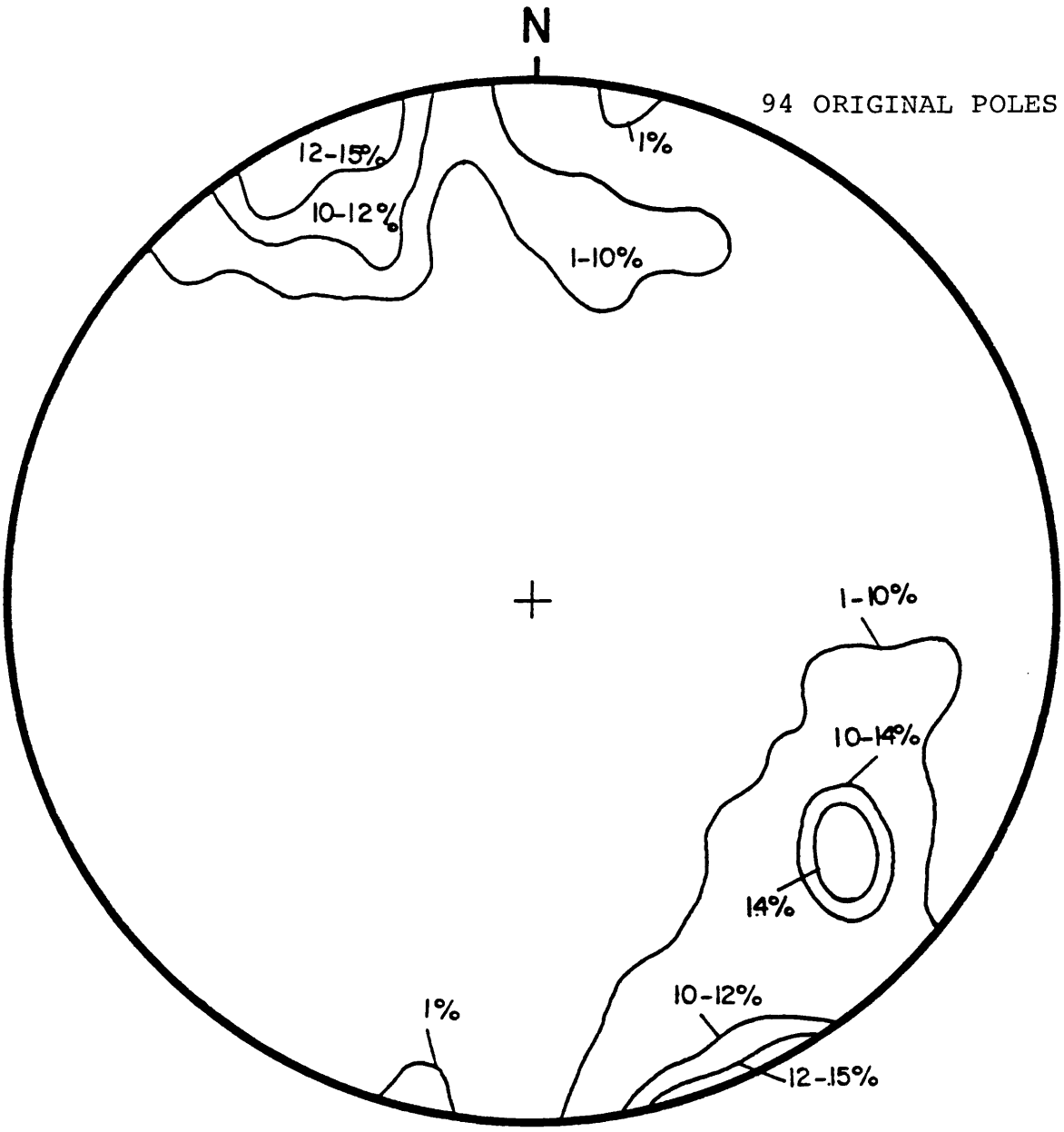

Figure 82. Quadrant N111,750 - N112,750
All data at elevations 6880 - 6920

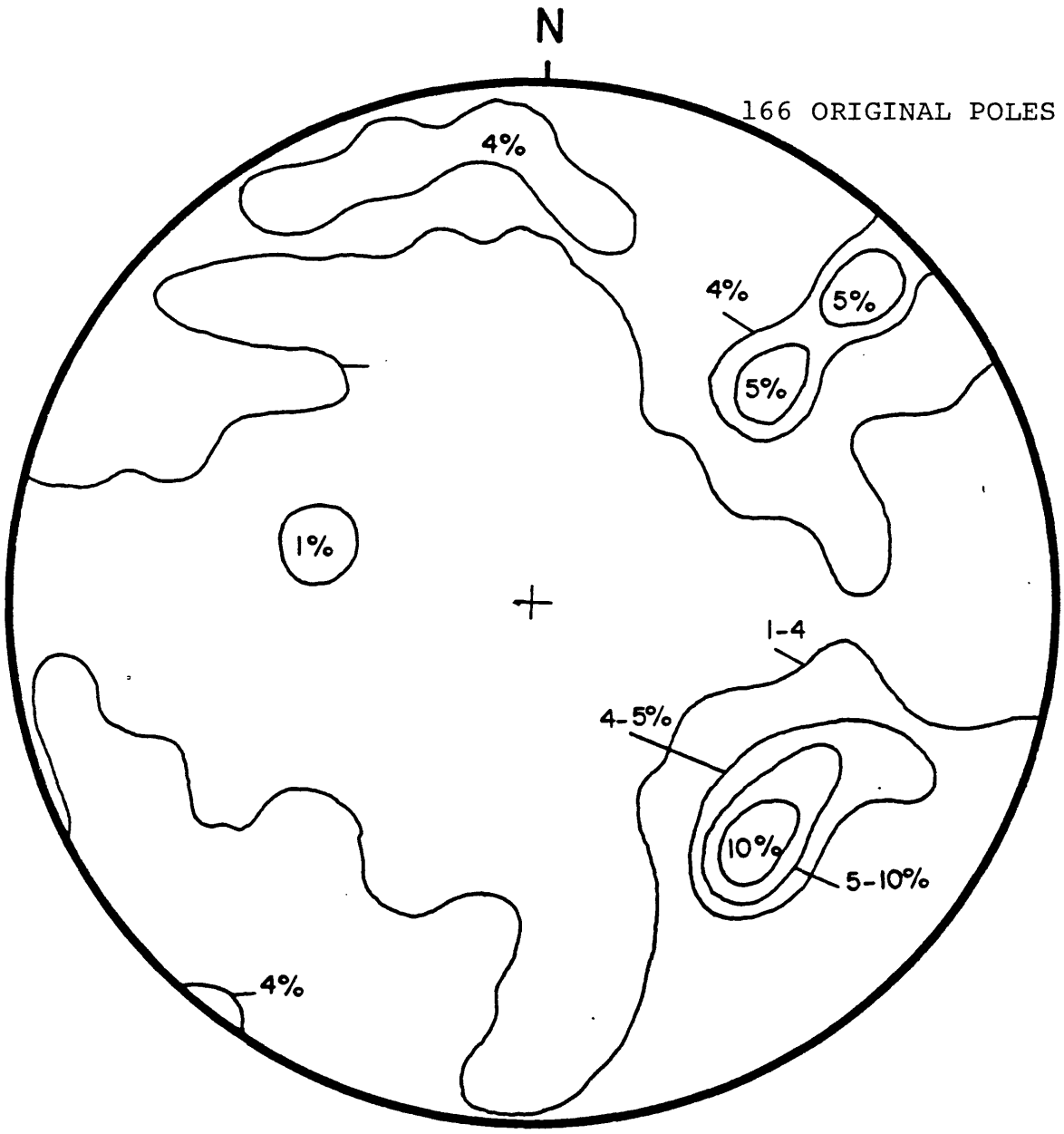

Figure 83. Quadrant N111,750 - N112,750
All data at elevations 6800 - 6840

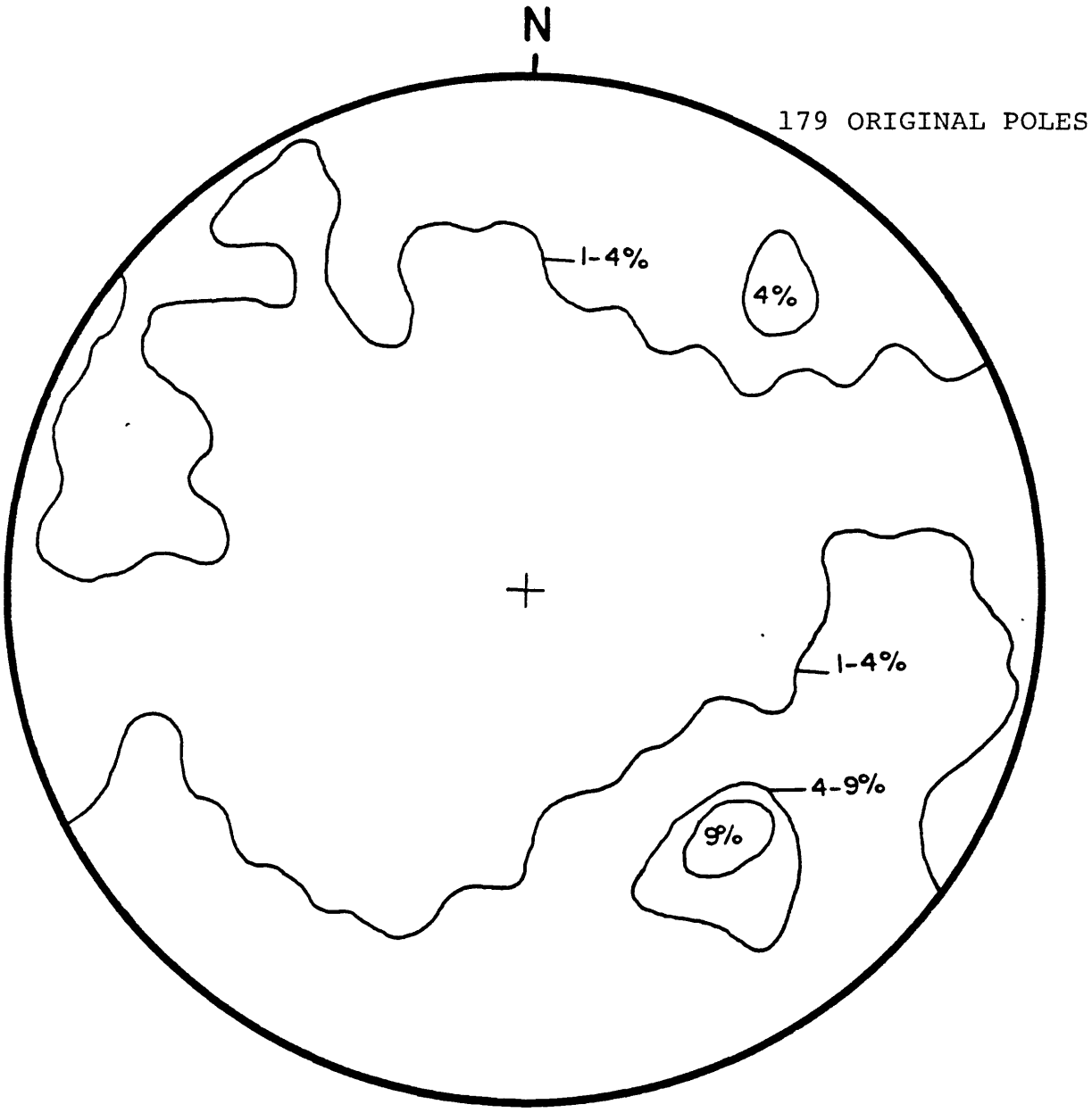

Figure 84. Quadrant N111,750 - N112,750
All data at elevations 6720 - 6760

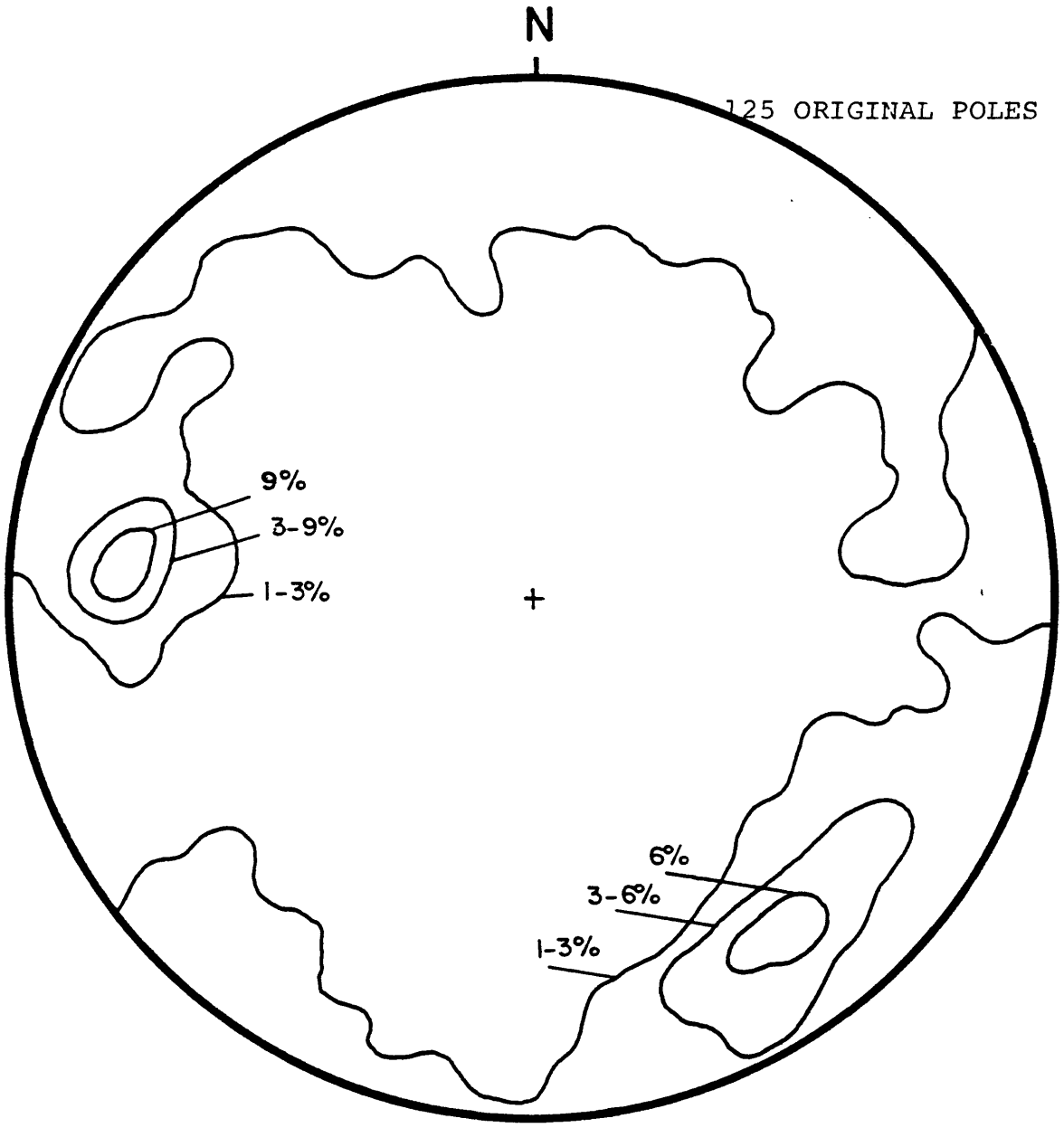

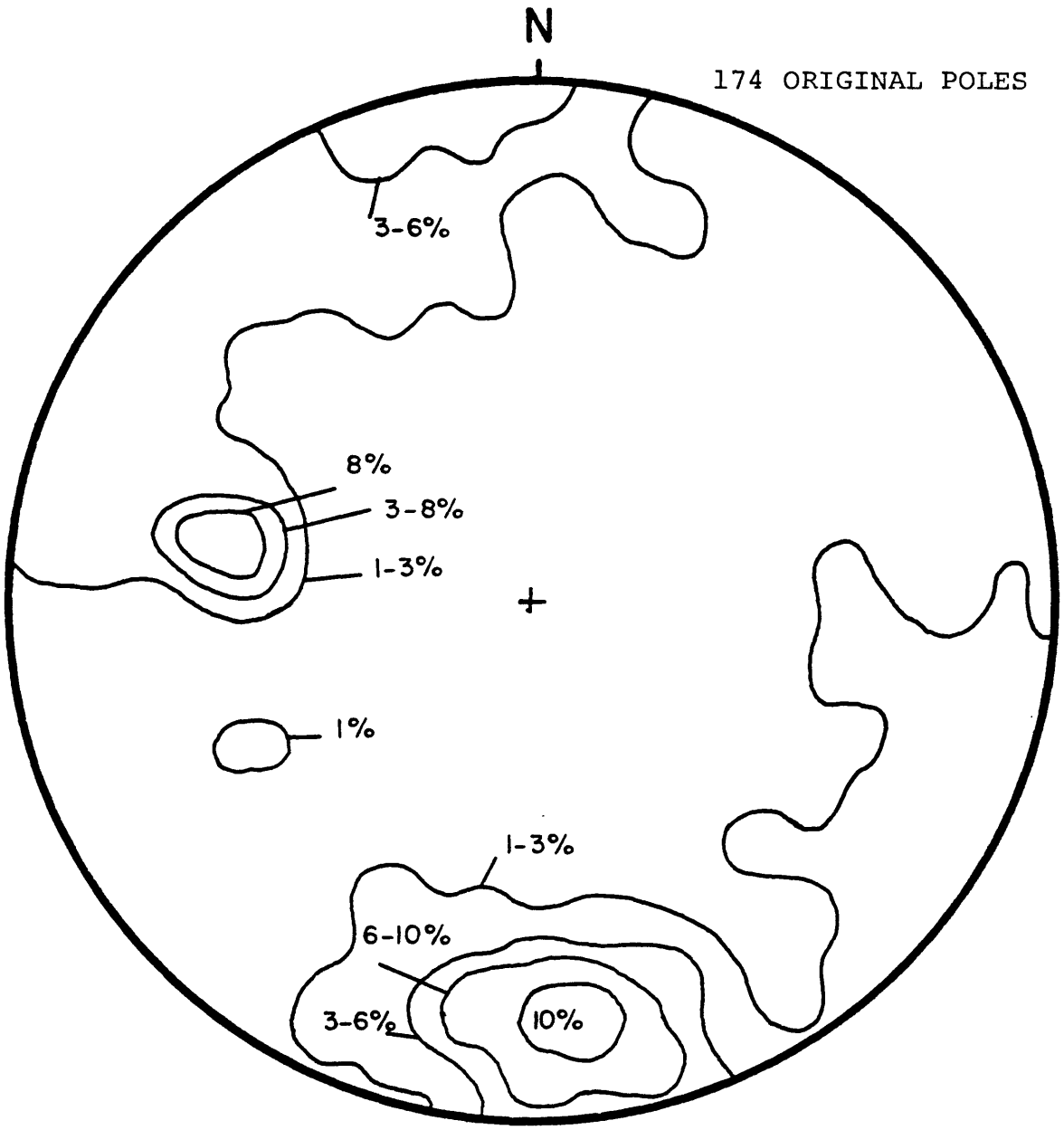


Figure 85. Quadrant E103,750 - E104,500
All data at elevations 6680 - 6760

Figure 86. Quadrant N110,000 - 111,000
All data at elevations 6760 - 6960

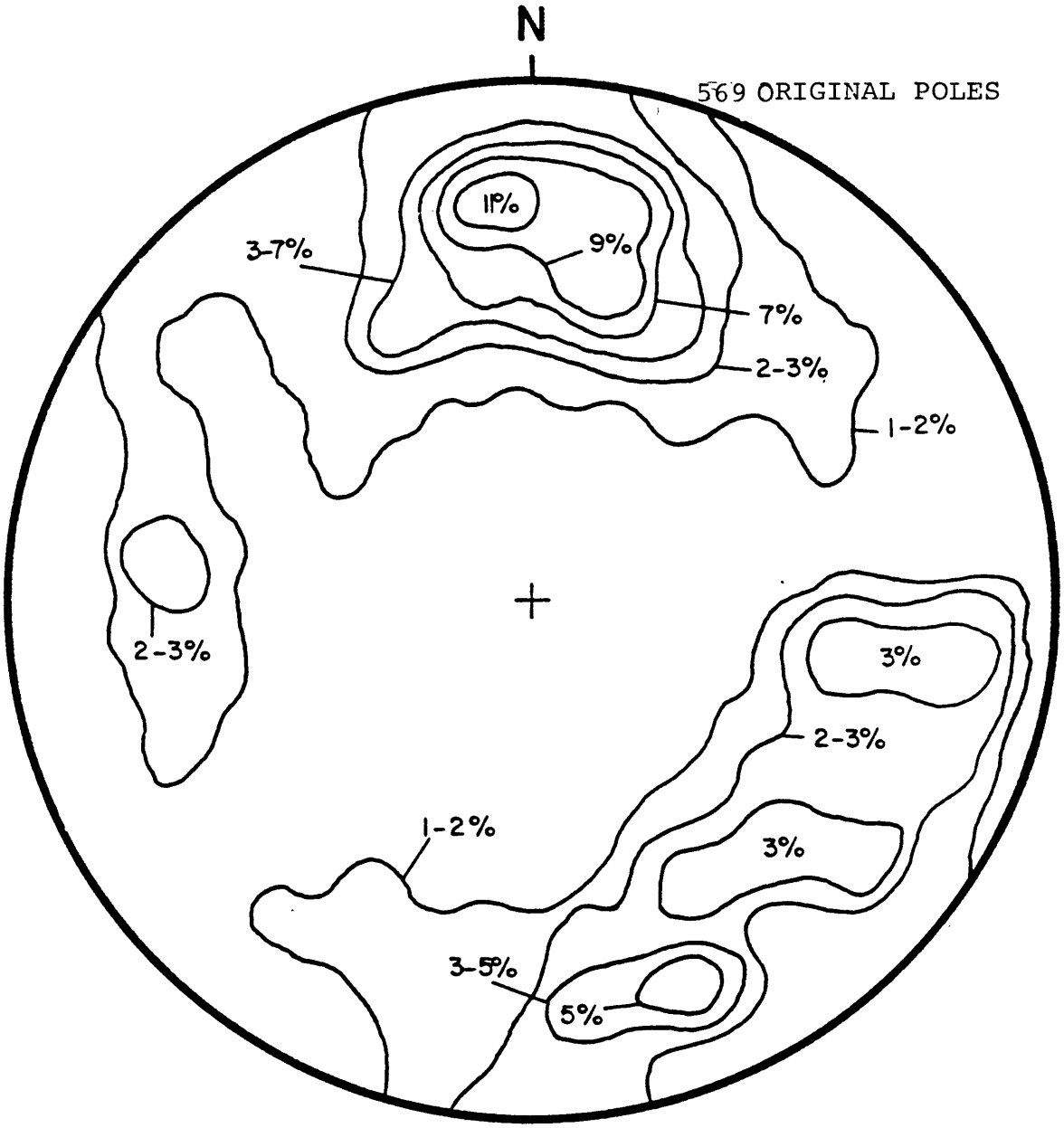

Figure 87. Quadrant N111,000 - N111,750
All data at elevations 6720 - 6920

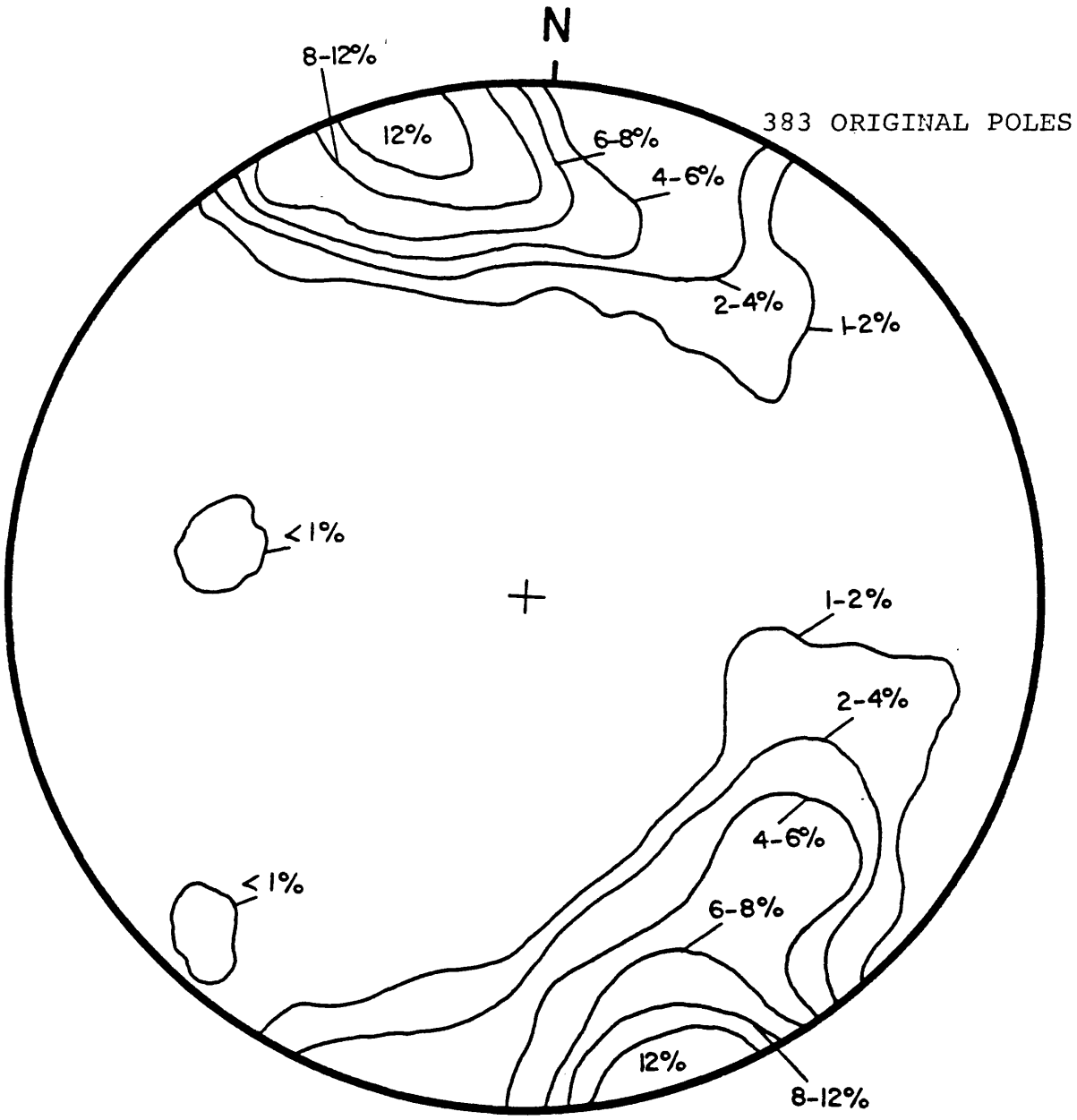

Figure 88. Quadrant N111,750 - N112,750
All data at elevations 6720 - 6920

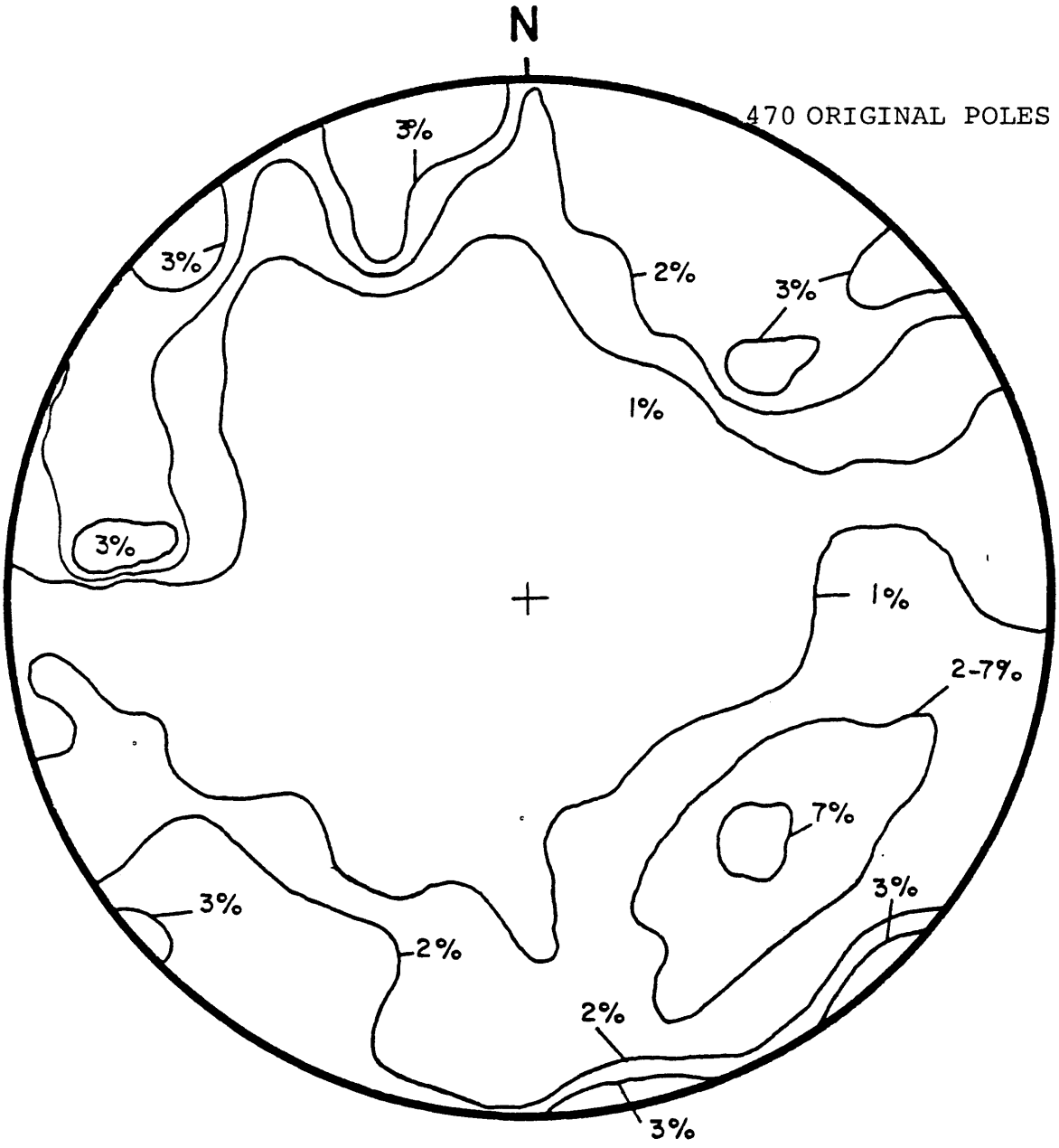

# REFERENCES

Aldrich, M. J., 1972, Tracing a subsurface structure by joints analysis: Santa Rita-Hanover axis, southwestern New Mexico.

Anderson, E., 1957, The metal resources of New Mexico and their economic features: New Mexico Bur. Mines Bull. 39.

Ballmer, G. J., 1953, Geology of the Santa Rita area: New Mexico Geol. Soc. Guidebook to 4th Field Conference.

Barnes, H. L., and Czamanske, G. K., 1967, Solubilities and transport of ore minerals, in Geochemistry of hydrothermal ore deposits: New York, Reinhard and Winston, Inc.

Bateman, A. M., 1950, Economic mineral deposits, 2nd ed.: New York, John Wiley and Sons.

Blackwelder, E., 1925, Exfoliation as a result of rock weathering: Jour. Geol., v. 33, p. 793-806.

Bryner, L., 1961, Breccia and pebble columns associated with epigenetic ore deposits: Econ. Geol., Vol. 56

Carpenter, R. H., 1960, A resume of hydrothermal alteration and ore deposition at Questa, New Mexico: Geol. Cong., 21st, Norway, Pt. 16, p. 79-86.

_____ 1968, Geology and ore deposits of the Questa molybdenum mine area, Taos County, New Mexico, in Ore deposits in the United States (Graton-Sales Volume) v. 2: New York, Am. Inst. Mining Metall. Petroleum Engineers, p. 1328-1350.

Cathles, L. M., 1977, An analysis of the cooling of intrusives by ground water convection which includes boiling: Econ. Geol., V. 72, no. 5.

Dana, J. D., 1895, Manual of geology: American Book Company, 127 p.

Dane, C. H., and Bachman, G. O., 1961, Preliminary geologic map of the southwestern part of New Mexico: U.S. Geol. Survey Misc. Geol. Inv. Map I-344.

Darton, N. H., 1917, Description of the Deming quadrangle (New Mexico): U.S. Geol. Survey Geol. Atlas, Folio 207, 15 p.

Denness, B., 1972, A revised method of contouring stereograms using variable curvilinear cells. Geol. Mag. v. 109, no. 2, pp. 157-163.

Forrester, J., 1972, Skarn formation and sulfide mineralization at the Continental mine, Fierro, New Mexico. (unpublished Ph.D. thesis, Cornell University).

Gilmour, P., 1977, Mineralized intrusive breccias as guides to concealed porphyry copper systems: Econ. Geol., vol. 72, no. 2.

Goldschmidt, V. M., 1911, Dristiania visensk. Skr. Math. Naturv. Kl. 11.

Goodman, R., 1976, Methods of geological engineering: West Publishing Co., New York.

_____ and Taylor, R. L., 1967, Methods of analysis for rock slopes and abutments: a review of recent developments, Proc. 8th Symp. on Rock Mechanics (AIME).

Gordon, C. H., 1907, Notes on the Pennsylvanian Formation in the Rio Grande Valley, New Mexico: Jour. Geol., v. 15, p. 805-816.

Grabau, Amaden W., 1920, A textbook of geology, part I, General geology: D.C. Heath and Company, p. 393-394.

Harker, R. I. and Tuttle, O., 1955, Am. Jr. Sci. v. 253, p. 209-244.

Harries, G. and Mercer, J. K., 1975, The science of blasting and its use to minimize cost. Proc. Australian Inst. Min. Metall. Annual Conf., Adelaide, part B.

Hernon, R. M., Jones, W. R., and Moore, S. L., 1953, Some geological features of the Santa Rita quadrangle, New Mexico: New Mexico Geol. Soc. Guidebook, 4th Field Conf., Southwestern New Mexico, 1953, p. 117-130.

Hobbs, W. H., 1929, Earth features and their meaning: The Macmillan Company, p. 150-152.

Hoek, E. and Sharp, J. C., 1970, Improving the stability of rock slopes by drainage: Planning open pit mines. Proc. of the symp. on the theoretical background to the planning of open pit mines, Johannesburg, South Africa.

_____ and Bray, J. W., 1977, Rock slope engineering. The Institution of Mining and Metallurgy, London. Second edition.

Hubert, L.B., 1967, Geochemistry of hydrothermal ore deposits: Holt, Rinehart and Winston, Inc.

Jaeger, J. C., 1957, The temperature in the neighborhood of a cooling intrusive sheet: Am. Jour. Sci., v. 255, p. 306-318.

Jennings, J.E. and Black, R. A., 1963, Factors affecting the angle of slope in opencast mines. Trans. A.I.M.E., vol. 226.

Jones, W. R., 1956, The central mining district, Grant County, New Mexico: U.S. Geol. Survey Open-File Rept.

_____ Case, J. E., and Pratt, W. P., 1964, Aeromagnetic and geologic map of part of the Silver City mining region, Grant County, New Mexico: U.S. Geol. Survey Geophys. Inv. Map GP-424.

_____ Hernon, R. M. and Moore, S. L., 1967, General geology of Santa Rita quadrangle, Grant County, New Mexico: U.S. Geol. survey prof. paper 555.

_____ Hernon, R. M. and Pratt, W. P., 1961, Geologic events culminating in primary metallization in the central mining district, Grant County, New Mexico, in short papers in the geologic and hydrologic sciences: U.S. Geol. Survey Prof. Paper 424-C, p. C11-C16.

Kelley, V., 1949, Geology and economics of New Mexico iron-ore deposits: New Mexico Univ., Pubs. Geology, no. 2, 246 p.

Kennedy, G. C., 1953, Geology and mineral deposits of Jumbo Basin, south eastern Alaska. U.S. Geol. Surv., prof. paper 251.

Kerr, Paul F., Kulp, J. L., Patterson, C. M., and Wright, R. J., 1950, Hydrothermal alteration at Santa Rita, New Mexico: Geol. Soc. America Bull., v. 61, no. 4, p. 275-347.

King, P. B., and others, 1944, Tectonic map of the United States (scale 1:2,500,000), with text: Am. Assoc. Petroleum Geologists, Prepared under direction of Natl. Research Council.

Kniffin, L. M., 1930, Mining and engineering methods and costs of the Hanover Bessemer Iron and Copper Co., Fierro, New Mexico: U.S. Bur. Mines Inf. Circ 6361, 20 p.

Korzhinskii, D. S., 1954, Physico-chemical principles of the analysis of mineral paragenesis: Pub. Acad. Sci., U.S.S.R.

Korzhinskii, D. S., 1970, Theory of metasomatic zoning: Oxford University Press, Ely House, London.

Landon, E., 1929, Metamorphism and ore deposition in the Santa Rita-Hanover-Fierro area, New Mexico - a study of igneous metamorphism: Chicago Univ., Unpub. Ph.D. thesis.

_____ 1932, Desericitization, a process operating during high temperature mineralization: Am. Min., v. 17, no. 9, p. 449-454.

Larsen, E. S., Jr., 1948, Batholith and associated rocks of Corona Elsinore, and San Luis Rey quadrangle, Southern California: Geol. Soc. Am. Mem. 29, p. 114-119.

Laskey, G., 1930, Geology and ore deposits of the Ground Hog mine, Central district, Grant County, New Mexico: New Mexico School Mines State Bur. Mines and Mineral Resources, circ. 2, 14 p.

_____ 1936, Geology and ore deposits of the Bayard area, Central mining district, New Mexico: U.S. Geol. Survey Bull. 870, 144 p.

_____ and Hoagland, A. D., 1948, Central mining district, New Mexico, in Dunham, K. C. ed., Symposium on the geology, paragenesis, and reserves of the ores of lead and zinc: Internat. Geol. Cong., 18th, London, 1948, p. 97-110.

Laudon, L. R., and Bowsher, A. L., 1941, Mississippian formations of Sacramento Mountains, New Mexico: Am. Assoc. Petroleum Geologists Bull., v. 25, no. 12, p. 2107-2160.

Lindgred, W., 1933, Mineral deposits, 695-712, New York, McGraw-Hill Book Co., Inc.

Locke, A., 1926, Formation of certain ore bodies by mineralization stoping: Eco. Geol., v. 21, p. 431-453.

Lowell, J.D., 1974, Regional characteristics of porphyry copper deposits of the southwest: Econ. Geol., v. 69, p. 601-618.

Lowell, J. D. and Guilbert, J. M., 1970, Lateral and vertical alteration-mineralization zoning in porphyry ore deposits: Econ. Geol., v. 65, p. 373-408.

Metz, P., and Winkler, H. G. F., 1963, Geochim. et Cosmochim. Acta. v. 27, p. 431-457.

Metz, P., 1967, Contr. Mineral. Petrol. v. 15, p. 272-280.

Miyashiro, A., 1953, Progressive metamorphism of the calcium-rich rocks of the Gasaisho Takanuki district, Abukuma Plateau, Japan: Jour. Geol. Geogr., v. 23, p. 82-107.

_____ 1973, Metamorphism and metamorphic belts: ed. by George A. and Unwin, London.

Morgan, B. A., 1975, Mineralogy and origin of skarns in the Mount Morrison Pendant, Sierra Nevada, California. Am. Jour. Sci., v. 275, p. 119-142.

Morgenstern, N. R., 1971, The influence of groundwater on stability: Proceedings of the first international conference on stability in open pit mining.

Muller, L., 1964, Application of rock mechanics in the design of rock slopes: state of stress in the earth's crust. American Elsevier Pub. Co., New York, p. 575-598.

Nielsen, R. L., 1968, Hypogene texture and mineral zoning in a copper bearing granodiorite porphyry stock, Santa Rita, New Mexico: Econ. Geol., v. 63, p. 37-50.

Paige, S., 1909, The Hanover iron-ore deposits, New Mexico: U.S. Geol. Survey Bull. 380-E, p. 199-214.

Patton, F. D., 1966, Multiple modes of shear failure in rock. Proc. 1st International Congress of Rock Mechanics. Lisbon. v. 1.

_____ and Deere, D. V., 1971. Geologic factors controlling slope stability in open pit mines. Proceedings of the first international conference on stability in open pit mining. Edited by Brawner and Milligan.

Pentz, D. L., 1971, Methods of analysis of stability of rock slopes. Proceedings of the first international conference on stability in open pit mining. Vancouver, B.C., Canada, edited by Brawner and Milligan.

Ramberg, H., 1952, The origin of metamorphic and metasomatic rocks.

Romdohr, P., 1969, The ore minerals and their intergrowths: Third edition, New York, Pergamon Press.

Schmitt, H. A., 1933a, Structural associations of certain metalliferous deposits in southwestern United States and northern Mexico: Am. Inst. Mining Metall. Engineers Contr. 38, 23 p., 1935a, Trans., v. 115, p. 36-58.

_____ 1933b, The Central mining district, New Mexico: Am. Inst. Mining Metall. Engineers Contr. 39, 22 p., 1935b, Trans., v. 115, p. 187-208.

_____ 1939a, The Pewabic mine (New Mexico): Geol. Soc. American Bull., v. 50, no. 5, p. 777-818.

Shoji, T., 1975, Role of temperature and $CO_2$ pressure in the formation of skarn and its bearing on mineralization: Econ. Geol., v. 70, p. 739-749.

Smirnov, S., 1934, Polymetallic deposits of eastern Transbaykaliya. Tr. Uses. Geolrazv. Ob"yed., no. 327.

Smirnov, V. I., 1976, Geology of mineral depoists: Mir Publisher, Moscow.

Spencer, A. D., and Paige, S., 1935, Geology of the Santa Rita mining area, New Mexico: U.S. Geol. Survey Bull. 859, 78 p.

Spry, A., 1969, Metamorphic textures: New York, Pergamon Press.

Terzaghi, R., 1965, Sources of error in joint surveys: Geotechnique, pp. 287-304.

Winkler, G. F., 1974, Petrogenesis of metamorphic rocks: Third Ed., Springer-Verlag, New York.

Yousefpour, M.V., 1977, Geology and contact pyrometasomatic ore deposits at the Continental mine, Fierro, New Mexico (unpublished M.Sc. thesis, Colorado School of Mines).

Zharikov, V. A., 1970, Skarns (Part I): Internat. Geol. Rev. v. 12, no. 5.

_____ 1970, Skarns (Part II): Internat. Geol. Rev. v. 12, no. 6.

_____ 1970, Skarns (Part III): Internat. Geol. Rev. v. 12, no. 7.